

**HIGH-THROUGHPUT SCREENING FOR SMALL-MOLECULE
INHIBITORS OF THE $G\alpha_{12/13}$ /RHOA SIGNALING PATHWAY**

by

Chris Richard Evelyn

A dissertation submitted in partial fulfillment
of the requirements for the degree of
Doctor of Philosophy
(Pharmacology)
in The University of Michigan
2009

Doctoral Committee:

Professor Richard Robert Neubig, Chair
Professor Sofia D. Merajver
Emeritus Professor William B. Pratt
Associate Professor Jorge A. Iñiguez-Lluhí
Assistant Professor Daniel A. Bochar

To Mom and Dad

ACKNOWLEDGEMENTS

I would first like to thank my thesis advisor, Dr. Richard R. Neubig for his scientific guidance and mentorship. I also will like to thank the other members of my thesis committee, Drs. Sofia Merajver, Jorge Iñiguez-Lluhí, William B. Pratt, and Daniel Bochar for their scientific guidance, mentorship, and helpful feedback during my committee meetings. I would like to thank members of the Sunahara and Tesmer Labs along with Drs. Roger Sunahara and John Tesmer for their helpful scientific feedback and discussion during lab meetings over the years. I would like to thank Drs. Li Li (Wayne State University, Detroit, MI), Michael Parmacek (University of Pennsylvania, Philadelphia, PA), Ron Prywes (Columbia University, NYC, NY), and John Tesmer (University of Michigan, Ann Arbor, MI) for kindly providing DNA plasmids. I would also like to thank Drs. Sofia Merajver, J. Menon, Kathleen Cho, Kenneth Pienta (University of Michigan, Ann Arbor, MI), and Richard Hynes (Massachusetts Institute of Technology, Cambridge, MA) for kindly providing cell lines. I would like to thank the Center for Chemical Genomics (CCG) at the University of Michigan, especially Dr. Stuart J. Decker, Ms. Martha Larsen, and Mr. Renju Jacob for their help with assay development, chemo-informatic analysis, and aid with carrying out my high-throughput screens. I would like to thank the Medicinal Chemistry Core Synthesis laboratory at the University of Michigan, especially Drs. Hollis D. Showalter and Scott D. Larsen, Ms. Jenny Ryu, Ms. Jessica L. Bell, and Ms. Nicole L. Harzdorf for chemical synthesis of my CCG-1423 analogs and for medicinal chemistry assistance and advice (especially Dr. Scott D. Larsen) for my structure-activity relationship studies. I would like to thank Drs.

John Sondek and Rafael Rojas at the University of North Carolina – Chapel Hill for a fun and productive collaboration for my Chapter 5 studies.

I would like to thank past and present members of the Neubig Lab for their support and help over the years, especially Ms. Susan M. Wade, Drs. Qin Wang, Pete Clapp, Xinyan Huang, Ying Fu, David L. Roman, Becky Roof, and Serge Thierry Omouessi. I also would like to thank the undergraduate students, Mr. Timothy Ferng, Mr. Melvin Rivera, and Mr. Andrew Kocab, whom I have mentored over the years for their hard work and dedication. I would like to thank all my friends and fellow graduate students whom I spent many joyous times with over the years and helped to make this experience memorable for me.

I would like to thank my parents, Norva and Richard Evelyn for their support and encouragement during my graduate school years and throughout my whole life. I also would like to thank my sister Tichar Evelyn and my brother Anthony Evelyn for their support and encouragement. I also would like to thank my little nephew John Charzuk for keeping me grounded and helping me to keep life in perspective during these graduate school years.

Lastly, I would like to acknowledge my NRSA funding from the National Cancer Institute, part of the National Institutes of Health – F31CA113268.

TABLE OF CONTENTS

DEDICATION.....	ii
ACKNOWLEDGEMENTS.....	iii
LIST OF FIGURES.....	viii
LIST OF TABLES.....	x
LIST OF ABBREVIATIONS.....	xi
CHAPTER I. INTRODUCTION.....	1
G-protein Coupled Receptors	1
GPCRs and Cancer	2
RhoA Transcriptional Signaling Pathway	5
RhoA Transcriptional Signaling Pathway and Cancer	7
Targeting the RhoA Transcriptional Pathway	12
My Work	13
References	19
CHAPTER II. CCG-1423: A SMALL-MOLECULE INHIBITOR OF RHOA TRANSCRIPTIONAL SIGNALING.....	30
Abstract	30
Introduction....	31
Materials and Methods	35
Results	42
Discussion	57
References	64

CHAPTER III. CHEMICAL SYNTHESIS, STRUCTURE-ACTIVITY RELATIONSHIPS, AND PROSTATE CELL-BASED STUDIES OF THE RHOA TRANSCRIPTIONAL PATHWAY INHIBITOR, CCG-1423.....	70
Abstract	70
Introduction	71
Materials and Methods	73
Results	76
Discussion	93
References	110
CHAPTER IV. THE EFFECT OF THE RHOA TRANSCRIPTIONAL PATHWAY INHIBITOR, CCG-1423, UPON GLOBAL GENE EXPRESSION.....	113
Abstract	113
Introduction	114
Materials and Methods	118
Results	122
Discussion	143
References	151
CHAPTER V. HIGH-THROUGHPUT SCREENING FOR SMALL-MOLECULE INHIBITORS OF LARG-STIMULATED RHOA NUCLEOTIDE BINDING VIA A NOVEL FLUORESCENCE POLARIZATION ASSAY.....	158
Abstract	158
Introduction	159
Materials and Methods	162
Results	.166

Discussion	176
References	185
CHAPTER VI. CONCLUSION.....	189
References	197
APPENDIX.....	201

LIST OF FIGURES

1-1.	GPCR-G $\alpha_{12/13}$ -RhoA-MKL1/SRF cellular mechanism.....	17
1-2.	G $\alpha_{12/13}$ -RhoA transcriptional signaling pathway.....	18
2-1.	Characterization of the SRE.L system in HEK293T cells.....	44
2-2.	Summary of high-throughput screening results and chemical structures.....	48
2-3.	Latrunculin B, CCG-977, and CCG-1423 inhibit G α_{13} Q226L-stimulated SRE.L luciferase expression in PC-3 cells.....	52
2-4.	CCG-1423 inhibits downstream of Rho and shows specificity for SRE.L-mediated transcription.....	53
2-5.	CCG-1423 inhibits cancer cell proliferation and survival.....	59
2-6.	CCG-1423 inhibits prostate cancer cell invasion.....	60
2-7.	Effect of Rho-Kinase inhibitor, Y-27632, on SRE.L-luciferase activated by transfection of ROCK or G α_{13} and effect of CCG-1423 on ROCK kinase activity.....	61
3-1.	Effect of the methyl group upon the SRE.L response.....	78
3-2.	Effect of the removal of the hydroxamate group and the methyl group position upon the SRE.L response.....	79
3-3.	Effects of the R-groups upon the SRE.L response.....	82
3-4.	Dose-dependent inhibition of the SRE.L response by the amide class of CCG-1423 analogs.....	83
3-5.	Dose-dependent inhibition of the SRE.L response by the conformationally restrictive class of CCG-1423 analogs.....	85

3-6.	Dose-dependent inhibition of the SRE.L response by the conformationally restrictive class of CCG-1423 analogs.....	86
3-7.	Dose-dependent inhibition of the SRE.L response by the amide replacement class of CCG-1423 analogs.....	89
3-8.	Dose-dependent inhibition of the SRE.L response by the amide replacement class of CCG-1423 analogs.....	90
3-9.	Correlation between the Matrigel Invasion Assay vs. the SRE.L-luciferase reporter assay.....	109
4-1.	Microarray analysis of regulated genes.....	126
4-2.	Time-course of CCG-1423 effect upon PC-3 cell gene expression.....	140
4-3.	Gene expression across 3 prostate epithelial cell lines.....	141
4-4.	Effect of CCG-1423 analogs upon PC-3 cell gene expression.....	144
5-1.	GTPase cycle, mechanisms of inhibition, and structure of guanosine triphosphate (GTP) analogs.....	171
5-2.	Fluorescence polarization RhoA nucleotide-binding assays.....	173
5-3.	Dose-dependent leukemia-associated RhoGEF (LARG)–stimulated RhoA nucleotide binding.....	174
5-4.	Fluorescence polarization screen for inhibitors of LARG-stimulated RhoA nucleotide binding.....	177
5-5.	Dose-response inhibition of leukemia-associated RhoGEF (LARG)–stimulated RhoA [³⁵ S] GTPγS binding by high-throughput screening (HTS) hits.....	180
5-6.	Compound selectivity for leukemia-associated RhoGEF (LARG)–stimulated RhoA [³⁵ S] GTPγS binding.....	181
6-1.	CCG-1423 analogs and affinity column for future mechanistic studies.....	193

LIST OF TABLES

3-1.	Summary of SRE.L-luciferase reporter results.....	96
3-2.	Summary of 24 hr cell viability results.....	101
3-3.	Summary of Matrigel invasion results.....	106
4-1.	Number of genes regulated in microarray.....	125
4-2.	Comparison of genes regulated by CCG-1423 with CArG-box or MKL1-dependent genes.....	129
4-3.	Rationale for candidate gene selection.....	132
4-4.	Comparison of microarray versus QRT-PCR results.....	134
5-1.	Chemical compound properties and IC ₅₀ values.....	178
A-1.	Summary of metastasis-related gene transcripts.....	201

LIST OF ABBREVIATIONS

ANGPTL4: angiopoietin-like 4

ATCC: American Type Culture Collection

AMPK: AMP-activated protein kinase

BB: bombesin receptor

BODIPY: 4,4-difluoro-4-bora-3a,4a-diaza-s-indacene or boron dipyrromethene, a fluorescent dye

BPE: bovine pituitary extract

BrdUrd: 5-Bromo-2'-deoxyuridine

CCG: Center for Chemical Genomics core facility at the University of Michigan – Ann Arbor

cDNA: complementary deoxyribonucleic acid

CO₂: carbon dioxide

CRM1: chromosome region maintenance 1

CTGF: connective tissue growth factor

DAG: diacylglycerol

DH: dbl homology domain

DMEM: Dulbecco's Modified Eagle's Medium

DMSO: dimethyl sulfoxide

DNA: deoxyribonucleic acid

DRB: 5,6-dichlorobenzimidazole-1-β-D-ribofuranoside, general transcription inhibitor

ED: erectile dysfunction

EGF: epidermal growth factor

EGFR: epidermal growth factor receptor

EMT: epithelial mesenchymal transition

EREG: epiregulin

ERK: extracellular signal-regulated protein kinase

F-Actin: filamentous actin

Farnesylation: covalent attachment of a 15 carbon saturated fatty acid farnesyl group

FBS: fetal bovine serum

FL: fluorescein fluorophore

FP: fluorescence polarization

G-Actin: globular actin

G $\alpha_{i/o}$: G-protein subfamily which inhibits adenylyl cyclase and stimulates K⁺ and inhibits Ca⁺² channels

GAP: GTPase-activating proteins

G $\alpha_{q/11}$: G-protein subfamily which signals through phospholipase C β

G α_s : G-protein which stimulates adenylyl cyclase

G $\alpha_{12/13}$: G-protein subfamily which signals through the RhoA subfamily (RhoA, B, C)

GDI: guanosine nucleotide dissociation inhibitor

GDP: guanosine diphosphate

GEF: guanosine nucleotide exchange factor

Geranylgeranylation: covalent attachment of a 20 carbon saturated fatty acid isoprenyl group

GO: gene ontology

GPCR: G-protein Coupled Receptor

G Proteins: heterotrimeric guanosine nucleotide binding proteins

GTP: guanosine triphosphate

GTP γ S: guanosine 5'-o-(3-thiophosphate), a non-hydrolyzable analog of GTP

h: hours

HAT: histone acetyltransferase

HCl: hydrochloric acid

HDAC: histone deacetyltransferase

HGF: hepatocyte growth factor

HIV: human immunodeficiency virus

HMT: histone methyltransferase

HTS: high-throughput screen

IC₅₀: half maximal inhibitory concentration

IL-11: interleukin 11

IL13R α 2: interleukin-13 decoy receptor

inhib: inhibition

IOSE: normal immortalized ovarian surface epithelial cells

IP₃: inositol-1,4,5-triphosphate

K_d: dissociation constant

kDA: kilodaltons

KLF6: kruppel-like factor 6

K-SFM: keratinocyte serum-free medium

LARG: leukemia-associated RhoGEF

LPA: lysophosphatidic acid

Luc: luciferase

MALDI: matrix-assisted laser desorption/ionization mass spectrometry

MANT: N-methyl-3'-O-anthranoyl, type of fluorophore

MCCSL: Medicinal Chemistry Core Synthesis Lab core facility at University of
Michigan – Ann Arbor

MEK: map (mitogen-activated protein kinase)-erk kinase

µg: micrograms

min: minutes

MKL1: megakaryoblastic leukemia 1

mL: milliliters

MLL: mixed-lineage leukemia

µmol/L: micromoles per liter or micromolar

µM: micromolar

mM: millimolar

MMP: matrix metalloproteinase protein

mol/L: moles per liter or molar

mP: measured values of polarization

mRNA: messenger ribonucleic acid

NA: no inhibitory activity

ng/mL: nanograms per milliliter

nm: nanometers

nM: nanomolar

PAR: protease-activated receptor

PH: pleckstrin homology domain

PIP₂: phosphatidylinositol-4,5-bisphosphate

PTGS2: prostaglandin G/H synthase 2

PTHrP: parathyroid hormone-related protein

PTX: pertussis toxin, ADP-ribosylates G α_i -subunit

QRT-PCR: quantitative real-time polymerase chain reaction

RBM15: RNA-binding motif protein 15

RGS4: regulator of G-protein signaling 4

RGS7: regulator of G-protein signaling 7

RH: regulator of G-protein signaling homology domain

RMA: robust multi-array average

RNA: ribonucleic acid

ROCK: Rho-associated coiled-coil forming protein serine/threonine kinase

SD: standard deviation

SEM: standard error of the mean

shRNA: small hairpin RNA or short hairpin RNA

siRNA: small interfering RNA

SOX9: SRY (sex determining region Y)-box 9 (campomelic dysplasia, autosomal sex reversal)

SRE: serum response element

SRF: serum response factor

T-Antigen: tumor antigen

3D: three-dimensional

TGF β : transforming growth factor beta

TIP30: Tat-interacting protein 30

TK: thymidine kinase

TR: texas-red fluorophore

UMCCC: University of Michigan Comprehensive Cancer Center

VEGF: vascular endothelial growth factor

CHAPTER I.

INTRODUCTION

G-Protein Coupled Receptors (GPCRs)

The G-protein Coupled Receptor (GPCR) family of receptors is responsible for a myriad of cellular and physiological functions through interactions with extracellular stimuli, such as hormones, neurotransmitters, cytokines, lipids, proteases, odorants, etc (1, 2). As a result, the pharmaceutical industry has placed much effort upon targeting this class of receptor proteins, which has resulted in nearly 50% of the current drugs on the market today (1). All GPCRs are characterized by seven transmembrane helices, three extracellular loops, three intracellular loops, and an extracellular N-terminal tail and an intracellular C-terminal tail. The G-proteins are made up of a heterotrimer of proteins consisting of $G\alpha$, $G\beta$, and $G\gamma$ subunits. Upon receptor activation, GTP for GDP exchange occurs on the $G\alpha$ subunit, and the $G\alpha$ and $G\beta\gamma$ subunits dissociate. The activated GTP-bound $G\alpha$ subunit and $G\beta\gamma$ subunit can now interact with their respective downstream effectors leading to cell signaling events regulating various cellular functions, such as motility, metabolism, calcium signaling, neurotransmitter release, and gene expression (1, 2).

The type of effector that a GPCR activates depends upon the type of $G\alpha$ subunit that it couples to. There are four main families of GPCRs, which include those that couple to $G\alpha_s$, $G\alpha_{i/o}$, $G\alpha_{q/11}$, and $G\alpha_{12/13}$. $G\alpha_s$ and $G\alpha_{i/o}$ coupled receptors lead to stimulation or inhibition of adenylyl cyclase, which results in increased production or

decreased production of cyclic-AMP, respectively. $G\alpha_s$ and $G\alpha_{i/o}$ coupled receptor regulated cyclic-AMP changes result in ion channel function (Na^+/Cl^- channel and K^+/Cl^- channel) within the cell. $G\alpha_{q/11}$ coupled receptors result in the activation of phospholipase $C\beta$. This enzyme converts phosphatidylinositol-4,5-bisphosphate (PIP_2) into diacylglycerol (DAG) and inositol-1,4,5-triphosphate (IP_3). The effect of phospholipase $C\beta$ activation and IP_3 production by $G\alpha_{q/11}$ coupled receptors results in increased intracellular calcium and signaling within the cell. Lastly, $G\alpha_{12/13}$ coupled receptors, which are the class of receptors that is the focus of the work I describe here, result in the activation of the small GTPase RhoA subfamily (RhoA, B, C). Activation of the RhoA subfamily results in both short-term cytoskeletal effects within the cell affecting cell motility and long-term transcriptional effects leading to gene expression (1, 2).

Among the many GPCRs, three GPCRs that are known to couple to $G\alpha_{12/13}$ are the lysophosphatidic acid, thrombin, and bombesin receptors (Fig. 1-1). These GPCRs also have the capacity to couple to $G\alpha_i$ and $G\alpha_q$ (3-6). As a result, the ability of these receptors to couple to multiple G-proteins enables them to control a variety of both cellular and biological functions, such as: cell migration, cell morphology changes, gene expression, cell cycle regulation, apoptosis, cell growth, DNA synthesis, mobilization of cellular calcium, platelet aggregation, endothelial cell and smooth muscle contraction, and tumor differentiation (3-5).

GPCRs and Cancer

These three GPCRs have been well-documented to play a major role in the pathogenesis of cancer and cancer metastasis. The LPA receptor family (LPA_1 , LPA_2 , and LPA_3) is well-known to play a major role in the pathogenesis of ovarian cancer, but

is also known to play a role in endometrial, gastric, and prostate cancers (7-16). LPA has been shown to promote *in vitro* cancer cell migration through an uncoated or collagen I coated matrix by Caov-3 and SKOV-3 ovarian cancer cells (7, 8, 16), AGS gastric cancer cells (13, 14), HEC1A endometrial cancer cells (11), PC-3 prostate cancer cells (10), and BT-20 breast cancer cells (9). In addition, ascites from ovarian cancer patients containing high concentrations of LPA as well as LPA itself were able to stimulate hADSC mesenchymal stem cells, which are key cells involved in ovarian cancer metastatic progression, to migrate through a collagen I coated matrix. This effect is dependent on both RhoA-Rho Kinase (ROCK) and $G\alpha_i$ -MEK-ERK pathways (17). In addition to cell migration, LPA has been shown to stimulate *in vitro* cancer cell invasion through a Matrigel-coated matrix by AGS gastric cancer cells (14) and PC-3 prostate cancer cells (12). More interestingly, the LPA receptor coupled $G\alpha_{12/13}$ -RhoA signaling pathway has been shown to play a role in cell migration or invasion of Caov-3 and SKOV-3 ovarian cancer cells (7, 16), AGS gastric cancer cells (14), BT-20 breast cancer cells (9), and PC-3 prostate cancer cells (12). In addition to metastasis, LPA has also been shown to play a role in general cancer pathogenesis through a pro-survival role and by stimulating cell cycle progression in PC-3 prostate cancer cells (15).

Like for the LPA receptor family, it has been well-established that the thrombin receptor family (PAR1, PAR2, PAR3, and PAR4) plays an important role in tumorigenesis. A fundamental example of this is that overexpression of the PAR1 receptor in the presence of thrombin-containing serum leads to focus formation by NIH-3T3 mouse fibroblasts (18). Thrombin has been shown to stimulate, in a dose-dependent manner, growth of A172 glioblastoma cells (19) and HT29 colon cancer cells. This

involves a PAR4-dependent mechanism (20). Thrombin has also been shown to stimulate *in vitro* cancer cell migration through an uncoated or collagen-coated matrix. This is primarily through a PAR1-dependent mechanism, but in a few cases PAR2 or PAR4 have also been shown to contribute. These studies utilized M24met melanoma cells (21), HCC 589 hepatocellular carcinoma cells (22), A-498 renal carcinoma cells (23), and PC-3 prostate cancer cells (24). In addition, thrombin stimulates *in vitro* invasion through a Matrigel-coated matrix by MDA-MB-231 and BT549 breast cancer cells (25, 26), PC-3 prostate cancer cells (27), and U2-OS osteosarcoma cells (28). Interestingly, thrombin stimulates the invasion by PC-3 cells in a Rho-dependent manner (27). With respect to *in vivo* studies, anti-PAR1 antibodies and PAR1 siRNA incorporated into liposomes have been shown to inhibit pulmonary metastases of M24met and A375SM melanoma cells, respectively (21, 29).

The bombesin receptor family (BB₁, BB₂, and BB₃) also plays a role in cancer progression. In a wound-healing assay, bombesin stimulates *in vitro* motility of both PC-3 prostate cancer cells (30, 31) and Isreco1 colon carcinoma cells (32) in a RhoA pathway dependent manner. In addition, in an invasion through a Matrigel matrix assay, bombesin stimulates invasion by Caco-2 and Isreco1 colon carcinoma cells in a Cox-2 and RhoA-dependent manner, respectively (32, 33). More interestingly, in an *in vivo* xenograft model using SK-N-SH neuroblastoma cells, bombesin increases both tumor growth and angiogenesis as measured by VEGF protein expression (34). Also, in several other xenograft tumor models, including both H-69 small cell- (35) and H460 non-small cell- (36) lung carcinoma, MDA-MB-435 breast cancer (37), and PC-3 prostate cancer models (38), bombesin signaling was shown to play a pivotal role since the bombesin

receptor antagonist, RC-3940-II, inhibited tumor growth. Clearly, these three $G\alpha_{12/13}$ coupled GPCR receptor families play a significant role in cancer progression and metastasis in a variety of cancer cell types, some of which show RhoA pathway dependent mechanisms (Fig. 1-1).

RhoA Transcriptional Signaling Pathway

The Rho family of small GTPases is a major subset of the Ras superfamily of GTPases. The Rho family of small GTPases can be subdivided into 10 subgroups including small GTPases that are related to RhoA, Rac1, Cdc42, RhoD, Rif/RhoF, Rnd3/RhoE, TTF/RhoH, Chp/RhoV, Miro1/RhoT1, or RhoBTB (39). In the cell, Rho GTPases are activated upon extracellular ligand activation of cell surface receptors, such as cytokine, tyrosine kinase, adhesion, integrin, and G-protein-coupled receptors (GPCRs) (Fig. 1-1) (40). This leads to membrane translocation and activation in which the Rho GTPase switches from its inactive GDP-bound to the active GTP-bound form, which leads to various downstream cellular events, such as cytoskeletal changes, cell migration, cell growth, and gene transcription (Fig. 1-1) (39). The Rho family of small GTPases is most well-known for downstream effects upon the cytoskeleton, which lead to cell motility (Fig. 1-1). The three main subgroups, RhoA, Rac1, and Cdc42, are responsible for orchestrating cell motility through their control of stress fiber and focal adhesion formation, lamellipodia formation, and filopodia formation, respectively (41).

The activation of small GTPases is regulated by several classes of proteins. The GTPase-activating proteins (GAPs) catalyze the GTP hydrolysis of the active GTP-bound form of Rho GTPases leading to their inactivation and to termination of their downstream

signaling events. The guanine-nucleotide-dissociation inhibitors (GDIs) sequester inactive GDP-bound Rho GTPases in the cytosol, thus preventing their membrane localization and activation. Finally, guanine nucleotide exchange factors (GEFs) stimulate the exchange of GTP for GDP upon Rho GTPases resulting in their activation. There are over 60 known human RhoGEFs that specifically activate the Rho family of small GTPases (39).

Rho GEFs are characterized by their Dbl homology (DH) and C-terminal adjacent pleckstrin homology (PH) domains, which are primarily responsible for catalyzing nucleotide exchange leading to activation of Rho GTPases (39). However, the PH domains have also been shown to play a role in membrane localization of Rho GEFs in addition to aiding the DH domain in catalysis (39). The $G\alpha_{12/13}$ coupled heterotrimeric G-protein coupled receptors activate the RhoA subgroup (RhoA, RhoB, RhoC) of GTPases through a special family of Rho GEFs (p115-RhoGEF, LARG, PDZ-RhoGEF), which are characterized by a regulator of G-protein signaling homology domain (RH) (42). The RH-domain-containing RhoGEF leukemia-associated RhoGEF (LARG) is a focus of the work described here (Fig. 1-1 and 1-2). LARG was originally identified as a chromosomal translocation fusion protein to the mixed-lineage leukemia (MLL) gene in a patient with acute myeloid leukemia (43).

In addition to the short term cytoskeletal effects, $G\alpha_{12/13}$ -dependent RhoA signaling can lead to more long term gene expression effects (Fig 1-1 and 1-2). These gene expression effects are modulated by the transcription factor, serum response factor (SRF), which is most well-known for stimulating immediate early gene expression (e.g. *c-fos* and *jun*) (Fig. 1-1) (44-46). In the RhoA signaling pathway, SRF stimulates gene

expression through collaboration with the transcriptional co-activator megakaryoblastic leukemia 1 (MKL1 a.k.a. MRTF-A and MAL). Like LARG, MKL1 was originally discovered as a chromosomal translocation fusion protein to RNA-binding motif protein-15 (RBM15) in patients with acute megakaryoblastic leukemia (47). Upon the loss of monomeric G-actin as a result of actin polymerization, MKL1 is released from its inactive G-actin bound state and translocates into the nucleus (Fig. 1-1) (44, 46). In addition, nuclear export of MKL1 through the chromosome region maintenance 1 (Crm1) protein is blocked upon activation of the $G\alpha_{12/13}$ -RhoA-dependent pathway (48).

RhoA Transcriptional Signaling Pathway and Cancer

G $\alpha_{12/13}$ /Rho GTPases and Cancer

Rho signaling has been well-established in the literature to play a role in cancer pathogenesis and metastasis. Two of the major Rho GTPases, Rac and Cdc42, have been implicated in tumor growth, migration, and invasion in both mouse skin and human breast tumors (49-51). Several of the atypical Rho GTPases, RhoD, RhoF, and RhoE have been implicated in anti-tumorigenic roles through the reduction of oncogenic src-dependent and A375 melanoma cell motility, induction of cell cycle arrest and apoptosis in prostate cancer cells, and gene deletion in T-cell lymphoma (52-55). However, the atypical Rho GTPase, Chp, has been implicated in tumor progression due to its ability to stimulate focus formation by NIH-3T3 cells (56).

The RhoA subgroup (RhoA, RhoB, RhoC) of Rho GTPases, which is the focus of the work described here, has been shown to play a significant role in cancer progression, with the exception of RhoB. Like several of the atypical Rho GTPases,

RhoB has been shown to play an anti-tumorigenic role, such as in the inhibition of melanoma pulmonary metastasis and ovarian tumor growth in mice, oncogenic ras-mediated focus formation by NIH-3T3 mouse fibroblasts, and thyroid cancer cell growth (57-60). Unlike RhoB, the other two RhoA subgroup members, RhoA and RhoC, have been implicated in the progression of multiple malignancies. RhoA has been shown to be overexpressed in hepatocellular carcinoma, gastric cancer, and esophageal squamous cell carcinoma patients (7, 61-64). High expression of RhoA correlates with poor prognosis and patient survival in both hepatocellular carcinoma and esophageal squamous cell carcinoma (61, 62, 64). In gastric cancer models, RhoA has been implicated in *in vitro* cell growth and cell cycle progression of gastric cancer cells (AGS and SGC7901 cells), whereas in *in vivo* xenograft nude mouse models, it has been shown to play a role in tumor growth as shown by siRNA and dominant negative RhoA overexpression approaches (63, 65). RhoA has been implicated in *in vitro* growth and Matrigel invasion by MDA-MB-231 breast cancer cells. Furthermore, *in vivo* MDA-MB-231 tumor growth was reduced by siRNA knockdown of RhoA (66). Interestingly, in an esophageal squamous cancer metastasis model in nude mice, RhoA was shown to play a role in tumor growth, but not in pulmonary metastasis (67). However, in head and neck squamous cell carcinoma, RhoA was shown to play a role in *in vitro* cell motility and Matrigel invasion by two highly metastatic cell lines (UMSCC11A and UMSCC36) (68).

RhoC plays a similar and perhaps greater role in the cancer progression and metastasis of gastric cancer, hepatocellular carcinoma, head and neck squamous cell carcinoma, breast cancer, and esophageal squamous cell carcinoma. In esophageal squamous cell carcinoma and hepatocellular carcinoma, RhoC appears to be more

important for tumor metastasis rather than for growth (63, 65-69). Interestingly, with invasive SUM-159 breast cancer cells, using individual siRNAs to knockdown RhoA and RhoC showed that RhoC stimulated, whereas RhoA inhibited *in vitro* Matrigel cell invasion (70). This highlights the mechanistic differences that occur across various types of cancers. In a very aggressive inflammatory breast cancer model, RhoC has been shown to be overexpressed and to play a significant role in the metastatic phenotype (71-73). More recently, RhoC overexpression has been shown to be correlated with inflammatory breast cancer and an increased number of tumor emboli in an Egyptian population of breast cancer patients (74). RhoC is most notable for its role in *in vitro* cancer cell migration and/or invasion and in *in vivo* metastatic models with various malignancies, such as melanoma (75, 76), pancreatic adenocarcinoma (77), prostate cancer (78-81), and lung cancer (82). Consistent with these results across various cancers, RhoC was shown to be critical for *in vivo* metastasis, but not for tumor initiation and growth of polyoma T-antigen-induced mammary tumors in a RhoC-deficient mouse model (83). In addition, $G\alpha_{12}$, which can activate the RhoA subgroup, has been shown to be overexpressed in both breast and prostate cancers. It also stimulates invasion through a Matrigel matrix in a RhoA signaling pathway-dependent manner (27, 84). $G\alpha_{12}$ was also shown to play a role in *in vivo* breast cancer metastasis in a RhoA signaling pathway-dependent manner (84). Therefore, the RhoA subgroup especially RhoA and RhoC have been well-established to play a role in cancer progression and metastasis and as result should serve as valuable cancer therapeutic targets.

ROCK and Cancer

The most notable Rho effector known to play a role in cancer progression and metastasis is the Rho-associated coiled-coil forming protein serine/threonine kinase (ROCK). ROCK can be directly activated by either RhoA or RhoC (85). Like RhoA and RhoC, ROCK has been observed to be overexpressed in a variety of malignancies, such as esophageal squamous cell carcinoma (86), pancreatic cancer (87), and hepatocellular carcinoma (88). In HT1080 lung cancer, MDA-MB-231 breast cancer, and B16 melanoma models, ROCK was implicated in both *in vitro* tumor cell migration and invasion and *in vivo* metastasis (89, 90). Mechanistically, ROCK has been shown to be vital for *in vitro* cell invasion through a 3D-Matrigel matrix by rounded bleb-forming cells versus more elongated cells (91, 92). However, more recently, in both colon cancer cells and hepatocellular carcinoma cells, ROCK was implicated in either cell migration or invasion through a collagen I or Matrigel matrix and in the regulation of matrix metalloproteinases (93, 94). Therefore, it is possible for ROCK to regulate metalloproteinase-dependent modes of cell movement depending on the type of cancer and cell type. As a result, ROCK potentially may serve as a valuable cancer therapeutic target within the RhoA transcriptional signaling pathway in future clinical studies.

MKL1/SRF and Gene Expression and Cancer

Although the Rho GTPases, their regulators, and effectors have been well-established to be involved in cancer, there is rather little known about the role of the transcriptional portion of the RhoA signaling pathway, which includes the co-activator MKL1 and its transcription factor SRF, in cancer progression and metastasis.

Interestingly, SRF has been implicated in several cell processes that may be relevant to cancer development in non-cancerous cells, including cell motility, cell growth, DNA synthesis, cell adhesion, and angiogenesis (45, 95, 96). More recently, there have been publications implicating a role for SRF in cancer progression and metastasis. Like RhoA, RhoC, and ROCK, SRF is overexpressed in hepatocellular carcinoma and has been implicated to play a role in *in vitro* hepatocellular carcinoma cell migration and invasion (97). In androgen-dependent (hormone-dependent) prostate cancer cells, SRF has been shown to play a role in *in vitro* cell growth and DNA synthesis (98). Also, in colon cancer, an exon 5 deleted splice variant of SRF has been shown to improve cell survival, *in vitro* (99). Therefore, SRF is beginning to elicit interest in the cancer biology community. More recently, Medjkane and colleagues (100) have shown for the first time that both the co-activator MKL1 and its transcription factor SRF play a role in both breast cancer and melanoma metastasis. The authors show a requirement of both MKL1 and SRF for cell motility and invasion but not for cell proliferation (100), which is consistent with the RhoC data described earlier in which similar functional effects were seen. Also, MKL1 and SRF were implicated in the production of pulmonary metastases in an *in vivo* nude mouse model for both breast cancer and melanoma (100).

Medjkane and colleagues also showed that two MKL1-dependent cytoskeletal genes, *Myl9* and *Myh9*, were critical for the breast cancer cell migration and invasion. A similar role was seen in *in vivo* breast cancer and melanoma cell pulmonary metastases. Several serum-mediated MKL1-dependent genes have also been implicated in tumorigenesis, including *SRF*, *adrenomedullin*, *epiregulin*, *interleukin-6*, *hexokinase 2*, and *zyxin* (101). These MKL1-dependent genes have been linked to cancer cell functional

processes, such as cell-growth, migration, invasion, and survival (102-107). In addition to SRF and MKL1, RhoC has also been shown to induce expression of genes that are critical for cancer metastasis, including *cyclin D1*, *VEGF-C*, *CXCL1*, *fibronectin*, and *IGFBP2* (108). Therefore, the transcriptional portion of the RhoA signaling pathway and RhoA pathway-mediated gene expression can also play an important role in cancer pathogenesis and metastasis.

Targeting the RhoA Transcriptional Signaling Pathway

Although there is a well-documented role for the RhoA transcriptional signaling pathway in cancer progression and metastasis, there are relatively few chemical inhibitors available that target this pathway. There has been significant effort focused on inhibiting the carboxy-terminal isoprenylation of the activated form of the Rho GTPase. This lipid modification is critical for membrane localization and function of the Rho GTPase. Inhibitors of this lipid modification include the farnesyltransferase and geranylgeranyl transferase inhibitors and the cholesterol lowering statin drugs (71, 76, 109), but these drugs are not selective for the Rho family of GTPases or the RhoA transcriptional signaling pathway. The Rho GTPase effector, ROCK, has also been targeted for chemical inhibitor development. Inhibitors, such as Y-27632, WF-536, and fasudil, have shown promising anti-metastatic activity in both *in vitro* and *in vivo* models (89, 90, 110). However, the drawback of these compounds is that they only inhibit one “arm” of the RhoA signaling pathway (Fig. 1-2), which would render them ineffective against tumors that are dependent upon the transcriptional portion and/or Rho GTPase-mediated gene expression of the RhoA pathway. There is also the marine toxin, latrunculin B, which

inhibits filamentous actin formation and the cytoskeletal functional effects of the pathway (111). However, this compound is a general actin polymerization inhibitor and is not specific for the RhoA transcriptional signaling pathway. Other than the ROCK inhibitors, there are only two published specific inhibitors of Rho GTPase signaling, but neither of these compounds target the RhoA transcriptional signaling pathway. These inhibitors, NSC23766 and EHT 1864, directly and specifically inhibit the Rho GTPase, Rac1 (112-114). However, there is still a need for inhibitors of RhoA and RhoC, their regulators or effectors, or other protein-protein interactions specific to the RhoA transcriptional signaling pathway.

My Work

The evidence presented above leads me to the goal of this thesis, which is to identify novel small-molecule inhibitors of the RhoA transcriptional signaling pathway as pharmacological tools to better understand the role of this pathway in cancer biology and metastasis. Such compounds could also serve as leads for the development of cancer therapeutics. The two approaches undertaken here used high-throughput chemical screening to identify novel inhibitors. One project utilized a cell-based Rho-specific SRE.L-luciferase reporter assay (Fig. 1-2), whereas the other utilized a biochemical guanine nucleotide binding functional fluorescence polarization assay targeting the interaction between the RhoGEF, LARG, and the Rho GTPase, RhoA.

In Chapter 2, using the cell-based Rho-specific SRE.L-luciferase reporter assay screening (Fig. 1-2) approach to screen two-thousand compounds, I identified two small-molecule inhibitors, CCG-977 and CCG-1423, of the RhoA transcriptional signaling pathway. CCG-977 was found to have an IC₅₀ of 2 μM, whereas CCG-1423 was found to

have an IC_{50} of 1 μ M. Therefore, the more potent CCG-1423 compound was selected to pursue follow-up studies. In assessing its mechanism of action, CCG-1423 was found to work at the transcriptional level, likely modulating MKL1/SRF stimulated gene expression. Interestingly, in cancer biology *in vitro* functional experiments, CCG-1423 inhibited LPA-mediated DNA synthesis in PC-3 prostate cancer cells, RhoC-overexpressing melanoma cell growth and survival, and spontaneous PC-3 cell Matrigel invasion but not $G\alpha_i$ -dependent SKOV-3 ovarian cancer cell Matrigel invasion.

In chapter 5, utilizing the biochemical guanine nucleotide binding functional fluorescence polarization assay screening approach targeting the interaction between the RhoGEF, LARG, and the Rho GTPase, RhoA to screen ten-thousand compounds, we identified five small-molecule inhibitors, CCG-13528, CCG-14631, CCG-7167, CCG-14113, and CCG-12529, of LARG-stimulated RhoA nucleotide binding. These compounds were found to selectively inhibit LARG-stimulated [35 S] GTP γ S binding to RhoA but not RhoA or $G\alpha_o$ [35 S] GTP γ S binding. Therefore, these five compounds were identified as leads for further development into both pharmacological tools and/or therapeutics. In addition, the novel fluorescence polarization guanosine nucleotide-binding assay developed to carryout this high-throughput screen should serve as a useful approach for general biological applications as well.

In Chapter 3, I describe the chemical synthesis of analogs of the RhoA transcriptional pathway inhibitor, CCG-1423, and describe their effects upon $G\alpha_{12}QL$ -stimulated SRE.L-luciferase expression, constitutive thymidine kinase (TK)-promoter-driven *Renilla* luciferase expression, the WST1 cell viability response, and spontaneous cell Matrigel invasion of PC-3 prostate cancer cells. In addition, I also tested the toxicity

of these analogs across a panel of normal prostate and prostate cancer cell lines. The most promising analogs described were found to be less potent than CCG-1423, but more selective and less toxic with respect to both the firefly and *Renilla* luciferase expression and WST1 cell viability of PC-3 cells. Also, none of the analogs described in this chapter showed any significant toxic selectivity across the panel of normal prostate and prostate cancer cell lines. Overall, the analogs showed similar potency, selectivity, and toxicity in the PC-3 cell Matrigel invasion experiments in comparison to the Rho-specific SRE.L-luciferase expression experiments. The most promising and selective analogs described in Chapter 3 should serve as lead compounds for both future mechanistic studies to identify the molecular target of CCG-1423 and for *in vivo* metastatic prostate cancer xenograft studies.

Lastly, in Chapter 4, I describe the effect of the RhoA transcriptional pathway inhibitor, CCG-1423, upon genome-wide gene expression in PC-3 prostate cancer cells in order to investigate both the general mechanism of action of CCG-1423 and its mechanism of action as it relates to spontaneous PC-3 prostate cancer cell Matrigel invasion. Using this approach, I was able to identify four candidate genes (*RGS4*, *RGS7*, *CTGF*, and *SOX9*) regulated by CCG-1423 to be potentially involved in CCG-1423 inhibition of spontaneous PC-3 cell Matrigel invasion. Two of these genes (*RGS4* and *SOX9*) were confirmed to be regulated by two more selective CCG-1423 analogs identified in Chapter 3, CCG-100602 and CCG-101425, in the same manner as CCG-1423 via quantitative real-time polymerase chain reaction (QRT-PCR) analysis. Future functional studies will determine if the genes, *RGS4* and *SOX9*, are involved in CCG-

1423-mediated inhibition of PC-3 prostate cancer cell Matrigel invasion and prostate cancer metastasis.

As a result, the high-throughput screens described here yielded promising lead compounds that inhibit the RhoA transcriptional signaling pathway (Fig. 1-1). These compounds should prove to be useful for the development of future pharmacological tools and therapeutics. One of these tools, CCG-1423, has already been utilized to elucidate the mechanism of action of its inhibition of spontaneous PC-3 cell Matrigel invasion in Chapter 4. Overall, the work described here lays a strong foundation for the further development of inhibitors of the RhoA transcriptional signaling pathway.

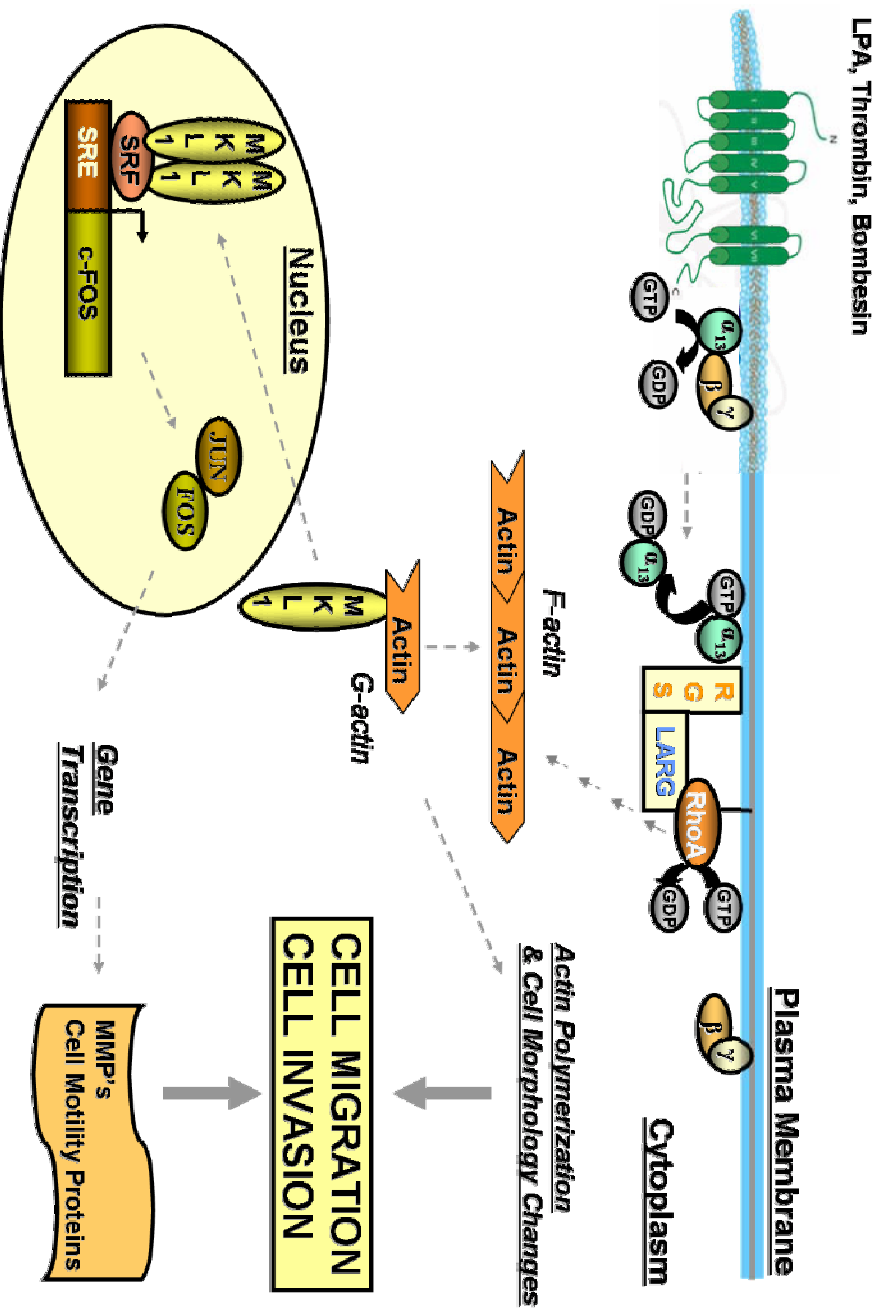


Figure 1-1. GPCR-G $\alpha_{12/13}$ -RhoA-MKLI/SRF Cellular Mechanism. A schematic of the general cellular mechanism of the RhoA transcriptional signaling pathway, included with the way the pathway contributes to tumor cell migration and invasion.

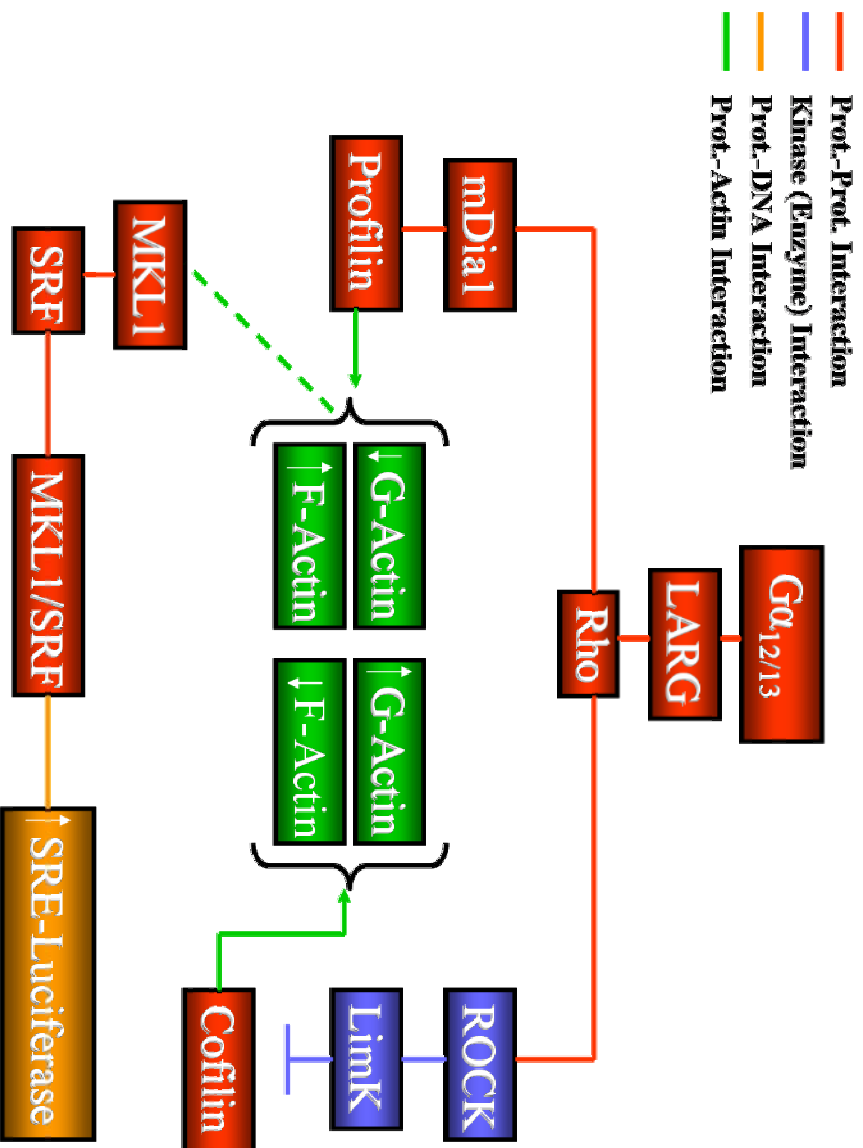


Figure 1-2. $G\alpha_{12/13}$ -RhoA Transcriptional Signaling Pathway. A schematic depicting the protein-protein and protein-DNA interactions involved in the $G\alpha_{12/13}$ -RhoA transcriptional signaling pathway that potentially can be targeted for chemical inhibition. The SRE-luciferase component represents the reporter readout utilized for the cell-based reporter high-throughput chemical screen.

References

1. Bridges, T. M. and Lindsley, C. W. G-protein-coupled receptors: from classical modes of modulation to allosteric mechanisms. *ACS Chem Biol*, 3: 530-541, 2008.
2. Gilman, A. G. G proteins: transducers of receptor-generated signals. *Annu Rev Biochem*, 56: 615-649, 1987.
3. Jensen, R. T., Battey, J. F., Spindel, E. R., and Benya, R. V. International Union of Pharmacology. LXVIII. Mammalian bombesin receptors: nomenclature, distribution, pharmacology, signaling, and functions in normal and disease states. *Pharmacol Rev*, 60: 1-42, 2008.
4. Macfarlane, S. R., Seatter, M. J., Kanke, T., Hunter, G. D., and Plevin, R. Proteinase-activated receptors. *Pharmacol Rev*, 53: 245-282, 2001.
5. Mills, G. B. and Moolenaar, W. H. The emerging role of lysophosphatidic acid in cancer. *Nat Rev Cancer*, 3: 582-591, 2003.
6. Trejo, J. Protease-activated receptors: new concepts in regulation of G protein-coupled receptor signaling and trafficking. *J Pharmacol Exp Ther*, 307: 437-442, 2003.
7. Bian, D., Mahanivong, C., Yu, J., Frisch, S. M., Pan, Z. K., Ye, R. D., and Huang, S. The G12/13-RhoA signaling pathway contributes to efficient lysophosphatidic acid-stimulated cell migration. *Oncogene*, 25: 2234-2244, 2006.
8. Bian, D., Su, S., Mahanivong, C., Cheng, R. K., Han, Q., Pan, Z. K., Sun, P., and Huang, S. Lysophosphatidic Acid Stimulates Ovarian Cancer Cell Migration via a Ras-MEK Kinase 1 Pathway. *Cancer Res*, 64: 4209-4217, 2004.
9. Chen, M., Towers, L. N., and O'Connor, K. L. LPA2 (EDG4) mediates Rho-dependent chemotaxis with lower efficacy than LPA1 (EDG2) in breast carcinoma cells. *Am J Physiol Cell Physiol*, 292: C1927-1933, 2007.
10. Hasegawa, Y., Murph, M., Yu, S., Tigyi, G., and Mills, G. B. Lysophosphatidic acid (LPA)-induced vasodilator-stimulated phosphoprotein mediates lamellipodia formation to initiate motility in PC-3 prostate cancer cells. *Mol Oncol*, 2: 54-69, 2008.
11. Hope, J. M., Wang, F. Q., Whyte, J. S., Ariztia, E. V., Abdalla, W., Long, K., and Fishman, D. A. LPA receptor 2 mediates LPA-induced endometrial cancer invasion. *Gynecol Oncol*, 112: 215-223, 2009.

12. Hwang, Y. S., Hodge, J. C., Sivapurapu, N., and Lindholm, P. F. Lysophosphatidic acid stimulates PC-3 prostate cancer cell Matrigel invasion through activation of RhoA and NF-kappaB activity. *Mol Carcinog*, *45*: 518-529, 2006.
13. Kim, M. H., Park, J. S., Chang, H. J., Baek, M. K., Kim, H. R., Shin, B. A., Ahn, B. W., and Jung, Y. D. Lysophosphatidic acid promotes cell invasion by up-regulating the urokinase-type plasminogen activator receptor in human gastric cancer cells. *J Cell Biochem*, *104*: 1102-1112, 2008.
14. Murray, D., Horgan, G., Macmathuna, P., and Doran, P. NET1-mediated RhoA activation facilitates lysophosphatidic acid-induced cell migration and invasion in gastric cancer. *Br J Cancer*, *99*: 1322-1329, 2008.
15. Raj, G. V., Sekula, J. A., Guo, R., Madden, J. F., and Daaka, Y. Lysophosphatidic acid promotes survival of androgen-insensitive prostate cancer PC3 cells via activation of NF-kappaB. *Prostate*, *61*: 105-113, 2004.
16. Sawada, K., Morishige, K., Tahara, M., Kawagishi, R., Ikebuchi, Y., Tasaka, K., and Murata, Y. Alendronate inhibits lysophosphatidic acid-induced migration of human ovarian cancer cells by attenuating the activation of rho. *Cancer Res*, *62*: 6015-6020, 2002.
17. Lee, M. J., Jeon, E. S., Lee, J. S., Cho, M., Suh, D. S., Chang, C. L., and Kim, J. H. Lysophosphatidic acid in malignant ascites stimulates migration of human mesenchymal stem cells. *J Cell Biochem*, *104*: 499-510, 2008.
18. Marinissen, M. J., Servitja, J. M., Offermanns, S., Simon, M. I., and Gutkind, J. S. Thrombin protease-activated receptor-1 signals through Gq- and G13-initiated MAPK cascades regulating c-Jun expression to induce cell transformation. *J Biol Chem*, *278*: 46814-46825, 2003.
19. Hayakawa, Y., Kurimoto, M., Nagai, S., Kurosaki, K., Tsuboi, Y., Hamada, H., Hayashi, N., and Endo, S. Thrombin-induced cell proliferation and platelet-derived growth factor-AB release from A172 human glioblastoma cells. *J Thromb Haemost*, *5*: 2219-2226, 2007.
20. Gratio, V., Walker, F., Lehy, T., Laburthe, M., and Darmoul, D. Aberrant expression of proteinase-activated receptor 4 promotes colon cancer cell proliferation through a persistent signaling that involves Src and ErbB-2 kinase. *Int J Cancer*, *124*: 1517-1525, 2009.
21. Shi, X., Gangadharan, B., Brass, L. F., Ruf, W., and Mueller, B. M. Protease-activated receptors (PAR1 and PAR2) contribute to tumor cell motility and metastasis. *Mol Cancer Res*, *2*: 395-402, 2004.

22. Kaufmann, R., Rahn, S., Pollrich, K., Hertel, J., Dittmar, Y., Hommann, M., Henklein, P., Biskup, C., Westermann, M., Hollenberg, M. D., and Settmacher, U. Thrombin-mediated hepatocellular carcinoma cell migration: cooperative action via proteinase-activated receptors 1 and 4. *J Cell Physiol*, *211*: 699-707, 2007.
23. Bergmann, S., Junker, K., Henklein, P., Hollenberg, M. D., Settmacher, U., and Kaufmann, R. PAR-type thrombin receptors in renal carcinoma cells: PAR1-mediated EGFR activation promotes cell migration. *Oncol Rep*, *15*: 889-893, 2006.
24. Loberg, R. D., Tantivejkul, K., Craig, M., Neeley, C. K., and Pienta, K. J. PAR1-mediated RhoA activation facilitates CCL2-induced chemotaxis in PC-3 cells. *J Cell Biochem*, *101*: 1292-1300, 2007.
25. Arora, P., Cuevas, B. D., Russo, A., Johnson, G. L., and Trejo, J. Persistent transactivation of EGFR and ErbB2/HER2 by protease-activated receptor-1 promotes breast carcinoma cell invasion. *Oncogene*, *27*: 4434-4445, 2008.
26. Booden, M. A., Eckert, L. B., Der, C. J., and Trejo, J. Persistent signaling by dysregulated thrombin receptor trafficking promotes breast carcinoma cell invasion. *Mol Cell Biol*, *24*: 1990-1999, 2004.
27. Kelly, P., Stemmler, L. N., Madden, J. F., Fields, T. A., Daaka, Y., and Casey, P. J. A role for the G12 family of heterotrimeric G proteins in prostate cancer invasion. *J Biol Chem*, *281*: 26483-26490, 2006.
28. Radjabi, A. R., Sawada, K., Jagadeeswaran, S., Eichbichler, A., Kenny, H. A., Montag, A., Bruno, K., and Lengyel, E. Thrombin induces tumor invasion through the induction and association of matrix metalloproteinase-9 and beta1-integrin on the cell surface. *J Biol Chem*, *283*: 2822-2834, 2008.
29. Villares, G. J., Zigler, M., Wang, H., Melnikova, V. O., Wu, H., Friedman, R., Leslie, M. C., Vivas-Mejia, P. E., Lopez-Berestein, G., Sood, A. K., and Bar-Eli, M. Targeting melanoma growth and metastasis with systemic delivery of liposome-incorporated protease-activated receptor-1 small interfering RNA. *Cancer Res*, *68*: 9078-9086, 2008.
30. Lacoste, J., Aprikian, A. G., and Chevalier, S. Focal adhesion kinase is required for bombesin-induced prostate cancer cell motility. *Mol Cell Endocrinol*, *235*: 51-61, 2005.
31. Zheng, R., Iwase, A., Shen, R., Goodman, O. B., Jr., Sugimoto, N., Takuwa, Y., Lerner, D. J., and Nanus, D. M. Neuropeptide-stimulated cell migration in prostate cancer cells is mediated by RhoA kinase signaling and inhibited by neutral endopeptidase. *Oncogene*, *25*: 5942-5952, 2006.

32. Saurin, J. C., Fallavier, M., Sordat, B., Gevrey, J. C., Chayvialle, J. A., and Abello, J. Bombesin stimulates invasion and migration of Isreco1 colon carcinoma cells in a Rho-dependent manner. *Cancer Res*, 62: 4829-4835, 2002.
33. Corral, R. S., Iniguez, M. A., Duque, J., Lopez-Perez, R., and Fresno, M. Bombesin induces cyclooxygenase-2 expression through the activation of the nuclear factor of activated T cells and enhances cell migration in Caco-2 colon carcinoma cells. *Oncogene*, 26: 958-969, 2007.
34. Kang, J., Ishola, T. A., Baregamian, N., Mourot, J. M., Rychahou, P. G., Evers, B. M., and Chung, D. H. Bombesin induces angiogenesis and neuroblastoma growth. *Cancer Lett*, 253: 273-281, 2007.
35. Kanashiro, C. A., Schally, A. V., Zarandi, M., Hammann, B. D., and Varga, J. L. Suppression of growth of H-69 small cell lung carcinoma by antagonists of growth hormone releasing hormone and bombesin is associated with an inhibition of protein kinase C signaling. *Int J Cancer*, 112: 570-576, 2004.
36. Hohla, F., Schally, A. V., Kanashiro, C. A., Buchholz, S., Baker, B., Kannadka, C., Moder, A., Aigner, E., Datz, C., and Halmos, G. Growth inhibition of non-small-cell lung carcinoma by BN/GRP antagonist is linked with suppression of K-Ras, COX-2, and pAkt. *Proc Natl Acad Sci U S A*, 104: 18671-18676, 2007.
37. Bajo, A. M., Schally, A. V., Krupa, M., Hebert, F., Groot, K., and Szepeshazi, K. Bombesin antagonists inhibit growth of MDA-MB-435 estrogen-independent breast cancers and decrease the expression of the ErbB-2/HER-2 oncoprotein and c-jun and c-fos oncogenes. *Proc Natl Acad Sci U S A*, 99: 3836-3841, 2002.
38. Stangelberger, A., Schally, A. V., Varga, J. L., Zarandi, M., Szepeshazi, K., Armatis, P., and Halmos, G. Inhibitory effect of antagonists of bombesin and growth hormone-releasing hormone on orthotopic and intraosseous growth and invasiveness of PC-3 human prostate cancer in nude mice. *Clin Cancer Res*, 11: 49-57, 2005.
39. Rossman, K. L., Der, C. J., and Sondek, J. GEF means go: turning on RHO GTPases with guanine nucleotide-exchange factors. *Nat Rev Mol Cell Biol*, 6: 167-180, 2005.
40. Kjoller, L. and Hall, A. Signaling to Rho GTPases. *Exp Cell Res*, 253: 166-179, 1999.
41. Whitehead, I. P., Zohn, I. E., and Der, C. J. Rho GTPase-dependent transformation by G protein-coupled receptors. *Oncogene*, 20: 1547-1555, 2001.
42. Schmidt, A. and Hall, A. Guanine nucleotide exchange factors for Rho GTPases: turning on the switch. *Genes Dev*, 16: 1587-1609, 2002.

43. Kourlas, P. J., Strout, M. P., Becknell, B., Veronese, M. L., Croce, C. M., Theil, K. S., Krahe, R., Ruutu, T., Knuutila, S., Bloomfield, C. D., and Caligiuri, M. A. Identification of a gene at 11q23 encoding a guanine nucleotide exchange factor: evidence for its fusion with MLL in acute myeloid leukemia. *Proc Natl Acad Sci U S A*, *97*: 2145-2150, 2000.
44. Cen, B., Selvaraj, A., Burgess, R. C., Hitzler, J. K., Ma, Z., Morris, S. W., and Prywes, R. Megakaryoblastic leukemia 1, a potent transcriptional coactivator for serum response factor (SRF), is required for serum induction of SRF target genes. *Mol Cell Biol*, *23*: 6597-6608, 2003.
45. Chai, J. and Tarnawski, A. S. Serum response factor: discovery, biochemistry, biological roles and implications for tissue injury healing. *J Physiol Pharmacol*, *53*: 147-157, 2002.
46. Miralles, F., Posern, G., Zaromytidou, A. I., and Treisman, R. Actin dynamics control SRF activity by regulation of its coactivator MAL. *Cell*, *113*: 329-342, 2003.
47. Ma, Z., Morris, S. W., Valentine, V., Li, M., Herbrick, J. A., Cui, X., Bouman, D., Li, Y., Mehta, P. K., Nizetic, D., Kaneko, Y., Chan, G. C., Chan, L. C., Squire, J., Scherer, S. W., and Hitzler, J. K. Fusion of two novel genes, RBM15 and MKL1, in the t(1;22)(p13;q13) of acute megakaryoblastic leukemia. *Nat Genet*, *28*: 220-221, 2001.
48. Vartiainen, M. K., Guettler, S., Larijani, B., and Treisman, R. Nuclear actin regulates dynamic subcellular localization and activity of the SRF cofactor MAL. *Science*, *316*: 1749-1752, 2007.
49. Baugher, P. J., Krishnamoorthy, L., Price, J. E., and Dharmawardhane, S. F. Rac1 and Rac3 isoform activation is involved in the invasive and metastatic phenotype of human breast cancer cells. *Breast Cancer Res*, *7*: R965-974, 2005.
50. Hirsch, D. S., Shen, Y., and Wu, W. J. Growth and motility inhibition of breast cancer cells by epidermal growth factor receptor degradation is correlated with inactivation of Cdc42. *Cancer Res*, *66*: 3523-3530, 2006.
51. Kwei, K. A., Finch, J. S., Ranger-Moore, J., and Bowden, G. T. The role of Rac1 in maintaining malignant phenotype of mouse skin tumor cells. *Cancer Lett*, *231*: 326-338, 2006.
52. Bektic, J., Pfeil, K., Berger, A. P., Ramoner, R., Pelzer, A., Schafer, G., Kofler, K., Bartsch, G., and Klocker, H. Small G-protein RhoE is underexpressed in prostate cancer and induces cell cycle arrest and apoptosis. *Prostate*, *64*: 332-340, 2005.

53. Carbone, A., Bernardini, L., Valenzano, F., Bottillo, I., De Simone, C., Capizzi, R., Capalbo, A., Romano, F., Novelli, A., Dallapiccola, B., and Amerio, P. Array-based comparative genomic hybridization in early-stage mycosis fungoides: recurrent deletion of tumor suppressor genes BCL7A, SMAC/DIABLO, and RHOA. *Genes Chromosomes Cancer*, *47*: 1067-1075, 2008.
54. Nguyen, Q. D., Faivre, S., Bruyneel, E., Rivat, C., Seto, M., Endo, T., Mareel, M., Emami, S., and Gespach, C. RhoA- and RhoD-dependent regulatory switch of G α subunit signaling by PAR-1 receptors in cellular invasion. *FASEB J*, *16*: 565-576, 2002.
55. Pinner, S. and Sahai, E. PDK1 regulates cancer cell motility by antagonising inhibition of ROCK1 by RhoE. *Nat Cell Biol*, *10*: 127-137, 2008.
56. Chenette, E. J., Abo, A., and Der, C. J. Critical and distinct roles of amino- and carboxyl-terminal sequences in regulation of the biological activity of the Cbp atypical Rho GTPase. *J Biol Chem*, *280*: 13784-13792, 2005.
57. Couderc, B., Pradines, A., Rafii, A., Golzio, M., Deviers, A., Allal, C., Berg, D., Penary, M., Teissie, J., and Favre, G. In vivo restoration of RhoB expression leads to ovarian tumor regression. *Cancer Gene Ther*, *15*: 456-464, 2008.
58. Jiang, K., Sun, J., Cheng, J., Djeu, J. Y., Wei, S., and Sebt, S. Akt mediates Ras downregulation of RhoB, a suppressor of transformation, invasion, and metastasis. *Mol Cell Biol*, *24*: 5565-5576, 2004.
59. Marlow, L. A., Reynolds, L. A., Cleland, A. S., Cooper, S. J., Gumz, M. L., Kurakata, S., Fujiwara, K., Zhang, Y., Sebo, T., Grant, C., McIver, B., Wadsworth, J. T., Radisky, D. C., Smallridge, R. C., and Copland, J. A. Reactivation of suppressed RhoB is a critical step for the inhibition of anaplastic thyroid cancer growth. *Cancer Res*, *69*: 1536-1544, 2009.
60. Mazieres, J., Tillement, V., Allal, C., Clanet, C., Bobin, L., Chen, Z., Sebt, S. M., Favre, G., and Pradines, A. Geranylgeranylated, but not farnesylated, RhoB suppresses Ras transformation of NIH-3T3 cells. *Exp Cell Res*, *304*: 354-364, 2005.
61. Faried, A., Nakajima, M., Sohda, M., Miyazaki, T., Kato, H., and Kuwano, H. Correlation between RhoA overexpression and tumour progression in esophageal squamous cell carcinoma. *Eur J Surg Oncol*, *31*: 410-414, 2005.
62. Li, X. R., Ji, F., Ouyang, J., Wu, W., Qian, L. Y., and Yang, K. Y. Overexpression of RhoA is associated with poor prognosis in hepatocellular carcinoma. *Eur J Surg Oncol*, *32*: 1130-1134, 2006.

63. Liu, N., Bi, F., Pan, Y., Sun, L., Xue, Y., Shi, Y., Yao, X., Zheng, Y., and Fan, D. Reversal of the malignant phenotype of gastric cancer cells by inhibition of RhoA expression and activity. *Clin Cancer Res*, *10*: 6239-6247, 2004.
64. Xiaorong, L., Wei, W., Liyuan, Q., and Kaiyan, Y. Underexpression of deleted in liver cancer 2 (DLC2) is associated with overexpression of RhoA and poor prognosis in hepatocellular carcinoma. *BMC Cancer*, *8*: 205, 2008.
65. Sun, H. W., Tong, S. L., He, J., Wang, Q., Zou, L., Ma, S. J., Tan, H. Y., Luo, J. F., and Wu, H. X. RhoA and RhoC -siRNA inhibit the proliferation and invasiveness activity of human gastric carcinoma by Rho/PI3K/Akt pathway. *World J Gastroenterol*, *13*: 3517-3522, 2007.
66. Pille, J. Y., Denoyelle, C., Varet, J., Bertrand, J. R., Soria, J., Opolon, P., Lu, H., Pritchard, L. L., Vannier, J. P., Malvy, C., Soria, C., and Li, H. Anti-RhoA and anti-RhoC siRNAs inhibit the proliferation and invasiveness of MDA-MB-231 breast cancer cells in vitro and in vivo. *Mol Ther*, *11*: 267-274, 2005.
67. Faried, A., Faried, L. S., Kimura, H., Nakajima, M., Sohda, M., Miyazaki, T., Kato, H., Usman, N., and Kuwano, H. RhoA and RhoC proteins promote both cell proliferation and cell invasion of human oesophageal squamous cell carcinoma cell lines in vitro and in vivo. *Eur J Cancer*, *42*: 1455-1465, 2006.
68. Pan, Q., Bao, L. W., Teknos, T. N., and Merajver, S. D. Targeted disruption of protein kinase C epsilon reduces cell invasion and motility through inactivation of RhoA and RhoC GTPases in head and neck squamous cell carcinoma. *Cancer Res*, *66*: 9379-9384, 2006.
69. Wang, W., Wu, F., Fang, F., Tao, Y., and Yang, L. Inhibition of invasion and metastasis of hepatocellular carcinoma cells via targeting RhoC in vitro and in vivo. *Clin Cancer Res*, *14*: 6804-6812, 2008.
70. Simpson, K. J., Dugan, A. S., and Mercurio, A. M. Functional analysis of the contribution of RhoA and RhoC GTPases to invasive breast carcinoma. *Cancer Res*, *64*: 8694-8701, 2004.
71. van Golen, K. L., Bao, L., DiVito, M. M., Wu, Z., Prendergast, G. C., and Merajver, S. D. Reversion of RhoC GTPase-induced inflammatory breast cancer phenotype by treatment with a farnesyl transferase inhibitor. *Mol Cancer Ther*, *1*: 575-583, 2002.
72. van Golen, K. L., Davies, S., Wu, Z. F., Wang, Y., Bucana, C. D., Root, H., Chandrasekharappa, S., Strawderman, M., Ethier, S. P., and Merajver, S. D. A novel putative low-affinity insulin-like growth factor-binding protein, LIBC (lost in inflammatory breast cancer), and RhoC GTPase correlate with the inflammatory breast cancer phenotype. *Clin Cancer Res*, *5*: 2511-2519, 1999.

73. van Golen, K. L., Wu, Z. F., Qiao, X. T., Bao, L. W., and Merajver, S. D. RhoC GTPase, a novel transforming oncogene for human mammary epithelial cells that partially recapitulates the inflammatory breast cancer phenotype. *Cancer Res*, *60*: 5832-5838, 2000.
74. Lo, A. C., Georgopoulos, A., Kleer, C. G., Banerjee, M., Omar, S., Khaled, H., Eissa, S., Hablas, A., Omar, H. G., Douglas, J. A., Merajver, S. D., and Soliman, A. S. Analysis of RhoC expression and lymphovascular emboli in inflammatory vs non-inflammatory breast cancers in Egyptian patients. *Breast*, *18*: 55-59, 2009.
75. Clark, E. A., Golub, T. R., Lander, E. S., and Hynes, R. O. Genomic analysis of metastasis reveals an essential role for RhoC. *Nature*, *406*: 532-535, 2000.
76. Collisson, E. A., Kleer, C., Wu, M., De, A., Gambhir, S. S., Merajver, S. D., and Kolodney, M. S. Atorvastatin prevents RhoC isoprenylation, invasion, and metastasis in human melanoma cells. *Mol Cancer Ther*, *2*: 941-948, 2003.
77. Lin, M., DiVito, M. M., Merajver, S. D., Boyanapalli, M., and van Golen, K. L. Regulation of pancreatic cancer cell migration and invasion by RhoC GTPase and caveolin-1. *Mol Cancer*, *4*: 21, 2005.
78. Hall, C. L., Dubyk, C. W., Riesenberger, T. A., Shein, D., Keller, E. T., and van Golen, K. L. Type I collagen receptor (alpha2beta1) signaling promotes prostate cancer invasion through RhoC GTPase. *Neoplasia*, *10*: 797-803, 2008.
79. Iizumi, M., Bandyopadhyay, S., Pai, S. K., Watabe, M., Hirota, S., Hosobe, S., Tsukada, T., Miura, K., Saito, K., Furuta, E., Liu, W., Xing, F., Okuda, H., Kobayashi, A., and Watabe, K. RhoC promotes metastasis via activation of the Pyk2 pathway in prostate cancer. *Cancer Res*, *68*: 7613-7620, 2008.
80. Sequeira, L., Dubyk, C. W., Riesenberger, T. A., Cooper, C. R., and van Golen, K. L. Rho GTPases in PC-3 prostate cancer cell morphology, invasion and tumor cell diapedesis. *Clin Exp Metastasis*, *25*: 569-579, 2008.
81. Yao, H., Dashner, E. J., van Golen, C. M., and van Golen, K. L. RhoC GTPase is required for PC-3 prostate cancer cell invasion but not motility. *Oncogene*, *25*: 2285-2296, 2006.
82. Ikoma, T., Takahashi, T., Nagano, S., Li, Y. M., Ohno, Y., Ando, K., Fujiwara, T., Fujiwara, H., and Kosai, K. A definitive role of RhoC in metastasis of orthotopic lung cancer in mice. *Clin Cancer Res*, *10*: 1192-1200, 2004.
83. Hakem, A., Sanchez-Sweetman, O., You-Ten, A., Duncan, G., Wakeham, A., Khokha, R., and Mak, T. W. RhoC is dispensable for embryogenesis and tumor initiation but essential for metastasis. *Genes Dev*, *19*: 1974-1979, 2005.

84. Kelly, P., Moeller, B. J., Juneja, J., Booden, M. A., Der, C. J., Daaka, Y., Dewhirst, M. W., Fields, T. A., and Casey, P. J. The G12 family of heterotrimeric G proteins promotes breast cancer invasion and metastasis. *Proc Natl Acad Sci U S A*, *103*: 8173-8178, 2006.
85. Sahai, E. and Marshall, C. J. ROCK and Dia have opposing effects on adherens junctions downstream of Rho. *Nat Cell Biol*, *4*: 408-415, 2002.
86. Zhou, J., Zhao, L. Q., Xiong, M. M., Wang, X. Q., Yang, G. R., Qiu, Z. L., Wu, M., and Liu, Z. H. Gene expression profiles at different stages of human esophageal squamous cell carcinoma. *World J Gastroenterol*, *9*: 9-15, 2003.
87. Kaneko, K., Satoh, K., Masamune, A., Satoh, A., and Shimosegawa, T. Expression of ROCK-1 in human pancreatic cancer: its down-regulation by morpholino oligo antisense can reduce the migration of pancreatic cancer cells in vitro. *Pancreas*, *24*: 251-257, 2002.
88. Wong, C. C., Wong, C. M., Tung, E. K., Man, K., and Ng, I. O. Rho-kinase 2 is frequently overexpressed in hepatocellular carcinoma and involved in tumor invasion. *Hepatology*, 2009.
89. Nakajima, M., Hayashi, K., Egi, Y., Katayama, K., Amano, Y., Uehata, M., Ohtsuki, M., Fujii, A., Oshita, K., Kataoka, H., Chiba, K., Goto, N., and Kondo, T. Effect of Wf-536, a novel ROCK inhibitor, against metastasis of B16 melanoma. *Cancer Chemother Pharmacol*, *52*: 319-324, 2003.
90. Ying, H., Biroc, S. L., Li, W. W., Alicke, B., Xuan, J. A., Pagila, R., Ohashi, Y., Okada, T., Kamata, Y., and Dinter, H. The Rho kinase inhibitor fasudil inhibits tumor progression in human and rat tumor models. *Mol Cancer Ther*, *5*: 2158-2164, 2006.
91. Sahai, E. and Marshall, C. J. Differing modes of tumour cell invasion have distinct requirements for Rho/ROCK signalling and extracellular proteolysis. *Nat Cell Biol*, *5*: 711-719, 2003.
92. Torka, R., Thuma, F., Herzog, V., and Kirfel, G. ROCK signaling mediates the adoption of different modes of migration and invasion in human mammary epithelial tumor cells. *Exp Cell Res*, *312*: 3857-3871, 2006.
93. Vishnubhotla, R., Sun, S., Huq, J., Bulic, M., Ramesh, A., Guzman, G., Cho, M., and Glover, S. C. ROCK-II mediates colon cancer invasion via regulation of MMP-2 and MMP-13 at the site of invadopodia as revealed by multiphoton imaging. *Lab Invest*, *87*: 1149-1158, 2007.
94. Xue, F., Takahara, T., Yata, Y., Xia, Q., Nonome, K., Shinno, E., Kanayama, M., Takahara, S., and Sugiyama, T. Blockade of Rho/Rho-associated coiled coil-

forming kinase signaling can prevent progression of hepatocellular carcinoma in matrix metalloproteinase-dependent manner. *Hepatol Res*, 38: 810-817, 2008.

95. Alberti, S., Krause, S. M., Kretz, O., Philippar, U., Lemberger, T., Casanova, E., Wiebel, F. F., Schwarz, H., Frotscher, M., Schutz, G., and Nordheim, A. Neuronal migration in the murine rostral migratory stream requires serum response factor. *Proc Natl Acad Sci U S A*, 102: 6148-6153, 2005.
96. Schrott, G., Philippar, U., Berger, J., Schwarz, H., Heidenreich, O., and Nordheim, A. Serum response factor is crucial for actin cytoskeletal organization and focal adhesion assembly in embryonic stem cells. *J Cell Biol*, 156: 737-750, 2002.
97. Park, M. Y., Kim, K. R., Park, H. S., Park, B. H., Choi, H. N., Jang, K. Y., Chung, M. J., Kang, M. J., Lee, D. G., and Moon, W. S. Expression of the serum response factor in hepatocellular carcinoma: implications for epithelial-mesenchymal transition. *Int J Oncol*, 31: 1309-1315, 2007.
98. Heemers, H. V., Regan, K. M., Dehm, S. M., and Tindall, D. J. Androgen induction of the androgen receptor coactivator four and a half LIM domain protein-2: evidence for a role for serum response factor in prostate cancer. *Cancer Res*, 67: 10592-10599, 2007.
99. Patten, L. C., Belaguli, N. S., Baek, M. J., Fagan, S. P., Awad, S. S., and Berger, D. H. Serum response factor is alternatively spliced in human colon cancer. *J Surg Res*, 121: 92-100, 2004.
100. Medjkane, S., Perez-Sanchez, C., Gaggioli, C., Sahai, E., and Treisman, R. Myocardin-related transcription factors and SRF are required for cytoskeletal dynamics and experimental metastasis. *Nat Cell Biol*, 11: 257-268, 2009.
101. Selvaraj, A. and Prywes, R. Expression profiling of serum inducible genes identifies a subset of SRF target genes that are MKL dependent. *BMC Mol Biol*, 5: 13, 2004.
102. Mathupala, S. P., Ko, Y. H., and Pedersen, P. L. Hexokinase II: cancer's double-edged sword acting as both facilitator and gatekeeper of malignancy when bound to mitochondria. *Oncogene*, 25: 4777-4786, 2006.
103. Vickers, E. R., Kasza, A., Kurnaz, I. A., Seifert, A., Zeef, L. A., O'Donnell, A., Hayes, A., and Sharrocks, A. D. Ternary complex factor-serum response factor complex-regulated gene activity is required for cellular proliferation and inhibition of apoptotic cell death. *Mol Cell Biol*, 24: 10340-10351, 2004.
104. Wegiel, B., Bjartell, A., Culig, Z., and Persson, J. L. Interleukin-6 activates PI3K/Akt pathway and regulates cyclin A1 to promote prostate cancer cell survival. *Int J Cancer*, 122: 1521-1529, 2008.

105. Yu, Y. P. and Luo, J. H. Myopodin-mediated suppression of prostate cancer cell migration involves interaction with zyxin. *Cancer Res*, *66*: 7414-7419, 2006.
106. Zhu, Z., Kleeff, J., Friess, H., Wang, L., Zimmermann, A., Yarden, Y., Buchler, M. W., and Korc, M. Epiregulin is Up-regulated in pancreatic cancer and stimulates pancreatic cancer cell growth. *Biochem Biophys Res Commun*, *273*: 1019-1024, 2000.
107. Zudaire, E., Martinez, A., and Cuttitta, F. Adrenomedullin and cancer. *Regul Pept*, *112*: 175-183, 2003.
108. Wu, M., Wu, Z. F., Kumar-Sinha, C., Chinnaiyan, A., and Merajver, S. D. RhoC induces differential expression of genes involved in invasion and metastasis in MCF10A breast cells. *Breast Cancer Res Treat*, *84*: 3-12, 2004.
109. Peterson, Y. K., Kelly, P., Weinbaum, C. A., and Casey, P. J. A novel protein geranylgeranyltransferase-I inhibitor with high potency, selectivity, and cellular activity. *J Biol Chem*, *281*: 12445-12450, 2006.
110. Lawler, K., Foran, E., O'Sullivan, G., Long, A., and Kenny, D. Mobility and invasiveness of metastatic esophageal cancer are potentiated by shear stress in a ROCK- and Ras-dependent manner. *Am J Physiol Cell Physiol*, *291*: C668-677, 2006.
111. Evelyn, C. R., Wade, S. M., Wang, Q., Wu, M., Iniguez-Lluhi, J. A., Merajver, S. D., and Neubig, R. R. CCG-1423: a small-molecule inhibitor of RhoA transcriptional signaling. *Mol Cancer Ther*, *6*: 2249-2260, 2007.
112. Desire, L., Bourdin, J., Loiseau, N., Peillon, H., Picard, V., De Oliveira, C., Bachelot, F., Leblond, B., Taverne, T., Beausoleil, E., Lacombe, S., Drouin, D., and Schweighoffer, F. RAC1 inhibition targets amyloid precursor protein processing by gamma-secretase and decreases Abeta production in vitro and in vivo. *J Biol Chem*, *280*: 37516-37525, 2005.
113. Gao, Y., Dickerson, J. B., Guo, F., Zheng, J., and Zheng, Y. Rational design and characterization of a Rac GTPase-specific small molecule inhibitor. *Proc Natl Acad Sci U S A*, *101*: 7618-7623, 2004.
114. Shutes, A., Onesto, C., Picard, V., Leblond, B., Schweighoffer, F., and Der, C. J. Specificity and mechanism of action of EHT 1864, a novel small molecule inhibitor of Rac family small GTPases. *J Biol Chem*, *282*: 35666-35678, 2007.

CHAPTER II

CCG-1423: A SMALL-MOLECULE INHIBITOR OF RHOA TRANSCRIPTIONAL SIGNALING

Abstract

Lysophosphatidic acid receptors stimulate a $G\alpha_{12/13}$ /RhoA-dependent gene transcription program involving the serum response factor (SRF) and its co-activator and oncogene, megakaryoblastic leukemia 1 (MKL1). Inhibitors of this pathway could serve as useful biological probes and potential cancer therapeutic agents. Through a transcription-based high-throughput serum response element-luciferase screening assay, we identified two small-molecule inhibitors of this pathway. Mechanistic studies on the more potent CCG-1423 show that it acts downstream of Rho because it blocks SRE.L-driven transcription stimulated by $G\alpha_{12}Q231L$, $G\alpha_{13}Q226L$, RhoA-G14V, and RhoC-G14V. The ability of CCG-1423 to block transcription activated by MKL1, but not that induced by SRF-VP16 or GAL4-VP16, suggests a mechanism targeting MKL/SRF-dependent transcriptional activation that does not involve alterations in DNA binding. Consistent with its role as a Rho/SRF pathway inhibitor, CCG-1423 displays activity in several *in vitro* cancer cell functional assays. CCG-1423 potently ($<1 \mu\text{mol/L}$) inhibits lysophosphatidic acid-induced DNA synthesis in PC-3 prostate cancer cells, and whereas it inhibits the growth of RhoC-overexpressing melanoma lines (A375M2 and SK-Mel-147) at nanomolar concentrations, it is less active on related lines (A375 and SK-Mel-28) that express lower

levels of Rho. Similarly, CCG-1423 selectively stimulates apoptosis of the metastasis-prone, RhoC-overexpressing melanoma cell line (A375M2) compared with the parental cell line (A375). CCG-1423 inhibited Rho-dependent invasion by PC-3 prostate cancer cells, whereas it did not affect the $G\alpha_i$ -dependent invasion by the SKOV-3 ovarian cancer cell line. Thus, based on its profile, CCG-1423 is a promising lead compound for the development of novel pharmacologic tools to disrupt transcriptional responses of the Rho pathway in cancer.

Introduction

Cancer metastasis is a significant medical problem responsible for thousands of deaths every year (1). Metastases arise when dysregulation of one or more cellular processes allows malignant cells to escape the confines of the tissue of origin and establish themselves in alternate sites. These processes include cell adhesion, migration, invasion, extravasation, survival, and proliferation (1). Multiple members of the Rho family of small GTPases play important roles in these cellular processes and in some human tumors (e.g., colon, esophageal, lung, pancreatic, and inflammatory breast cancers), up-regulation of RhoA or RhoC is associated with a poor clinical outcome (2, 3).

Rho GTPases are best known for their effects on the actin cytoskeleton. The three main Rho GTPase subfamilies, RhoA, Rac, and Cdc42, control stress fiber formation, lamellipodia, and filopodia (4), respectively, which are structures important for cell motility. Rac and Cdc42 have been implicated in tumor growth, migration, and invasion in both mouse skin and human breast tumors (5-7). Within the RhoA family (RhoA,

RhoB, RhoC, etc.), there is evidence for involvement of both RhoA and RhoC in cancer, with the latter being clearly implicated in multiple malignancies. RhoC is essential for inflammatory breast cancer cell growth, invasion, and survival (8, 9) and more recently was found to be critical for invasion by PC-3 prostate cancer cells (10). Similarly, RhoC is critical for *in vivo* metastasis of polyoma T antigen–induced mammary tumors (11). Clearly, the RhoA family GTPases play important roles in multiple cellular processes central to tumor growth and metastasis.

Heterotrimeric G protein–coupled receptors (GPCR), especially those activating the $G\alpha_{12/13}$ family of $G\alpha$ subunits, are upstream regulators of the Rho pathway and are also implicated in metastasis. Lysophosphatidic acid (LPA), thrombin, and bombesin, acting on their respective GPCRs, stimulate Rho signaling and migration of various cancer cell lines (12-14). A family of three rhoGEFs containing a regulator of G protein signaling homology (RH) domain serves to couple receptors and $G\alpha_{12/13}$ subunits to RhoA (15). The three RH domain-containing RhoGEFs are p115RhoGEF, PDZ-RhoGEF, and leukemia-associated RhoGEF (LARG). The latter was initially found as a fusion to the mixed lineage leukemia gene in a patient with acute myelogenous leukemia (16). Binding of activated $G\alpha$ subunits (i.e., $G\alpha_{12}$ and $G\alpha_{13}$) to the RH domain of the RhoGEF stimulates the DH-PH domain-mediated guanine nucleotide exchange on the small GTPase RhoA, leading to its activation (17-19). Another G protein–activated RhoGEF, p63-RhoGEF, is activated by $G\alpha_q$ but does not contain an RH domain (20). Furthermore, the downstream Rho effector Rho-associated coiled coil–forming protein kinase (ROCK) is implicated in migration and invasion of cancer cells (21). Thus,

$G\alpha_{12/13}$ -coupled receptors can stimulate activation of RhoA as well as downstream cellular processes involved in cancer metastasis.

In addition to its established effects on motility, RhoA-dependent actin polymerization in response to activation of $G\alpha_{12/13}$ -coupled GPCRs leads to changes in gene expression. The loss of free G-actin resulting from actin polymerization leads to its dissociation from the transcriptional co-activator megakaryoblastic leukemia 1 (MKL1), which then translocates into the nucleus where it collaborates with serum response factor (SRF) to induce gene expression (22, 23). SRF participates in many cellular processes, including cell growth and differentiation, apoptosis, and angiogenesis (24, 25). Although the role of gene transcription in Rho-related cancer biology is poorly understood, both RhoA and RhoC regulate genes important for cell growth and proliferation, such as c-fos and cyclin D1 (24, 26). RhoC overexpression has been linked to vascular endothelial growth factor-C, CXCL1 chemokine, and fibronectin up-regulation, which are important for angiogenesis and formation of the extracellular matrix (26). In addition, several serum-stimulated genes shown to be MKL1-dependent have been implicated in cancer, including SRF itself, adrenomedullin, epiregulin, interleukin-6, hexokinase 2, and zyxin (27). These MKL1-dependent genes participate in various cancer-linked processes, including cell growth, migration, invasion, and survival (24, 25, 28-32). Thus, alterations in gene expression are likely to be an integral part of Rho effects on cancer metastasis.

Currently, there are relatively few drugs or pharmacologic tools that target Rho GTPase family signaling pathways. Much of the effort to date has focused on inhibiting the COOH-terminal isoprenylation of the Rho GTPases. This lipid modification is necessary for membrane localization and function of the activated Rho proteins. The

most widely used inhibitors of this modification include farnesyltransferase and geranylgeranyltransferase inhibitors and the cholesterol-lowering statin drugs (33). However, these compounds are not specific for the Rho family of small GTPases so their effects are difficult to interpret mechanistically. There have also been significant efforts aimed at inhibiting the Rho effector molecule ROCK. The ROCK inhibitors Y-27632 and Wf-536 have shown promising anti-metastatic activity both *in vitro* and *in vivo* (34-36). To date, the only specific and direct inhibitor of Rho GTPases is the Rac1 inhibitor NSC23766 (37). Although it is relatively specific, it is not very potent (IC_{50} , $\sim 50 \mu\text{mol/L}$). Thus, there is a clear need and opportunity for specific inhibitors of Rho GTPase signaling pathways.

In this study, we took advantage of a modified serum response element (SRE)-luciferase reporter to undertake a high-throughput screen aiming to identify novel small molecule inhibitors of the RhoA family signaling pathway. We chose to use a firefly luciferase expression vector driven by a mutant SRE (SRE.L) lacking the ternary complex factor binding sites because this construct is a selective probe of RhoA-induced gene transcription (38). We initiated Rho pathway signaling through the upstream signals $G\alpha_{13}$ and LARG so that inhibition at any step from $G\alpha_{13}$ to the SRE could be detected. By this approach, we identified two novel and structurally similar small-molecule inhibitors of RhoA-stimulated transcription. Mechanistic analysis showed that the more potent compound (CCG-1423) elicits its effects downstream of RhoA and actin polymerization by a mechanism targeting MKL/SRF-dependent transcriptional activation. Interestingly, we find that CCG-1423 inhibits LPA receptor-stimulated DNA synthesis, cell growth, cell survival, and Matrigel invasion for several cancer cell lines.

Materials and Methods

Plasmids and Reagents

The Rho-responsive SRE.L-luciferase reporter construct and myc-tagged human LARG expression plasmid were described previously (38). The p(GAL4)₂-Luc luciferase reporter was generated by ligation of a 50-bp double-stranded oligonucleotide bearing two idealized GAL4 sites into the BamHI and BglII sites of pDODLO2 (39). Control expression vectors driving *Renilla* luciferase from different promoters, pRL-cytomegalovirus and pRL-thymidine kinase (TK), were from Promega. Human G α_{12} Q231L, G α_{13} Q226L, RhoA-G14V, and RhoC-G14V expression plasmids were from the UMR cDNA Resource Center. Expression plasmids for MKL1 (40), SRF-VP16 (41), GAL4-MKL1 (amino acids 601 – 931; (22), and C3 exotoxin (42) were kindly provided by Dr. Michael Parmacek (University of Pennsylvania, Philadelphia, PA), Dr. Li Li (Wayne State University, Detroit, MI), Dr. Ron Prywes (Columbia University, New York, NY), and Dr. John Williams (University of Michigan, Ann Arbor, MI), respectively. The cytomegalovirus-driven NH₂-terminally HA-tagged GAL4-VP16 expression vector was generated by sub-cloning the coding sequence from a Rous sarcoma virus-driven version (43) into pcDNA3.1. The pcDNA3.1-zeo expression plasmid and mouse laminin were from Invitrogen. The marine toxin latrunculin B as well as daunorubicin, LPA, Igepal, anti-mouse IgG peroxidase conjugate, and anti-rabbit IgG peroxidase conjugate were from Sigma. Pertussis toxin (PTX) was from List Biological Laboratories, Inc. BD BioCoat Matrigel invasion chambers (8 μ m) were from Becton Dickinson. 5-Bromo-2'-deoxyuridine (BrdUrd), anti-BrdUrd-peroxidase, BM blue peroxidase substrate, and cell proliferation reagent WST-1 were from Roche Diagnostics.

The caspase-3 fluorescent peptide substrate, rhodamine 110, bis-N-CBZ-L-aspartyl-L-glutamyl-L-valyl-L-aspartic acid amide was from Biotium. The chemical compounds CCG-977 [N1-(4-([3,5-di(trifluoromethyl)anilino]sulfonyl)-phenyl)-4-chlorobenzamide] and CCG-1423 [N-[2-(4-chloroanilino)-1-methyl-2-oxoethoxy]-3,5-bis(trifluoromethyl)benzamide] were from Maybridge. A plasmid expressing ROCK kinase (p160ROCK-dN3) from a CMV promoter in the pCAG vector was kindly provided by Dr. S. Narumiya (Kyoto University). ROCK-2 kinase and its biotinylated peptide substrate and detecting antibody were purchased as elements of the HTScan ROCK-2 kinase assay kit from Cell Signaling Technologies (Danvers, MA). Lumavidin beads were purchased from Luminex Corp. (Austin, TX). R-phycoerythrin-labelled Goat Anti-Rabbit antibody was purchased from Invitrogen (Carlsbad, CA). The HEK293T, PC-3, SKOV-3, and A375M2 cell lines were kind gifts from Drs. J. Menon, Kenneth Pienta, and Kathleen Cho (University of Michigan) and Dr. Richard Hynes (Massachusetts Institute of Technology, Cambridge, MA). The A375, WI-38, and SW962 cell lines were obtained from the American Type Culture Collection. The SK-Mel-28 and SK-Mel-147 cell lines were obtained from Dr. Sofia Merajver (University of Michigan) and have been described previously (44, 45).

Cell Culture, Transfections, and Dual-Luciferase Assay

Cell lines were normally maintained in DMEM containing 10% fetal bovine serum (FBS), 100 units/mL penicillin, and 100 µg/mL streptomycin at 37°C in 5% CO₂. HEK293T or PC-3 cells were seeded into 96-well plates (3 x 10⁴ to 4 x 10⁴ per well) approximately 24 hr before transfection. Cells were transiently transfected by incubation

with the indicated amounts of DNA plasmids plus 1 μ L of LipofectAMINE 2000 (Invitrogen) per μ g of DNA in antibiotic-free culture medium. For dual-luciferase measurements, various activator plasmids (i.e., $G\alpha_{12}Q231L$, $G\alpha_{13}Q226L$, RhoA-G14V, RhoC-G14V, MKL1, SRF-VP16, GAL4-VP16, and GAL4-MKL1) were included along with the SRE.L or p(GAL4)2-Luc luciferase reporter and PRL-TK or PRL cytomegalovirus *Renilla* control plasmids. The total amount of DNA was kept constant by inclusion of the appropriate amount of pcDNA3.1. Transfection efficiencies determined with pcDNA3.1-eGFP were approximately 90% to 100% and 30% to 50% for HEK293T and PC-3 cells, respectively. Five to 6 hr after transfection, the transfection mixture was removed and cells were starved overnight in DMEM containing 0.5% FBS and 1% penicillin-streptomycin. Firefly and *Renilla* luciferase activities were determined 18 to 19 h later using the dual-luciferase assay kit (Promega) according to the manufacturer's instructions. Luminescence was read on a Victor² plate reader with dual injectors (Perkin-Elmer). In the site of action studies, firefly luciferase activity was normalized to *Renilla* luciferase activity. For testing chemical compounds, 1 μ L of compound or DMSO was added to the cells (final concentration, 1% DMSO) at the beginning of the serum starvation step.

High-throughput SRE.L Luciferase Screen

HEK293T cells (6×10^6 per dish) were seeded into 10-cm dishes 24 h before transfection. Cells were co-transfected with 5 ng of $G\alpha_{13}Q226L$ and 150 ng of LARG expression plasmids, and 3 μ g of the SRE.L reporter plasmid. Two thousand chemical compounds (Maybridge) were pre-spotted onto white 96-well Costar tissue culture plates (Corning)

in 1 μ L DMSO (final concentration of compounds, 10 μ mol/L) using a Biomek FX Workstation (Beckman Coulter). Cells were trypsinized 5 to 6 hr after transfection and transferred to the compound-containing assay plates (3×10^4 per well) in 100 μ L DMEM containing 0.5% FBS and 1% penicillin-streptomycin. After an additional 18 to 19 h of incubation, the robotic workstation was used to remove 70 μ L of medium from each well and to add 30 μ L of Steady-Glo reagent (Promega). Plates were incubated for 30 min at room temperature with rocking and luminescence was read for 1 s/well on the Victor² plate reader. The statistical Z' factor (46, 47) for high-throughput assays was calculated by using the following formula: $Z' = 1 - [(3\sigma_{c+} + 3\sigma_{c-}) / |\mu_{c+} - \mu_{c-}|]$ (σ = SD, μ = mean, $c+$ = latrunculin B, and $c-$ = DMSO-negative control).

Stress Fiber Formation

NIH-3T3 mouse fibroblast cells (5.0×10^5 per well) were plated onto coverslips in six well plates. After attachment, cells were starved overnight in serum-free DMEM (0% calf serum). Cells were pre-treated with compounds for 1 hr before the addition of LPA (30 μ mol/L) or calf serum (10%). On addition of the stimuli, the cells were incubated for an additional 1 hr. Wells were then washed with PBS and fixed for 15 min with 4% paraformaldehyde. Cells were then washed again with PBS and then lysed in buffer containing 0.3% Triton X-100 in PBS for 15 min. After washing in buffer containing 0.5% Igepal in PBS, cells were incubated for 1 h with rhodamine-phalloidin (1:200) stain in PBS containing 0.5% Igepal and 1% bovine serum albumin. Cells were then washed twice in 0.5% Igepal in PBS and then mounted onto slides with Gel Mount antifade

solution (Biomeda). Cell images were obtained with an Olympus FluoView 500 microscope with a 60x oil objective.

DNA Synthesis

PC-3 human prostate cancer cells (1.2×10^4 per well) were plated onto 96-well plates coated with laminin. After attachment, cells were serum-starved overnight in serum-free (0% FBS) DMEM and treated with LPA (100 $\mu\text{mol/L}$) or FBS (10%) for 27 hr. BrdUrd (10 $\mu\text{mol/L}$ final) was added to the wells during the final 4.5 h of the incubation. Wells were then washed with PBS and fixed for 20 min with 100 μL of 70% ethanol in 2.3 mol/L HCl. After washing with 10% FCS in PBS, cells were incubated for 1 hr at room temperature with anti-BrdUrd-peroxidase. Wells were washed with PBS and then BM blue peroxidase substrate was added, and after 30 min, the reaction was stopped by the addition of 2 N H_2SO_4 . The absorbance was read at 450 nm using a Victor² plate reader. To determine cell viability, the tetrazolium salt WST-1 was added to the wells during the last 1 h of incubation with BrdUrd. The mitochondrial metabolite of WST-1 cleavage was detected spectrophotometrically at 450 nm just before washing and fixing the cells for BrdUrd measurements.

Cell Growth

Cells in normal culture medium were plated (2,000 per well) in a 96-well plate coated with laminin. After attachment, the medium was replaced with serum-free medium (0% FBS) with 30 $\mu\text{mol/L}$ LPA with or without 300 nmol/L CCG-1423. Fresh LPA with or without CCG-1423 was added at day 5 to ensure that LPA and compound were present

throughout the experiment. On day 8, WST-1 reagent was added to the wells for 1 hr and absorbance at 450 nm was read using a Victor² plate reader.

Caspase-3 Activity

Cells in normal culture medium were plated (2×10^4 per well) in a black 96-well plate coated with laminin. After overnight attachment, the medium in the wells was replaced with serum-free DMEM (0% FBS) with CCG-1423 or daunorubicin for 25 h. An equal volume of 2x reaction buffer [20 mmol/L PIPES (pH 7.4), 2 mmol/L EDTA, 0.2% CHAPS, 10 mmol/L DTT] containing 50 μ mol/L of the fluorogenic caspase-3 substrate Z-DEVD-R110 was then added. After an additional 90 min of incubation at 37°C, fluorescence was measured in a Victor² plate reader using excitation at 485 nm and emission detection at 520 nm.

Matrigel Cell Invasion

PC-3 or SKOV-3 cells (5×10^4) were transferred to 24-well Matrigel inserts in serum-free medium with or without CCG-1423. Serum-free medium (0% FBS) with or without 30 μ mol/L LPA as chemoattractant was added to the lower well, and the invasion chambers were returned to the incubator for 24 hr. Inserts were fixed in methanol for 10 min and then stained 30 min with 0.5% crystal violet in 20% methanol. After wiping the top surface of the filter to remove non-invaded cells, the number of remaining cells was determined by counting four non-overlapping 20x fields. For PTX experiments, cells were treated with 100 ng/mL PTX overnight before being transferred to the Matrigel inserts and 100 ng/mL PTX was maintained in the medium.

Effect of Y-27632 on SRE-Luciferase

HEK293T cells were transiently transfected with the SRE.L Luciferase reporter and CMV-*Renilla* reporter along with an expression vector for either the constitutively active G α ₁₃ QL mutant or ROCK kinase using Lipofectamine 2000 at a ratio of 4 μ l Lipofectamine per μ g DNA. Six hours after transfection, the medium was replaced with low serum (0.5% FBS) DMEM and the transfected cells were incubated overnight with various concentrations of the Rho kinase inhibitor Y-27632. Expression of firefly and *Renilla* luciferase was measured as described in the accompanying paper and data are expressed as % of the control Firefly/*Renilla* ratio without Y-27632. Data are mean \pm SEM of triplicate determinations.

Effect of CCG-1423 on Rho kinase activity

Biotinylated ROCK-2 peptide substrate (10 nM) was bound to Lumavidin beads, washed three times in PBS then re-suspended in kinase assay buffer. Beads were diluted into samples containing the indicated concentrations of CCG-1423 then ROCK-2 enzyme (50 ng) was added to each sample and incubated for 10 minutes at RT. Primary antibody (1:4000) was added and samples were incubated for 60 minutes at room temperature. Then R-phycoerythrin-labelled secondary (1:2000) antibody was added and incubations continued for an additional 30 minutes. Bound secondary antibody was quantitated on a Luminex 200 instrument and expressed as median fluorescence intensity (MFI). Values without added kinase were nearly undetectable. Data are mean \pm SEM of triplicate determinations from one experiment repeated three times with similar results.

Results

Rho-Dependent SRE.L Luciferase Regulation

To assess the suitability of the mutant SRE.L luciferase reporter (which lacks the ternary complex factor-binding sites present in the normal SRE) as a high-throughput assay for inhibitors of GPCR-regulated Rho-dependent pathways (Fig. 2-1A), we tested a series of Rho pathway activators beginning with $G\alpha_{13}$ and LARG. As shown in Fig. 2-1B, co-transfection of HEK293T cells with expression vectors for the constitutively active mutant $G\alpha$ subunit $G\alpha_{13}Q226L$ together with LARG activates the SRE.L-driven reporter synergistically (i.e., 1.6-fold above the sum of the independent stimulation by $G\alpha_{13}Q226L$ and LARG). In Fig. 2-1C, effective stimulation is also observed for a constitutively active $G\alpha_{12}$ guanine nucleotide-binding protein, $G\alpha_{12}Q231L$, as well as the active Rho GTPases RhoA-G14V and RhoC-G14V. In addition, the SRE.L-driven reporter can be directly stimulated by expression of either the SRF coactivator MKL1 or the chimeric activator SRF-VP16 in which the potent VP16 viral transactivation domain is fused to full-length SRF (Fig. 2-1C). Thus, the pathway can be activated using signals either upstream ($G\alpha_{13}$ and/or LARG) or downstream (MKL1 or SRF-VP16) of RhoA and RhoC. As shown in the signaling pathway diagram (Fig. 2-1A), Rho-mediated SRE.L luciferase stimulation is dependent on actin polymerization and the ensuing monomeric G-actin depletion. Therefore, we examined the effect of the marine toxin latrunculin B, which binds to G-actin and inhibits actin polymerization, for its ability to inhibit $G\alpha_{13}Q226L$ -stimulated SRE.L-driven luciferase expression. As shown in Fig. 2-1D, 0.5 $\mu\text{mol/L}$ latrunculin B completely abrogates the $G\alpha_{13}Q226L$ stimulation, confirming that our SRE.L system is indeed dependent on actin polymerization. Lastly, to ensure that the

SRE.L reporter response is Rho-dependent, we co-transfected cells with expression vectors for both $G\alpha_{13}Q226L$ and the *Clostridium botulinum* exotoxin C3. ADP-ribosylation of Rho by the C3 exotoxin results in Rho inactivation. $G\alpha_{13}Q226L$ -stimulated SRE.L luciferase expression is nearly abolished by the C3 exotoxin (Fig. 2-1D), showing the Rho dependence of the response.

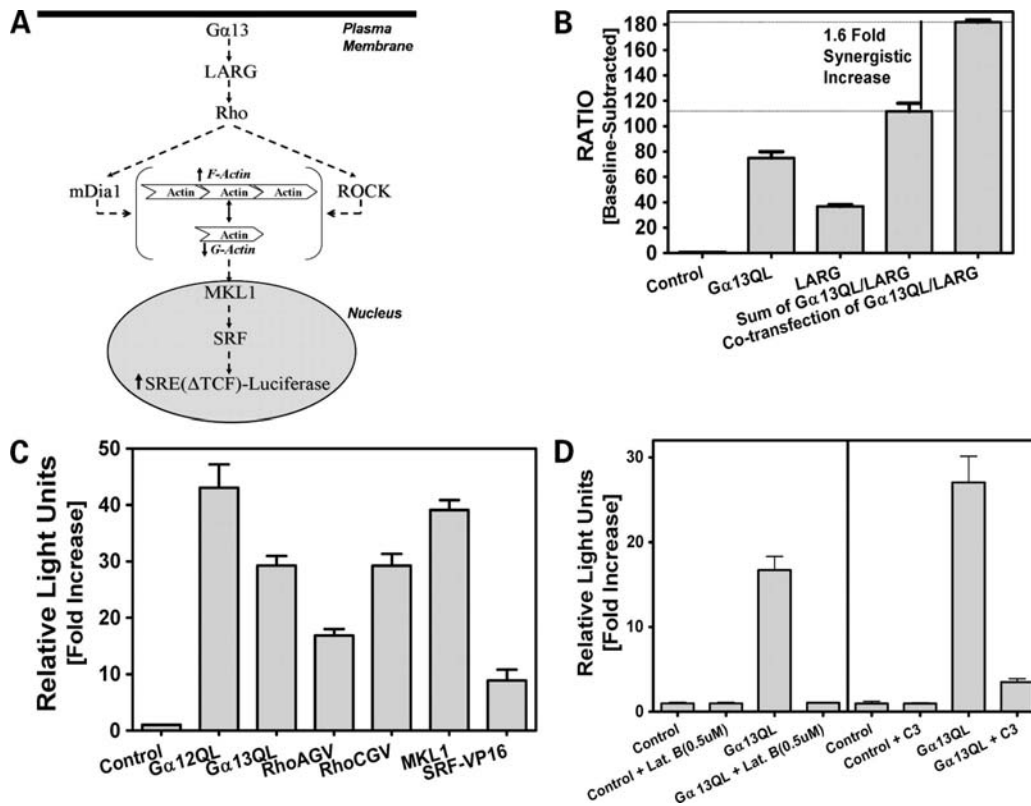


Figure 2-1. Characterization of the SRE.L system in HEK293T cells. A) $G\alpha_{13}$ activates the rhoGEF LARG, which activates Rho. This leads to actin polymerization through mDia1 and ROCK. On actin polymerization, the co-activator MKL1 is released from actin and translocates into the nucleus. There, MKL1 interacts with the transcription factor SRF and the complex activates the SRE(Δ TCF) response element, leading to luciferase expression. B) $G\alpha_{13}Q226L$ and LARG synergistically stimulate SRE.L-mediated transcription. HEK293T cells were co-transfected with 0.5 ng of $G\alpha_{13}Q226L$ and/or 0.2 ng of LARG expression plasmids along with 30 ng of SRE.L and 3 ng of PRL-TK reporter plasmids. *Dotted line*, sum of luciferase activities for $G\alpha_{13}$ and LARG expressed individually. Co-transfection produces a 1.6-fold synergistic activation. C) Constitutively active mutants of several activators stimulate SRE.L expression. Plasmids for constitutive activators (0.1 ng of $G\alpha_{12}Q231L$ and $G\alpha_{13}Q226L$, 10 ng of RhoA-G14V and RhoC-G14V, and 1 ng SRF-VP16) or for wild-type MKL1 (3 ng) were individually co-transfected with 15 ng of SRE.L reporter plasmid. D) The actin polymerization inhibitor latrunculin B and the Rho inactivator C3-exotoxin inhibit $G\alpha_{13}Q226L$ -stimulated SRE.L-driven luciferase expression. Cells were co-transfected with 0.3 ng of the $G\alpha_{13}Q226L$ expression plasmid and 15 ng of the SRE.L reporter plasmid with or without 50 ng of the C3 expression plasmid. At the beginning of serum starvation, cells were treated with 0.5 μ mol/L latrunculin B or 1% DMSO for 18 to 19 h and harvested as described in Materials and Methods. The pcDNA3.1-zeo plasmid was used as carrier DNA in all experiments, which were done in triplicate. Data from B were baseline-subtracted and normalized to the *Renilla* internal control and expressed as a ratio of

Figure 2-1.(continued) firefly to *Renilla* luciferase activities. Data from C and D are expressed as fold-increase above baseline. Data in B, C, and D were measured in triplicate and are representative data of $n = 3$. The raw firefly luciferase counts (in thousands) for the *left half of the graph* in D were 200 ± 40 and $3,300 \pm 600$ for control and $G\alpha_{13}Q226L$, respectively. The raw firefly luciferase counts (in thousands) for the *right half of the graph* in D were 18 ± 8 and 492 ± 97 for control and $G\alpha_{13}Q226L$, respectively.

High-Throughput Screen for Rho Pathway Inhibitors

To identify novel chemical inhibitors of the RhoA pathway, we first adapted the SRE.L luciferase assay to a high-throughput format using 293T cells co-expressing G α_{13} Q226L and LARG. Statistical analysis to determine the robustness and reproducibility of the assay for high-throughput screening yielded a Z' factor of 0.7 (see Materials and Methods), which indicates that it is well suited for our purposes. Using this assay, we screened a 2,000-compound subset of the Maybridge diverse chemical compound collection. The results of the screen are summarized in Fig. 2-2A. Applying a stringent cutoff of >75% inhibition and using the actin polymerization inhibitor latrunculin B as a positive control, we obtained 39 candidates. We used the dual-luciferase format (see Materials and Methods) as a follow-up assay to confirm the initial results and to test for nonspecific cellular toxicity or general transcriptional inhibition. Of the original 39 hits, we confirmed inhibition of the SRE.L luciferase expression for 18 compounds. Of these, 13 also inhibited cytomegalovirus *Renilla* luciferase expression, suggesting a generalized transcriptional inhibition or nonspecific cellular toxicity. This yielded five confirmed hits, of which four were available for resupply from Maybridge. A common problem in high-throughput, luciferase-based inhibitor screens is the potential for the recovery of direct luciferase enzyme inhibitors. Of the four compounds isolated in the screen, two inhibited firefly luciferase in cell lysates, indicating that they inhibited the reporter enzyme directly rather than its cellular expression. Thus, out of 2,000 compounds screened, we identified 2 lead compounds, CCG-977 and CCG-1423, as specific inhibitors of the RhoA pathway based on our criteria. Strikingly, these compounds share substantial structural similarity because they contain identical R₁ (3,5-

bis-trifluoromethylphenyl) and R₂ (p-chlorophenyl) groups connected by distinct linkers. CCG-977 has an aromatic linker with eight atoms separating the two R-groups, whereas CCG-1423 has an aliphatic linker with six atoms between R₁ and R₂ (Fig. 2-2B).

CCG-977 and CCG-1423 Inhibit Rho Pathway-Induced Transcription

To further assess whether CCG-977 and CCG-1423 selectively inhibit transcription induced by the Rho pathway, we examined the effect of these compounds on Gα₁₃Q226L-stimulated firefly luciferase expression driven by the SRE.L response element and *Renilla* expression from the constitutively active TK promoter in PC-3 prostate cancer cells. Both compounds inhibited SRE.L luciferase expression with IC₅₀ values of 1 to 5 μmol/L while only modestly inhibiting TK-driven *Renilla* expression (Fig. 2-3A and 2-3B). The extent of inhibition of *Renilla* expression correlated with inhibition of cell viability as detected by WST-1 absorbance (data not shown). Similar to the effect of CCG-977 and CCG-1423, latrunculin B potently inhibited the luciferase signal and also showed a modest effect on the TK *Renilla* signal at the highest concentrations (Fig. 2-3C). In contrast, the general inhibitor of transcription 5,6-

A	Total # of Compounds Screened	2000
	Hits from Primary Screen (Steady-Glo Luciferase Assay)	39 (2%)
	Secondary Screen/Dose Response (Dual Flash Luciferase Assay)	21 – Didn't inhibit SRE-Luciferase 13 – Inhibited Renilla 5 – Confirmed hits (0.25%)
	Available for Re-Supply	4 (0.2%)
	Direct inhibition of Firefly Luciferase	2 – Direct inhibitors of Firefly Luciferase 2 – True Positives (0.1%)

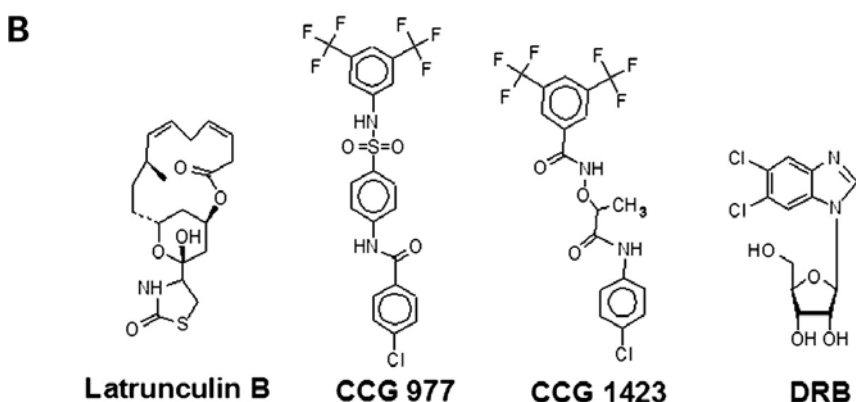


Figure 2-2. Summary of high-throughput screening results and chemical structures.

A) Two-thousand chemical compounds from the Maybridge Diverse Chemical Library collection were screened using the SRE.L assay as described in Materials and Methods. Thirty-nine compounds inhibited the SRE.L response by greater than or equal to 75%. Five of the 39 compounds selectively inhibited firefly luciferase but not cytomegalovirus *Renilla* luciferase expression. Four compounds were available for resupply from Maybridge and two did not directly inhibit firefly luciferase activity. All studies were done in HEK293T cells. B) The actin polymerization inhibitor latrunculin B was our positive control for the screen. Structures of CCG-977 and CCG-1423, the two lead compounds that came out of the screen. The kinase inhibitor 5,6-dichlorobenzimidazole-1- β -D-ribofuranoside (*DRB*) is a general transcription inhibitor.

dichlorobenzimidazole-1- β -D-ribofuranoside, which functions as an inhibitor of casein-2 kinase and RNA polymerase activity, inhibited firefly and *Renilla* luciferase expression equally (Fig. 2-3D). Thus, CCG-1423 and CCG-977 have selective effects on SRF-mediated transcription activated by Rho pathway signaling in comparison with TK promoter-mediated transcription.

CCG-1423 Inhibits Downstream of Rho

To determine the site of action of CCG-1423, we activated the Rho signaling pathway in PC-3 cells at multiple steps. CCG-1423 (10 μ mol/L) inhibited SRE.L activation by heterotrimeric G-proteins ($G\alpha_{12}Q231L$ and $G\alpha_{13}Q226L$; Fig. 2-4A). Control experiments testing the effect of CCG-1423 on activator protein expression (e.g., LARG, RhoA, and MKL1) could not be interpreted as we were unable to detect the expression of the tagged proteins in PC-3 cells by Western blots with concentrations of plasmids relevant to the luciferase assay. This result indicates that the inhibitor is not specific for $G\alpha_{13}$ because $G\alpha_{12}$ signals are also affected. Notably, CCG-1423 does not seem to interfere with Rho activation per se (by targeting LARG for example) because acute treatment with CCG-1423 did not inhibit LPA- or serum-stimulated stress fiber formation in NIH-3T3 mouse fibroblasts (Fig. 2-4B). The effects of CCG-1423 on serum- and LPA-induced stress fibers were minimal. There were some LPA-stimulated cells showing a change in the morphology of phalloidin staining with 5 μ mol/L CCG-1423, but most samples showed nearly normal stress fiber formation. CCG-1423, however, inhibited the activity elicited by expression of RhoA-G14V and RhoC-G14V. Because activation by these proteins is not dependent on upstream activators, this further supports an action of

the compound at a downstream step. The ability to block signals initiated by both RhoA and RhoC indicates that the step inhibited by CCG-1423 is engaged by both proteins. This does not seem to be the Rho kinase (ROCK) because CCG-1423 does not inhibit ROCK kinase activity *in vitro* nor does the known ROCK inhibitor Y-27632 fully inhibit $G\alpha_{13}$ -stimulated SRE-luciferase expression (Fig. 2-7). Thus, CCG-1423 should be capable of disrupting cancer cell functions elicited by RhoC as well as RhoA.

Because the data above indicate that CCG-1423 does not interfere with upstream components of the pathway, we probed steps more proximal to the transcriptional machinery. To this end, we tested effects of the compound on the transcriptional response induced by several transcription factors/co-activators. SRE.L-driven transcription is dependent on the ability of SRF to bind to this DNA element and nucleate the assembly of productive transcription complexes. CCG-1423 could therefore act by interfering with SRE-SRF recognition or by altering SRF-specific mechanisms of transcriptional activation. To distinguish between these possibilities, we examined the ability of CCG-1423 to inhibit activity elicited by an SRF-VP16 fusion protein. This chimera depends on the SRF-SRE interaction for its recruitment to the promoter but can activate transcription through the VP16 activation domain. As can be seen in Fig. 2-4A, CCG-1423 failed to inhibit the activity elicited by this protein, suggesting that the compound does not interfere with SRE-SRF interactions and implies that it does not affect transcriptional activation pathways used by the VP16 activation domain. This last point is confirmed by the observation that CCG-1423 does not inhibit the transcriptional response elicited by the chimeric activator GAL4-VP16 at a promoter-bearing GAL4 sites (Fig. 2-4A). To examine the effects of CCG-1423 on transcriptional activation mechanisms used by SRF,

we tested the ability of this compound to inhibit SRE.L-driven transcription stimulated by expression of the SRF coactivator MKL. As can be seen in Fig. 2-4A, despite the fact that expression of MKL1 led to a robust activation, reaching levels comparable with those achieved with the SRF-VP16 fusion ($31,100 \pm 17,500$ and $28,500 \pm 13,200$, respectively), CCG-1423 was able to inhibit this response effectively, whereas it had no effect on SRF-VP16-mediated activity. Together with the lack of effect on GAL4-VP16 or TK-driven *Renilla* luciferase expression, this result suggests that the compound specifically interferes with SRF/MKL1-dependent transcriptional activation mechanisms. The ability of CCG-1423 to inhibit MKL1-stimulated activity could be due to alterations in the recruitment of MKL to SRF or to effects on MKL1-dependent post-recruitment transcriptional activation mechanisms. As an initial step to explore these possibilities,

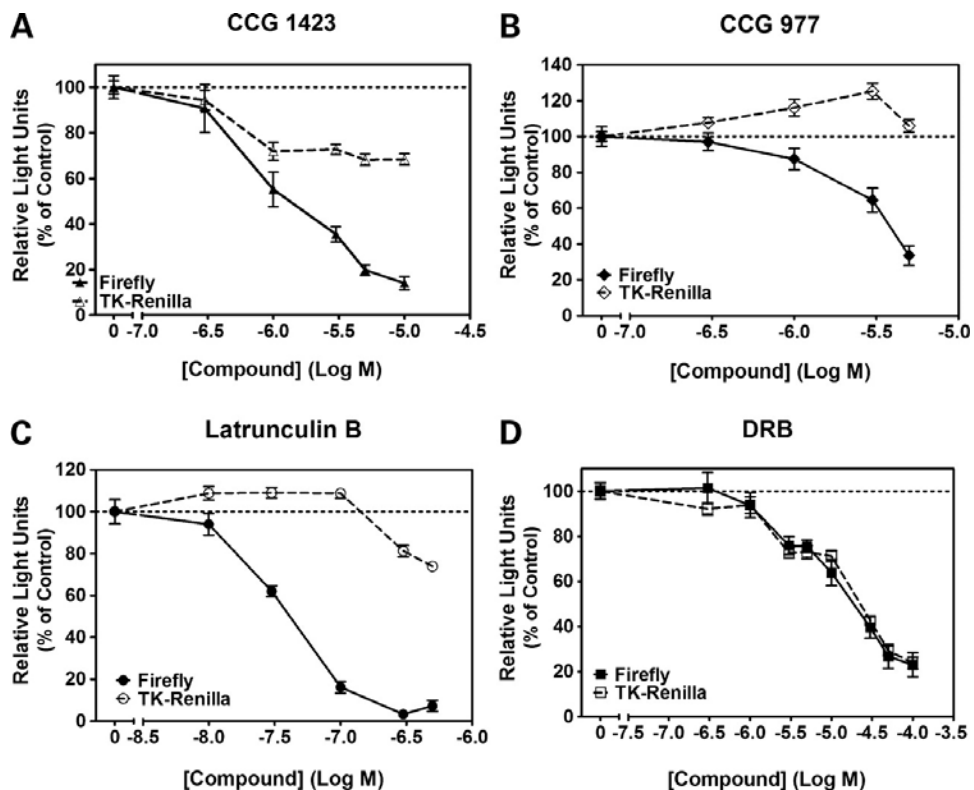


Figure 2-3. Latrunculin B, CCG-977, and CCG-1423 inhibit $G\alpha_{13}Q226L$ -stimulated SRE.L luciferase expression in PC-3 cells. Cells were co-transfected with 1 ng of the $G\alpha_{13}Q226L$ expression plasmid along with 30 ng of SRE.L and 7 ng of PRL-TK reporter plasmids as described in Materials and Methods. Cells were treated with the indicated concentrations of compounds, CCG-1423 (A), CCG-977 (B), latrunculin B (C), and 5,6-dichlorobenzimidazole-1- β -D-ribofuranoside (D), for 18 to 19 h after transfection before lysis and reading luminescence in the plate reader as described in Materials and Methods. The pcDNA3.1-zeo expression plasmid was used as carrier DNA in all experiments. Data are graphed as a percentage of the DMSO-negative control. *Points*, mean of three separate experiments done in triplicate; *bars*, SE. For the firefly luciferase, data with reporter alone (i.e., without activator) were subtracted.

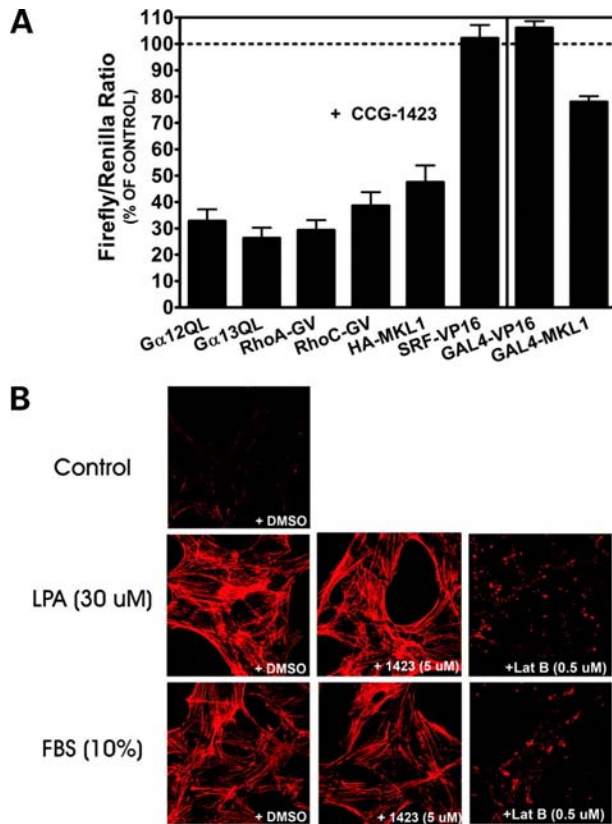


Figure 2-4. CCG-1423 inhibits downstream of Rho and shows specificity for SRE.L-mediated transcription. A) PC-3 cells were individually co-transfected with various activator expression plasmids (1 ng Gα₁₂Q231L, 1 ng Gα₁₃Q226L, 3 ng RhoA-G14V, 3 ng RhoC-G14V, 0.2 ng MKL1, 1 ng SRF-VP16, 0.03 ng GAL4-VP16, and 0.01 ng GAL4-MKL1) along with 30 ng of SRE.L or 50 ng of p(GAL4)₂-Luc and 7 ng of PRL-TK reporter plasmids. Cells were treated with 10 μmol/L CCG-1423 for 18 to 19 hr after transfection during serum starvation. B) Serum-starved NIH-3T3 cells were pre-treated with CCG-1423 (5 μmol/L) or latrunculin B (0.5 μmol/L) for 1 hr before treatment with LPA (30 μmol/L) and calf serum (10%) for 1 h to stimulate stress fiber formation. Cells were then fixed, lysed, and stained as described in Materials and Methods. Data in A are baseline-subtracted (reporter alone without activator), and the ratio of firefly to *Renilla* counts is expressed as a percentage of the DMSO control. Experiments were done in triplicate and represent $n = 3$.

we bypassed the SRF-dependent MKL recruitment step by fusing a COOH-terminal region of MKL, which harbors a strong activation function to the GAL4 DNA-binding domain. Activity of this fusion protein at a promoter-bearing GAL4 sites was partially inhibited by CCG-1423 (Fig. 2-4A). The partial nature of the response argues that CCG-1423 may function by altering steps both upstream of MKL recruitment as well as by interfering with post-recruitment functions of MKL at the promoter. Thus, in the context of the current view of the Rho signaling pathway shown in Fig. 2-1A, our overall analysis indicates that the site of action of CCG-1423 lies at a common step downstream of RhoA and RhoC distinct from the SRF-SRE interaction. Actions on some aspect of MKL1/SRF function (e.g., nuclear translocation, posttranslational modifications, MKL/SRF interaction, or MKL interactions with the transcriptional machinery) seem most likely.

CCG-1423 Inhibits Cancer Cell Functions In vitro

The above data show that CCG-1423 exerts selective effects on Rho-stimulated transcription. To determine whether the influence of this compound extends to Rho-mediated cellular responses central to malignant cell growth and metastasis, we have examined the effect of this compound on the growth and invasiveness of cancer cell lines that differ in their Rho pathway properties. Initially, we examined the effects of CCG-1423 on proliferation in response to activation of the Rho pathway. LPA is a major mitogen acting through GPCRs. Specific LPA receptors can activate signaling through at least three different G protein families ($G\alpha_i$, $G\alpha_q$, and $G\alpha_{12}/G\alpha_{13}$). $G\alpha_i$ signaling is sensitive to PTX, whereas $G\alpha_q$ and $G\alpha_{12/13}$ signaling are not. The downstream effects are also distinct because $G\alpha_i$ activates ras (48), $G\alpha_{13}$ strongly activates Rho, whereas $G\alpha_q$

activation leads to both Rho and ras signals (49, 50). Our laboratory has previously shown that LPA stimulates Rho in PC-3 cells through PDZ-RhoGEF (51). We therefore examined the effect of CCG-1423 on LPA-stimulated DNA synthesis in PC-3 cells using a BrdUrd incorporation assay. CCG-1423 specifically inhibited LPA-stimulated DNA synthesis in a dose-dependent manner and completely suppressed this response at 3 $\mu\text{mol/L}$ (Fig. 2-5A). In this context, PTX had no effect on LPA-stimulated DNA synthesis (data not shown). This is consistent with a model in which LPA activates Rho through non- $G\alpha_i$ pathways, such as $G\alpha_{12}/G\alpha_{13}$ or $G\alpha_q$, which in turn leads to Rho pathway signaling events that are blocked by CCG-1423. Notably, over the 24-h time course of this study, the compound did not affect cell viability as measured by WST-1 metabolism, showing that, at these doses, the compound does not have acute non-specific toxic effects on PC-3 cells (data not shown).

To assess the anti-proliferative effects of CCG-1423, we analyzed the sensitivity of a panel of cell lines that differ in their Rho pathway properties. The panel includes melanoma lines that overexpress RhoC (A375M2 and SKMel-147) as well as related low RhoC-expressing lines (A375 and SK-Mel-28). In addition, we also examined transformed (SW962, PC-3, and SKOV-3) and nontransformed (WI-38) cell lines. The A375M2 line was originally derived from the A375 melanoma line by selection for high metastatic potential by two passages through a mouse lung metastasis system (52). In this line, RhoC mRNA expression is 3- to 5-fold higher than in the non-metastatic cells remaining in the primary tumor site (52). The SK-Mel-147 line shows substantially higher RhoC protein expression compared with SK-Mel-28 cells as assessed by Western blot (44). In an 8-day growth assay in the presence of LPA (Fig. 2-5B), a low

concentration of CCG-1423 (300 nmol/L) markedly inhibited the proliferation of RhoC-overexpressing melanoma cells (A375M2 and SK-Mel-147) while not affecting their related low RhoC-expressing counterparts (A375 and SK-Mel-28). The squamous cell cancer line SW962, shown by Sahai and Marshal (21) to exhibit Rho-independent invasion, in contrast to the Rho-dependent A375M2, was similarly unaffected. PC-3 prostate cancer cells, SKOV-3 ovarian carcinoma cells, as well as the non-transformed WI-38 human fibroblasts were inhibited only marginally at this low concentration. However, growth of PC-3 prostate cancer cells was inhibited in this 8-day study with an IC_{50} of 1 μ mol/L in good agreement with its potency in effects on DNA synthesis and SRE-mediated gene transcription. The spectrum of activity of CCG-1423 in this panel of cell lines is consistent with its role as a Rho/SRF pathway inhibitor because its antiproliferative effects display selectivity toward RhoC-overexpressing melanoma cell lines. One potential mechanism for reduced growth in the presence of CCG-1423 could be enhanced apoptosis. We therefore measured caspase-3 activation in response to either CCG-1423 or daunorubicin in the RhoC-overexpressing A375M2 and low RhoC-expressing A375 melanoma cell lines. Compared with the low RhoC-expressing A375 line, CCG-1423 induced a 2-fold higher caspase-3 activity in the RhoC-overexpressing (A375M2) derivative (Fig. 2-5C, left). In this cell line, the activity induced by CCG-1423 was nearly as large as the effect of daunorubicin. In contrast to CCG-1423, the effect of daunorubicin (Fig. 2-5C, right) is substantially higher in the low RhoC-expressing A375 cells compared with the RhoC-overexpressing A375M2 cells. These data indicate that CCG-1423 displays selectivity toward Rho-overexpressing lines and the reversal of specificity of the two compounds (CCG-1423 versus daunorubicin) between A375 and

A375M2 cells suggests a distinct mechanism of action for CCG-1423 compared with daunorubicin. A critical process in metastasis is the ability of malignant cells to invade heterologous tissues. Recently, the invasiveness of PC-3 prostate cancer cells was shown to be dependent on RhoC and $G\alpha_{12}$ (10, 53). Thus, we compared the effects of CCG-1423 on matrix invasion by PC-3 prostate cancer cells and SKOV-3 ovarian cancer cells. In a Matrigel invasion assay, PC-3 cells display high invasion rates and do not require an exogenous stimulus for invasion (Fig. 2-6A, left). In contrast, invasion by SKOV-3 cells is greatly stimulated in the presence of LPA (Fig. 2-6A, right). Invasion in these two cell lines relies on different pathways because LPA-stimulated invasion by SKOV-3 cells was completely eliminated by PTX ($G\alpha_i$ -pathway dependent), whereas PC-3 cell invasion was not affected (Fig. 2-6B). Consistent with a Rho pathway inhibitor function, CCG-1423 (3 $\mu\text{mol/L}$) strongly suppressed the Rho-dependent invasion by PC-3 cells. A similar effect was seen on PC-3 cells in the presence of LPA (data not shown). In contrast, CCG-1423 did not affect the $G\alpha_i$ -pathway-dependent invasion by SKOV-3 cells (Fig. 2-6B).

Discussion

Recent developments in cancer therapeutics have highlighted the importance of molecularly targeted therapies with a current major emphasis on tyrosine kinases (54, 55). However, there is a strong body of evidence supporting efforts to disrupt signaling by oncogenic GTPases, such as Ras and Rho family members. These include blockade of critical lipid modifications by farnesyltransferase and geranylgeranyltransferase inhibitors, statins, and bisphosphonates (33). Inhibitors of Rho kinase have also been evaluated in cancer models (35, 36). In this report, we describe a novel small-molecule

inhibitor, which disrupts transcriptional signaling by the RhoA GTPase family. The compound described here (CCG-1423) has nanomolar to low micromolar potency as well as selectivity toward Rho-overexpressing and invasive cancer cell lines for inhibition of DNA synthesis, cell growth, and/or invasion. The role of RhoA family members, particularly RhoA and RhoC, in cancer cell growth and/or metastasis has become quite clear. Multiple studies correlate RhoA or RhoC overexpression and tumor aggressiveness (2, 3). Suppression of RhoC protein expression reduces invasiveness *in vitro* (10). Furthermore, breast tumors induced by the polyoma virus middle T antigen in a RhoC-deficient mouse show normal growth but a dramatic reduction in metastasis (11). The role of GPCR signaling to Rho is also relevant. A recent study found that a non-synonymous polymorphism in the RH-containing rhoGEF, PDZ-rhoGEF, was associated with reduced lung cancer risk in a case-control study of Mexican-Americans (56). In addition, Yao et al. (10) report that RhoC plays an important role in Rho-dependent prostate cancer cell invasion. This result correlates with our observation that CCG-1423 inhibits PC-3 prostate cancer cell matrix invasion (Fig. 2-6B). In the strongly Rho-overexpressing cell lines (A375M2 and SK-Mel-147), we see an effect of nanomolar concentrations of CCG-1423 on cell growth. Rho-mediated regulation of the cell cycle is complex, involving both Rho and ras pathway components, leading to effects on cyclins A and D1 and on the cyclin-dependent kinase inhibitors p21^{Waf1/Cip1} and p27^{kip1} (57, 58). Interestingly, the induction of cyclin D1 by the Rho effector ROCK (57) could be due to Rho-mediated gene transcriptional events. Thus, differential dependence on these cell cycle regulators could underlie the functional differences in cell growth and DNA synthesis that we observe with CCG-1423 on the various cancer cell types. Furthermore,

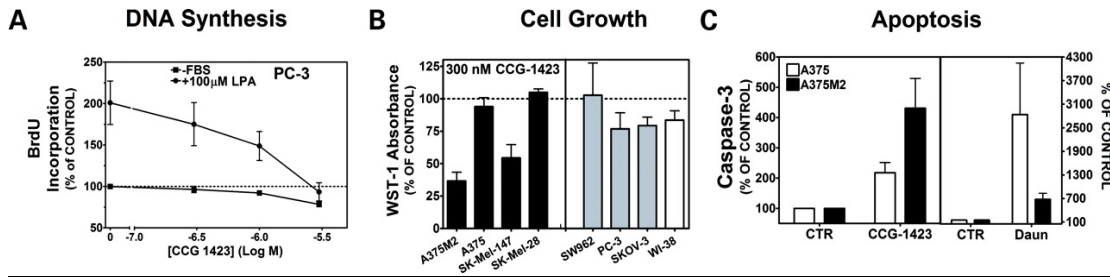


Figure 2-5. CCG-1423 inhibits cancer cell proliferation and survival. A) PC-3 cells were treated for 27 h with 100 $\mu\text{mol/L}$ LPA in the presence or absence of various concentrations of CCG-1423, labeled with BrdUrd, and stained, and absorbance was read as described in Materials and Methods. B) Various cell lines were treated with 30 $\mu\text{mol/L}$ LPA with or without 0.3 $\mu\text{mol/L}$ CCG-1423, and then on day 8, WST-1 absorbance was read as described in Materials and Methods. *Black columns*, four melanoma lines with differing expression of RhoC [A375M2 and SK-Mel-147 have high expression (see text), whereas the parental line A375 (used to derive A375M2) and SK-Mel-28 have lower expression]; *gray columns*, several other cancer cell lines; *white column*, non-transformed fibroblast line, WI-38. C) A375 and A375M2 cells were treated with 3 $\mu\text{mol/L}$ CCG-1423 or 3 $\mu\text{mol/L}$ daunorubicin for 25 hr, and then caspase-3 activity was measured with a fluorescent substrate as described in Materials and Methods. In A and C, data are expressed as a percentage of the no FBS control. In B, data are expressed as percentage of the LPA + DMSO control. All data represent $n = 3$.

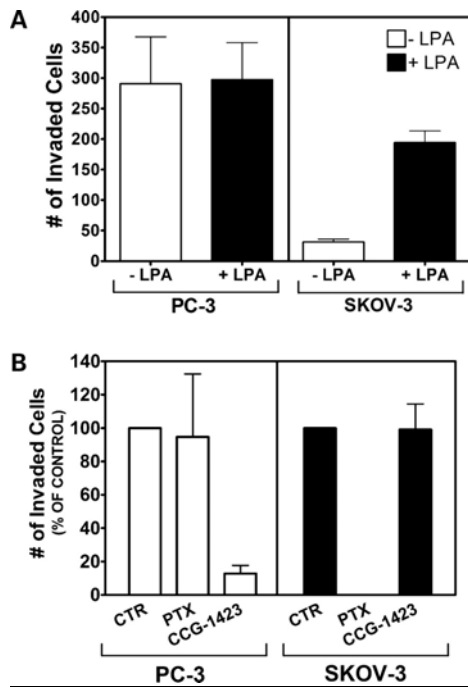


Figure 2-6. CCG-1423 inhibits prostate cancer cell invasion. A) LPA stimulates invasion of SKOV-3 but not PC-3 cells. Invasion of Matrigel-coated filters by serum-starved PC-3 prostate cancer or SKOV-3 ovarian cancer cells was measured with or without 30 $\mu\text{mol/L}$ LPA as chemo-attractant as described in Materials and Methods. B) CCG-1423 inhibits PC-3 cell invasion, whereas PTX inhibits SKOV-3 cell invasion. The effects of CCG-1423 (3 $\mu\text{mol/L}$) and PTX (100 ng/mL) on spontaneous (PC-3) or LPA-stimulated (SKOV-3) invasion through Matrigel were measured as described in Materials and Methods. In B, data are expressed as a percentage of control. All data represent $n = 3$.

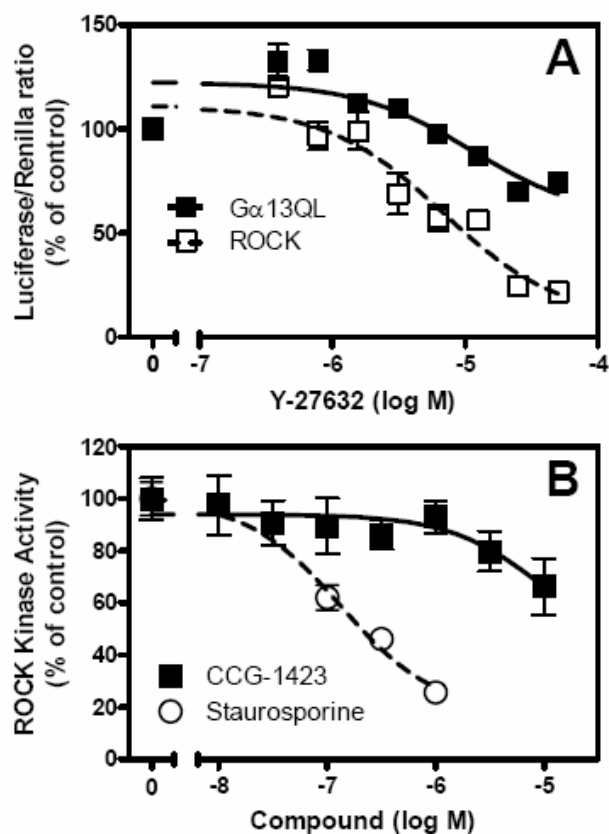


Figure 2-7. Effect of Rho-Kinase Inhibitor, Y-27632, on SRE.L-luciferase Activated by Transfection of ROCK or Gα13 and Effect of CCG-1423 on ROCK Kinase Activity. A) HEK293T cells transiently transfected with SRE-Luciferase reporter and an activator (ROCK or Gα13) were incubated overnight with the indicated concentrations of the Rho kinase inhibitor Y-27632 as described in Materials and Methods. Luciferase expression (normalized to expression of the co-transfected *Renilla* reporter) is expressed as percent of the no-drug control. Data are mean ± SEM of triplicate determinations. B) Rho kinase activity *in vitro* was measured as described in Materials and Methods. The indicated concentrations of staurosporine or CCG-1423 were added. Data are means ± SEM of triplicate determinations.

the growth inhibition in the 8-day experiments could also involve enhanced cell death as well as inhibition of cell cycle progression. Consistent with this, caspase-3 activation in the highly metastatic RhoC-overexpressing A375M2 melanoma cell line was enhanced by CCG-1423 whereas a smaller increase was seen with the parental A375 cell line, whereas just the opposite pattern was seen with daunorubicin. The precise molecular mechanism of action of CCG-1423 is not clear but our findings indicate that CCG-1423 may disrupt Rho signaling through functional inhibition of SRF transcriptional activity. The data suggest that effects on the co-activator MKL1 are likely, although effects on other SRF regulatory cofactors cannot be ruled out. Nuclear MKL1 function depends on Rho-mediated actin polymerization, which leads to dissociation from G-actin and nuclear translocation of MKL1. Free from G-actin, MKL1 can bind the transcription factor SRF and stimulate transcription (22, 23). MKL1 function is also regulated by post-translational modifications, including covalent modification by members of the small ubiquitin-like modifier family. Consistent with the effects of sumoylation on sequence-specific transcription factors (59), small ubiquitin-like modifier modification of MKL1 attenuates its transcriptional activation potential (60). Thus, CCG-1423 could modify several aspects of MKL1 function, for example (a) preventing release from actin or blocking nuclear translocation of MKL1, (b) enhancing sumoylation causing transcriptional repression, (c) inhibiting the protein-protein interaction between MKL1 and SRF, or (d) disrupting MKL1 coactivator function. The ability of CCG-1423 to partially inhibit the GAL4-MKL1 transcriptional signal supports at least in part this latter point, although definitive conclusions will require additional experiments. Alternatively, CCG-1423 might disrupt some other aspect of SRF function, such as recruitment or

activity of other SRF transcription partners [e.g., Nkx3.1 and GATA-4; refs. (61, 62)]. The role of different Rho signaling events in cancer biology has been difficult to decipher because RhoA family members activate many effectors, such as Rho kinases (ROCK-I and ROCK-II), rhotekin, and mDia1. The downstream events from Rho signals are similarly diverse, with alterations in actin cytoskeletal organization and gene transcription being two prominent effects. Our identification of CCG-1423 as an inhibitor of Rho-mediated transcription provides a useful tool to further elucidate the role of this process in cancer biology. Given the strong inhibition of PC-3 cell matrix invasion and A375M2 cell growth, it is likely that Rho-stimulated transcriptional processes play a role in these phenomena. Indeed, enhanced Rho-dependent matrix metalloproteinase expression induced by the chemokine CXCL12 acting at CXCR4 receptors is involved in melanoma cell matrix invasion (63). It will clearly be of interest to identify which Rho-dependent genes show reduced expression with CCG-1423. In summary, our identification of CCG-1423 provides a novel lead compound for the development of more potent and specific inhibitors of Rho-mediated transcription. CCG-1423 should serve both as a pharmacologic tool and as a potential lead for therapeutics for Rho-dependent cancers. Further exploration on the mechanism of action of CCG-1423 and identification of even more potent analogues will be important steps for the future.

References

1. Sawyer, T. K. Cancer metastasis therapeutic targets and drug discovery: emerging small-molecule protein kinase inhibitors. *Expert Opin Investig Drugs*, *13*: 1-19, 2004.
2. Sahai, E. and Marshall, C. J. RHO-GTPases and cancer. *Nat Rev Cancer*, *2*: 133-142, 2002.
3. Faried, A., Nakajima, M., Sohda, M., Miyazaki, T., Kato, H., and Kuwano, H. Correlation between RhoA overexpression and tumour progression in esophageal squamous cell carcinoma. *Eur J Surg Oncol*, *31*: 410-414, 2005.
4. Whitehead, I. P., Zohn, I. E., and Der, C. J. Rho GTPase-dependent transformation by G protein-coupled receptors. *Oncogene*, *20*: 1547-1555, 2001.
5. Kwei, K. A., Finch, J. S., Ranger-Moore, J., and Bowden, G. T. The role of Rac1 in maintaining malignant phenotype of mouse skin tumor cells. *Cancer Lett*, *231*: 326-338, 2006.
6. Hirsch, D. S., Shen, Y., and Wu, W. J. Growth and motility inhibition of breast cancer cells by epidermal growth factor receptor degradation is correlated with inactivation of Cdc42. *Cancer Res*, *66*: 3523-3530, 2006.
7. Baugher, P. J., Krishnamoorthy, L., Price, J. E., and Dharmawardhane, S. F. Rac1 and Rac3 isoform activation is involved in the invasive and metastatic phenotype of human breast cancer cells. *Breast Cancer Res*, *7*: R965-974, 2005.
8. van Golen, K. L., Davies, S., Wu, Z. F., Wang, Y., Bucana, C. D., Root, H., Chandrasekharappa, S., Strawderman, M., Ethier, S. P., and Merajver, S. D. A novel putative low-affinity insulin-like growth factor-binding protein, LIBC (lost in inflammatory breast cancer), and RhoC GTPase correlate with the inflammatory breast cancer phenotype. *Clin Cancer Res*, *5*: 2511-2519, 1999.
9. van Golen, K. L., Wu, Z. F., Qiao, X. T., Bao, L. W., and Merajver, S. D. RhoC GTPase, a novel transforming oncogene for human mammary epithelial cells that partially recapitulates the inflammatory breast cancer phenotype. *Cancer Res*, *60*: 5832-5838, 2000.
10. Yao, H., Dashner, E. J., van Golen, C. M., and van Golen, K. L. RhoC GTPase is required for PC-3 prostate cancer cell invasion but not motility. *Oncogene*, *25*: 2285-2296, 2006.
11. Hakem, A., Sanchez-Sweetman, O., You-Ten, A., Duncan, G., Wakeham, A., Khokha, R., and Mak, T. W. RhoC is dispensable for embryogenesis and tumor initiation but essential for metastasis. *Genes Dev*, *19*: 1974-1979, 2005.

12. Lacoste, J., Aprikian, A. G., and Chevalier, S. Focal adhesion kinase is required for bombesin-induced prostate cancer cell motility. *Mol Cell Endocrinol*, 235: 51-61, 2005.
13. Sawada, K., Morishige, K., Tahara, M., Kawagishi, R., Ikebuchi, Y., Tasaka, K., and Murata, Y. Alendronate inhibits lysophosphatidic acid-induced migration of human ovarian cancer cells by attenuating the activation of rho. *Cancer Res*, 62: 6015-6020, 2002.
14. Shi, X., Gangadharan, B., Brass, L. F., Ruf, W., and Mueller, B. M. Protease-activated receptors (PAR1 and PAR2) contribute to tumor cell motility and metastasis. *Mol Cancer Res*, 2: 395-402, 2004.
15. Fukuhara, S., Chikumi, H., and Gutkind, J. S. RGS-containing RhoGEFs: the missing link between transforming G proteins and Rho? *Oncogene*, 20: 1661-1668, 2001.
16. Kourlas, P. J., Strout, M. P., Becknell, B., Veronese, M. L., Croce, C. M., Theil, K. S., Krahe, R., Ruutu, T., Knuutila, S., Bloomfield, C. D., and Caligiuri, M. A. Identification of a gene at 11q23 encoding a guanine nucleotide exchange factor: evidence for its fusion with MLL in acute myeloid leukemia. *Proc Natl Acad Sci U S A*, 97: 2145-2150, 2000.
17. Hart, M. J., Jiang, X., Kozasa, T., Roscoe, W., Singer, W. D., Gilman, A. G., Sternweis, P. C., and Bollag, G. Direct stimulation of the guanine nucleotide exchange activity of p115 RhoGEF by G α 13. *Science*, 280: 2112-2114, 1998.
18. Kozasa, T., Jiang, X., Hart, M. J., Sternweis, P. M., Singer, W. D., Gilman, A. G., Bollag, G., and Sternweis, P. C. p115 RhoGEF, a GTPase activating protein for G α 12 and G α 13. *Science*, 280: 2109-2111, 1998.
19. Vogt, S., Grosse, R., Schultz, G., and Offermanns, S. Receptor-dependent RhoA activation in G12/G13-deficient cells: genetic evidence for an involvement of Gq/G11. *J Biol Chem*, 278: 28743-28749, 2003.
20. Lutz, S., Freichel-Blomquist, A., Yang, Y., Rumenapp, U., Jakobs, K. H., Schmidt, M., and Wieland, T. The guanine nucleotide exchange factor p63RhoGEF, a specific link between Gq/11-coupled receptor signaling and RhoA. *J Biol Chem*, 280: 11134-11139, 2005.
21. Sahai, E. and Marshall, C. J. Differing modes of tumour cell invasion have distinct requirements for Rho/ROCK signalling and extracellular proteolysis. *Nat Cell Biol*, 5: 711-719, 2003.
22. Cen, B., Selvaraj, A., Burgess, R. C., Hitzler, J. K., Ma, Z., Morris, S. W., and Prywes, R. Megakaryoblastic leukemia 1, a potent transcriptional coactivator for

- serum response factor (SRF), is required for serum induction of SRF target genes. *Mol Cell Biol*, 23: 6597-6608, 2003.
23. Miralles, F., Posern, G., Zaromytidou, A. I., and Treisman, R. Actin dynamics control SRF activity by regulation of its coactivator MAL. *Cell*, 113: 329-342, 2003.
 24. Schwartz, D. R., Kardia, S. L., Shedden, K. A., Kuick, R., Michailidis, G., Taylor, J. M., Misek, D. E., Wu, R., Zhai, Y., Darrah, D. M., Reed, H., Ellenson, L. H., Giordano, T. J., Fearon, E. R., Hanash, S. M., and Cho, K. R. Gene expression in ovarian cancer reflects both morphology and biological behavior, distinguishing clear cell from other poor-prognosis ovarian carcinomas. *Cancer Res*, 62: 4722-4729, 2002.
 25. Vickers, E. R., Kasza, A., Kurnaz, I. A., Seifert, A., Zeef, L. A., O'Donnell, A., Hayes, A., and Sharrocks, A. D. Ternary complex factor-serum response factor complex-regulated gene activity is required for cellular proliferation and inhibition of apoptotic cell death. *Mol Cell Biol*, 24: 10340-10351, 2004.
 26. Wu, M., Wu, Z. F., Kumar-Sinha, C., Chinnaiyan, A., and Merajver, S. D. RhoC induces differential expression of genes involved in invasion and metastasis in MCF10A breast cells. *Breast Cancer Res Treat*, 84: 3-12, 2004.
 27. Selvaraj, A. and Prywes, R. Expression profiling of serum inducible genes identifies a subset of SRF target genes that are MKL dependent. *BMC Mol Biol*, 5: 13, 2004.
 28. Andela, V. B. Correspondence Re S. S. Virtanen et al., Alendronate inhibits invasion of PC-3 prostate cancer cells by affecting the mevalonate pathway. *Cancer Res* 2002;62:2708-14. Re K. Sawada et al., Alendronate inhibits lysophosphatidic acid-induced migration of human ovarian cancer cells by attenuating the activation of Rho. *Cancer Res* 2002;62:6015-20. *Cancer Res*, 64: 2934-2935; author reply 2935-2936, 2004.
 29. Mathupala, S. P., Ko, Y. H., and Pedersen, P. L. Hexokinase II: cancer's double-edged sword acting as both facilitator and gatekeeper of malignancy when bound to mitochondria. *Oncogene*, 25: 4777-4786, 2006.
 30. Yu, Y. P. and Luo, J. H. Myopodin-mediated suppression of prostate cancer cell migration involves interaction with zyxin. *Cancer Res*, 66: 7414-7419, 2006.
 31. Zhu, Z., Kleeff, J., Friess, H., Wang, L., Zimmermann, A., Yarden, Y., Buchler, M. W., and Korc, M. Epiregulin is Up-regulated in pancreatic cancer and stimulates pancreatic cancer cell growth. *Biochem Biophys Res Commun*, 273: 1019-1024, 2000.

32. Zudaire, E., Martinez, A., and Cuttitta, F. Adrenomedullin and cancer. *Regul Pept*, *112*: 175-183, 2003.
33. Aznar, S., Fernandez-Valeron, P., Espina, C., and Lacal, J. C. Rho GTPases: potential candidates for anticancer therapy. *Cancer Lett*, *206*: 181-191, 2004.
34. Lawler, K., Foran, E., O'Sullivan, G., Long, A., and Kenny, D. Mobility and invasiveness of metastatic esophageal cancer are potentiated by shear stress in a ROCK- and Ras-dependent manner. *Am J Physiol Cell Physiol*, *291*: C668-677, 2006.
35. Nakajima, M., Hayashi, K., Egi, Y., Katayama, K., Amano, Y., Uehata, M., Ohtsuki, M., Fujii, A., Oshita, K., Kataoka, H., Chiba, K., Goto, N., and Kondo, T. Effect of Wf-536, a novel ROCK inhibitor, against metastasis of B16 melanoma. *Cancer Chemother Pharmacol*, *52*: 319-324, 2003.
36. Nakajima, M., Katayama, K., Tamechika, I., Hayashi, K., Amano, Y., Uehata, M., Goto, N., and Kondo, T. WF-536 inhibits metastatic invasion by enhancing the host cell barrier and inhibiting tumour cell motility. *Clin Exp Pharmacol Physiol*, *30*: 457-463, 2003.
37. Gao, Y., Dickerson, J. B., Guo, F., Zheng, J., and Zheng, Y. Rational design and characterization of a Rac GTPase-specific small molecule inhibitor. *Proc Natl Acad Sci U S A*, *101*: 7618-7623, 2004.
38. Suzuki, N., Nakamura, S., Mano, H., and Kozasa, T. G α 12 activates Rho GTPase through tyrosine-phosphorylated leukemia-associated RhoGEF. *Proc Natl Acad Sci U S A*, *100*: 733-738, 2003.
39. Subramanian, L., Benson, M. D., and Iniguez-Lluhi, J. A. A synergy control motif within the attenuator domain of CCAAT/enhancer-binding protein α inhibits transcriptional synergy through its PIASy-enhanced modification by SUMO-1 or SUMO-3. *J Biol Chem*, *278*: 9134-9141, 2003.
40. Du, K. L., Chen, M., Li, J., Lepore, J. J., Mericko, P., and Parmacek, M. S. Megakaryoblastic leukemia factor-1 transduces cytoskeletal signals and induces smooth muscle cell differentiation from undifferentiated embryonic stem cells. *J Biol Chem*, *279*: 17578-17586, 2004.
41. Hart, M. J., Sharma, S., elMasry, N., Qiu, R. G., McCabe, P., Polakis, P., and Bollag, G. Identification of a novel guanine nucleotide exchange factor for the Rho GTPase. *J Biol Chem*, *271*: 25452-25458, 1996.
42. Le Page, S. L., Bi, Y., and Williams, J. A. CCK-A receptor activates RhoA through G α 12/13 in NIH3T3 cells. *Am J Physiol Cell Physiol*, *285*: C1197-1206, 2003.

43. Chupreta, S., Holmstrom, S., Subramanian, L., and Iniguez-Lluhi, J. A. A small conserved surface in SUMO is the critical structural determinant of its transcriptional inhibitory properties. *Mol Cell Biol*, 25: 4272-4282, 2005.
44. Collisson, E. A., Kleer, C., Wu, M., De, A., Gambhir, S. S., Merajver, S. D., and Kolodney, M. S. Atorvastatin prevents RhoC isoprenylation, invasion, and metastasis in human melanoma cells. *Mol Cancer Ther*, 2: 941-948, 2003.
45. Soengas, M. S., Capodiceci, P., Polsky, D., Mora, J., Esteller, M., Opitz-Araya, X., McCombie, R., Herman, J. G., Gerald, W. L., Lazebnik, Y. A., Cordon-Cardo, C., and Lowe, S. W. Inactivation of the apoptosis effector Apaf-1 in malignant melanoma. *Nature*, 409: 207-211, 2001.
46. Owicki, J. C. Fluorescence polarization and anisotropy in high throughput screening: perspectives and primer. *J Biomol Screen*, 5: 297-306, 2000.
47. Zhang, J. H., Chung, T. D., and Oldenburg, K. R. A Simple Statistical Parameter for Use in Evaluation and Validation of High Throughput Screening Assays. *J Biomol Screen*, 4: 67-73, 1999.
48. Bian, D., Su, S., Mahanivong, C., Cheng, R. K., Han, Q., Pan, Z. K., Sun, P., and Huang, S. Lysophosphatidic Acid Stimulates Ovarian Cancer Cell Migration via a Ras-MEK Kinase 1 Pathway. *Cancer Res*, 64: 4209-4217, 2004.
49. Chikumi, H., Fukuhara, S., and Gutkind, J. S. Regulation of G protein-linked guanine nucleotide exchange factors for Rho, PDZ-RhoGEF, and LARG by tyrosine phosphorylation: evidence of a role for focal adhesion kinase. *J Biol Chem*, 277: 12463-12473, 2002.
50. Mills, G. B. and Moolenaar, W. H. The emerging role of lysophosphatidic acid in cancer. *Nat Rev Cancer*, 3: 582-591, 2003.
51. Wang, Q., Liu, M., Kozasa, T., Rothstein, J. D., Sternweis, P. C., and Neubig, R. R. Thrombin and lysophosphatidic acid receptors utilize distinct rhoGEFs in prostate cancer cells. *J Biol Chem*, 279: 28831-28834, 2004.
52. Clark, E. A., Golub, T. R., Lander, E. S., and Hynes, R. O. Genomic analysis of metastasis reveals an essential role for RhoC. *Nature*, 406: 532-535, 2000.
53. Kelly, P., Stemmler, L. N., Madden, J. F., Fields, T. A., Daaka, Y., and Casey, P. J. A role for the G12 family of heterotrimeric G proteins in prostate cancer invasion. *J Biol Chem*, 281: 26483-26490, 2006.
54. Buchdunger, E., Zimmermann, J., Mett, H., Meyer, T., Muller, M., Druker, B. J., and Lydon, N. B. Inhibition of the Abl protein-tyrosine kinase in vitro and in vivo by a 2-phenylaminopyrimidine derivative. *Cancer Res*, 56: 100-104, 1996.

55. Pollack, V. A., Savage, D. M., Baker, D. A., Tsaparikos, K. E., Sloan, D. E., Moyer, J. D., Barbacci, E. G., Pustilnik, L. R., Smolarek, T. A., Davis, J. A., Vaidya, M. P., Arnold, L. D., Doty, J. L., Iwata, K. K., and Morin, M. J. Inhibition of epidermal growth factor receptor-associated tyrosine phosphorylation in human carcinomas with CP-358,774: dynamics of receptor inhibition in situ and antitumor effects in athymic mice. *J Pharmacol Exp Ther*, *291*: 739-748, 1999.
56. Gu, J., Wu, X., Dong, Q., Romeo, M. J., Lin, X., Gutkind, J. S., and Berman, D. M. A nonsynonymous single-nucleotide polymorphism in the PDZ-Rho guanine nucleotide exchange factor (Ser1416Gly) modulates the risk of lung cancer in Mexican Americans. *Cancer*, *106*: 2716-2724, 2006.
57. Croft, D. R. and Olson, M. F. The Rho GTPase effector ROCK regulates cyclin A, cyclin D1, and p27Kip1 levels by distinct mechanisms. *Mol Cell Biol*, *26*: 4612-4627, 2006.
58. Olson, M. F., Paterson, H. F., and Marshall, C. J. Signals from Ras and Rho GTPases interact to regulate expression of p21Waf1/Cip1. *Nature*, *394*: 295-299, 1998.
59. Holmstrom, S., Van Antwerp, M. E., and Iniguez-Lluhi, J. A. Direct and distinguishable inhibitory roles for SUMO isoforms in the control of transcriptional synergy. *Proc Natl Acad Sci U S A*, *100*: 15758-15763, 2003.
60. Nakagawa, K. and Kuzumaki, N. Transcriptional activity of megakaryoblastic leukemia 1 (MKL1) is repressed by SUMO modification. *Genes Cells*, *10*: 835-850, 2005.
61. Belaguli, N. S., Sepulveda, J. L., Nigam, V., Charron, F., Nemer, M., and Schwartz, R. J. Cardiac tissue enriched factors serum response factor and GATA-4 are mutual coregulators. *Mol Cell Biol*, *20*: 7550-7558, 2000.
62. Ju, J. H., Maeng, J. S., Zemedkun, M., Ahronovitz, N., Mack, J. W., Ferretti, J. A., Gelmann, E. P., and Gruschus, J. M. Physical and functional interactions between the prostate suppressor homeoprotein NKX3.1 and serum response factor. *J Mol Biol*, *360*: 989-999, 2006.
63. Bartolome, R. A., Galvez, B. G., Longo, N., Baleux, F., Van Muijen, G. N., Sanchez-Mateos, P., Arroyo, A. G., and Teixido, J. Stromal cell-derived factor-1alpha promotes melanoma cell invasion across basement membranes involving stimulation of membrane-type 1 matrix metalloproteinase and Rho GTPase activities. *Cancer Res*, *64*: 2534-2543, 2004.

CHAPTER III

CHEMICAL SYNTHESIS, STRUCTURE-ACTIVITY RELATIONSHIPS, AND PROSTATE CELL-BASED STUDIES OF THE RHOA TRANSCRIPTIONAL PATHWAY INHIBITOR, CCG-1423

Abstract

In this chapter, I describe the chemical synthesis of analogs of the RhoA transcriptional pathway inhibitor, CCG-1423 (2-([3,5-bis(trifluoromethyl)phenyl]formamido}oxy)-N-(4-chlorophenyl)propanamide), and describe their effect upon the cellular function of prostate epithelial cells. The most promising analogs described here were less potent than CCG-1423, but were more selective and less toxic with respect to the Rho-specific SRE.L luciferase response versus both the thymidine kinase (TK)-promoter-driven *Renilla* response and WST-1 cell viability response. These analogs also inhibited PC-3 prostate cancer cell Matrigel invasion with an activity profile similar to their effect on the SRE.L-luciferase response. They did not show major toxicity differences across a panel of prostate epithelial cell lines, with the exception of a few compounds. As a result, these structure-activity relationship studies have identified key lead compounds for both future mechanistic studies to identify the molecular target of CCG-1423 and for *in vivo* prostate cancer xenograft studies.

Introduction

Cancer metastasis is a major medical problem, which is responsible for 90% of deaths of patients with solid tumors (1). It involves several complex cellular processes that are responsible for the movement of malignant cells from the site of tissue origin of the primary tumor to an alternate tissue site, such as the bone, lungs, liver, or brain. These cellular processes include cell adhesion, migration, invasion, angiogenesis, survival, and proliferation (1, 2). The RhoA transcriptional signaling pathway plays an important role in these cellular processes and in several solid human tumors such as colon, esophageal, lung, pancreatic, and inflammatory breast cancer (3-5).

A major mechanism of activating the RhoA transcriptional pathway is through activation of heterotrimeric G-protein coupled receptors (GPCR) that activate the $G\alpha_{12/13}$ family of $G\alpha$ -subunits. Three GPCRs that can couple to the $G\alpha_{12/13}$ family of $G\alpha$ -subunits are the lysophosphatidic acid (LPA), thrombin, and bombesin receptors (6, 7). Upon receptor activation, RhoA is activated by one of the regulator of G-protein signaling homology (RH) domain containing RhoGEFs (p115RhoGEF, PDZ-RhoGEF, and leukemia-associated RhoGEF), which stimulates the nucleotide exchange of GTP for GDP (8-11). Upon activation, RhoA is most well-known for its short-term effects upon cytoskeletal changes within the cell, which are important for the process of cell motility. RhoA is required for stress fiber formation, whereas the two other main Rho GTPases, Rac and Cdc42, are required for formation of lamellipodia and filipodia, respectively (12). In addition to these effects, RhoA activation can have more long-term effects upon gene transcription through the activation of the transcription factor, serum response factor (SRF), and its co-activator megakaryoblastic leukemia 1 (MKL1) (13-16).

The RhoA transcriptional signaling pathway has been implicated in cellular processes that are important for cancer metastasis. The LPA, thrombin, and bombesin GPCRs have been shown to stimulate migration of ovarian and prostate cancer cells (17-19). The downstream Rho effector, Rho-associated coiled coil-forming protein kinase (ROCK) has been implicated in cell migration, invasion, and metastasis (20, 21). In addition, the transcription factor SRF has been shown to play a crucial role in the cellular processes of cell migration, invasion, growth, and survival (22-24). More recently, Medjkane et al. (25) have shown that MKL1 is required for breast cancer and melanoma cell adhesion, spreading, migration, and invasion, *in vitro*, and for lung metastasis of melanoma cells, *in vivo*. Therefore, there is a clear role for the RhoA transcriptional signaling pathway in the process of cancer metastasis.

I described in Chapter 2 the identification of a small-molecule inhibitor, CCG-1423, of the RhoA transcriptional signaling pathway that prevents PC-3 prostate cancer cell invasion (26). Previous work reported that PC-3 prostate cancer cell invasion is RhoC-dependent (27-29). We also showed previously that RhoC is capable of activation of the RhoA transcriptional signaling pathway through activation of MKL1/SRF dependent gene transcription (26). Therefore, here we undertook a structure-activity relationship study through chemical synthesis of analogs of CCG-1423 in order to improve potency, selectivity (with respect to the Rho-specific SRE.L-luciferase transcriptional response versus the constitutively active thymidine kinase *Renilla* luciferase response), and toxicity (monitored by the WST1 cell viability response). In our original study, CCG-1423 inhibited SRE.L-luciferase expression with an IC₅₀ of 1 μM. It also inhibited both the thymidine kinase driven *Renilla* luciferase expression and WST1

cell viability response approximately 30% at a maximum concentration of 10 μ M. Therefore, we hypothesize that more potent, selective, and less toxic lead compounds in both the Rho-specific SRE.L-luciferase reporter assay and PC-3 prostate cancer cell Matrigel invasion assay will enable future mechanistic studies to identify the molecular target, and future *in vivo* prostate cancer cell metastatic xenograft studies for the development of cancer therapeutics.

Materials and Methods

Plasmids, Cell Lines, and Reagents

The Rho-pathway selective SRE.L luciferase reporter construct was described previously (26). The control pRL-thymidine kinase (TK) *Renilla* luciferase reporter construct was purchased from Promega (Madison, WI). The human $G\alpha_{12}Q231L$ expression plasmid was from the Missouri S&T cDNA Resource Center (www.cdna.org). The pcDNA 3.1-zeo expression plasmid was from Invitrogen (Carlsbad, CA). The BD BioCoat Matrigel invasion chambers (8 μ m) were from Becton Dickinson (Franklin Lakes, NJ). Crystal violet was purchased from Sigma (St. Louis, MO). The WST-1 cell proliferation reagent was from Roche Applied Science (Indianapolis, IN). The chemical compound CCG-1423 [*N*-[2-(4-chloroanilino)-1-methyl-2-oxoethoxy]-3,5-bis(trifluoromethyl)benzamide] was from Cayman Chemical (Ann Arbor, MI). The synthetic analog compounds of CCG-1423 were synthesized at the Medicinal Chemistry Core Synthesis Laboratory at the University of Michigan. The PC-3 cell line was a kind gift from Dr. Kenneth Pienta (University of Michigan). The RWPE-1 and LNCaP cell lines were obtained from the American Type Culture Collection (Manassas, VA).

Cell Culture

The PC-3 cell line was normally maintained in DMEM medium (Invitrogen, cat.#: 11995) containing 10% fetal bovine serum (FBS), 100 units/mL penicillin, and 100 µg/mL streptomycin at 37°C in 5% CO₂. The LNCaP cell line was normally maintained in RPMI-1640 medium (Invitrogen, cat.#: 11875) containing 10% fetal bovine serum (FBS), 100 units/mL penicillin, and 100 µg/mL streptomycin at 37°C in 5% CO₂. The RWPE-1 immortalized prostate epithelium cell line was normally maintained in Keratinocyte Serum Free medium (K-SFM) (Invitrogen, cat.#: 17005-042) containing 0.05 mg/ml of bovine pituitary extract (BPE), 5 ng/ml of human recombinant epidermal growth factor (EGF), 100 units/mL penicillin, and 100 µg/mL streptomycin at 37°C in 5% CO₂.

Dual Luciferase Reporter Assay

PC-3 cells were seeded into 96-well plates at a cell density of 4×10^4 cells per well 24 hour prior to transfection. Cells were transiently transfected with the Gα₁₂Q231L activator expression plasmid along with both the SRE.L luciferase and pRL-TK *Renilla* luciferase reporter plasmids. The DNA plasmids were transfected using the lipid-based LipofectAMINE 2000 (Invitrogen) transfection reagent at a concentration of 1 µL per µg of DNA in antibiotic-free, Opti-MEM I medium. The total amount of DNA was kept constant by inclusion of the appropriate amount of the pcDNA3.1-zeo plasmid. Six hours after transfection, the transfection mixture was removed and cells were serum-starved overnight in DMEM medium containing 0.5% FBS and 1% penicillin-streptomycin. Firefly and *Renilla* luciferase activities were determined 19 hours later using the dual-

luciferase assay kit (Promega) according to the manufacturer's instructions. Luminescence was read on a Victor² plate reader with dual injectors (Perkin-Elmer). Chemical compounds were tested by adding 1 μ L of compound or DMSO to the cells (final concentration, 1% DMSO) at the beginning of the serum starvation step.

Cell Viability

Fifty microliters (μ l) of low serum (0.5% FBS) DMEM medium or RPMI-1640 medium were added to each well of 96-well plates receiving PC-3 and LNCaP cells, respectively. Fifty microliters (μ l) of K-SFM medium were added to each well of 96-well plates receiving RWPE-1 cells. Chemical compounds were added via 2-fold serial-dilutions in duplicate to each plate over a concentration range of 100 μ M to 0.78125 μ M. 1% DMSO was added to sixteen control wells per plate. Using a Multidrop 384 (Thermo), cells were added in 50 μ l of the appropriate medium to a final cell density of 4×10^4 cells per well. Twenty-three hours later, 10 μ l per well of the tetrazolium salt WST-1 was added to each well. Plates were incubated at 37°C in 5% CO₂ for 1 hour. The mitochondrial metabolite of WST-1 cleavage was detected using absorbance at a wavelength of 450 nm with the Victor² plate reader. For WST-1 cell viability assays performed in conjunction with the luciferase reporter assays, the WST-1 reagent was added to each well 1 hour prior to the cell lysis step in the dual luciferase assay instructions. For WST-1 cell viability assays performed in conjunction with the Matrigel invasion assay, cells were seeded in parallel in 96-well plates at a cell density of 4×10^4 cells per well, and subsequently assayed twenty-four hours later in the Victor² plate reader.

Matrigel Cell Invasion

PC-3 cells (2×10^5) were transferred to 24-well Matrigel inserts in low-serum DMEM medium (0.5% FBS) with DMSO or chemical compounds in the lower chamber. Low-serum DMEM medium (0.5% FBS) was added to the lower well and the invasion chambers were incubated at 37°C in 5% CO₂ for 24 hours. Inserts were fixed in methanol for 10 min and then stained for 60 min with 0.5% crystal violet in 20% methanol. After wiping the top surface of the filter with cotton swabs to remove non-invaded cells, the inserts were allowed to dry overnight. Inserts were incubated in 20% acetic acid on a plate shaker for 15 min to extract the crystal violet stain. The number of invaded cells was quantitated by measuring the absorbance of the extracted crystal violet stain at a wavelength of 595 nm with the Victor² plate reader.

Compound Synthesis and Characterization

The chemical synthesis of the analogs will be described elsewhere, in the Thesis dissertation of Jessica L. Bell (Thesis Advisor: Dr. Scott D. Larsen – Department of Medicinal Chemistry, College of Pharmacy, University of Michigan-Ann Arbor).

Results

Effect of CCG-1423 Analogs Upon the SRE.L-luciferase Response

Table 3-1 summarizes the effects of the CCG-1423 analogs upon G α_{12} Q231L stimulated SRE.L-luciferase expression in PC-3 prostate cancer cells. As expected, our original RhoA transcriptional pathway inhibitor, CCG-1423, inhibited the Rho-specific

SRE.L response with low micromolar potency (IC_{50} - 1.2 μ M) (Fig. 3-1A). It also produced significant inhibition of the constitutively active thymidine-kinase-driven *Renilla* response and the WST-1 cell viability response 44% and 41%, respectively, at the maximum concentration of 10 μ M (Table 3-1, Fig. 3-1A). Removal of the methyl group as in CCG-100596 (2-([3-tert-butyl-5-(trifluoromethyl)phenyl]formamido)oxy)-N-(4-chlorophenyl)acetamide) resulted in a half log change in the potency (IC_{50} - 4.7 μ M) and no significant improvement in selectivity (53% inhibition of TK-*Renilla*, 42% for WST-1) (Table 3-1) at a concentration of 10 μ M. At a concentration of 100 μ M, CCG-100596 was highly toxic (Table 3-1). In addition, the di-methyl analog, CCG-100689 (2-([3,5-bis(trifluoromethyl)phenyl]formamido)oxy)-N-(4-chlorophenyl)-2-methylpropanamide) does not improve potency, selectivity, or efficacy, and also is toxic at 100 μ M (Table 3-1, Fig. 3-1B-C).

By changing the reactive hydroxamate functional group within the linker region of CCG-1423 to an amide (CCG-100595 - 3-[3,5-bis(trifluoromethyl)phenyl]formamido)-N-(4-chlorophenyl)-2-methylpropanamide), we largely eliminated the toxic effect, but drastically reduced potency (IC_{50} - 62.2 μ M). However, selectivity was significantly improved at a concentration of 100 μ M (Table 3-1, Fig. 3-2A). Methyl group analogs of the amide compound (CCG-100601 - 3-[3,5-bis(trifluoromethyl)phenyl]formamido)-N-(4-chlorophenyl)butanamide; CCG-100604 - 3-[3,5-bis(trifluoromethyl)phenyl]formamido)-N-(4-chlorophenyl)-3-methylbutanamide; CCG-100598 - 2-[3-tert-butyl-5-(trifluoromethyl)phenyl]formamido)-N-(4-chlorophenyl)propanamide) did not show any

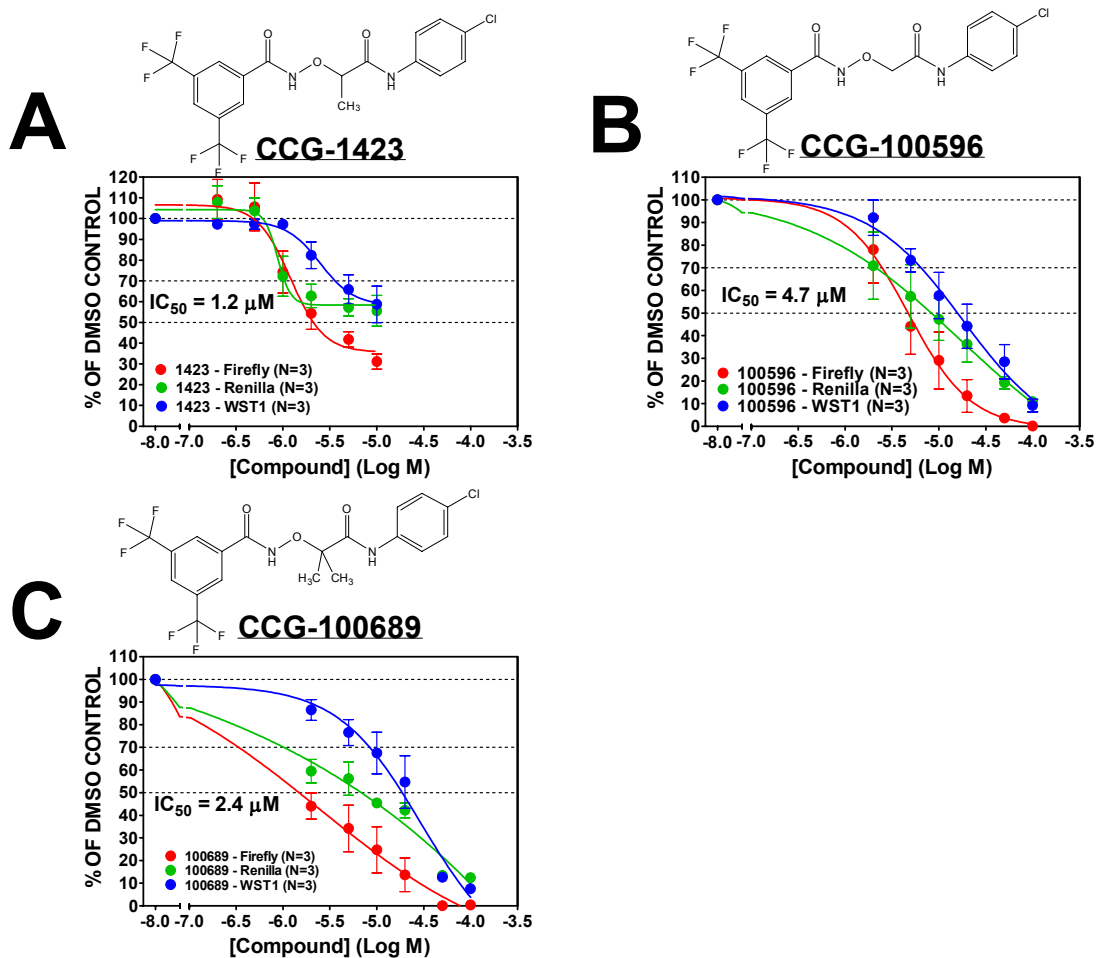


Figure 3-1. Effect of the Methyl Group Upon the SRE.L Response. Cells were co-transfected with 2 ng of the $G\alpha_{12}Q231L$ expression plasmid along with 50 ng of SRE.L and 7 ng of PRL-TK reporter plasmids as described in Materials and Methods. Cells were treated with the indicated concentrations of compounds, CCG-1423 (A), CCG-100596 (B), and CCG-100689 (C), for 19 h after transfection before lysis and reading luminescence in the plate reader as described in Materials and Methods. Just before lysis cell viability was measured by absorbance in the plate reader as described in the Materials and Methods. The pcDNA3.1-zeo expression plasmid was used as carrier DNA in all experiments. Data are graphed as a percentage of the DMSO-negative control. Each data point represents the mean \pm SEM of three separate experiments done in triplicate. For the firefly luciferase, data with reporter alone (i.e., without activator) were subtracted.

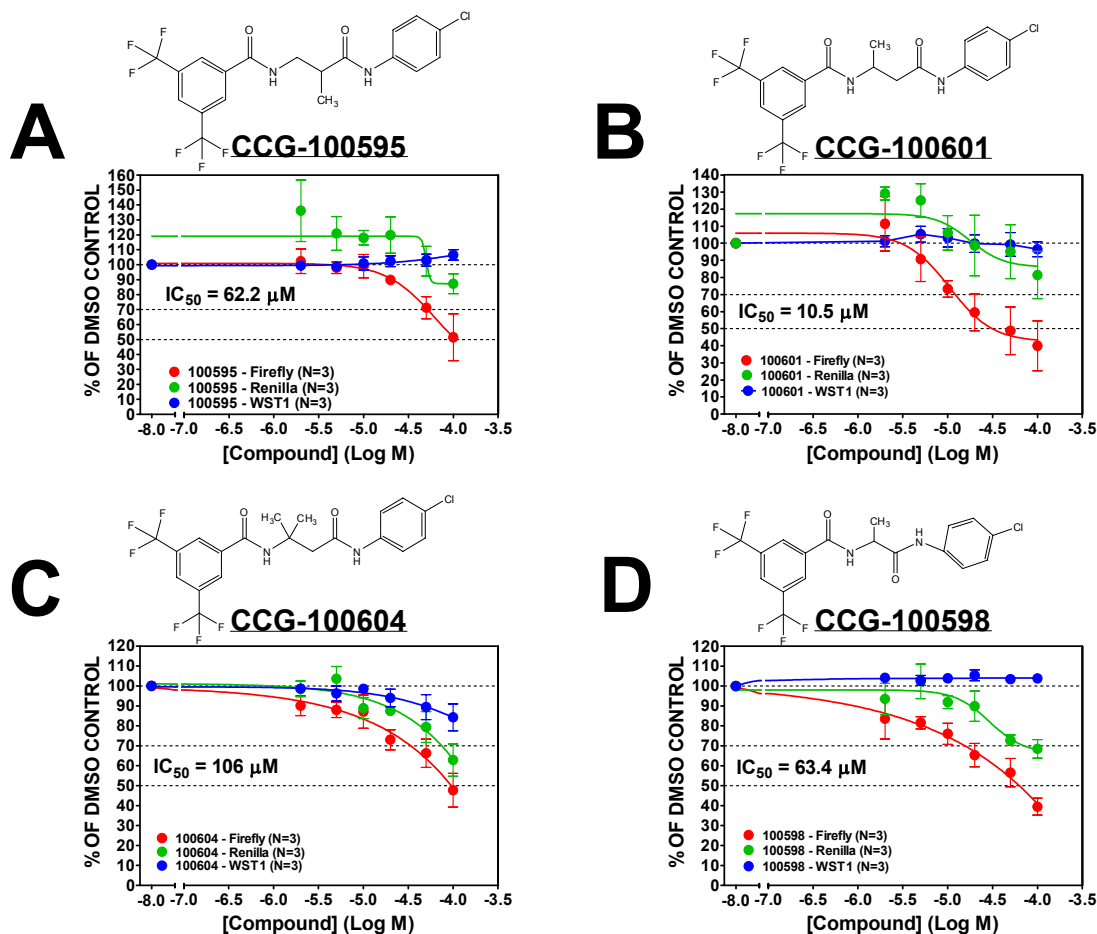


Figure 3-2. Effect of the Removal of the Hydroxamate Group and the Methyl Group Position Upon the SRE.L Response. Cells were co-transfected with 2 ng of the $\text{G}\alpha_{12}\text{Q231L}$ expression plasmid along with 50 ng of SRE.L and 7 ng of PRL-TK reporter plasmids as described in Materials and Methods. Cells were treated with the indicated concentrations of compounds, CCG-100595 (A), CCG-100601 (B), CCG-100604 (C), and CCG-100598 (D), for 19 h after transfection before lysis and reading luminescence in the plate reader as described in Materials and Methods. Just before lysis cell viability was measured by absorbance in the plate reader as described in the Materials and Methods. The pcDNA3.1-zeo expression plasmid was used as carrier DNA in all experiments. Data are graphed as a percentage of the DMSO-negative control. Each data point represents the mean \pm SEM of three separate experiments done in triplicate. For the firefly luciferase, data with reporter alone (i.e., without activator) were subtracted.

improvement in potency or selectivity in comparison to CCG-100595 (Fig. 3-2). Interestingly, these methyl group analogs also have very low toxicity (< 16% inhibition of WST1 at 100 μ M) with reasonable SRE.L-luciferase inhibition (60% - CCG-100601, -100598 and 52% - CCG-100604), which is consistent with our hypothesis that the hydroxamate functional group is the major cause of toxicity (Fig. 3-2B-D).

In our original publication (26), we identified two compounds, CCG-1423 and CCG-977, which contained two identical R₁ and R₂ functional groups, but distinct linkers. Therefore, we tested the importance of these two functional groups (a 2,4-bis-trifluoro-phenyl and 3-chlorophenyl) using the SRE.L-luciferase reporter assay. We chose to use CCG-100596 as our parental compound rather than CCG-1423 in order to simplify the synthetic scheme (Fig. 3-3). Removal of the two trifluoro functional groups from the phenyl ring, CCG-100701 (N-(4-chlorophenyl)-2-[(phenylformamido)oxy]acetamide), completely abolished both the SRE.L and WST-1 cell viability responses (Table 3-1, Fig. 3-3B). Interestingly, TK-*Renilla* expression was stimulated by CCG-100701 (Table 3-1, Fig. 3-3B). Removal of one of the bis-trifluoro groups (CCG-101202 -N-(4-chlorophenyl)-2-([3-(trifluoromethyl)phenyl]formamido)oxy)acetamide; CCG-100723 -N-(4-chlorophenyl)-2-([4-(trifluoromethyl)phenyl]formamido)oxy)acetamide) reduces potency (IC₅₀, 52 and 29 μ M, respectively) (Fig. 3-3C-D). The compounds are also less efficacious on SRE.L-luciferase, but are more selective with respect to the TK-*Renilla* response in comparison to CCG-100596 (Table 3-1, Fig. 3-3A,B-D). Removal of the chloro-group on the phenyl ring, CCG-100703 (2-([3,5-bis(trifluoromethyl)phenyl]formamido)oxy)-N-phenylacetamide), did not completely abolish activity, but reduced potency, efficacy, and selectivity in comparison to CCG-100596 (Table 3-1, Fig. 3-

3A,E). Movement of the p-chloro-group to the meta position (CCG-101200 - 2-([3,5-bis(trifluoromethyl)phenyl]formamido)oxy)-N-(3-chlorophenyl)acetamide) did not have any significant effect upon potency, selectivity, or efficacy in comparison to CCG-100596 (Table 3-1, Fig. 3-3A,F). Therefore, the bis-trifluoro-phenyl functional group is more important for activity, than the chloro-phenyl group.

We also hypothesized that the length of the linker region of CCG-1423 would be critical for its inhibitory activity. Therefore, we utilized the amide analog (CCG-100594) to assess the importance of length of the linker region (Fig. 3-4). We found that reducing the number of carbons to one (CCG-100600 - (2-([3,5-bis(trifluoromethyl)phenyl]formamido)-N-(4-chlorophenyl)acetamide) or increasing the number of carbons to three (CCG-100597 - 4-([3-tert-butyl-5-(trifluoromethyl)phenyl]formamido)-N-(4-chlorophenyl)butanamide) did not significantly affect potency, efficacy, or selectivity (Table 3-1, Fig. 3-4A,C). However, increasing the number of carbons to four (CCG-100686 - 5-([3,5-bis(trifluoromethyl)phenyl]formamido)-N-(4-chlorophenyl)pentanamide) dramatically reduced activity (< 12% inhibition at 100 μ M) (Table 3-1, Fig. 3-4D). As a result, a four carbon linker region results in loss of activity due to either lack of permeability or loss of interaction of the compound with its molecular target.

We next hypothesized that conformationally restricting the linker region through introducing a piperidine ring, pyrrolidine ring, or phenyl ring would improve potency, selectivity, and efficacy. The two piperidine ring analogs, CCG-100602 (1-([3,5-bis(trifluoromethyl)phenyl]carbonyl)-N-(4-chlorophenyl)piperidine-3-carboxamide) and

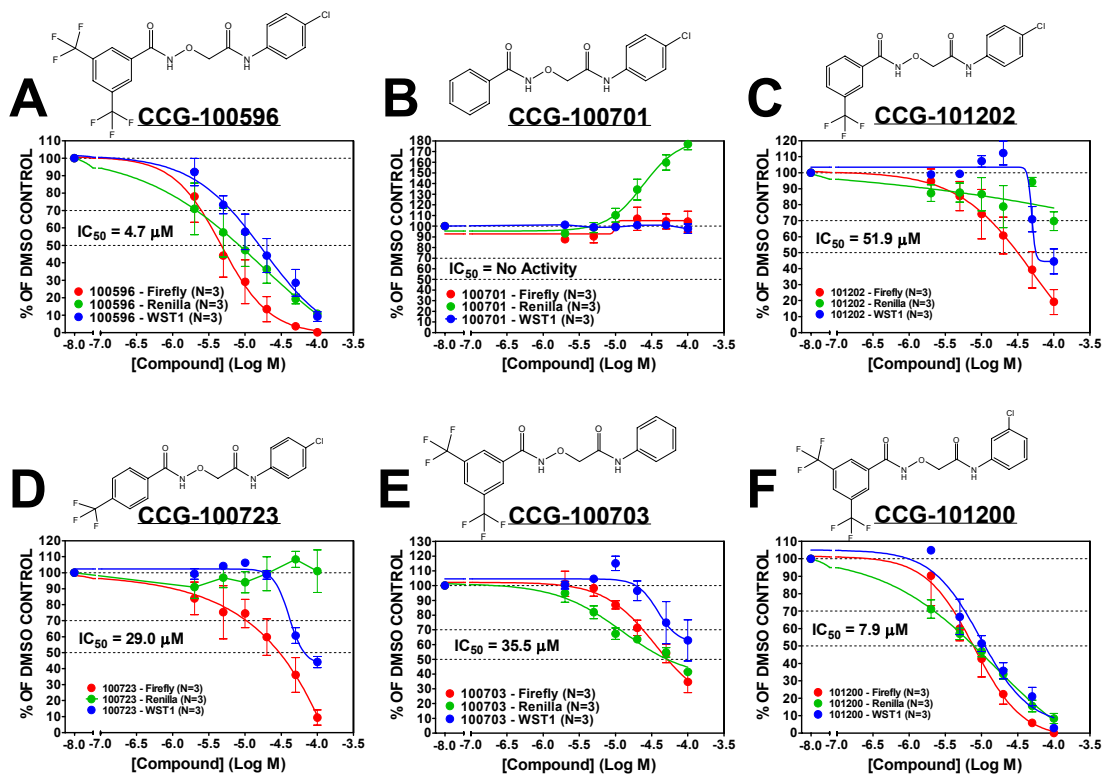


Figure 3-3. Effects of the R-groups Upon the SRE.L Response. Cells were co-transfected with 2 ng of the $Ga_{12}Q231L$ expression plasmid along with 50 ng of SRE.L and 7 ng of PRL-TK reporter plasmids as described in Materials and Methods. Cells were treated with the indicated concentrations of compounds, CCG-100596 (A), CCG-100701 (B), CCG-101202 (C), CCG-100723 (D), CCG-100703 (E), and CCG-101200 (F), for 19 h after transfection before lysis and reading luminescence in the plate reader as described in Materials and Methods. Just before lysis cell viability was measured by absorbance in the plate reader as described in the Materials and Methods. The pcDNA3.1-zeo expression plasmid was used as carrier DNA in all experiments. Data are graphed as a percentage of the DMSO-negative control. Each data point represents the mean \pm SEM of three separate experiments done in triplicate. For the firefly luciferase, data with reporter alone (i.e., without activator) were subtracted.

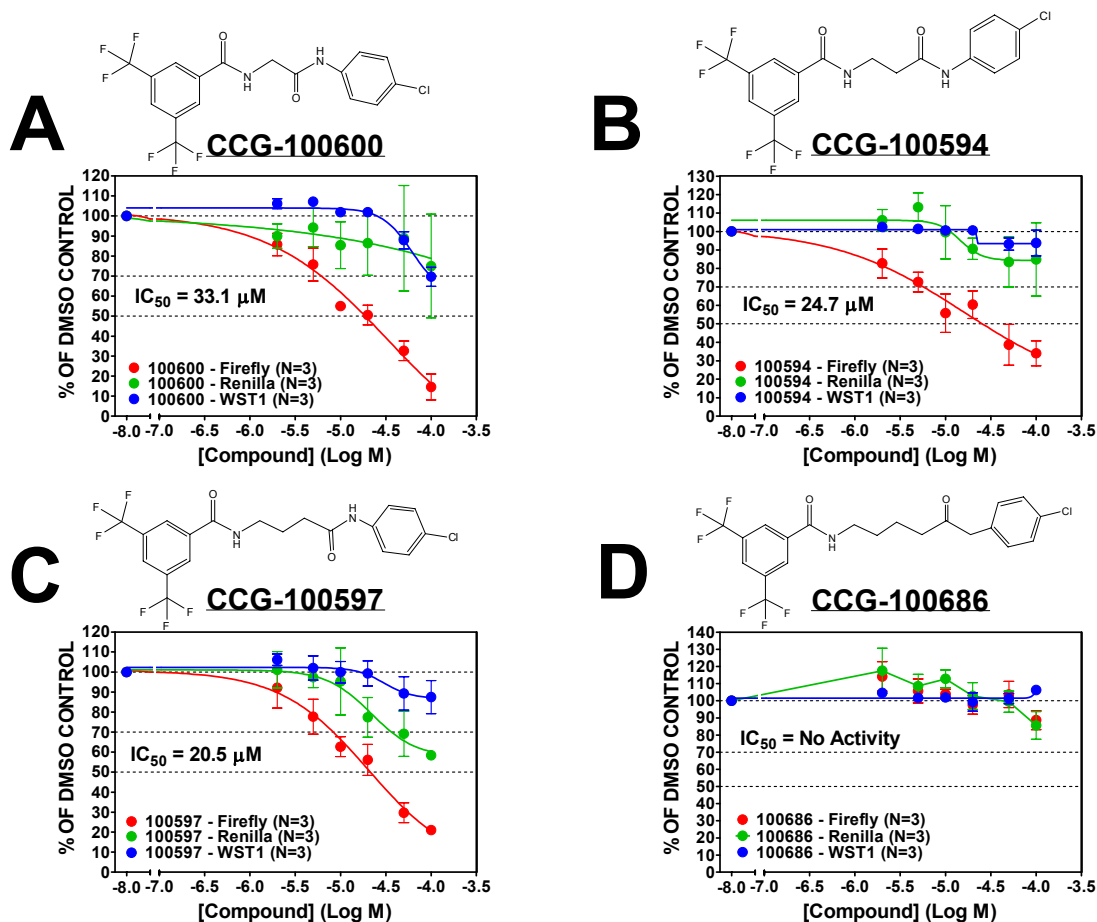


Figure 3-4. Dose-Dependent Inhibition of the SRE.L Response by the Amide Class of CCG-1423 Analogs. Cells were co-transfected with 2 ng of the $G\alpha_{12}Q231L$ expression plasmid along with 50 ng of SRE.L and 7 ng of PRL-TK reporter plasmids as described in Materials and Methods. Cells were treated with the indicated concentrations of compounds, CCG-100600 (A), CCG-100594 (B), CCG-100597 (C), and CCG-100686 (D), for 19 h after transfection before lysis and reading luminescence in the plate reader as described in Materials and Methods. Just before lysis cell viability was measured by absorbance in the plate reader as described in the Materials and Methods. The pcDNA3.1-zeo expression plasmid was used as carrier DNA in all experiments. Data are graphed as a percentage of the DMSO-negative control. Each data point represents the mean \pm SEM of three separate experiments done in triplicate. For the firefly luciferase, data with reporter alone (i.e., without activator) were subtracted.

CCG-100690 (1-{{[3,5-bis(trifluoromethyl)phenyl]carbonyl}}-N-(4-chlorophenyl)piperidine-4-carboxamide), both significantly improved selectivity and reduced toxicity (< 39% inhibition – WST-1) in comparison to CCG-1423 (Table 3-1, Fig. 3-5A-B). In addition, the piperidine ring analogs improved efficacy (CCG-100602: 75.4% SRE.L-Luc. inhib. at 100 μM, CCG-100690: 81.8% SRE.L-Luc inhib. at 100 μM) in comparison to the amide analogs, CCG-100595 and CCG-100594 (Table 3-1, Fig. 3-5A-B). The pyrrolidine ring analog, CCG-100692 (1-{{[3,5-bis(trifluoromethyl)phenyl]carbonyl}}-N-(4-chlorophenyl)pyrrolidine-2-carboxamide), improved selectivity and reduced toxicity in comparison to CCG-1423, but only significantly improved efficacy (83.2% SRE.L-Luc. inhib.) in comparison to the amide analogs (Table 3-1, Fig. 3-5C). However, the other pyrrolidine ring analog which constrains the chloro-phenyl group, CCG-102443 (N-(3-(5-chloroindolin-1-yl)-3-oxopropyl)-3,5-bis(trifluoromethyl)benzamide), improved selectivity in comparison to CCG-1423 and abrogated toxicity. CCG-102443 did improve potency in comparison to the amide analogs, but did not improve selectivity or efficacy (Table 3-1, Fig. 3-5D). Interestingly, the phenyl ring linker analogs had varying effects upon activity. CCG-101343 (N-(3-(4-chlorophenylcarbamoyl)phenyl)-3,5-bis(trifluoromethyl)benzamide), with a meta-substitution markedly improved potency back to the one micromolar range, but did not improve toxicity in comparison to CCG-1423 (Table 3-1, Fig. 3-6A). In addition, CCG-101343 initially decreased, but then increased the TK-*Renilla* expression linker analog, CCG-101329 (N-(4-(4-chlorophenylcarbamoyl)phenyl)-3,5-bis(trifluoromethyl)benzamide), was completely inactive, whereas the ortho-analog, CCG-101433 (N-(2-(4-chlorophenylcarbamoyl)phenyl)-3,5-

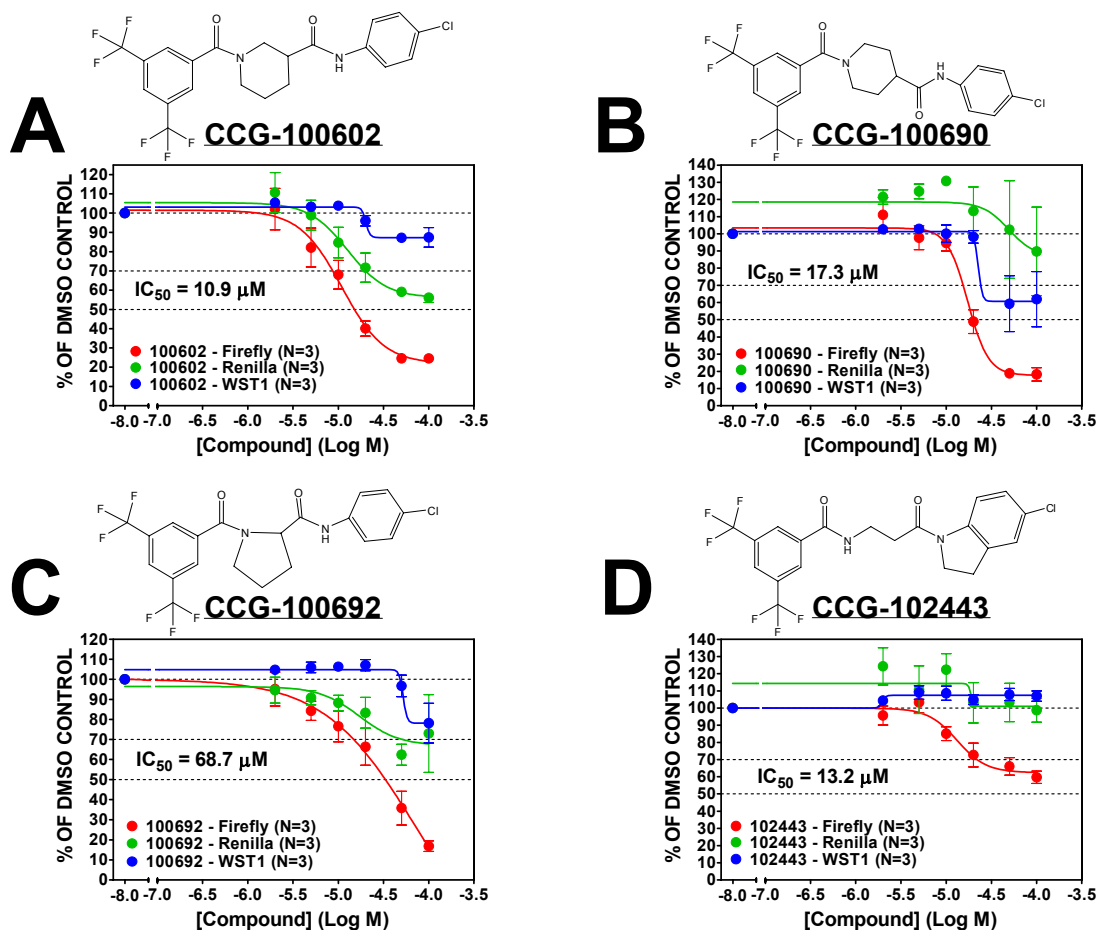


Figure 3-5. Dose-Dependent Inhibition of the SRE.L Response by the Conformationally Restrictive Class of CCG-1423 Analogs. Cells were co-transfected with 2 ng of the $G\alpha_{12}Q231L$ expression plasmid along with 50 ng of SRE.L and 7 ng of PRL-TK reporter plasmids as described in Materials and Methods. Cells were treated with the indicated concentrations of compounds, CCG-100602 (A), CCG-100690 (B), CCG-100692 (C), and CCG-102443 (D), for 19 h after transfection before lysis and reading luminescence in the plate reader as described in Materials and Methods. Just before lysis cell viability was measured by absorbance in the plate reader as described in the Materials and Methods. The pcDNA3.1-zeo expression plasmid was used as carrier DNA in all experiments. Data are graphed as a percentage of the DMSO-negative control. Each data point represents the mean \pm SEM of three separate experiments done in triplicate. For the firefly luciferase, data with reporter alone (i.e., without activator) were subtracted.

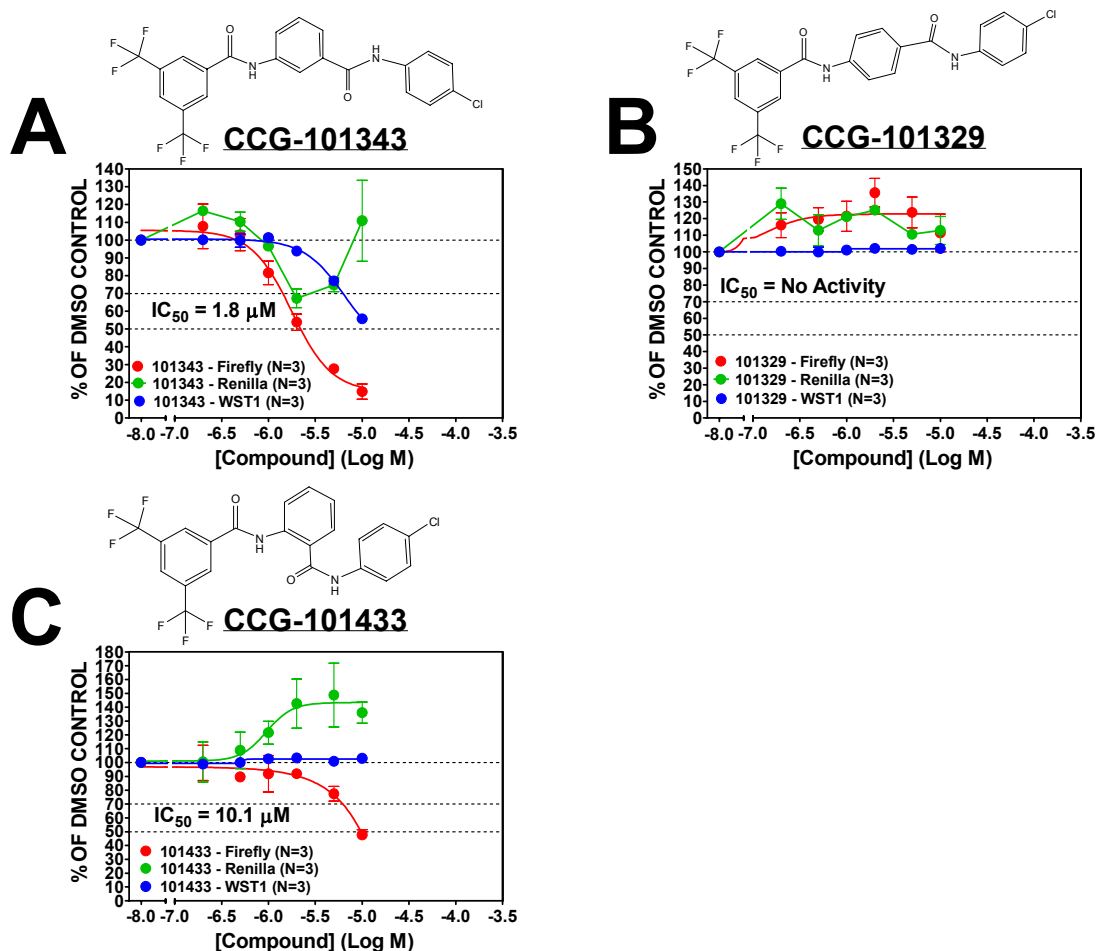


Figure 3-6. Dose-Dependent Inhibition of the SRE.L Response by the Conformationally Restrictive Class of CCG-1423 Analogs. Cells were co-transfected with 2 ng of the $G\alpha_{12}Q231L$ expression plasmid along with 50 ng of SRE.L and 7 ng of PRL-TK reporter plasmids as described in Materials and Methods. Cells were treated with the indicated concentrations of compounds, CCG-101343 (A), CCG-101329 (B), and CCG-101433 (C), for 19 h after transfection before lysis and reading luminescence in the plate reader as described in Materials and Methods. Just before lysis cell viability was measured by absorbance in the plate reader as described in the Materials and Methods. The pcDNA3.1-zeo expression plasmid was used as carrier DNA in all experiments. Data are graphed as a percentage of the DMSO-negative control. Each data point represents the mean \pm SEM of three separate experiments done in triplicate. For the firefly luciferase, data with reporter alone (i.e., without activator) were subtracted.

bis(trifluoromethyl)benzamide), did not improve selectivity or efficacy in comparison to CCG-1423 or the amide analogs (Table 3-1, Fig. 3-6B-C). In addition, CCG-101433 increased the TK-*Renilla* expression in a similar manner to CCG-100701 (Fig. 3-6C). Overall, the conformationally restricted class of analogs improved selectivity and efficacy in comparison to CCG-1423 and the amide analogs.

In order to further improve activity, we hypothesized that removal of one or both amide groups would improve permeability of the compounds. Replacement of the amide groups nearest the chloro-phenyl with an amine, CCG-101425 (N-(3-(4-chlorophenylamino)propyl)-3,5-bis(trifluoromethyl)benzamide), markedly enhanced potency and slightly improved efficacy in comparison to CCG-1423 with reduced toxicity (IC₅₀ – 4.9 μM, 73.3% inhib. of SRE.L-luc. at 10 μM, 77.6% inhib. of SRE.L-luc up to 100 μM, < 5% Inhib. of WST1 up to 100 μM) (Table 3-1, Fig. 3-7A). However, replacement of the amide group nearest the bis-trifluoro-phenyl group (CCG-102585–3-(3,5-bis(trifluoromethyl)benzylamino)-N-(4-chlorophenyl)propanamide) or replacement of both amide groups (CCG-102532–N1-(3,5-bis(trifluoromethyl)benzyl)-N3-(4-chlorophenyl)propane-1,3-diamine) resulted in similar potency (CCG-102585 – IC₅₀ – 8.3 μM; CCG-102532 – IC₅₀ - 9.1 μM) and efficacy at 10 μM (CCG-102585 – 59.0% inhib.; CCG-102532 – 65.2% inhib.) in comparison to CCG-101425 (Table 3-1, Fig. 3-7), but the selectivity of CCG-102585 and CCG-102532 suffered. Concentrations greater than 10 μM resulted in extreme toxicity of the cells (Table 3-1, Fig. 3-7B-C). Other amide replacement analogs (CCG-101325-N-(2-((4-chlorophenyl)(methyl)amino)-2-oxoethoxy)-3,5-bis(trifluoromethyl)benzamide ; CCG-101435-N-(3-((4-chlorophenyl)(methyl)amino)-3-oxopropyl)-3,5-bis(trifluoromethyl)benzamide; 102441-

(3,5-bis(trifluoromethyl)phenyl)(4-(4-chlorophenylamino)piperidin-1-yl)methanone;
CCG-102445–N-((2-(4-chlorophenyl)thiazol-4-yl)methyl)bis(trifluoromethyl)benzamide;
CCG-102447–N-(3-(4-chlorophenoxy)propyl)-3,5-bis(trifluoromethyl)benzamide) did not show significant improvement of potency, selectivity, or efficacy in comparison to the amide analogs or the other analogs within their class (Table 3-1, Fig. 3-8). Nevertheless, the amine replacement analogs (e.g. CCG-101425) represent our most promising group of compounds to date with low micromolar potency and improved selectivity compared to both CCG-1423 and the amide analogs.

CCG-1423, along with several of our analogs, contains a chiral center, so we hypothesized that some of our compounds may show stereoselectivity, which could improve potency, selectivity, toxicity, and efficacy. Therefore, enantiomers were synthesized for the following compounds: CCG-100598 (CCG-100599–(S)-N-(1-(4-chlorophenylamino)-1-oxopropan-2-yl)-3,5-bis(trifluoromethyl)benzamide; CCG-100603–(R)-N-(1-(4-chlorophenylamino)-1-oxopropan-2-yl)-3,5-bis(trifluoromethyl)benzamide), CCG-100601 (CCG-100709–(S)-N-(4-(4-chlorophenylamino)-4-oxobutan-2-yl)-3,5-bis(trifluoromethyl)benzamide; CCG-100711(R)-N-(4-(4-chlorophenylamino)-4-oxobutan-2-yl) 3,5-bis(trifluoromethyl)benzamide), and CCG-100602 (CCG-100687-(R)-1-(3,5-bis(trifluoromethyl)benzoyl)-N-(4-chlorophenyl)piperidine-3-carboxamide; CCG-100688-(S)-1-(3,5-bis(trifluoromethyl)benzoyl)-N-(4-chlorophenyl)piperidine-3-

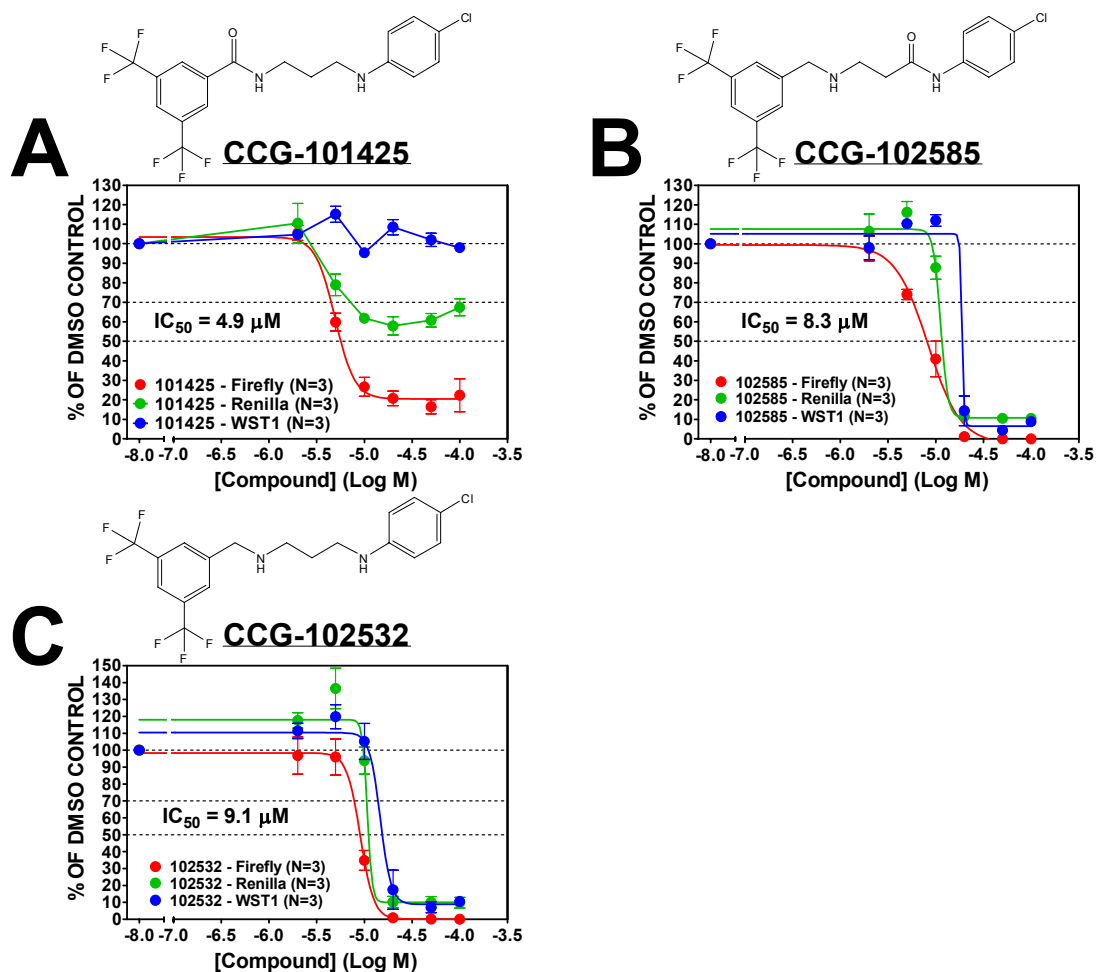


Figure 3-7. Dose-Dependent Inhibition of the SRE.L Response by the Amide Replacement Class of CCG-1423 Analogs. Cells were co-transfected with 2 ng of the $G\alpha_{12}Q231L$ expression plasmid along with 50 ng of SRE.L and 7 ng of PRL-TK reporter plasmids as described in Materials and Methods. Cells were treated with the indicated concentrations of compounds, CCG-101425 (A), CCG-102585 (B), and CCG-102532 (C), for 19 h after transfection before lysis and reading luminescence in the plate reader as described in Materials and Methods. Just before lysis cell viability was measured by absorbance in the plate reader as described in the Materials and Methods. The pcDNA3.1-zeo expression plasmid was used as carrier DNA in all experiments. Data are graphed as a percentage of the DMSO-negative control. Each data point represents the mean \pm SEM of three separate experiments done in triplicate. For the firefly luciferase, data with reporter alone (i.e., without activator) were subtracted.

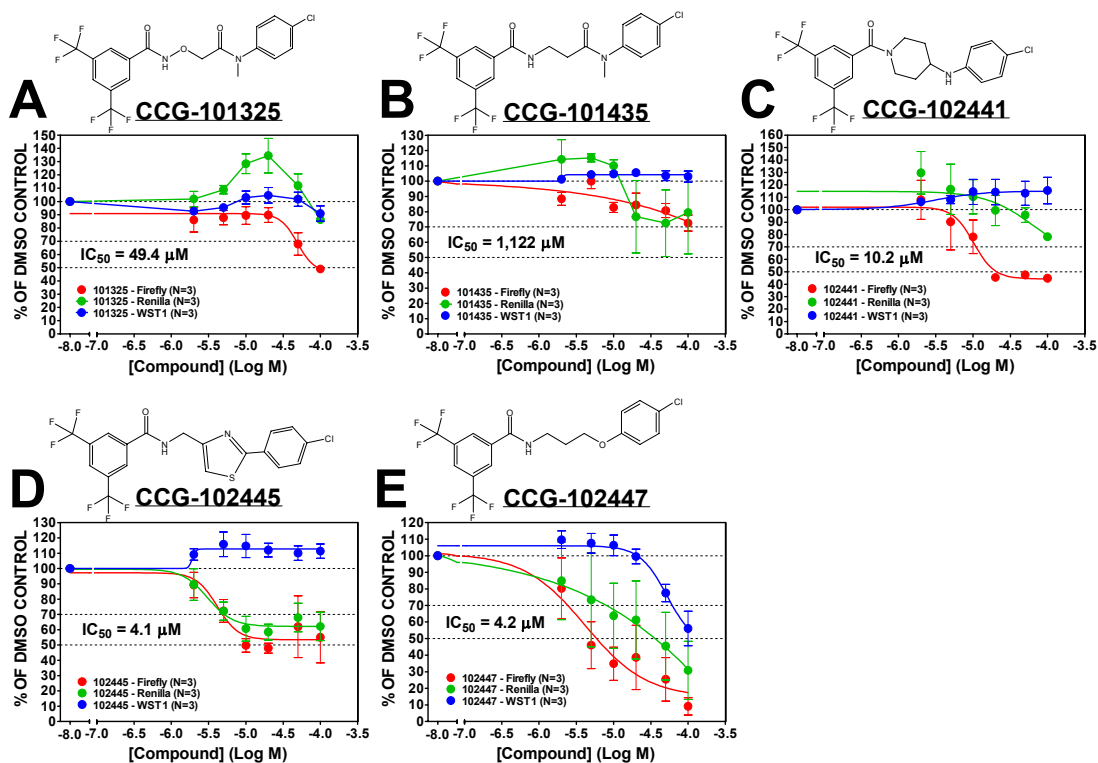


Figure 3-8. Dose-Dependent Inhibition of the SRE.L Response by the Amide Replacement Class of CCG-1423 Analogs. Cells were co-transfected with 2 ng of the $G\alpha_{12}Q231L$ expression plasmid along with 50 ng of SRE.L and 7 ng of PRL-TK reporter plasmids as described in Materials and Methods. Cells were treated with the indicated concentrations of compounds, CCG-101325 (A), CCG-101435 (B), CCG-102441 (C), CCG-102445 (D), and CCG-102447 (E), for 19 h after transfection before lysis and reading luminescence in the plate reader as described in Materials and Methods. Just before lysis cell viability was measured by absorbance in the plate reader as described in the Materials and Methods. The pcDNA3.1-zeo expression plasmid was used as carrier DNA in all experiments. Data are graphed as a percentage of the DMSO-negative control. Each data point represents the mean \pm SEM of three separate experiments done in triplicate. For the firefly luciferase, data with reporter alone (i.e., without activator) were subtracted.

carboxamide). However, none of these analogs showed any stereo-selectivity (Table 3-1).

In addition, reverse analogs were synthesized for several analogs by swapping the bis-trifluoro-phenyl and chloro-phenyl groups to assess the importance of the position of these groups upon activity. Therefore, these groups were swapped for CCG-100690 (CCG-100721–N-(3,5-bis(trifluoromethyl)phenyl)-1-(4-chlorobenzoyl)piperidine-4-carboxamide) and CCG-100596 (CCG-100691–N-(2-(3,5-bis(trifluoromethyl)phenylamino)-2-oxoethoxy)-4-chlorobenzamide), but neither of these analogs showed any significant difference in their activity profiles in comparison to their parental compounds (Table 3-1).

Toxicity Assesment of the CCG-1423 Analogs

Since all of the functional transcriptional reporter studies were performed in the highly-metastatic and hormone-independent PC-3 prostate cancer cell line, it is possible that the toxicity we observe could be cell line selective due to a pathway-specific mechanism. Therefore, we tested the effect of the CCG-1423 and its analogs upon cell survival of a normal epithelial prostate cell line, RWPE-1, and a hormone-dependent epithelial prostate cancer cell line, LNCaP in addition to the hormone-independent epithelial prostate cancer cell line, PC-3, under low serum conditions for twenty-four hours. We observed no major selectivity for cell survival across the prostate epithelial cell lines with CCG-1423, the toxic hydroxamate analogs, or toxic conformationally restrictive analogs (Table 3-2). Therefore, the cell toxicity that we observe with CCG-1423 and our toxic analogs is not due to a pathway-specific mechanism, but rather a

general non-specific toxicity most likely due to the chemical structures of the compounds.

Effect of CCG-1423 Analogs Upon PC-3 cell Matrigel Invasion

In Chapter 2 and our original publication, we showed that CCG-1423 selectively inhibited spontaneous PC-3 prostate cancer cell invasion through a Matrigel matrix, but did not inhibit $G\alpha_i$ -dependent lysophosphatidic acid stimulated SKOV-3 ovarian cancer cell invasion through Matrigel, *in vitro* (26). Therefore, we tested several classes of our analogs for their ability to inhibit PC-3 prostate cancer cell Matrigel invasion and tested for selectivity for invasion versus toxicity in comparison to CCG-1423. Removal of the hydroxamate group or the methyl group (CCG-100595 and CCG-100596) did not significantly improve selectivity for the Matrigel invasion inhibition (Table 3-3). The amide class of analogs (CCG-100600, CCG-100594, CCG-100597, CCG-100686) showed improved selectivity, but were not as efficacious as CCG-1423 (Table 3-3). Interestingly, CCG-100686, which was inactive in the Rho-specific SRE.L reporter assay, showed modest activity (25.3% inhib. at 100 μ M) in the Matrigel invasion assay. Overall, the conformationally restrictive class of analogs (CCG-100602, CCG-100690, CCG-100692, CCG-102443, CCG-101343, and CCG-101329) showed a similar activity profile in the Matrigel invasion assay as in the Rho-specific SRE.L reporter assay (Fig. 3-1). In addition, the conformationally restrictive class of analogs showed better selectivity and similar efficacy in comparison to CCG-1423 in the Matrigel invasion assay (Table 3-3). The amide replacement class of analogs (CCG-102441, CCG-102445, CCG-102447, CCG-101425, CCG-102585, and CCG-102532) also showed a similar activity profile in

the Matrigel invasion assay as in the Rho-specific SRE.L reporter assay (Table 3-1, Table 3-3, Fig. 3-1). This class of analogs showed the best selectivity and improved efficacy in comparison to CCG-1423 in the Matrigel invasion assay. Within this class of compounds, CCG-101425 shows the best activity and selectivity to date. In general, the analogs tested in the PC-3 cell Matrigel invasion assay showed similar activity profiles in comparison to the Rho-specific SRE.L-luciferase reporter assay (Fig. 3-1) and improved selectivity in comparison to CCG-1423 in the Matrigel invasion assay.

Discussion

In the structure-activity relationship study described here, we were able to improve selectivity, efficacy, and reduce toxicity, but not improve potency in comparison to our originally identified RhoA transcriptional signaling pathway inhibitor, CCG-1423. By removing the biologically reactive hydroxamate functional group, we were able to reduce toxicity, but not improve potency or efficacy with the amide or methyl amide class of analogs. However, given that most of our studies were performed in the aggressive metastatic PC-3 prostate cancer cell line, it is possible that the toxicity we see with the hydroxamate compound could be due to a RhoA transcriptional signaling pathway-dependent mechanism. This would be consistent with the concept of “oncogene addiction” in the field of cancer, where cancer cells are dependent upon a particular oncogene for their survival (30). However, we found this phenomenon not to apply to the toxic compounds studied here, since there was no selectivity across a panel of prostate epithelial cell lines, including PC-3 cells along with the low metastatic LNCaP cell line and the normal RWPE-1 cell line.

In addition, in this study, we found that the maximum length of the carbon linker for the amide class of compounds in the SRE.L-luciferase reporter assay was three carbons. Four carbons proved to be too long and resulted in a complete loss of inhibitory activity. This could be a result of a lack of permeability or loss of binding of the compound to its molecular target. Interestingly, in the PC-3 prostate cancer cell Matrigel invasion assay, the three carbon amide had limited inhibitory activity, whereas the four carbon amide showed modest inhibitory activity. A possible explanation for the discrepancy of results between the assays could be mechanistic. In addition to the RhoA transcriptional signaling pathway, it is possible that there are multiple mechanisms to inhibit PC-3 cell Matrigel invasion. Therefore, the four carbon linker amide could have an extracellular and receptor-dependent mechanism of inhibition of the PC-3 cell Matrigel invasion, which is not dependent upon the RhoA transcriptional signaling pathway.

Overall, we found the conformationally restrictive class of analogs to be less toxic, more selective, and more efficacious than CCG-1423 and the amide class of analogs in both the Rho-specific SRE.L luciferase reporter assay and the PC-3 cell Matrigel invasion assay. A few of piperidine and pyrrolidine ring analogs showed some toxicity across the panel of prostate cell lines at higher doses. This could potentially be due to a general off-target toxic effect. In addition, the phenyl ring linker analog, CCG-101343, showed similar toxicity across cell lines to CCG-1423. It is unclear why this analog shows toxicity, but it could potentially be targeting a similar mechanism as CCG-1423 for its toxic effect.

In our previous study (26), we found that the bis-trifluoro-phenyl and chloro-phenyl functional groups were identical in both of the RhoA transcriptional pathway inhibitors that we identified (CCG-1423 and CCG-977). Therefore, in the present study, we investigated the importance of these functional groups. We found that the bis-trifluoro-phenyl group to be critical for activity, with the chloro phenyl group being less so. Therefore, there could potentially be future SAR studies with modifications of the chloro-phenyl group with maintenance of the bis-trifluoro-phenyl group. Interestingly, we also found that swapping the bis-trifluoro-phenyl and chloro phenyl groups with one another had no effect upon activity. Also, surprisingly, there was no stereoselectivity observed with the enantiomers synthesized in this study.

Our most promising class of analogs in this study proved to be the amide replacement class of analogs. This class of analogs returned potency to a low micromolar range similar to that of CCG-1423, and showed improved selectivity and reduced toxicity. A possible explanation for the dramatic improvement in activity with this class of analogs could be due to improved cell permeability due to the removal of one or both of the amide groups. CCG-101425 is the most promising analog to date within this class of analogs showing the best potency, selectivity, and improved toxicity out of all the analogs in both the Rho-specific SRE.L-luciferase assay and the PC-3 cell Matrigel invasion assay. This compound along with a few others within the amide replacement class of analogs and the conformationally restrictive class of analogs should serve as promising lead compounds for both future mechanistic and *in vivo* xenograft studies for the continued development of a cancer therapeutic.

<u>Compound</u>	<u>Structure</u>	<u>SRE1-C₅₀</u> ($\mu\text{mol/L}$)	<u>Hill</u> <u>Slope</u>	<u>SRE1-</u> <u>Efficacy</u> (10 $\mu\text{mol/L}$)	<u>PR1-TK</u> <u>Efficacy</u> (10 $\mu\text{mol/L}$)	<u>WST1-</u> <u>Efficacy</u> (10 $\mu\text{mol/L}$)	<u>SRE1-</u> <u>Efficacy</u> (100 $\mu\text{mol/L}$)	<u>PR1-TK</u> <u>Efficacy</u> (100 $\mu\text{mol/L}$)	<u>WST1-</u> <u>Efficacy</u> (100 $\mu\text{mol/L}$)
1423		1.2	-2.5	68.8	44.0	41.3	ND ²	ND ²	ND ²
100595		62.2	-1.6	0.9	-18.1	-0.9	48.5	12.7	-6.6
100596		4.7	-1.3	70.9	52.8	42.3	99.9	89.1	90.8
100594		24.7	-0.5	44.2	0.4	-0.5	66.0	15.2	6.2
100701		NA ¹	NA ¹	0.2	-10.2	0.9	-4.3	-76.9	2.4
100703		35.5	-1.2	13.1	32.6	-15.1	65.3	58.5	37.2
101202		51.9	-0.8	25.9	13.4	-7.2	80.2	30.2	55.5
100723		29.0	-1.2	25.5	6.0	-6.2	90.6	-0.9	55.9
101200		7.9	-1.3	57.4	53.1	48.6	99.9	91.6	97.1

Compound	Structure	SRE1-G ₅₀ ($\mu\text{mol/L}$)	Hill Slope	SRE1- Efficacy (10 $\mu\text{mol/L}$)	PR1-TK Efficacy (10 $\mu\text{mol/L}$)	WST1- Efficacy (10 $\mu\text{mol/L}$)	SRE1- Efficacy (100 $\mu\text{mol/L}$)	PR1-TK Efficacy (100 $\mu\text{mol/L}$)	WST1- Efficacy (100 $\mu\text{mol/L}$)
100689		2.4	-0.4	75.3	54.6	32.5	99.6	87.5	92.5
100601		10.5	-1.8	26.7	-6.1	-3.2	60.0	18.6	3.5
100604		106	-0.7	12.9	11.1	1.4	52.3	37.1	15.7
100598		63.4	-0.6	24.0	8.0	-3.8	60.5	31.5	-3.8
100600		33.1	-0.6	45.0	14.6	-2.0	85.4	25.0	30.3
100597		20.5	-0.9	37.3	4.7	0.1	78.9	41.6	12.5
100686		NA ¹	NA ¹	-3.8	-12.7	-1.9	11.3	14.4	-6.2
100602		10.9	-1.9	32.0	15.3	-3.9	75.4	44.0	12.5
100690		17.3	-3.8	5.3	-30.7	-0.1	81.8	10.2	38.0

Compound	Structure	SRE1-G₅₀ ($\mu\text{mol/L}$)	Hill Slope	SRE1- Efficacy (10 $\mu\text{mol/L}$)	PR1-TK Efficacy (10 $\mu\text{mol/L}$)	WST1- Efficacy (10 $\mu\text{mol/L}$)	SRE1- Efficacy (100 $\mu\text{mol/L}$)	PR1-TK Efficacy (100 $\mu\text{mol/L}$)	WST1- Efficacy (100 $\mu\text{mol/L}$)
100692		68.7	-0.9	23.4	11.7	-6.3	83.2	27.0	38.0
101343		1.8	-2.0	85.1	-10.8	44.2	ND ²	ND ²	ND ²
101329		NA ¹	NA ¹	-11.5	-13.0	-2.1	ND ²	ND ²	ND ²
101433		10.1	-1.9	52.2	-36.0	-3.0	ND ²	ND ²	ND ²
102443		13.2	-2.7	14.9	-22.4	-8.6	40.3	1.3	-7.0
101325		49.4	-3.8	10.5	-28.4	-3.0	51.0	13.7	9.1
101435		1122	-0.4	17.3	-10.0	-4.7	27.5	20.6	-3.0
102441		10.2	-3.1	21.8	-10.4	-14.4	55.1	21.8	-15.4
102445		4.1	-3.1	50.2	39.3	-14.8	44.9	37.8	-11.4

Compound	Structure	SRE1-G ₅₀ ($\mu\text{mol/L}$)	Hill Slope	SRE1- Efficacy (10 $\mu\text{mol/L}$)	PR1-TK Efficacy (10 $\mu\text{mol/L}$)	WST1- Efficacy (10 $\mu\text{mol/L}$)	SRE1- Efficacy (100 $\mu\text{mol/L}$)	PR1-TK Efficacy (100 $\mu\text{mol/L}$)	WST1- Efficacy (100 $\mu\text{mol/L}$)
102447		4.2	-1.0	65.2	36.2	-6.4	90.9	69.2	43.8
101425		4.9	-4.2	73.3	38.2	4.6	77.6	32.6	2.0
102585		8.3	-2.5	59.0	12.2	-12.0	99.9	89.5	91.2
102532		9.1	-6.1	65.2	6.1	-5.2	99.9	90.2	89.4
100599		152	-0.8	8.3	-3.4	-2.5	44.9	11.1	-6.7
100603		209	-0.9	2.3	-18.8	-2.3	66.3	30.0	-3.0
100688		9.7	-0.8	48.9	23.1	-2.5	90.0	43.5	6.7
100687		9.8	-2.7	41.0	11.9	-2.5	78.0	16.4	4.5
100709		NA ¹	NA ¹	21.8	-31.4	-5.3	28.1	-17.0	-12.5

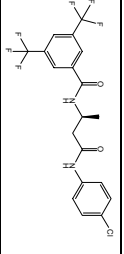
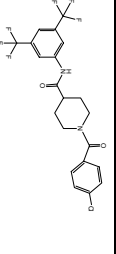
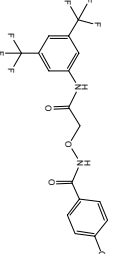
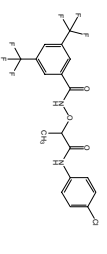
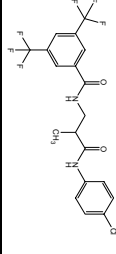
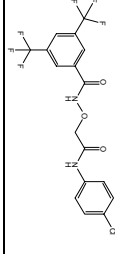
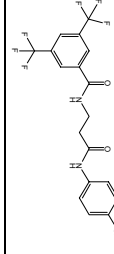
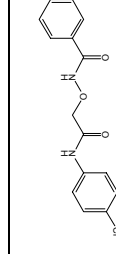
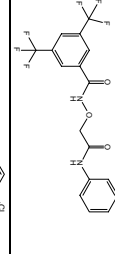
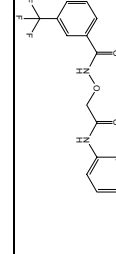
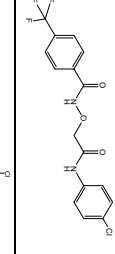
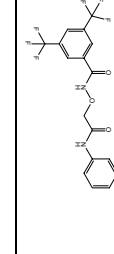
Compound	Structure	SRE.L-IC ₅₀ ($\mu\text{mol/L}$)	Hill Slope	SRE.L- Efficacy (10 $\mu\text{mol/L}$)	PRL-TK Efficacy (10 $\mu\text{mol/L}$)	WSTL- Efficacy (10 $\mu\text{mol/L}$)	SRE.L- Efficacy (100 $\mu\text{mol/L}$)	PRL-TK Efficacy (100 $\mu\text{mol/L}$)	WSTL- Efficacy (100 $\mu\text{mol/L}$)
100711		NA ¹	NA ¹	10.5	-22.0	-2.0	8.8	-27.2	-9.6
100721		9.9	-4.2	51.0	29.5	9.5	99.7	90.5	87.8
100691		8.6	-2.2	57.8	19.0	10.8	99.9	87.2	95.6

Table 3-1. Summary of SRE.L-Luciferase Reporter Results. Biological activity of the synthetic chemical analogs of CCG-1423 were assessed in the SRE.L Luciferase reporter assay. PC-3 prostate cancer cells were co-transfected with 2 ng of the Gd₁₂Q231L expression plasmid along with 50 ng of the SRE.L and 7 ng of the pRL-TK luciferase reporter plasmids as described in the Materials and Methods. Cells were treated with 0 (DMSO alone), 1, 3, 10, 30, and 100 μM of compound for 19 hrs after transfection before lysis and luminescence was read in the plate reader as described in the Materials and Methods. For some compounds, the concentrations of 30 and 100 μM were not tested as indicated by ND in the table. Just before cell lysis, the viability of the cells was measured using the WST-1 cell proliferation reagent as described in the Materials and Methods. Data are expressed as percentage of inhibition (DMSO alone = 0%). The experiments were performed three separate times for a n = 3 in triplicate.

Footnotes: 1. NA represents No Activity in the assay; 2. ND represents No Data for that compound in the assay

Compound	Structure	RWPE-1 Efficacy- %Inhibition (12.5 µmol/L)	LNCaP Efficacy- %Inhibition (12.5 µmol/L)	PC-3 Efficacy- %Inhibition (12.5 µmol/L)	RWPE-1 Efficacy- %Inhibition (100 µmol/L)	LNCaP Efficacy- %Inhibition (100 µmol/L)	PC-3 Efficacy- %Inhibition (100 µmol/L)
1423		54.8	78.2	63.2	54.7	81.2	94.0
100595		-1.5	-57.7	-6.5	38.2	-12.6	-2.8
100596		80.0	74.7	40.0	93.7	90.3	77.6
100594		3.4	-70.3	-8.9	14.2	-11.3	-13.2
100701		-36.8	-66.5	-11.9	0.8	11.2	-6.7
100703		49.8	42.3	-36.9	83.0	76.8	34.9
101202		-0.4	-4.7	-17.3	82.9	81.7	36.7
100723		7.9	-28.5	-13.2	74.4	78.9	35.1
101200		83.4	76.5	46.9	98.1	89.4	79.2

Compound	Structure	RWPE-1 Efficacy- %Inhibition (12.5 µmol/L)	INCAP Efficacy- %Inhibition (12.5 µmol/L)	PC-3 Efficacy- %Inhibition (12.5 µmol/L)	RWPE-1 Efficacy- %Inhibition (100 µmol/L)	INCAP Efficacy- %Inhibition (100 µmol/L)	PC-3 Efficacy- %Inhibition (100 µmol/L)
100689		81.0	75.4	47.1	83.8	88.9	88.6
100601		-66.2	-51.2	-2.5	38.7	0.6	-2.3
100604		-19.2	-32.8	-6.1	16.4	-0.9	-2.6
100598		-24.8	-24.7	-5.6	-15.7	-2.0	-11.1
100600		-19.3	-64.0	-8.6	46.5	35.9	7.3
100597		-42.7	-30.5	-5.7	-20.3	-5.5	-3.5
100686		-18.8	-62.3	-10.7	-5.4	-33.4	-9.2
100602		-51.9	-96.4	-26.5	59.8	83.7	22.1
100690		-9.8	-48.0	-5.8	43.9	89.1	56.5

Compound	Structure	RWPE-1 Efficacy- %Inhibition (12.5 µmol/L)	INCAP Efficacy- %Inhibition (12.5 µmol/L)	PC-3 Efficacy- %Inhibition (12.5 µmol/L)	RWPE-1 Efficacy- %Inhibition (100 µmol/L)	INCAP Efficacy- %Inhibition (100 µmol/L)	PC-3 Efficacy- %Inhibition (100 µmol/L)
100692		-46.2	-51.4	-15.7	51.2	85.0	34.4
101343		18.1	77.4	34.8	73.6	78.7	70.2
101329		-77.8	-40.2	-8.8	-26.3	-13.9	-9.4
101433		-51.3	-56.8	-24.0	63.4	22.7	58.8
102443		-72.7	-94.2	-22.9	-1.2	-1.8	0.1
101325		2.9	9.7	-15.9	81.1	80.7	13.0
101435		-82.3	-55.4	-20.8	-33.2	3.4	-2.6
102441		-118.7	-67.9	-24.2	-44.0	1.3	-10.3
102445		-122.7	-47.2	-24.3	55.3	13.6	21.0

Compound	Structure	RWPE-1 Efficacy- %Inhibition (12.5 µmol/L)	LNcap Efficacy- %Inhibition (12.5 µmol/L)	PC-3 Efficacy- %Inhibition (12.5 µmol/L)	RWPE-1 Efficacy- %Inhibition (100 µmol/L)	LNcap Efficacy- %Inhibition (100 µmol/L)	PC-3 Efficacy- %Inhibition (100 µmol/L)
102447		-98.3	-41.7	-19.6	-6.6	-7.9	-4.5
101425		-74.1	61.9	-18.6	18.0	53.2	5.3
102585		-83.6	-87.3	-12.8	80.9	74.5	92.1
102532		-102.3	-94.8	-14.0	84.8	73.9	92.1
100599		-13.5	-61.7	-4.2	8.6	-7.8	10.0
100603		-26.3	-45.6	-5.2	3.8	-0.9	4.0
100688		-18.9	-89.8	-23.2	59.1	74.1	23.8
100687		-53.2	-61.7	-9.1	45.8	70.6	12.6
100709		-2.1	-60.8	-5.9	26.4	-22.4	-18.9

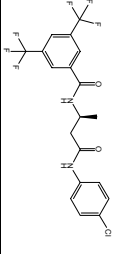
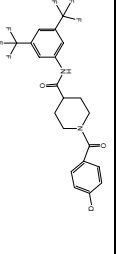
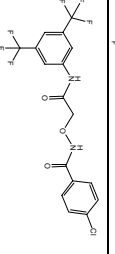
Compound	Structure	RWPE-1 Efficacy- %Inhibition (12.5 μmol/L)	LNCaP Efficacy- %Inhibition (12.5 μmol/L)	PC-3 Efficacy- %Inhibition (12.5 μmol/L)	RWPE-1 Efficacy- %Inhibition (100 μmol/L)	LNCaP Efficacy- %Inhibition (100 μmol/L)	PC-3 Efficacy- %Inhibition (100 μmol/L)
100711		-13.6	-47.2	-3.6	0.9	-11.4	-16.3
100721		12.3	-1.6	18.2	76.4	82.1	89.4
100691		23.8	59.4	20.7	96.4	92.7	96.9

Table 3-2. Summary of 24 hr Cell Viability Results. The effect of the synthetic chemical analogs of CCG-1423 upon 24 hour prostate cell viability under low serum conditions was assessed. The RWPE-1 normal epithelial prostate cell line, the hormone-dependent LNCaP epithelial prostate cancer cell line, and the hormone-independent PC-3 prostate cancer cell line were assessed. Compounds were added to the cells 2-fold serially over the concentration range of 0.78125 to 100 μM, and incubated with the cells for 24 hours as described in the Materials and Methods. Cell viability was measured by absorbance using the WST-1 reagent and the Victor² plate reader as described in the Materials and Methods. This table includes the effect of the compounds only at the concentrations of 12.5 μM and 100 μM. Data are expressed as percentage of inhibition (DMSO alone = 0%). The experiments were performed three separate times for a n = 3 in duplicate.

Compound	Structure	Matrigel Invasion- Efficacy-%/Inhibition (10.0 μmol/L)	WST1- Efficacy-%/Inhibition (10.0 μmol/L)	Matrigel Invasion Efficacy-%/Inhibition (100 μmol/L)	WST1- Efficacy-%/Inhibition (100 μmol/L)
1423		70.9	53.6	75.6	96.2
100595		-7.8	-5.2	50.8	43.4
100596		49.6	14.4	88.4	78.2
100594		13.3	-4.2	62.2	28.1
100600		14.1	-8.3	74.8	38.4
100597		6.4	-6.3	14.6	1.1
100686		15.0	-6.6	25.3	1.2
100602		19.8	-8.4	71.9	23.5
100690		13.6	-6.5	79.1	35.9

Compound	Structure	Matrigel Invasion- Efficacy-%/Inhibition (10.0 µmol/L)	WST1- Efficacy-%/Inhibition (10.0 µmol/L)	Matrigel Invasion Efficacy-%/Inhibition (100 µmol/L)	WST1- Efficacy-%/Inhibition (100 µmol/L)
100692		11.8	-8.4	78.0	44.1
101343		63.1	30.8	86.0	69.6
101329		1.8	-4.0	-7.8	1.2
102443		0.0	-4.8	-3.6	-3.4
102441		17.9	-6.3	56.0	-6.9
102445		18.4	-2.6	7.6	0.2
102447		3.3	-0.3	25.6	0.3
101425		53.5	-3.5	83.6	27.1
102585		47.3	-7.9	96.2	95.4

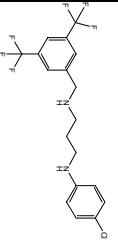
Compound	Structure	Matrigel Invasion- Efficacy-%Inhibition (10.0 μmol/L)	WST1- Efficacy-%Inhibition (10.0 μmol/L)	Matrigel Invasion Efficacy-%Inhibition (100 μmol/L)	WST1- Efficacy-%Inhibition (100 μmol/L)
102532		30.4	-4.8	85.9	96.7

Table 3-3. Summary of Matrigel Invasion Results. Biological activity of the synthetic chemical analogs of CCG-1423 were assessed for their ability to inhibit PC-3 prostate cancer cell invasion through a Matrigel-coated filter under low serum (0.5% FBS) conditions in the absence of a chemoattractant as described in the Materials and Methods. Compounds were incubated with the cells at concentrations of 10 μM and 100 μM for 24 hours, then fixed, stained, and measured by absorbance as described in the Materials and Methods. In parallel, cells were plated in a 96-well plate at a cell density of 4×10^4 cell per well for WST-1 cell viability measurements as described in the Materials and Methods. Both invasion and WST-1 cell viability data are expressed as percentage of inhibition (DMSO alone = 0%). The invasion experiments were performed three separate times for a n = 3 in duplicate. The WST-1 cell viability experiments were performed three separate times for a n = 3 in triplicate.

Footnotes: 1. NA represents No Activity in the assay; 2. ND represents No Data for that compound in the assay

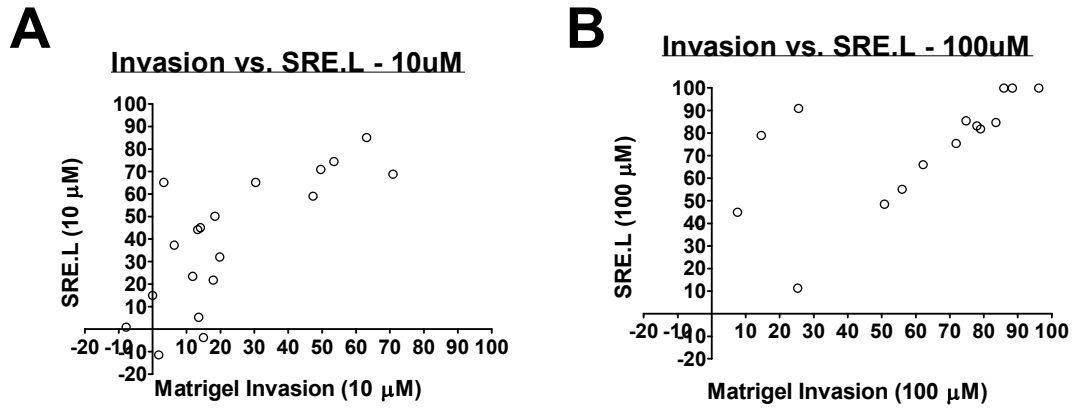


Figure 3-9. Correlation between the Matrigel Invasion Assay vs. the SRE.L-luciferase reporter assay. A. and B.) Correlation graph between the average inhibition of the PC-3 Matrigel invasion assay results on the x-axis versus the average inhibition of the $G\alpha_{12}QL$ -stimulated SRE.L-luciferase expression in PC-3 cells on the y-axis at 10 μM and 100 μM , respectively. Panel A and B represent the average data of experiments performed 3 separate times for a $n = 3$ in duplicate and triplicate, respectively.

References

1. Gupta, G. P. and Massague, J. Cancer metastasis: building a framework. *Cell*, *127*: 679-695, 2006.
2. Sawyer, T. K. Cancer metastasis therapeutic targets and drug discovery: emerging small-molecule protein kinase inhibitors. *Expert Opin Investig Drugs*, *13*: 1-19, 2004.
3. Sahai, E. and Marshall, C. J. RHO-GTPases and cancer. *Nat Rev Cancer*, *2*: 133-142, 2002.
4. van Golen, K. L., Davies, S., Wu, Z. F., Wang, Y., Bucana, C. D., Root, H., Chandrasekharappa, S., Strawderman, M., Ethier, S. P., and Merajver, S. D. A novel putative low-affinity insulin-like growth factor-binding protein, LIBC (lost in inflammatory breast cancer), and RhoC GTPase correlate with the inflammatory breast cancer phenotype. *Clin Cancer Res*, *5*: 2511-2519, 1999.
5. van Golen, K. L., Wu, Z. F., Qiao, X. T., Bao, L. W., and Merajver, S. D. RhoC GTPase, a novel transforming oncogene for human mammary epithelial cells that partially recapitulates the inflammatory breast cancer phenotype. *Cancer Res*, *60*: 5832-5838, 2000.
6. Ridley, A. J. and Hall, A. The small GTP-binding protein rho regulates the assembly of focal adhesions and actin stress fibers in response to growth factors. *Cell*, *70*: 389-399, 1992.
7. Wang, Q., Liu, M., Kozasa, T., Rothstein, J. D., Sternweis, P. C., and Neubig, R. R. Thrombin and lysophosphatidic acid receptors utilize distinct rhoGEFs in prostate cancer cells. *J Biol Chem*, *279*: 28831-28834, 2004.
8. Fukuhara, S., Chikumi, H., and Gutkind, J. S. RGS-containing RhoGEFs: the missing link between transforming G proteins and Rho? *Oncogene*, *20*: 1661-1668, 2001.
9. Hart, M. J., Jiang, X., Kozasa, T., Roscoe, W., Singer, W. D., Gilman, A. G., Sternweis, P. C., and Bollag, G. Direct stimulation of the guanine nucleotide exchange activity of p115 RhoGEF by Galpha13. *Science*, *280*: 2112-2114, 1998.
10. Kourlas, P. J., Strout, M. P., Becknell, B., Veronese, M. L., Croce, C. M., Theil, K. S., Krahe, R., Ruutu, T., Knuutila, S., Bloomfield, C. D., and Caligiuri, M. A. Identification of a gene at 11q23 encoding a guanine nucleotide exchange factor: evidence for its fusion with MLL in acute myeloid leukemia. *Proc Natl Acad Sci U S A*, *97*: 2145-2150, 2000.

11. Kozasa, T., Jiang, X., Hart, M. J., Sternweis, P. M., Singer, W. D., Gilman, A. G., Bollag, G., and Sternweis, P. C. p115 RhoGEF, a GTPase activating protein for Galpha12 and Galpha13. *Science*, *280*: 2109-2111, 1998.
12. Whitehead, I. P., Zohn, I. E., and Der, C. J. Rho GTPase-dependent transformation by G protein-coupled receptors. *Oncogene*, *20*: 1547-1555, 2001.
13. Cen, B., Selvaraj, A., Burgess, R. C., Hitzler, J. K., Ma, Z., Morris, S. W., and Prywes, R. Megakaryoblastic leukemia 1, a potent transcriptional coactivator for serum response factor (SRF), is required for serum induction of SRF target genes. *Mol Cell Biol*, *23*: 6597-6608, 2003.
14. Cen, B., Selvaraj, A., and Prywes, R. Myocardin/MKL family of SRF coactivators: key regulators of immediate early and muscle specific gene expression. *J Cell Biochem*, *93*: 74-82, 2004.
15. Miralles, F., Posern, G., Zaromytidou, A. I., and Treisman, R. Actin dynamics control SRF activity by regulation of its coactivator MAL. *Cell*, *113*: 329-342, 2003.
16. Ma, Z., Morris, S. W., Valentine, V., Li, M., Herbrick, J. A., Cui, X., Bouman, D., Li, Y., Mehta, P. K., Nizetic, D., Kaneko, Y., Chan, G. C., Chan, L. C., Squire, J., Scherer, S. W., and Hitzler, J. K. Fusion of two novel genes, RBM15 and MKL1, in the t(1;22)(p13;q13) of acute megakaryoblastic leukemia. *Nat Genet*, *28*: 220-221, 2001.
17. Lacoste, J., Aprikian, A. G., and Chevalier, S. Focal adhesion kinase is required for bombesin-induced prostate cancer cell motility. *Mol Cell Endocrinol*, *235*: 51-61, 2005.
18. Sawada, K., Morishige, K., Tahara, M., Kawagishi, R., Ikebuchi, Y., Tasaka, K., and Murata, Y. Alendronate inhibits lysophosphatidic acid-induced migration of human ovarian cancer cells by attenuating the activation of rho. *Cancer Res*, *62*: 6015-6020, 2002.
19. Shi, X., Gangadharan, B., Brass, L. F., Ruf, W., and Mueller, B. M. Protease-activated receptors (PAR1 and PAR2) contribute to tumor cell motility and metastasis. *Mol Cancer Res*, *2*: 395-402, 2004.
20. Nakajima, M., Hayashi, K., Egi, Y., Katayama, K., Amano, Y., Uehata, M., Ohtsuki, M., Fujii, A., Oshita, K., Kataoka, H., Chiba, K., Goto, N., and Kondo, T. Effect of Wf-536, a novel ROCK inhibitor, against metastasis of B16 melanoma. *Cancer Chemother Pharmacol*, *52*: 319-324, 2003.

21. Sahai, E. and Marshall, C. J. Differing modes of tumour cell invasion have distinct requirements for Rho/ROCK signalling and extracellular proteolysis. *Nat Cell Biol*, 5: 711-719, 2003.
22. Alberti, S., Krause, S. M., Kretz, O., Philippar, U., Lemberger, T., Casanova, E., Wiebel, F. F., Schwarz, H., Frotscher, M., Schutz, G., and Nordheim, A. Neuronal migration in the murine rostral migratory stream requires serum response factor. *Proc Natl Acad Sci U S A*, 102: 6148-6153, 2005.
23. Somogyi, K. and Rorth, P. Evidence for tension-based regulation of Drosophila MAL and SRF during invasive cell migration. *Dev Cell*, 7: 85-93, 2004.
24. Vickers, E. R., Kasza, A., Kurnaz, I. A., Seifert, A., Zeef, L. A., O'Donnell, A., Hayes, A., and Sharrocks, A. D. Ternary complex factor-serum response factor complex-regulated gene activity is required for cellular proliferation and inhibition of apoptotic cell death. *Mol Cell Biol*, 24: 10340-10351, 2004.
25. Medjkane, S., Perez-Sanchez, C., Gaggioli, C., Sahai, E., and Treisman, R. Myocardin-related transcription factors and SRF are required for cytoskeletal dynamics and experimental metastasis. *Nat Cell Biol*, 11: 257-268, 2009.
26. Evelyn, C. R., Wade, S. M., Wang, Q., Wu, M., Iniguez-Lluhi, J. A., Merajver, S. D., and Neubig, R. R. CCG-1423: a small-molecule inhibitor of RhoA transcriptional signaling. *Mol Cancer Ther*, 6: 2249-2260, 2007.
27. Hall, C. L., Dubyk, C. W., Riesenberger, T. A., Shein, D., Keller, E. T., and van Golen, K. L. Type I collagen receptor (alpha2beta1) signaling promotes prostate cancer invasion through RhoC GTPase. *Neoplasia*, 10: 797-803, 2008.
28. Sequeira, L., Dubyk, C. W., Riesenberger, T. A., Cooper, C. R., and van Golen, K. L. Rho GTPases in PC-3 prostate cancer cell morphology, invasion and tumor cell diapedesis. *Clin Exp Metastasis*, 25: 569-579, 2008.
29. Yao, H., Dashner, E. J., van Golen, C. M., and van Golen, K. L. RhoC GTPase is required for PC-3 prostate cancer cell invasion but not motility. *Oncogene*, 25: 2285-2296, 2006.
30. Luo, J., Solimini, N. L., and Elledge, S. J. Principles of cancer therapy: oncogene and non-oncogene addiction. *Cell*, 136: 823-837, 2009.

Chapter IV

THE EFFECT OF THE RHOA TRANSCRIPTIONAL PATHWAY INHIBITOR, CCG-1423, UPON GLOBAL PC-3 PROSTATE CANCER CELL GENE EXPRESSION

Abstract

Cancer metastasis is a major health problem that results in many cancer patient deaths every year. The complex process of metastasis requires tumor cells to escape from their tissue of origin and to re-establish themselves at an alternate secondary tissue site, such as the bone, lungs, liver, and brain. Gene expression has been implicated to play a pivotal role in the process of metastasis. The RhoA transcriptional signaling pathway has been shown to play an important mechanistic role in the process of metastasis in a variety of malignancies, such as breast cancer, prostate cancer, head and neck cancer, and melanoma. I have previously shown that the RhoA transcriptional pathway inhibitor, CCG-1423, which inhibits megakaryoblastic leukemia 1 (MKL1)/serum-response factor (SRF) mediated gene transcription, also inhibits PC-3 prostate cancer cell Matrigel invasion (1). Therefore, I undertook a genome-wide Affymetrix gene chip study to further investigate both the general mechanism of action of CCG-1423 and its mechanism of action as it relates to PC-3 prostate cancer cell Matrigel invasion. Using metastasis-related gene ontology (GO) categories, an 8-fold-change in gene expression cut-off in either a stimulatory or inhibitory direction, and the literature (2-11), I was able to identify 4 candidate genes (*RGS4*, *RGS7*, *CTGF*, *SOX9*) that are regulated by CCG-1423. These 4

candidate genes were confirmed to be CCG-1423 regulated by quantitative real-time polymerase chain reaction (QRT-PCR). Interestingly, only 2 (*RGS4* and *SOX9*) of these 4 candidate genes were confirmed to be regulated by two more selective CCG-1423 analogs, CCG-100602 and CCG-101425, via QRT-PCR. Future functional studies will determine if the genes, *RGS4* and *SOX9*, are involved in CCG-1423-mediated inhibition of prostate cancer metastasis.

Introduction

Cancer metastasis is one of the major causes of cancer patient deaths (15-19). Metastasis is defined as a multi-step process that enables tumor cells to disseminate from their site of origin in order to colonize distant tissue and organ sites. The basic steps involved in this complex process include: local tissue invasion, intravasation, survival in the blood circulation, extravasation, and colonization at a distant site (15-19). There are several key cancer cell functions that are necessary for the metastasis to occur, which include cell proliferation, adhesion, migration, invasion, survival, and angiogenesis (15-19). The complex process of cancer metastasis and its related cellular functions can be mediated by several classes of genes, which can be grouped as metastasis initiation, metastasis progression, and metastasis virulence genes (18). Metastasis initiation genes can be defined as genes that enable tumor cells to invade the surrounding tissue, mediate tumor cell dissemination, and intravasate (18), such as the epithelial-mesenchymal transition (EMT) genes (*Twist1*, *Snai1*, *Snai2*) (20) and hepatocyte growth factor (HGF) pathway-dependent genes (*metadherin*) (21). Genes that enable tumor cells to extravasate and survive at the secondary tissue site are defined as metastasis progression genes, such

as prostaglandin G/H synthase 2 (PTGS2), epiregulin, and angiopoietin-like 4 (ANGPTL4) (18, 22, 23). Lastly, the metastasis virulence class of genes is defined by genes that enable tumor cells to colonize and survive at the distant secondary tumor site, such as parathyroid hormone-related protein (PTHrP) and interleukin 11 (IL-11) (18, 24-26). Therefore, clearly gene expression plays a vital role in the complex process of cancer metastasis.

The RhoA transcriptional signaling pathway is known to play a role in the complex process of metastasis and in many of the cellular processes that are associated with it. Both the RhoA and RhoC GTPases have been well-established to play a role in the process of cancer metastasis and related cellular processes. RhoA has been implicated in both *in vitro* and *in vivo* MDA-MB-231 breast cancer cell growth and *in vitro* Matrigel cell invasion (27). In addition, RhoA has been implicated in *in vitro* cell motility and Matrigel invasion of highly metastatic head neck squamous cell carcinoma cells (28). However, RhoC has been shown to play a more prominent role to date than RhoA in metastasis. RhoC has been shown to strongly correlate with the inflammatory breast cancer metastatic phenotype (29-31). RhoC has also been implicated to play a role in *in vitro* cancer cell migration and/or invasion and in *in vivo* metastatic nude mouse models across several malignancies, including melanoma (32, 33), pancreatic adenocarcinoma (34), prostate cancer (35-38), and lung cancer (39). In a polyoma T-antigen-induced mammary tumor model, RhoC-deficiency was found to nearly eliminate lung metastasis, but did not affect tumor initiation and growth (40). Also, the $G\alpha_{12}$ -subunit, which activates Rho, was found to be over-expressed in both breast and prostate cancers. It also mediates *in vitro* cancer cell Matrigel invasion through a RhoA-signaling pathway-

dependent mechanism (41, 42). Interestingly, genome-wide gene expression analysis of NIH-3T3 mouse fibroblast cells transformed with constitutively activated RhoA or RhoC revealed no major differences in regulated gene expression. Genes involved in both cell proliferation and in cytoskeletal changes necessary for cell motility were regulated by both RhoA and RhoC (43). Also, in another microarray study, RhoC was shown to mediate gene expression of several metastasis-related genes, including *cyclin D1*, *VEGF-C*, *CXCL1*, *fibronectin*, and *IGFBP2* (44).

The downstream transcriptional portion of the RhoA transcriptional pathway has been implicated in metastasis and related cellular processes, but its specific role is not as well-established as an overall role for RhoA and RhoC. The RhoA/C-mediated serum-response factor (SRF) transcription factor has been implicated in several metastasis-related cellular processes in non-cancerous cells, including cell motility, growth, adhesion, DNA synthesis, and angiogenesis (45-47). More interestingly, SRF has been shown to play a role in *in vitro* cell migration and invasion of hepatocellular carcinoma cells (48), and in *in vitro* cell growth and DNA synthesis of prostate cancer cells (49). More recently, Medjkane and colleagues have shown that both the SRF co-activator, megakaryoblastic leukemia 1 (MKL1), and SRF itself play a role in both *in vitro* and *in vivo* breast cancer and melanoma metastasis (14). Consistent with the data from RhoC-deficient mice (40), MKL1 and SRF were shown to be required for cell migration and invasion, but not proliferation (14). More interestingly, upon microarray analysis of MKL1-dependent gene expression in breast cancer and melanoma cells, two cytoskeleton genes, *Myh9* and *Myh9*, were identified. These genes were required for *in vivo* pulmonary metastasis for both breast cancer and melanoma cells (14). In addition, several serum-

mediated MKL1-dependent genes, including *SRF*, *adrenomedullin*, *epiregulin*, *interleukin-6*, *hexokinase 2*, and *zyxin*, (13), have been implicated in metastasis-related cellular processes, such as cell growth, migration, invasion, and survival (50-55). Therefore, the RhoA transcriptional pathway and pathway-mediated gene expression clearly play a role in the process of cancer metastasis and related cellular processes.

Previously, we identified the small-molecule, CCG-1423, as an inhibitor of the RhoA and RhoC transcriptional signaling pathway (1). We also showed that CCG-1423 could inhibit *in vitro* Matrigel invasion by PC-3 prostate cancer cells, but not $G\alpha_i$ -dependent SKOV-3 ovarian cancer cells (1). Therefore, to gain further insight into the mechanism of action of CCG-1423, we undertook a genome-wide gene expression analysis of CCG-1423, latrunculin B, and DRB effects on PC-3 prostate cancer cell gene expression utilizing conditions employed in our PC-3 cell Matrigel invasion assays. Latrunculin B is an actin polymerization inhibitor, which we utilized as our positive control inhibitor of the RhoA transcriptional signaling pathway. DRB is a casein-2 kinase inhibitor that disrupts RNA polymerase II-mediated gene transcription, which we utilized as our negative control. These compounds had a very modest effect upon PC-3 cell gene regulation at an early 2 hour time point, but a much greater effect at a later 24 hour time point. Surprisingly, there was relatively poor overlap between CCG-1423 regulated genes and latrunculin B regulated genes, CArG-box genes (12), and MKL1-dependent genes (13, 14).

Therefore, we hypothesized that the functional effect of CCG-1423 upon PC-3 cell Matrigel invasion was dependent upon CCG-1423 regulation of metastasis-related gene expression. Using metastasis-related gene ontology (GO) categories, an 8-fold-

change in gene expression in either a stimulatory or inhibitory direction, and the cancer literature, we were able to identify four candidate genes, *RGS4*, *RGS7*, *CTGF*, and *SOX9*, that may play a role in CCG-1423-mediated inhibition of PC-3 cell Matrigel invasion. We show here the confirmation of these four CCG-1423-regulated candidate genes in follow-up quantitative real-time polymerase chain reaction (QRT-PCR) experiments. In addition, only two (*RGS4* and *SOX9*) of these four candidate genes were confirmed to be regulated by two of the more selective CCG-1423 analogs identified in Chapter 3, CCG-100602 and CCG-101425, that also inhibit Matrigel invasion by PC-3 cells. Future functional experiments will determine if one or both of these candidate genes are involved in *in vitro* PC-3 prostate cancer cell Matrigel invasion along with cell migration, growth, and survival, and *in vivo* bone metastasis.

Materials and Methods

Cell lines and Reagents

Dimethyl Sulfoxide (DMSO), the marine toxin latrunculin b, and the casein kinase-2 RNA synthesis inhibitor DRB (5,6-Dichlorobenzimidazole 1- β -D-ribofuranoside) were all purchased from Sigma (St. Louis, MO). The RhoA transcriptional pathway inhibitor, CCG-1423 [N-[2-(4-chloroanilino)-1-methyl-2-oxoethoxy]-3,5-bis(trifluoromethyl)benzamide], was from Cayman Chemical (Ann Arbor, MI). The chemical compounds CCG-100686 [5-{{3,5-bis(trifluoromethyl)phenyl}formamido}-N-(4-chlorophenyl)pentanamide], CCG-100602 [1-{{3,5-bis(trifluoromethyl)phenyl}carbonyl}-N-(4-chlorophenyl)piperidine-3-carboxamide], and CCG-101425 [N-(3-(4-chlorophenylamino)propyl)-3,5-bis(trifluoromethyl)benzamide]

were synthesized at the Medicinal Chemistry Core Synthesis Laboratory at the University of Michigan. The PC-3 cell line was a kind gift from Dr. Kenneth Pienta (University of Michigan). The RWPE-1 and LNCaP cell lines were obtained from the American Type Culture Collection (ATCC) (Manassas, VA). The RNAqueous® RNA isolation kit was purchased from Ambion (Austin, TX). The TURBO DNase-*free* kit was purchased from Ambion (Austin, TX). The TaqMan® Reverse-Transcription Reagents Kit was purchased from Applied Biosystems (Foster City, CA). The Brilliant® II SYBR® Green QPCR Master Mix with low Rox dye was purchased from Stratagene (La Jolla, CA).

Cell Culture

The PC-3 prostate cancer epithelial cell line was normally maintained in DMEM medium (Invitrogen, cat.#: 11995) containing 10% fetal bovine serum (FBS), 100 units/mL penicillin, and 100 µg/mL streptomycin at 37°C in 5% CO₂. The LNCaP prostate cancer epithelial cell line was normally maintained in RPMI-1640 medium (Invitrogen, cat.#: 11875) containing 10% fetal bovine serum (FBS), 100 units/mL penicillin, and 100 µg/mL streptomycin at 37°C in 5% CO₂. The normal RWPE-1 prostate epithelial cell line was normally maintained in Keratinocyte Serum Free medium (K-SFM) (Invitrogen, cat.#: 17005-042) containing 0.05 mg/ml of bovine pituitary extract (BPE), 5 ng/ml of human recombinant epidermal growth factor (EGF), 100 units/mL penicillin, and 100 µg/mL streptomycin at 37°C in 5% CO₂.

Microarray Analysis

PC-3 cells (9×10^5) were seeded into individual 60 mm dishes. Twenty-four hours later, PC-3 cells were serum-starved (0.5% FBS) for twenty-four hours. Cells were then treated for an additional two or twenty-four hours with DMSO (1.0%), 3 μ M of CCG-1423, 0.5 μ M of latrunculin B, or 50 μ M of DRB under serum-starved conditions (0.5% FBS). Cells from three dishes for each condition were lysed and RNA was isolated using the RNeasy[®] kit from Ambion following the manufacturer's directions. cDNA and biotin-labeled cRNA synthesis, hybridization to the human U133 plus 2.0 Affymetrix gene chips, scanning of the gene chips, and analysis of the data images were all performed at the University of Michigan Comprehensive Cancer Center (UMCCC) Affymetrix and Microarray Core Facility in Ann Arbor, MI. Expression values for each probeset on the chip were calculated using a robust multi-array average (RMA) (56) and were expressed as \log_2 transformed data. Fold changes for each probeset were calculated by dividing the average expression values for the compound samples by the average expression values of the DMSO samples. A record for each probeset showing a two-fold change (i.e. \log_2 fold change > 1 for a decrease or < -1 for an increase in expression) was then imported into a MySQL[®] database (Sun Microsystems, Santa Clara, CA). Queries on the MySQL[®] database was utilized to obtain counts for genes with altered gene expression, identify highly regulated genes (\log_2 fold change > 3 or < -3), identify overlaps between datasets, filter by gene ontology (GO) categories, and to generate the data in the tables and the Venn diagram described here. Comparisons to gene sets from literature studies were done both manually and by importing gene symbols into our MySQL[®] database for comparison by queries.

Quantitative Real-Time Polymerase Chain Reaction (QRT-PCR)

PC-3 cells, LNCaP cells, or RWPE-1 cells (9×10^5) were seeded into 60 mm dishes. For Figure 4-4, 5×10^5 cells of PC-3 cells were plated into individual wells of a 6 well-plate. Twenty-four hours after-plating, PC-3 and LNCaP cells were serum-starved (0.5% FBS), while RWPE-1 cells were re-fed with fresh complete K-SFM medium, for twenty-four hours. Cells were then treated for an additional twenty-four hours with DMSO (0.03% or 1.0%) or compound under serum-starved conditions (0.5% FBS) for PC-3 cells and LNCaP cells or under normal conditions for RWPE-1 cells. Cells were lysed and RNA was isolated using the RNeasy[®] kit from Ambion following the manufacturer's directions. 10 μ g of RNA was DNase treated using the TURBO DNA-free kit from Ambion following the manufacturer's directions. 1 μ g of DNase-treated RNA was used as a template for synthesizing cDNA utilizing the Taqman[®] Reverse-Transcription Reagents kit. The components used for the reverse-transcription reaction were 1x reverse transcription buffer, 5.6 mM MgCl₂, 2 mM dNTPs, oligo dT, RNase inhibitor, reverse transcriptase enzyme, sterile water, and 1 μ g of RNA. The sequential order of reaction conditions was: (i) 25°C for 10 minutes, (ii) 48°C for 30 minutes, (iii) 95°C for 5 minutes and carried out in a Biometra TGradient thermocycler. The QRT-PCR reaction was performed using 5 μ l of cDNA sample per well in a 25 μ l final reaction volume in a 96-well qpcr plate, and the Brilliant[®] II SYBR[®] Green QPCR Master Mix with low Rox dye from Stratagene in a Stratagene MX3000P[®] QPCR System. The reaction mix consisted of 1x of the Brilliant[®] II SYBR[®] Green QPCR Master Mix with low Rox dye, 200 nM each of both forward and reverse primers, and sterile water. The sequential order of reaction conditions was: (i) 95°C for 10 minutes, (ii) 95°C for 30 seconds, (iii) 55°C for 1 minute,

and (iv) 72°C for 30 seconds. Steps 2 through 4 were carried out for 50 cycles. The primer sequences used were *GAPDH*: *Fwd*-5'-GGAAGGACTCATGACCACAG-3', *Rev*-5'-ACAGTCTTCTGGGTGGCAGTGATG-3' (base-pairs were corrected to match human sequence) (13); *RGS4*: *Fwd*-5'-TTCCCACAACAAGAAGGACAAAG-3', *Rev*-5'-TGATTCAGCCCATTCTTGAC-3' (base-pairs were corrected to match human sequence) (57); *RGS7*: *Fwd*-5'-CCTTCTAACCCATGGCTGTC-3', *Rev*-5'-TTTTTCAGGTCCTCCACTGC-3' (58); *CTGF*: *Fwd*-5'-CAGAGTGGAGCGCCTGTTC-3', *Rev*-5'-CTGCAGGAGGCGTTGTCAT-3' (59); *SOX9*: *Fwd*-5'-CAACCAGAATTCCCTTTGGA-3', *Rev*-5'-TGCTCCATTTAGCCAAGGTT-3' (60). *GAPDH* gene expression was utilized as an internal control. The relative mRNA gene expression was calculated using the following formula: $2^{-(\Delta Ct)}$, where the ΔCt value = Ct value of Sample – Ct value of *GAPDH*. Fold Changes were calculated by dividing the $2^{-(\Delta Ct)}$ of the compound sample by the $2^{-(\Delta Ct)}$ of the DMSO control sample.

Results

Microarray Analysis – Stimulatory vs. Inhibitory Regulated Gene Expression

In order to gain further insight into both the general cellular mechanism of action and the mechanism of action of my RhoA transcriptional pathway inhibitor, CCG-1423, upon *in vitro* PC-3 prostate cancer cell Matrigel invasion, I undertook a microarray approach to test the effect of CCG-1423 upon global PC-3 cell gene expression. I also utilized the actin cytoskeleton inhibitor, latrunculin B, as a positive control compound that inhibits the RhoA transcriptional pathway, along with the casein-2 kinase inhibitor, DRB, as a negative control compound that inhibits general RNA Polymerase II-mediated

transcription. I tested the effects of the compound both at an early 2-hour time point to capture effects upon genes with short half-lives, and a later time point of 24 hours to capture effects upon genes with longer half-lives and to be consistent with our Matrigel invasion assay conditions. I observed significantly fewer genes regulated at the early 2 hour time point in comparison to the 24 hour time point (Table 4-1). Interestingly, at the 2 hour time point, I observed both CCG-1423 and latrunculin B to have primarily a stimulatory regulatory effect upon gene expression (CCG-1423 – 47 gene transcripts out of 49 total gene transcripts, latrunculin B – 15 genes out of 17 total gene transcripts) in comparison to an inhibitory regulatory effect (Table 4-1). However, our control compound, DRB, had the opposite effect at the 2 hour time point, where it had primarily an inhibitory regulatory effect upon gene expression (DRB – 714 gene transcripts out of 719 total gene transcripts) (Table 4-1). The correlation at the 2 hour time point between CCG-1423 and latrunculin B is an interesting observation, but does not correlate with the number of genes shared, because only 4 total genes are both regulated by CCG-1423 and latrunculin B. At the 24 hour time point, there was an abundance of genes both stimulated and inhibited by all three compounds.

Microarray Analysis – Shared Gene Expression

In order to gain better insight into regulated gene expression at the 24 hour time point, we decided to build a Venn Diagram for comparison between the various compound treatments, along with a table depicting the percentage of regulated genes shared between compound treatments (Figure 4-1). As expected, our negative control compound, DRB, selectively regulated the most number of genes (2,205 gene

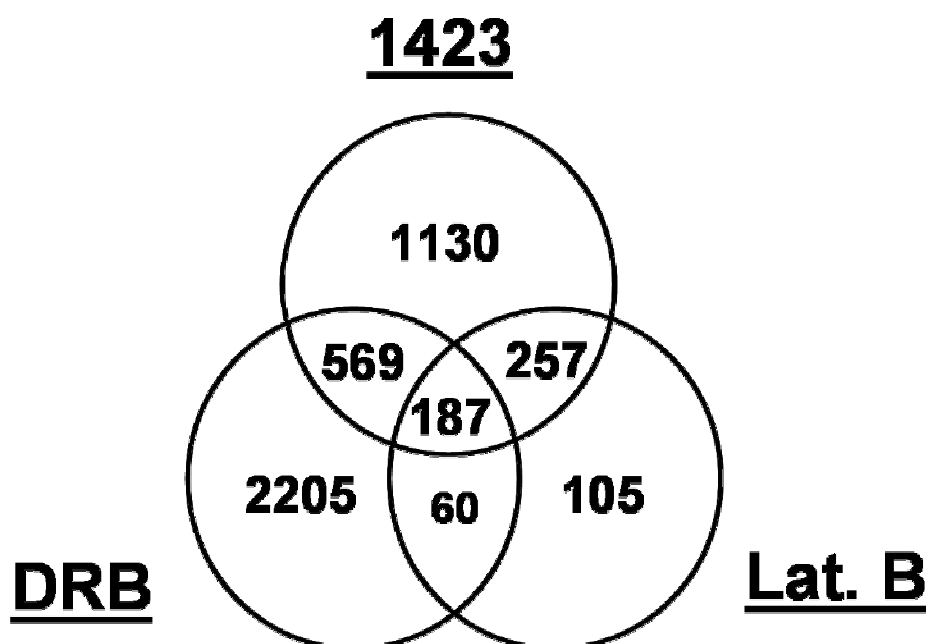
transcripts), and our positive control compound selectively regulated the least number of genes (105 gene transcripts) (Figure 4-1). Our RhoA transcriptional pathway inhibitor, CCG-1423, was in the middle with respect to the number of genes it regulated (1,130 gene transcripts) (Figure 4-1). This is consistent with our hypothesis that our inhibitor, CCG-1423, is selective for the RhoA transcriptional pathway, but does have some non-specific effects, as described in Chapter 2. Interestingly, CCG-1423 did regulate significantly fewer genes than did our general transcriptional negative control inhibitor, DRB, which further supports our argument in Chapter 1 that CCG-1423 is indeed a selective RhoA transcriptional pathway inhibitor. However, it is interesting to note that our general transcriptional negative control inhibitor, DRB, did regulate a much smaller number of genes than we hypothesized. However, this could be due to DRB being an indirect inhibitor of RNA Polymerase II by inhibiting one of its regulatory kinases.

In looking at the percentage of genes shared between the different treatments at the 24 hour time point, we did find a correlation between CCG-1423 and latrunculin B similar to the correlation we observed at the 2 hour time point. Interestingly, although CCG-1423 regulated a significant greater number of genes than latrunculin B, it did regulate 72.9% of the total number of latrunculin B regulated genes in comparison to DRB which only regulated 40.6% (Figure 4-1). On the other hand, latrunculin B only regulated 20.7% of the total number of CCG-1423 regulated genes, but also only regulated 8.2% of the total number of DRB regulated genes. Therefore, overall there is some correlation between regulated genes by CCG-1423 and latrunculin B, which is consistent with our hypothesis of CCG-1423 being a selective RhoA

	<u>2 hours</u>			<u>24 hours</u>		
<u>Treatment</u>	<u>Stimulated</u>	<u>Inhibited</u>	<u>Total</u>	<u>Stimulated</u>	<u>Inhibited</u>	<u>Total</u>
CCG-1423	47	2	49	837	1305	2142
Lat. B	15	2	17	225	383	608
DRB	5	714	719	1058	2026	3020*

Note. * total number of genes changes does not equal the sum of stimulated and inhibited gene totals because some genes have probesets that are stimulated and others that are inhibited.

Table 4-1. Number of Genes Regulated in Microarray. This table shows the number of genes stimulated and inhibited using a 2-fold criterion by 3 μ M of CCG-1423, 0.5 μ M of latrunculin B, and 50 μ M of DRB after 2 hours and 24 hours of treatment of PC-3 prostate cancer cells under serum-starved conditions (0.5% FBS). The total number of genes changed by each treatment is also displayed.



% OVERLAP

	1423	Lat. B	DRB
1423	100	20.7	35.3
Lat. B	72.9	100	40.6
DRB	25.0	8.2	100

Figure 4-1. Microarray analysis of Regulated Genes. PC-3 cells were treated with 3 μM of CCG-1423, 0.5 μM of latrunculin B, and 50 μM of DRB under serum-starved conditions (0.5% FBS) for 24 hours and gene expression assessed with an Affymetrix gene chip. The number of genes regulated (stimulated or inhibited) by CCG-1423, latrunculin B, and DRB with ≥ 2 -fold change are indicated in the Venn didagram. The percentages of genes coordinately regulated by CCG-1423 and latrunculin B, or latrunculin B, and DRB are indicated in the table below the Venn diagram.

transcriptional pathway inhibitor, but clearly CCG-1423 has other potentially interesting effects upon gene expression.

In chapter 2, I hypothesized that CCG-1423 selectively modulated MKL1/SRF-mediated gene transcription. Therefore, I investigated this hypothesis by comparing our gene expression data with three independent studies from the literature. First, I compared our data to a study in which the authors performed a bioinformatics experiment where they did an *in silico* genome-wide screen to identify novel CArG-box containing genes, which have been well-established to be SRF-mediated (12). In total, the authors were able to identify 194 known and novel CArG-box genes with CArG-box consensus sequences at least 4 kb upstream of the transcription start site (12). In comparison to our microarray dataset, CCG-1423 only regulated 12.9% of the CArG-box genes, but surprisingly latrunculin B only regulated 2.6% of the CArG-box genes (Table 4-2). This clearly indicates that latrunculin B is not a completely selective inhibitor of the RhoA transcriptional signaling pathway and SRF-mediated CArG-box gene expression. Clearly, there is not a strong correlation between CCG-1423 regulated gene expression and CArG-box genes.

We also compared our data with two studies in which the authors performed microarray studies to assess what genes are regulated by the co-activator MKL1. One study looked at the effect of overexpressing an MKL1-dominant negative protein upon serum-mediated gene expression, whereas the other looked at the effect of MKL1 shRNA knockdown upon global gene expression in both an invasive breast cancer and melanoma cell line (13, 14). Interestingly, CCG-1423 regulated 17.8% of the serum-mediated MKL1-dependent genes, 25.5% of the MKL1-dependent genes in the breast cancer cell

line, and 22.6% of the MKL1-dependent genes in the melanoma cell line (Table 4-2). Like the CArG-box genes, latrunculin B regulated a small percentage of the MKL1-dependent genes (0% - serum-mediated MKL1-dependent genes; 7.8% - MKL1-dependent breast cancer cell genes; 16.7% -MKL1-dependent melanoma cell genes) (Table 4-2). On the other hand, DRB regulated a similar percentage of genes as CCG-1423 (25.0% - serum-mediated MKL1-dependent genes; 25.3% - MKL1-dependent breast cancer cell genes; 18.0% -MKL1-dependent melanoma cell genes) (Table 4-2). Although, there is not a striking correlation between CCG-1423 and MKL1 regulated gene expression, it is interesting to note that CCG-1423 regulates similar percentages of MKL1-dependent genes as latrunculin B regulated genes (Figure 4-1, Table 4-2).

Microarray analysis - CCG-1423 regulation of metastasis-related gene expression

Due to the lack of a strong correlation of CCG-1423 regulated gene expression with latrunculin B and MKL1 regulated gene expression, we decided to investigate the effect of the compound more globally upon metastasis-related genes in order to gain insight into the mechanism of CCG-1423 inhibition of PC-3 prostate cancer cell *in vitro* Matrigel invasion. Therefore, utilizing metastasis-related gene ontology (GO) categories, which included *angiogenesis, cell migration, cell adhesion, epithelial to mesenchymal transition, extracellular matrix, G-protein coupled receptor protein signaling pathway, inflammatory response, metalloendopeptidases*, as a filter, we identified 203 gene Matrigel invasion. Therefore, utilizing metastasis-related gene ontology (GO) categories, which included *angiogenesis, cell migration, cell adhesion, epithelial to mesenchymal*

	<u>CCG-1423</u>	<u>Latrunculin B</u>	<u>DRB</u>
¹ CArG-Box Genes (#)	25 out 194	5 out 194	32 out of 194
¹ CArG-Box Genes (%)	12.9%	2.6%	16.5%
² FBS-MKL1-Dependent Genes (#) (NIH3T3)	5 out of 28	0 out of 28	7 out of 28
² FBS-MKL1-Dependent Genes (%) (NIH3T3)	17.8%	0.0%	25.0%
³ MKL1-Dependent Genes (#) (MDA-MB-231)	273 out 1,070	83 out of 1,070	271 out of 1,070
³ MKL1-Dependent Genes (%) (MDA-MB-231)	25.5%	7.8%	25.3%
³ MKL1-Dependent Genes (#) (B16F2)	73 out of 323	54 out of 323	58 out of 323
³ MKL1-Dependent Genes (%) (B16F2)	22.6%	16.7%	18.0%

Footnotes (References):

- 1.) Sun Q. et al., *Genome Research*, 2006, 16(2): 197-207 {4 kb upstream of the TSS} (12)
- 2.) Selvaraj A. and Prywes R., *BMC Mol. Biol.*, 2004, 5: 13 (13)
- 3.) Medjkane S. et al., *Nat. Cell Biol.*, 2009, 11(3): 257-268 (14)

Table 4-2. Comparison of Genes Regulated by CCG-1423 with CArG-Box or MKL1-Dependent Genes. The number and percentage of genes regulated by CCG-1423, latrunculin B, and DRB that share identity with genes identified to be CArG-Box, Serum (10% FBS)-mediated MKL1-dependent in NIH3T3 mouse fibroblast cells, or MKL1-dependent in aggressive MDA-MB-231 breast cancer cells or B16F2 melanoma cells are displayed in the table. The references used to build the table are indicated below the table.

transition, extracellular matrix, G-protein coupled receptor protein signaling pathway, inflammatory response, metalloendopeptidases, as a filter, we identified 203 gene transcripts out of the 2,142 total gene transcripts (Table A-1) that are regulated by CCG-1423 to be metastasis-related (Table 4-3, Table A-1). To further narrow the number of candidate genes to follow-up upon, we filtered the 203 gene transcripts for genes where CCG-1423 stimulated or inhibited by at least an 8-fold change in gene expression (Table 4-3). This left us with 16 candidate gene transcripts to follow-up upon (Table 4-3). We ruled out 12 of these gene transcripts based on the fact that the cancer biology literature on these gene transcripts did not correlate with the CCG-1423 regulated gene expression microarray results (Table 4-3). Therefore, we were left with 4 candidate genes, including *regulator of G-protein signaling 4 (RGS4)*, *regulator of G-protein signaling 7 (RGS7)*, *connective tissue growth factor (CTGF)*, and *SRY (sex determining region Y)-box 9 (campomelic dysplasia, autosomal sex reversal) (SOX9)*, to follow-up upon based on the cancer biology literature (Table 4-3).

Both RGS4 and RGS7 gene expression were stimulated by CCG-1423 in PC-3 prostate cancer cells. Interestingly, in ovarian cells RGS4 was previously found to be differentially expressed with RGS4 being expressed about 5,000-fold less in ovarian cancer cell lines (SKOV-3, Caov-3, OVCAR-3) in comparison to normal immortalized ovarian surface epithelial cells (IOSE) (4). Therefore, stimulation of RGS4 gene expression by CCG-1423 may prove useful in inhibiting cancer progression. In NIH3T3 mouse fibroblast cells, constitutively activated $G\alpha_o$ -subunit stimulated focus formation in a Stat3-dependent manner (8). Given that RGS7 can regulate $G\alpha_o$ -mediated signaling

mechanisms, stimulation of RGS7 gene expression by CCG-1423 may prove useful in inhibiting cancer progression dependent upon $G\alpha_o$ signaling pathways.

In contrast, both CTGF and SOX9 gene expression were inhibited by CCG-1423 in PC-3 prostate cancer cells. In the literature, CTGF has been shown to be over expressed in several types of cancers, including head and neck squamous cell carcinoma (7), pancreatic cancer (2), gastric cancer (5), and in pre-B acute lymphoblastic leukaemia (ALL) (3). In gastric cancer, CTGF overexpression was strongly correlated with poor patient survival (5), whereas in pancreatic cancer CTGF mediated tumor growth both *in vitro* and *in vivo* (2). SOX9 has been shown to be overexpressed in both colorectal cancer (6) and hormone-refractory prostate cancer (11). Overexpression of SOX9 has been correlated with poor patient survival in colorectal cancer (6), and enhanced *in vivo* tumor growth, angiogenesis, and invasion in a LNCaP prostate cancer xenograft model (10). Therefore, inhibition of CTGF and/or SOX9 by CCG-1423 may potentially play a role in preventing cancer progression.

<u>Total # of Transcripts on Affymetrix Chip</u>	50,000
<u>Genes changed by CCG-1423 (3 μM)</u>	2,143
<u>Genes w/ metastasis-related function based on GO Categories</u>	203
<u>Genes w/ +/- 8-fold change</u>	16
<u>Literature Validated Genes (Prostate or Cancer-Related)</u>	4 (RGS4, RGS7, CTGF, SOX9)

Table 4-3. Rationale for Candidate Gene Selection. Using metastasis-related gene ontologies as a filter, we were able to narrow the 2,143 candidate genes regulated by CCG-1423 down 203 gene transcripts. Then, using a stringent 8-fold change cutoff in either the stimulatory or inhibitory direction, we were able to narrow the candidate genes down to 16 gene transcripts. Finally, using literature to validate the 16 candidate genes as it potentially would correlate with CCG-1423 regulation, we were able to rule out 12 genes, and identify 4 candidate genes (RGS4, RGS7, CTGF, SOX9) that may play a role in PC-3 cell Matrigel invasion

Microarray vs. QRT-PCR Results

In order to confirm the microarray results for the 4 candidate genes, we tested the ability of CCG-1423 to regulate RGS4, RGS7, CTGF, and SOX9 gene expression in PC-3 prostate cancer cells in a quantitative-real time polymerase chain reaction (QRT-PCR) experiment. Both RGS4 and RGS7 gene expression was confirmed to be up-regulated, meanwhile both CTGF and SOX9 gene expression was confirmed to be down-regulated, by 3 μ M of CCG-1423 in the QRT-PCR experiment. The mean fold change for RGS4 up-regulation by CCG-1423 was slightly lower (12.4 fold-change) in the QRT-PCR results in comparison to the mean fold changes (21.7 fold-change, 21.6 fold-change, 19.4 fold-change) of the three RGS4 probesets in the microarray results (Table 4-4). The difference in mean fold changes for RGS7 upregulation by CCG-1423 between the QRT-PCR (9.9 fold-change) and microarray (9.6 fold-change) results was negligible (Table 4-4). With respect to CCG-1423-mediated down-regulation of CTGF gene expression, the mean fold change observed in the QRT-PCR results (0.12 fold-change) was lower than in the microarray results (0.05 fold-change) (Table 4-4). The mean fold change of SOX9 by CCG-1423 was very similar (0.19 fold-change) in the QRT-PCR results in comparison to the mean fold changes (0.12 fold-change, 0.13 fold-change) of the two SOX9 probesets in the microarray results (Table 4-4). Overall, the 4 candidate genes were confirmed by QRT-PCR to be regulated by CCG-1423.

Time-Course of CCG-1423 Regulated Gene Expression

In order to better understand the timing of CCG-1423 regulated gene expression, we studied the effect of CCG-1423 upon RGS4, RGS7, CTGF, and SOX9 gene

	<u>Microarray</u>	<u>QRT-PCR</u>
Gene	Fold Change	Fold Change
RGS4	21.7, 21.6*, 19.4*	12.4
RGS7	9.6	9.9
CTGF	0.05	0.12
SOX9	0.12, 0.13*	0.19

*Note. * indicates mean fold-change values of different probesets for RGS4 or SOX9.*

Table 4-4. Comparison of Microarray versus QRT-PCR Results. PC-3 cells were treated with 3 μ M of CCG-1423 under serum-starved conditions (0.5% FBS) for 24 hours and gene expression was assessed with an affymetrix gene chip or in a quantitative real-time-PCR (QRT-PCR)reaction assay. The genes RGS4, RGS7, CTGF, and SOX9, which were identified as candidate follow-up genes using our stringent criteria, were confirmed using a QRT-PCR assay. The mean fold-change values (over DMSO Control) of these genes for three separate experiments are displayed in the table for both the Affymetrix gene chip and QRT-PCR results. For the Microarray data, the \log_2 transformed expression values were converted to their natural scale by exponentiating the values using 2^x , where x equals the expression value. Then, the fold changes were calculated by dividing the expression values of the compound samples by the expression values of the DMSO samples.

expression over a time frame between 1 hour and 24 hours in PC-3 prostate cancer cells (Figure 4-2). CCG-1423 stimulated RGS4 gene expression in a time-dependent manner peaking at the 24 hour time point (Figure 4-2A). However, CCG-1423 stimulated RGS7 gene expression peaked at 6 hours (Figure 4-2B). Interestingly, CCG-1423 stimulated CTGF gene expression at the early 6 hour time point, but inhibited CTGF gene expression at the late 24 hour time point (Figure 4-2D). This suggests that if PC-3 prostate cancer cell Matrigel invasion is CTGF-dependent, then it would take at least 24 hours of CCG-1423 treatment for inhibition. Lastly, CCG-1423 inhibited SOX9 gene expression in a time-dependent manner, and inhibition was maximized after 12 hours of CCG-1423 treatment (Figure 4-2C). Overall, with the exception of RGS7 (6 hours), it takes between 12 hours and 24 hours of CCG-1423 treatment to maximize its regulation of RGS4, CTGF, and SOX9 gene expression.

Candidate Gene Expression across Prostate Epithelial Cell Lines

In order to determine if the 4 candidate genes were differentially expressed between two prostate cancer epithelial cell lines (LNCaP and PC-3) and a normal prostate epithelial cell line (RWPE-1), endogenous mRNA expression of these genes were tested via QRT-PCR. We hypothesized that RGS4 and RGS7 mRNA expression would be lower and CTGF and SOX9 mRNA expression would be higher in the prostate cancer cell lines versus the normal prostate cell line. In contrast with this expectation, RGS4 mRNA expression was strongly up-regulated in the hormone-independent PC-3 cancer cell line in comparison to both the hormone-dependent LNCaP cancer cell line and normal RWPE-1 cell line (Figure 4-3A). Interestingly, RGS4 mRNA expression was

slightly lower (~ 1.4 fold) in the hormone-dependent LNCaP cancer cell line versus the normal RWPE-1 cell line (Figure 4-3A). These data are not consistent with our hypothesis in relation to the hormone-independent PC-3 cells, but suggest that CCG-1423-mediated up-regulation of RGS4 gene expression may potentially play an inhibitory role in hormone-dependent prostate cancer progression. RGS7 mRNA expression was up-regulated in both the hormone-dependent LNCaP (~ 4-fold) and hormone-independent PC-3 (~ 4-fold) cancer cell lines in comparison to the normal RWPE-1 cell line (Figure 4-3C). This RGS7 result is also inconsistent with our hypothesis.

CTGF mRNA expression is up-regulated (~ 45-1,900 fold) in the hormone-independent PC-3 prostate cancer cells in comparison to both the hormone-dependent LNCaP prostate cancer cells and normal RWPE-1 prostate cells (Figure 4-3G). However, CTGF is down-regulated (~ 41-fold) in the hormone-dependent LNCaP prostate cancer cells versus the normal RWPE-1 prostate cells (Figure 4-3G). These CTGF results are partially consistent with our hypothesis with respect to the PC-3 cells, but not with respect to the LNCaP cells. Therefore, these data suggest that CCG-1423-mediated down-regulation of CTGF mRNA expression would potentially have an inhibitory effect upon hormone-independent prostate cancer progression and metastasis, but not hormone-dependent prostate cancer progression and metastasis. SOX9 mRNA expression is up-regulated (~ 30-45 fold) in hormone-independent PC-3 prostate cancer cells in comparison to both the hormone-dependent LNCaP prostate cancer cells and normal RWPE-1 prostate cells (Figure 4-3E). However, SOX9 mRNA expression is higher (~ 1.5 fold) in normal RWPE-1 prostate cells than hormone-dependent LNCaP prostate cancer cells (Figure 4-3E). These SOX9 data are partially consistent with my hypothesis

in relation to PC-3 cells, but not LNCaP cells. Therefore, similar to the CTGF data, the SOX9 data suggest that CCG-1423-mediated down-regulation of SOX9 gene expression potentially would have a positive inhibitory role in hormone-independent prostate cancer progression and metastasis, but not hormone-dependent prostate cancer progression and metastasis.

I also hypothesized that the CCG-1423-mediated effects upon gene expression of the 4 candidate genes would be selective for the prostate cancer cell lines versus the normal prostate cell line. Interestingly, CCG-1423 had a selective greater stimulatory effect upon RGS4 gene expression in both the hormone-dependent LNCaP (~ 13 fold-change) and hormone-independent PC-3 (~ 13 fold-change) prostate cancer cell lines versus the normal RWPE-1 (~ 3 fold-change) prostate cell line (Figure 4-3B), but no difference in its effect upon RGS7 gene expression across the prostate cell lines (Figure 4-3D). With respect to CTGF gene expression, CCG-1423 selectively stimulates CTGF gene expression in the hormone-dependent LNCaP (~ 80 fold-change) prostate cancer cell line, but selectively inhibits CTGF gene expression in the hormone-independent PC-3 (~ 0.5 fold-change) prostate cancer cell line, in comparison to the normal RWPE-1 prostate cells (Figure 4-3H). These effects upon CTGF gene expression may potentially serve useful in inhibiting both hormone-dependent and -independent prostate cancer progression and metastasis, if the endogenous mRNA expression of CTGF correlates with disease pathogenesis. CCG-1423 selectively inhibits SOX9 gene expression in hormone-independent PC-3 (~ 0.2 fold-change) prostate cancer cells, but only modestly inhibits SOX9 gene expression in hormone-dependent LNCaP (~ 0.77 fold-change) prostate cancer cells (Figure 4-3F). However, interestingly, CCG-1423 modestly

stimulates SOX9 gene expression the normal RWPE-1 (~ 1.6 fold-change) prostate cells (Figure 4-3F). Overall, CCG-1423 has selective effects upon RGS4, CTGF, and SOX9 gene expression in the two prostate cancer cell lines versus the normal prostate cell line, which make them viable candidate genes to further investigate the mechanism of CCG-1423-mediated inhibition of PC-3 prostate cancer cell Matrigel invasion.

Effect of CCG-1423 analogs Upon Candidate Gene Expression

In chapter 3, we identified several synthetic analogs of CCG-1423 with reduced toxicity and improved selectivity of the Rho-specific SRE.L-luciferase response in comparison to the thymidine kinase-mediated *Renilla* luciferase response. We hypothesized that these improved selective CCG-1423 analogs would have similar effects upon RGS4, RGS7, CTGF, and SOX9 gene expression in PC-3 prostate cancer cells, considering these analogs also had inhibitory effects upon PC-3 prostate cancer cell Matrigel invasion. We chose to test the effects of the RhoA transcriptional response inactive CCG-100686 analog and two active, CCG-100602 and CCG-101425, analogs upon candidate gene expression. As expected, we observed the CCG-100686 to be inactive and both CCG-100602 and CCG-101425 to stimulate RGS4 gene expression in a similar manner as CCG-1423 (Figure 4-4A). CCG-101425 stimulates RGS4 gene expression in a dose-dependent manner, but surprisingly CCG-100602 did not (Figure 4-4A). Surprisingly, the inactive, CCG-100686, and two active, CCG-100602 and CCG-101425, analogs all stimulated RGS7 gene expression (Figure 4-4B). There was no

significant difference in CCG-100602 stimulation of RGS7 gene expression at 30 μ M and 100 μ M, but CCG-101425 surprisingly did not stimulate RGS7 gene expression at 30 μ M (Figure 4-4B). The effects of the CCG-1423 analogs upon CTGF gene expression were

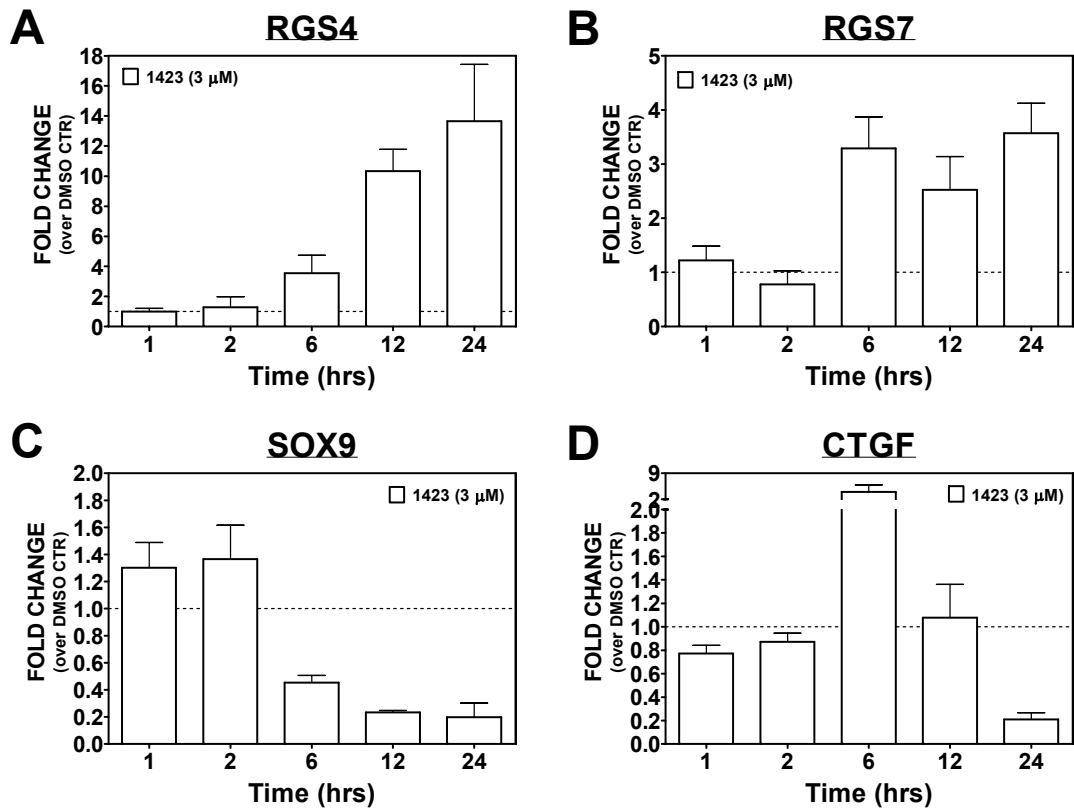


Figure 4-2. Time-Course of CCG-1423 Effect Upon PC-3 Cell Gene Expression. PC-3 cells were treated with 3 μ M of CCG-1423 under serum-starved (0.5% FBS) conditions for 1 hr, 2hrs, 6, hrs, 12 hrs, and 24 hrs. The genes, RGS4 (A), RGS7 (B), SOX9 (C), and CTGF (D), which were identified as candidate follow-up genes using our stringent criteria, were tested using QRT-PCR as described in the Materials and Methods. Data in Panels A-D represent mean \pm SEM fold-change values (over DMSO Control) for three separate experiments.

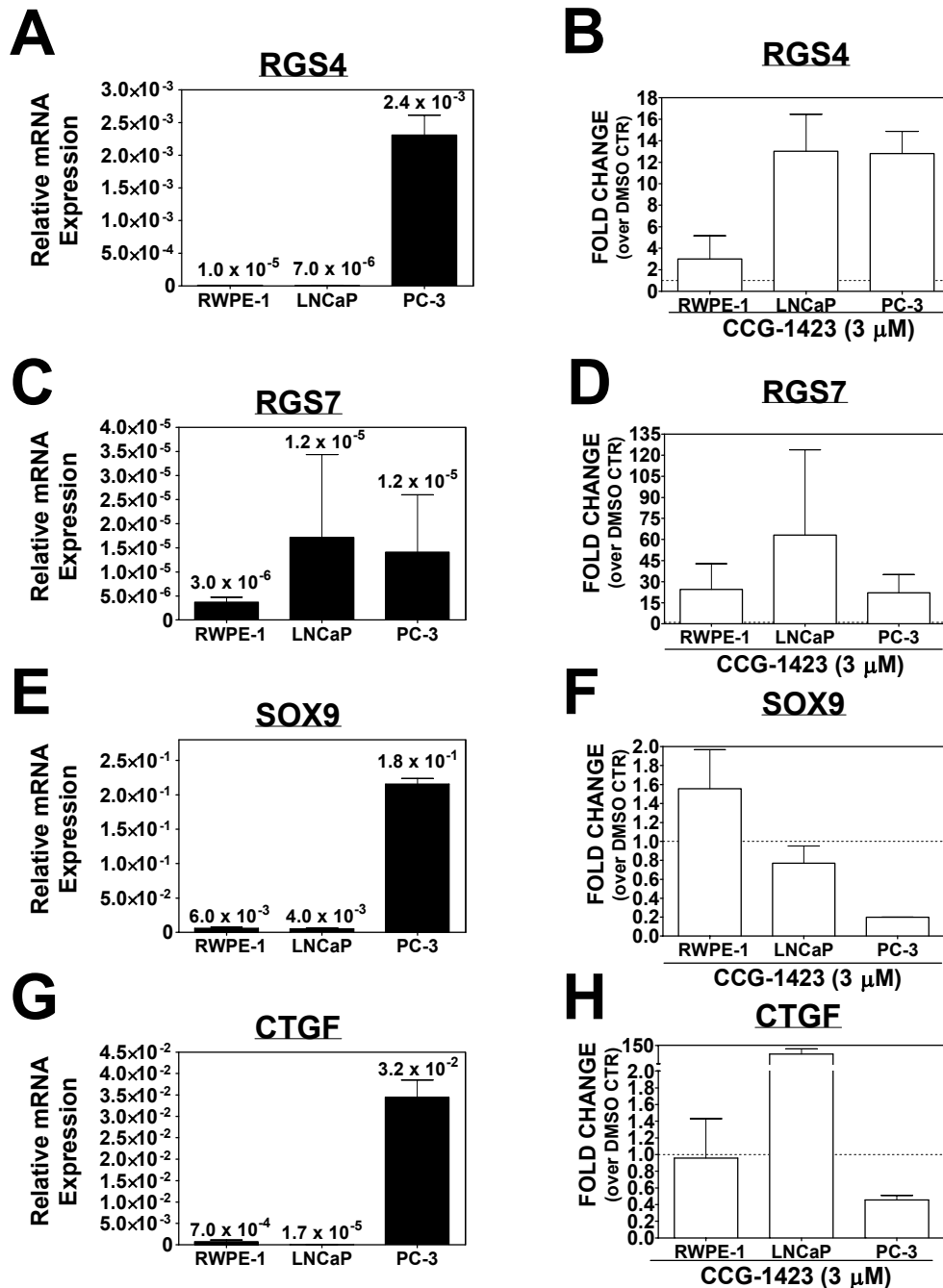


Figure 4-3. Gene Expression across 3 Prostate Epithelial Cell Lines. Normal RWPE-1 prostate epithelial cells, hormone-dependent LNCaP prostate cancer epithelial cells, and hormone-independent PC-3 prostate cancer epithelial cells were tested under serum-starved conditions (0.5% FBS) in the presence of DMSO (0.03%) for 24 hours for their basal levels of gene expression of RGS4 (A), RGS7 (C), SOX9 (E), and CTGF (G) mRNA using QRT-PCR as described in the Materials and Methods. The three prostate epithelial cell lines were also tested under serum-starved conditions (0.5% FBS) in the presence of 3 μ M of CCG-1423 for 24 hours to assess the effect of the compound upon RGS4 (B), RGS7 (D), SOX9 (F), and CTGF (H) gene expression using the QRT-PCR

Figure 4-3. Gene Expression across 3 Prostate Epithelial Cell Lines (continued). assay as described in the Materials and Methods. Data in Panels A, C, E, and G represent mean \pm SEM $2^{-(\Delta\text{ct value})}$ relative expression values for three separate experiments. Data in Panels B, D, F, and H mean \pm SEM fold-change (over DMSO control) values for three separate experiments.

drastically different in comparison to CCG-1423. As expected, the inactive CCG-100686 analog had no effect upon CTGF expression (Figure 4-4C). However, interestingly the active CCG-100602 analog had a stimulatory effect, whereas CCG-101425 had a very modest inhibitory effect upon CTGF gene expression (Figure 4-4C). In terms of SOX9 gene expression, the inactive CCG-100686 analog had no significant effect, whereas both active analogs, CCG-100602 and CCG-101425, had similar inhibitory effects as CCG-1423 (Figure 4-4D). However, the inhibitory effect of CCG-101425 was not as strong as CCG-1423 (Figure 4-4D). Therefore, considering the differential effects of the CCG-1423 analogs upon RGS7 and CTGF gene expression in comparison to CCG-1423, we are left with both RGS4 and SOX9 as a two best candidate genes that CCG-1423 may mediate its inhibitory effect upon PC-3 prostate cancer cell Matrigel invasion.

Discussion

In the study described here, we undertook a gene expression microarray analysis of CCG-1423 regulation of basal PC-3 prostate cancer cell gene expression. The goal of this study was to investigate the mechanism of action of CCG-1423 as it relates to both the RhoA transcriptional signaling pathway and spontaneous PC-3 prostate cancer cell Matrigel invasion. In order to investigate the mechanism of action as it relates to the RhoA transcriptional signaling pathway, we compared the effects of CCG-1423 regulated gene expression with the effects of both the actin cytoskeleton inhibitor,

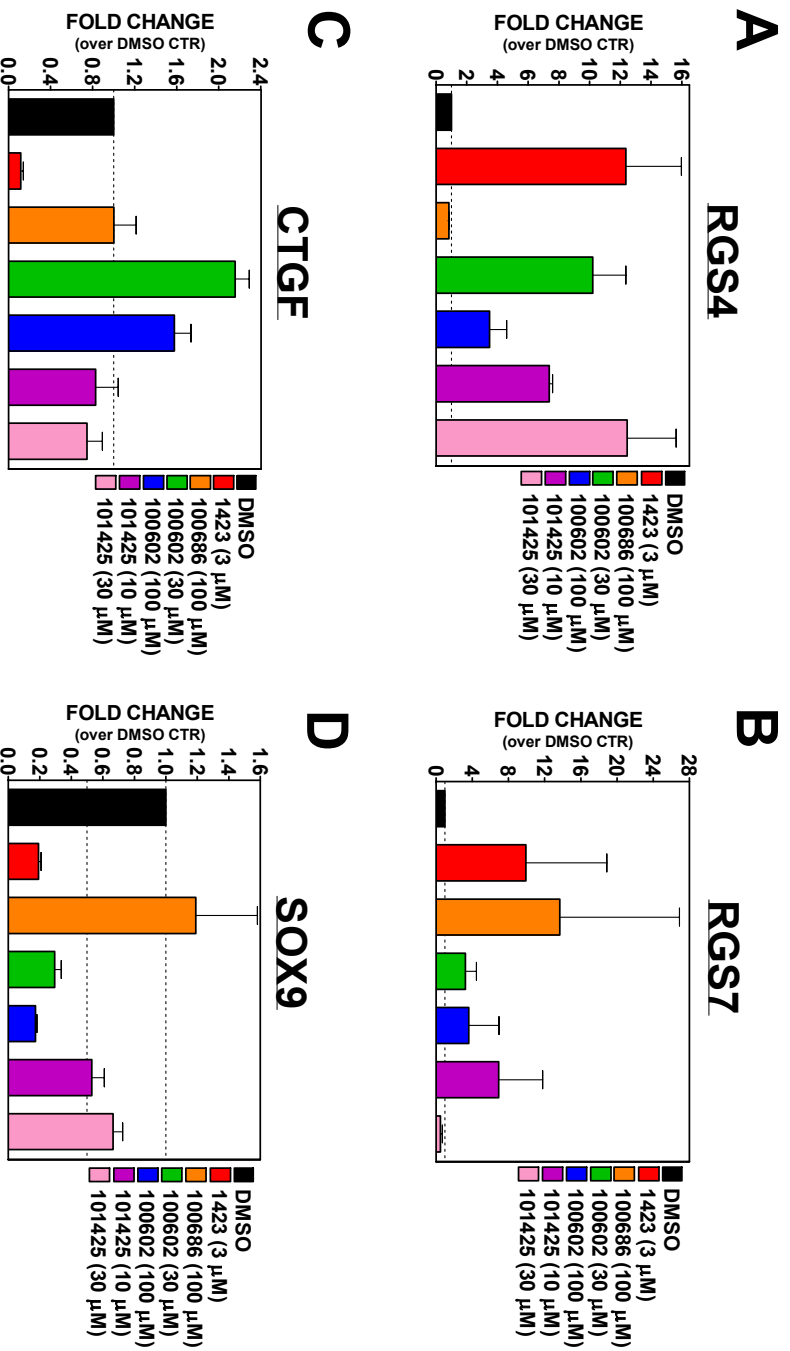


Figure 4-4. Effect of CCG-1423 Analogs Upon PC-3 Cell Gene Expression. PC-3 cells were treated with CCG-1423 (3 μ M), CCG-100686 (100 μ M), CCG-100602 (30 μ M and 100 μ M), and CCG-101425 (10 μ M and 30 μ M) for 24 hours under serum-starved conditions (0.5% FBS). The effect of these compounds upon gene expression of RGS4 (A), RGS7 (B), CTGF (C), and SOX9 (D), in PC-3 prostate cancer cells was assessed using QRT-PCR as described in the Materials and Methods. Data in Panels A-D represent the mean \pm SEM fold-change (over DMSO control) values of three separate experiments.

latrunculin B, as a positive control inhibitor of the pathway and the casein kinase II inhibitor, DRB, as a non-specific negative control inhibitor of general transcription. As expected, at both the 2 hour and 24 hour time point, DRB regulated the expression of the greatest number of gene transcripts, and the selective inhibitor, latrunculin B, regulated the least number of gene transcripts. Interestingly, CCG-1423 regulated a smaller number of gene transcripts than DRB, but a greater number of gene transcripts than latrunculin B. Therefore, these microarray results are consistent with our hypothesis that CCG-1423 is not a general non-specific gene transcription inhibitor, but it is a signaling pathway inhibitor with some non-specific effects based on the number of genes regulated by CCG-1423 and our control compounds. Interestingly, our general transcription inhibitor, DRB, regulated a surprisingly small number of gene transcripts at both the 2 hour (719 gene transcripts) and 24 hour (3021 gene transcripts) out of a possible total of about 50,000 gene transcripts. This is surprising since DRB was originally identified as an inhibitor of RNA-Polymerase II-mediated general transcription both biochemically and in cell culture through inhibition of the casein II kinase (61, 62). However, in early studies (61, 62), only a few gene promoters were tested. Interestingly, our genome-wide gene expression data suggest that casein kinase II-mediated regulation of RNA-Polymerase II driven transcription is specific only for a subset of genes, but this may partially be attributed to mRNA stability since only two time points were tested. Therefore, although not the focus of the work described here, our data suggest that DRB may not be completely selective for general RNA Polymerase II transcriptional activity. Different genes most likely utilize different kinases for mediating RNA Polymerase II activity. It would be interesting if

others in future studies investigate other potential kinases that may regulate RNA Polymerase II-mediated transcriptional activity.

Interestingly, at the 2 hour time point both CCG-1423 and latrunculin B stimulated all except two of the genes they each regulated. However, this is unlikely due to a correlation that both target the RhoA transcriptional signaling pathway since they only shared the regulation of four gene transcripts. At the 24 hour time point, CCG-1423 only shared 20.7% of its regulated transcripts with latrunculin B, but interestingly latrunculin B shared 72.9% of its regulated gene transcripts with CCG-1423, which would suggest some correlation due to pathway specificity between both inhibitors. However, the lack of strong correlation of CCG-1423 regulated gene transcripts with latrunculin B raises questions about this interpretation. However, it should be noted that latrunculin B is not specific for the RhoA transcriptional signaling pathway because the actin cytoskeleton is involved in many other cell signaling pathways, such as NF-kappaB (63), Rac (64), merlin-protein kinase A (PKA) (65), and insulin (66) signaling. This lack of pathway specificity could contribute to the lack of correlation between the CCG-1423 and latrunculin B data described here. We also tried to compare shared gene symbols identified in our gene expression compound results to an *in silico* study identifying known and novel SRF-mediated CArG-box genes (12) and to micorarray studies utilizing dominant negative overexpression and shRNA knockdown of MKL1 in different cell lines (13, 14), but found no significant correlation with our data. The lack of correlation could be partially attributed to most of these studies being performed in different types of cell lines. Therefore, future microarray experimental results in PC-3 cells utilizing more specific inhibitors or siRNA knockdown and/or dominant-negative overexpression of

components of the RhoA transcriptional signaling pathway, such as the Rho-kinase inhibitor, Y-27632, the Rho ADP-ribosylating toxin, C3, or siRNA knockdown and/or dominant-negative overexpression of RhoA, RhoC, MKL1, and/or SRF, would be useful to compare to the compound regulated gene expression results described here.

Due to the lack of a strong correlation of CCG-1423 regulated gene expression with the RhoA transcriptional signaling pathway in the study undertaken here, it is possible that CCG-1423 may not be as selective for the RhoA pathway as I originally hypothesized. Therefore, I decided to more generally look at the mechanism of CCG-1423 as it relates to global PC-3 cell gene expression. As a result, I switched my focus to investigating the mechanism of action of CCG-1423 as it relates to regulated genes that potentially may play a role in spontaneous PC-3 prostate cancer cell Matrigel invasion and metastasis. In the literature, gene expression has been implicated to play a role in the complex process of metastasis (18). In a genome-wide gene expression study comparing low versus high metastatic breast cancer cells, a subset of 54 genes were identified to be biologically relevant to lung metastasis (67). Out of these 54 genes, 9 genes were functionally validated to play a biological role in *in vivo* lung metastasis models, including the epidermal-growth-factor family epiregulin (*EREG*), the chemokine *GRO1/CXCL1*, the matrix metalloproteinases *MMPI* and *MMP2*, the cell adhesion molecule *SPARC*, the interleukin-13 decoy receptor *IL13Ra2*, the cell adhesion receptor *VCAMI*, the transcriptional inhibitor of cell differentiation and senescence *IDI*, and the prostaglandin-endoperoxide synthase *PTGS2/COX2* (67). Also, in another study, TGF β -mediated SMAD signaling and induction of angiotensin-like 4 (*ANGPTL4*) gene expression in lung metastatic breast cancer cells was found to promote lung metastasis of

breast cancer cells in a xenograft model (23). More interestingly, in prostate cancer, overexpression of the Tat-interacting protein 30 (TIP30) and the ADP-ribosylation factor GTPase-activating protein (ASAP1) in metastatic prostate cancer cell lines were shown to play a role in *in vitro* cell migration and invasion (68, 69), whereas the overexpression of a splice-variant of Kruppel-like factor 6 (KLF6-SV1) was shown to play a role in *in vivo* bone, lymph node, and brain metastasis in an orthotopic prostate cancer metastasis xenograft model (70). Therefore, using metastasis-related gene ontology (GO) categories (*angiogenesis, cell migration, cell adhesion, epithelial to mesenchymal transition, extracellular matrix, G-protein coupled receptor protein signaling pathway, inflammatory response, metalloendopeptidases*), an eight-fold change in gene expression in either the stimulatory or inhibitory direction, and the cancer literature, we were able to identify four candidate genes (*RGS4, RGS7, CTGF, and SOX9*) that were regulated by CCG-1423 to potentially play a role in PC-3 prostate cancer cell invasion and metastasis. Then, upon using two more selective CCG-1423 analogs (CCG-100602 and CCG-101425) identified in Chapter 3, we were able to rule out two out of the four candidate genes to not play a role in PC-3 prostate cancer cell invasion and metastasis, due to the more selective compounds having a differential effect upon gene expression of these genes in comparison to CCG-1423. Therefore, we were able to identify *RGS4* and *SOX9* as two potential genes that may play a role in PC-3 prostate cancer cell invasion and metastasis.

RGS4 is a regulator of G-protein signaling protein that regulates the inactivation of $G\alpha_{i/o}$ and $G\alpha_q$ coupled G-protein coupled receptor (GPCR) signaling through stimulating the hydrolysis of GTP to GDP on the nucleotide bound $G\alpha$ -subunit (71, 72).

Interestingly, RGS4 has been shown to play a role in tumorigenesis in a variety of cancer types. In thyroid cancer, RGS4 was found to be up-regulated in comparison to normal human tissue, and siRNA knockdown of RGS4 in thyroid cancer cells led to a functional reduction in viability (73), whereas in a pancreatic cancer metastatic xenograft model, RGS4 was found to be up-regulated in the liver metastasis cells in comparison to the primary tumor cells (74). However, in several ovarian cancer cell lines dependent upon lysophosphatidic acid (LPA) signaling, RGS4 was found to be at least 5,000-fold down-regulated in comparison to normal ovarian epithelial cells, which suggests a role for RGS4 in ovarian cancer pathogenesis (4). More interestingly, ovarian cancer ascites stimulated OV-90 ovarian cancer cell invasion through a Matrigel matrix, and this invasion directly correlated with an up-regulation of RGS4 gene expression. Also, RGS4 was found to be up-regulated in fast-migrating glioma cells versus slow-migrating glioma cells (9), thus suggesting a role of RGS4 regulated pathways in glioma invasion and metastasis. Therefore, the implication of RGS4 in the pathogenesis of a variety of cancers makes it a viable gene candidate that may play a role in PC-3 prostate cancer cell invasion and metastasis.

SOX9 (SRY (sex determining region Y)-box 9) is a transcription factor downstream of β -catenin signaling that has been well-established to be involved in male testis development and sex determination (75). However, in adulthood, aberrant SOX9 regulation can play a key role in tumorigenesis of colorectal and prostate cancers. In a 5-year colorectal cancer patient study, patients with high SOX9 expression showed a reduced survival rate in comparison to patients with low SOX9 expression (6). More interestingly, SOX9 was observed to be expressed in a higher percentage of prostate

cancer patients with recurrent tumors versus those with primary tumors (11). Also, SOX9 was shown to be over-expressed in hormone-refractory prostate cancer cell lines, and down-regulation in these cell lines led to a reduction of cell-cycle progression, and reduction of *in vivo* CWR22Rv1 cell growth (10, 11). In a xenograft model utilizing LNCaP cells overexpressing SOX9, tumor growth, invasion, and angiogenesis were enhanced (10). Therefore, SOX9 should be a viable gene candidate for the regulation of PC-3 prostate cancer cell invasion and metastasis.

In the microarray study described here, we were able to identify two viable candidate genes that may play a pivotal role in PC-3 prostate cancer cell invasion and metastasis. Future *in vitro* functional studies addressing the role of RGS4 and/or SOX9 in PC-3 cell growth, adhesion, migration, and invasion through retroviral overexpression of RGS4 and shRNA knockdown of SOX9 will produce insights into the role of these CCG-1423 regulated genes in prostate cancer progression and metastasis. Additional, *in vivo* PC-3 prostate cancer cell metastasis xenograft studies through retroviral overexpression of RGS4 and shRNA knockdown of SOX9 will also be useful in assessing the role of these CCG-1423 regulated genes in prostate cancer progression and metastasis, but in a more physiologically relevant context.

References

1. Evelyn, C. R., Wade, S. M., Wang, Q., Wu, M., Iniguez-Lluhi, J. A., Merajver, S. D., and Neubig, R. R. CCG-1423: a small-molecule inhibitor of RhoA transcriptional signaling. *Mol Cancer Ther*, *6*: 2249-2260, 2007.
2. Bennewith, K. L., Huang, X., Ham, C. M., Graves, E. E., Erler, J. T., Kambham, N., Feazell, J., Yang, G. P., Koong, A., and Giaccia, A. J. The role of tumor cell-derived connective tissue growth factor (CTGF/CCN2) in pancreatic tumor growth. *Cancer Res*, *69*: 775-784, 2009.
3. Boag, J. M., Beesley, A. H., Firth, M. J., Freitas, J. R., Ford, J., Brigstock, D. R., de Klerk, N. H., and Kees, U. R. High expression of connective tissue growth factor in pre-B acute lymphoblastic leukaemia. *Br J Haematol*, *138*: 740-748, 2007.
4. Hurst, J. H., Mendpara, N., and Hooks, S. B. Regulator of G-protein signalling expression and function in ovarian cancer cell lines. *Cell Mol Biol Lett*, *14*: 153-174, 2009.
5. Liu, L., Li, Z., Feng, G., You, W., and Li, J. Expression of connective tissue growth factor is in agreement with the expression of VEGF, VEGF-C, -D and associated with shorter survival in gastric cancer. *Pathol Int*, *57*: 712-718, 2007.
6. Lu, B., Fang, Y., Xu, J., Wang, L., Xu, F., Xu, E., Huang, Q., and Lai, M. Analysis of SOX9 expression in colorectal cancer. *Am J Clin Pathol*, *130*: 897-904, 2008.
7. Mullis, T. C., Tang, X., and Chong, K. T. Expression of connective tissue growth factor (CTGF/CCN2) in head and neck squamous cell carcinoma. *J Clin Pathol*, *61*: 606-610, 2008.
8. Ram, P. T., Horvath, C. M., and Iyengar, R. Stat3-mediated transformation of NIH-3T3 cells by the constitutively active Q205L Galphao protein. *Science*, *287*: 142-144, 2000.
9. Tatenhorst, L., Senner, V., Puttmann, S., and Paulus, W. Regulators of G-protein signaling 3 and 4 (RGS3, RGS4) are associated with glioma cell motility. *J Neuropathol Exp Neurol*, *63*: 210-222, 2004.
10. Wang, H., Leav, I., Ibaragi, S., Wegner, M., Hu, G. F., Lu, M. L., Balk, S. P., and Yuan, X. SOX9 is expressed in human fetal prostate epithelium and enhances prostate cancer invasion. *Cancer Res*, *68*: 1625-1630, 2008.

11. Wang, H., McKnight, N. C., Zhang, T., Lu, M. L., Balk, S. P., and Yuan, X. SOX9 is expressed in normal prostate basal cells and regulates androgen receptor expression in prostate cancer cells. *Cancer Res*, *67*: 528-536, 2007.
12. Sun, Q., Chen, G., Streb, J. W., Long, X., Yang, Y., Stoeckert, C. J., Jr., and Miano, J. M. Defining the mammalian CARome. *Genome Res*, *16*: 197-207, 2006.
13. Selvaraj, A. and Prywes, R. Expression profiling of serum inducible genes identifies a subset of SRF target genes that are MKL dependent. *BMC Mol Biol*, *5*: 13, 2004.
14. Medjkane, S., Perez-Sanchez, C., Gaggioli, C., Sahai, E., and Treisman, R. Myocardin-related transcription factors and SRF are required for cytoskeletal dynamics and experimental metastasis. *Nat Cell Biol*, *11*: 257-268, 2009.
15. Christofori, G. New signals from the invasive front. *Nature*, *441*: 444-450, 2006.
16. Fidler, I. J. The pathogenesis of cancer metastasis: the 'seed and soil' hypothesis revisited. *Nat Rev Cancer*, *3*: 453-458, 2003.
17. Gupta, G. P. and Massague, J. Cancer metastasis: building a framework. *Cell*, *127*: 679-695, 2006.
18. Nguyen, D. X., Bos, P. D., and Massague, J. Metastasis: from dissemination to organ-specific colonization. *Nat Rev Cancer*, *9*: 274-284, 2009.
19. Sawyer, T. K. Cancer metastasis therapeutic targets and drug discovery: emerging small-molecule protein kinase inhibitors. *Expert Opin Investig Drugs*, *13*: 1-19, 2004.
20. Yang, J. and Weinberg, R. A. Epithelial-mesenchymal transition: at the crossroads of development and tumor metastasis. *Dev Cell*, *14*: 818-829, 2008.
21. Hu, G., Chong, R. A., Yang, Q., Wei, Y., Blanco, M. A., Li, F., Reiss, M., Au, J. L., Haffty, B. G., and Kang, Y. MTDH activation by 8q22 genomic gain promotes chemoresistance and metastasis of poor-prognosis breast cancer. *Cancer Cell*, *15*: 9-20, 2009.
22. Gupta, G. P., Nguyen, D. X., Chiang, A. C., Bos, P. D., Kim, J. Y., Nadal, C., Gomis, R. R., Manova-Todorova, K., and Massague, J. Mediators of vascular remodelling co-opted for sequential steps in lung metastasis. *Nature*, *446*: 765-770, 2007.
23. Padua, D., Zhang, X. H., Wang, Q., Nadal, C., Gerald, W. L., Gomis, R. R., and Massague, J. TGFbeta primes breast tumors for lung metastasis seeding through angiopoietin-like 4. *Cell*, *133*: 66-77, 2008.

24. Kang, Y., Siegel, P. M., Shu, W., Drobnjak, M., Kakonen, S. M., Cordon-Cardo, C., Guise, T. A., and Massague, J. A multigenic program mediating breast cancer metastasis to bone. *Cancer Cell*, 3: 537-549, 2003.
25. Mundy, G. R. Metastasis to bone: causes, consequences and therapeutic opportunities. *Nat Rev Cancer*, 2: 584-593, 2002.
26. Yin, J. J., Selander, K., Chirgwin, J. M., Dallas, M., Grubbs, B. G., Wieser, R., Massague, J., Mundy, G. R., and Guise, T. A. TGF-beta signaling blockade inhibits PTHrP secretion by breast cancer cells and bone metastases development. *J Clin Invest*, 103: 197-206, 1999.
27. Pille, J. Y., Denoyelle, C., Varet, J., Bertrand, J. R., Soria, J., Opolon, P., Lu, H., Pritchard, L. L., Vannier, J. P., Malvy, C., Soria, C., and Li, H. Anti-RhoA and anti-RhoC siRNAs inhibit the proliferation and invasiveness of MDA-MB-231 breast cancer cells in vitro and in vivo. *Mol Ther*, 11: 267-274, 2005.
28. Pan, Q., Bao, L. W., Teknos, T. N., and Merajver, S. D. Targeted disruption of protein kinase C epsilon reduces cell invasion and motility through inactivation of RhoA and RhoC GTPases in head and neck squamous cell carcinoma. *Cancer Res*, 66: 9379-9384, 2006.
29. van Golen, K. L., Bao, L., DiVito, M. M., Wu, Z., Prendergast, G. C., and Merajver, S. D. Reversion of RhoC GTPase-induced inflammatory breast cancer phenotype by treatment with a farnesyl transferase inhibitor. *Mol Cancer Ther*, 1: 575-583, 2002.
30. van Golen, K. L., Davies, S., Wu, Z. F., Wang, Y., Bucana, C. D., Root, H., Chandrasekharappa, S., Strawderman, M., Ethier, S. P., and Merajver, S. D. A novel putative low-affinity insulin-like growth factor-binding protein, LIBC (lost in inflammatory breast cancer), and RhoC GTPase correlate with the inflammatory breast cancer phenotype. *Clin Cancer Res*, 5: 2511-2519, 1999.
31. van Golen, K. L., Wu, Z. F., Qiao, X. T., Bao, L. W., and Merajver, S. D. RhoC GTPase, a novel transforming oncogene for human mammary epithelial cells that partially recapitulates the inflammatory breast cancer phenotype. *Cancer Res*, 60: 5832-5838, 2000.
32. Clark, E. A., Golub, T. R., Lander, E. S., and Hynes, R. O. Genomic analysis of metastasis reveals an essential role for RhoC. *Nature*, 406: 532-535, 2000.
33. Collisson, E. A., Kleer, C., Wu, M., De, A., Gambhir, S. S., Merajver, S. D., and Kolodney, M. S. Atorvastatin prevents RhoC isoprenylation, invasion, and metastasis in human melanoma cells. *Mol Cancer Ther*, 2: 941-948, 2003.

34. Lin, M., DiVito, M. M., Merajver, S. D., Boyanapalli, M., and van Golen, K. L. Regulation of pancreatic cancer cell migration and invasion by RhoC GTPase and caveolin-1. *Mol Cancer*, 4: 21, 2005.
35. Hall, C. L., Dubyk, C. W., Riesenberger, T. A., Shein, D., Keller, E. T., and van Golen, K. L. Type I collagen receptor ($\alpha 2\beta 1$) signaling promotes prostate cancer invasion through RhoC GTPase. *Neoplasia*, 10: 797-803, 2008.
36. Iizumi, M., Bandyopadhyay, S., Pai, S. K., Watabe, M., Hirota, S., Hosobe, S., Tsukada, T., Miura, K., Saito, K., Furuta, E., Liu, W., Xing, F., Okuda, H., Kobayashi, A., and Watabe, K. RhoC promotes metastasis via activation of the Pyk2 pathway in prostate cancer. *Cancer Res*, 68: 7613-7620, 2008.
37. Sequeira, L., Dubyk, C. W., Riesenberger, T. A., Cooper, C. R., and van Golen, K. L. Rho GTPases in PC-3 prostate cancer cell morphology, invasion and tumor cell diapedesis. *Clin Exp Metastasis*, 25: 569-579, 2008.
38. Yao, H., Dashner, E. J., van Golen, C. M., and van Golen, K. L. RhoC GTPase is required for PC-3 prostate cancer cell invasion but not motility. *Oncogene*, 25: 2285-2296, 2006.
39. Ikoma, T., Takahashi, T., Nagano, S., Li, Y. M., Ohno, Y., Ando, K., Fujiwara, T., Fujiwara, H., and Kosai, K. A definitive role of RhoC in metastasis of orthotopic lung cancer in mice. *Clin Cancer Res*, 10: 1192-1200, 2004.
40. Hakem, A., Sanchez-Sweetman, O., You-Ten, A., Duncan, G., Wakeham, A., Khokha, R., and Mak, T. W. RhoC is dispensable for embryogenesis and tumor initiation but essential for metastasis. *Genes Dev*, 19: 1974-1979, 2005.
41. Kelly, P., Moeller, B. J., Juneja, J., Booden, M. A., Der, C. J., Daaka, Y., Dewhirst, M. W., Fields, T. A., and Casey, P. J. The G12 family of heterotrimeric G proteins promotes breast cancer invasion and metastasis. *Proc Natl Acad Sci U S A*, 103: 8173-8178, 2006.
42. Kelly, P., Stemmler, L. N., Madden, J. F., Fields, T. A., Daaka, Y., and Casey, P. J. A role for the G12 family of heterotrimeric G proteins in prostate cancer invasion. *J Biol Chem*, 281: 26483-26490, 2006.
43. Berenjano, I. M., Nunez, F., and Bustelo, X. R. Transcriptomal profiling of the cellular transformation induced by Rho subfamily GTPases. *Oncogene*, 26: 4295-4305, 2007.
44. Wu, M., Wu, Z. F., Kumar-Sinha, C., Chinnaiyan, A., and Merajver, S. D. RhoC induces differential expression of genes involved in invasion and metastasis in MCF10A breast cells. *Breast Cancer Res Treat*, 84: 3-12, 2004.

45. Alberti, S., Krause, S. M., Kretz, O., Philippar, U., Lemberger, T., Casanova, E., Wiebel, F. F., Schwarz, H., Frotscher, M., Schutz, G., and Nordheim, A. Neuronal migration in the murine rostral migratory stream requires serum response factor. *Proc Natl Acad Sci U S A*, *102*: 6148-6153, 2005.
46. Chai, J. and Tarnawski, A. S. Serum response factor: discovery, biochemistry, biological roles and implications for tissue injury healing. *J Physiol Pharmacol*, *53*: 147-157, 2002.
47. Schrott, G., Philippar, U., Berger, J., Schwarz, H., Heidenreich, O., and Nordheim, A. Serum response factor is crucial for actin cytoskeletal organization and focal adhesion assembly in embryonic stem cells. *J Cell Biol*, *156*: 737-750, 2002.
48. Park, M. Y., Kim, K. R., Park, H. S., Park, B. H., Choi, H. N., Jang, K. Y., Chung, M. J., Kang, M. J., Lee, D. G., and Moon, W. S. Expression of the serum response factor in hepatocellular carcinoma: implications for epithelial-mesenchymal transition. *Int J Oncol*, *31*: 1309-1315, 2007.
49. Heemers, H. V., Regan, K. M., Dehm, S. M., and Tindall, D. J. Androgen induction of the androgen receptor coactivator four and a half LIM domain protein-2: evidence for a role for serum response factor in prostate cancer. *Cancer Res*, *67*: 10592-10599, 2007.
50. Mathupala, S. P., Ko, Y. H., and Pedersen, P. L. Hexokinase II: cancer's double-edged sword acting as both facilitator and gatekeeper of malignancy when bound to mitochondria. *Oncogene*, *25*: 4777-4786, 2006.
51. Vickers, E. R., Kasza, A., Kurnaz, I. A., Seifert, A., Zeef, L. A., O'Donnell, A., Hayes, A., and Sharrocks, A. D. Ternary complex factor-serum response factor complex-regulated gene activity is required for cellular proliferation and inhibition of apoptotic cell death. *Mol Cell Biol*, *24*: 10340-10351, 2004.
52. Wegiel, B., Bjartell, A., Culig, Z., and Persson, J. L. Interleukin-6 activates PI3K/Akt pathway and regulates cyclin A1 to promote prostate cancer cell survival. *Int J Cancer*, *122*: 1521-1529, 2008.
53. Yu, Y. P. and Luo, J. H. Myopodin-mediated suppression of prostate cancer cell migration involves interaction with zyxin. *Cancer Res*, *66*: 7414-7419, 2006.
54. Zhu, Z., Kleeff, J., Friess, H., Wang, L., Zimmermann, A., Yarden, Y., Buchler, M. W., and Korc, M. Epiregulin is Up-regulated in pancreatic cancer and stimulates pancreatic cancer cell growth. *Biochem Biophys Res Commun*, *273*: 1019-1024, 2000.

55. Zudaire, E., Martinez, A., and Cuttitta, F. Adrenomedullin and cancer. *Regul Pept*, *112*: 175-183, 2003.
56. Irizarry, R. A., Hobbs, B., Collin, F., Beazer-Barclay, Y. D., Antonellis, K. J., Scherf, U., and Speed, T. P. Exploration, normalization, and summaries of high density oligonucleotide array probe level data. *Biostatistics*, *4*: 249-264, 2003.
57. Wang, X., Adams, L. D., Pabon, L. M., Mahoney, W. M., Jr., Beaudry, D., Gunaje, J., Geary, R. L., Deblois, D., and Schwartz, S. M. RGS5, RGS4, and RGS2 expression and aortic contractility are dynamically co-regulated during aortic banding-induced hypertrophy. *J Mol Cell Cardiol*, *44*: 539-550, 2008.
58. Chertkow, Y., Weinreb, O., Youdim, M. B., and Silver, H. Gene expression changes in peripheral mononuclear cells from schizophrenic patients treated with a combination of antipsychotic with fluvoxamine. *Prog Neuropsychopharmacol Biol Psychiatry*, *31*: 1356-1362, 2007.
59. Li, M. H., Sanchez, T., Pappalardo, A., Lynch, K. R., Hla, T., and Ferrer, F. Induction of antiproliferative connective tissue growth factor expression in Wilms' tumor cells by sphingosine-1-phosphate receptor 2. *Mol Cancer Res*, *6*: 1649-1656, 2008.
60. Vincourt, J. B., Vignaud, J. M., Lionneton, F., Sirveaux, F., Kawaki, H., Marchal, S., Lomazzi, S., Plenat, F., Guillemin, F., Netter, P., Takigawa, M., Mainard, D., and Magdalou, J. Increased expression of matrilin-3 not only in osteoarthritic articular cartilage but also in cartilage-forming tumors, and down-regulation of SOX9 via epidermal growth factor domain 1-dependent signaling. *Arthritis Rheum*, *58*: 2798-2808, 2008.
61. Zandomeni, R. and Weinmann, R. Inhibitory effect of 5,6-dichloro-1-beta-D-ribofuranosylbenzimidazole on a protein kinase. *J Biol Chem*, *259*: 14804-14811, 1984.
62. Zandomeni, R., Zandomeni, M. C., Shugar, D., and Weinmann, R. Casein kinase type II is involved in the inhibition by 5,6-dichloro-1-beta-D-ribofuranosylbenzimidazole of specific RNA polymerase II transcription. *J Biol Chem*, *261*: 3414-3419, 1986.
63. Eswarappa, S. M., Pareek, V., and Chakravorty, D. Role of actin cytoskeleton in LPS-induced NF-kappaB activation and nitric oxide production in murine macrophages. *Innate Immun*, *14*: 309-318, 2008.
64. Mitchell, T., Lo, A., Logan, M. R., Lacy, P., and Eitzen, G. Primary granule exocytosis in human neutrophils is regulated by Rac-dependent actin remodeling. *Am J Physiol Cell Physiol*, *295*: C1354-1365, 2008.

65. Laulajainen, M., Muranen, T., Carpen, O., and Gronholm, M. Protein kinase A-mediated phosphorylation of the NF2 tumor suppressor protein merlin at serine 10 affects the actin cytoskeleton. *Oncogene*, *27*: 3233-3243, 2008.
66. Stanley, F. M. Insulin-increased prolactin gene expression requires actin treadmilling: potential role for p21 activated kinase. *Endocrinology*, *148*: 5874-5883, 2007.
67. Minn, A. J., Gupta, G. P., Siegel, P. M., Bos, P. D., Shu, W., Giri, D. D., Viale, A., Olshen, A. B., Gerald, W. L., and Massague, J. Genes that mediate breast cancer metastasis to lung. *Nature*, *436*: 518-524, 2005.
68. Lin, D., Watahiki, A., Bayani, J., Zhang, F., Liu, L., Ling, V., Sadar, M. D., English, J., Fazli, L., So, A., Gout, P. W., Gleave, M., Squire, J. A., and Wang, Y. Z. ASAP1, a gene at 8q24, is associated with prostate cancer metastasis. *Cancer Res*, *68*: 4352-4359, 2008.
69. Zhang, H., Zhang, Y., Duan, H. O., Kirley, S. D., Lin, S. X., McDougal, W. S., Xiao, H., and Wu, C. L. TIP30 is associated with progression and metastasis of prostate cancer. *Int J Cancer*, *123*: 810-816, 2008.
70. Narla, G., DiFeo, A., Fernandez, Y., Dhanasekaran, S., Huang, F., Sangodkar, J., Hod, E., Leake, D., Friedman, S. L., Hall, S. J., Chinnaiyan, A. M., Gerald, W. L., Rubin, M. A., and Martignetti, J. A. KLF6-SV1 overexpression accelerates human and mouse prostate cancer progression and metastasis. *J Clin Invest*, *118*: 2711-2721, 2008.
71. Neubig, R. R. and Siderovski, D. P. Regulators of G-protein signalling as new central nervous system drug targets. *Nat Rev Drug Discov*, *1*: 187-197, 2002.
72. Roman, D. L., Talbot, J. N., Roof, R. A., Sunahara, R. K., Traynor, J. R., and Neubig, R. R. Identification of small-molecule inhibitors of RGS4 using a high-throughput flow cytometry protein interaction assay. *Mol Pharmacol*, *71*: 169-175, 2007.
73. Nikolova, D. N., Zembutsu, H., Sechanov, T., Vidinov, K., Kee, L. S., Ivanova, R., Becheva, E., Kocova, M., Toncheva, D., and Nakamura, Y. Genome-wide gene expression profiles of thyroid carcinoma: Identification of molecular targets for treatment of thyroid carcinoma. *Oncol Rep*, *20*: 105-121, 2008.
74. Niedergethmann, M., Alves, F., Neff, J. K., Heidrich, B., Aramin, N., Li, L., Pilarsky, C., Grutzmann, R., Allgayer, H., Post, S., and Gretz, N. Gene expression profiling of liver metastases and tumour invasion in pancreatic cancer using an orthotopic SCID mouse model. *Br J Cancer*, *97*: 1432-1440, 2007.
75. Kiefer, J. C. Back to basics: Sox genes. *Dev Dyn*, *236*: 2356-2366, 2007.

Chapter V

HIGH-THROUGHPUT SCREENING FOR SMALL-MOLECULE INHIBITORS OF LARG-STIMULATED RHOA NUCLEOTIDE BINDING VIA A NOVEL FLUORESCENCE POLARIZATION ASSAY

Abstract

Guanine nucleotide exchange factors (GEFs) stimulate guanine nucleotide exchange and the subsequent activation of Rho family proteins in response to extracellular stimuli acting upon cytokine, tyrosine kinase, adhesion, integrin, and G-protein coupled receptors (GPCRs). Upon Rho activation, several downstream events occur, such as morphological and cytoskeletal changes, motility, growth, survival, and gene transcription. The leukemia-associated RhoGEF (LARG) is a member of the regulators of G-protein signaling homology domain (RH) family of GEFs originally identified as a result of chromosomal translocation in acute myeloid leukemia. Using a novel fluorescence polarization guanine nucleotide-binding assay using BODIPY–Texas Red–GTP γ S (BODIPY-TR-GTP γ S), we performed a 10,000-compound high-throughput screen for inhibitors of LARG-stimulated RhoA nucleotide binding. Five compounds identified from the high-throughput screen were confirmed in a non-fluorescent radioactive guanine nucleotide-binding assay measuring LARG-stimulated [35 S] GTP γ S binding to RhoA, thus ruling out nonspecific fluorescent effects. All 5 compounds selectively inhibited LARG-stimulated RhoA [35 S] GTP γ S binding but had little to no effect on RhoA or Gao [35 S] GTP γ S binding. Therefore, these 5 compounds should serve as promising starting

points for the development of small-molecule inhibitors of LARG-mediated nucleotide exchange as both pharmacological tools and therapeutics. In addition, the fluorescence polarization guanine nucleotide-binding assay described here should serve as a useful approach for both high-throughput screening and general biological applications.

Introduction

The Rho-family of small GTPases are a main subset of the Ras superfamily of small GTPases (~20-25 kDa) (1). The Rho-family of GTPases is further subdivided into 10 subgroups based on their identity. In this work, we focus on the small GTPase RhoA, which is a member of the RhoA subgroup (RhoA, RhoB, and RhoC) within the Rho-family of proteins. In the cell, Rho GTPases are activated upon ligand activation of cell surface receptors, such as cytokine, tyrosine kinase, adhesion, integrin, and G-protein-coupled receptors (GPCRs) (2). As a result, this causes Rho GTPases to switch from their inactive guanosine diphosphate (GDP)-bound form to their active guanosine triphosphate (GTP)-bound form, leading to various downstream cellular events, such as cytoskeletal and morphological changes, migration, growth, survival, and gene transcription (1).

The activation state of Rho GTPases is controlled by several classes of regulatory proteins. The GTPase-activating proteins (GAPs) catalyze GTP hydrolysis by active Rho proteins, leading to their inactivation. The guanine nucleotide-dissociation inhibitors (GDIs) sequester GDP-bound Rho GTPases in the cytosol, thus preventing their subcellular localization to the plasma membrane and activation. Last, the guanine nucleotide exchange factors (GEFs) stimulate the exchange of GTP for GDP upon Rho

GTPases, leading to their activation. The GEFs are the focus of this work. There are more than 60 identified human Rho GEFs that specifically activate Rho GTPases (1).

Rho GEFs are characterized by their Dbl homology (DH) (~200 residues) and C-terminal adjacent pleckstrin homology (PH) (~100 residues) domains. DH domains are primarily responsible for catalyzing the guanine nucleotide exchange (GTP for GDP) upon Rho GTPases (1). PH domains are responsible for membrane localization of Rho GEFs and aid the DH domain in catalysis of guanine nucleotide exchange (1). The focus of this work is on the leukemia-associated RhoGEF (LARG), which was originally identified as a chromosomal translocation fusion protein to the mixed-lineage leukemia (MLL) gene in a patient with acute myeloid leukemia (3). LARG is a member of the regulators of the G-protein signaling homology domain (RH) containing the RhoGEF family of proteins (LARG, p115-RhoGEF, PDZ-RhoGEF) (4). This family of Rho GEFs is linked to Rho-dependent signaling pathways controlled by heterotrimeric GPCRs coupled to the $G\alpha_{12}$ and $G\alpha_{13}$ subunits, such as the lysophosphatidic acid, bombesin, and thrombin receptors (4-7).

LARG is an important regulatory protein in several clinical disorders. Considering its original identification in acute myeloid leukemia, LARG largely has been thought to be a key player in cancer progression. In conjunction with the Raf-1 kinase, LARG has been shown to transform mouse fibroblasts (8). It has also been shown to play a role in cell migration and growth of head and neck squamous cancer cells through adhesion and tyrosine kinase receptor interaction and subsequent RhoA activation (9). LARG has also been shown, through overexpression and siRNA knockdown, to play a role in thrombin and bombesin receptor-mediated prostate cancer cell morphology

changes and migration (6, 7). In addition to cancer, LARG has been implicated in lectin signaling in dendritic cells, which is important in the sequestration of human immunodeficiency virus (HIV) virions leading to the progression of the HIV disease (10). LARG also has been shown to play a role in vascular biology and calcium signaling. It has been directly linked to a role in salt-induced hypertension in transgenic mice and it has been speculated to play a role in erectile dysfunction (11-13). As a result, considering the implication of LARG in multiple diseases and disorders, it is an attractive molecular target for drug discovery.

Currently, there are limited pharmacological tools targeting RhoGEFs and Rho GTPases. To date, most of the efforts have focused on inhibiting the lipid modification of Rho GTPases, which is necessary for plasma membrane localization and activation. The inhibitors of this modification include farnesyltransferase and geranylgeranyl transferase inhibitors and the cholesterol-lowering statin drugs (14, 15). Unfortunately, these inhibitors and drugs are not specific to Rho GTPases, which complicates the mechanistic interpretation of results using these inhibitors. To date, there are only 2 reported specific inhibitors of Rho GTPases. Both inhibitors selectively inhibit Rac1, but they differ in their mechanism of inhibition. The inhibitor NSC23766 (IC_{50} , $\sim 50 \mu M$) inhibits by binding to the GEF binding pocket on Rac1, (16) and EHT 1864 (K_d , 40 nM) inhibits by binding to the nucleotide-binding pocket on Rac1 (17, 18). Although there are a few examples of selective Rho GTPase inhibitors, there are no published examples to date of inhibitors that target RhoGEFs.

Therefore, in this study, we performed a 10,000-compound high-throughput screen for small-molecule inhibitors of LARG-stimulated RhoA nucleotide exchange. To

do this screen, we first developed a novel fluorescence polarization (FP) RhoA nucleotide-binding assay using BODIPY-TR-GTP γ S. We chose fluorescence polarization rather than both the standard fluorescence intensity and radioactive [35 S] GTP γ S binding approaches because it proved to be more environmentally friendly, robust, reliable, and reproducible. Of the 10,000 compounds screened, 6 were confirmed to inhibit LARG-mediated guanine nucleotide exchange. Of these 6 compounds, 5 were confirmed in a non-fluorescent, radioactive [35 S] GTP γ S guanine nucleotide-binding assay with IC₅₀ values in the micromolar range. These compounds showed selectivity for LARG-stimulated RhoA [35 S] GTP γ S binding by having little to no effect on RhoA and Gao [35 S] GTP γ S binding. Therefore, as a result of the high-throughput screen with this novel FP guanine nucleotide-binding assay, 5 promising compounds were identified as inhibitors of LARG-stimulated RhoA nucleotide binding. Therefore, with further synthetic chemistry follow-up, these compounds may lead to useful inhibitors of LARG-stimulated RhoA nucleotide binding for both research and therapeutic purposes.

Materials and Methods

Plasmids, protein purification, and chemical reagents

Human RhoA (residues 1-189, C189S) was expressed in *Escherichia coli* as described previously (19). Human LARG encoding the DH/PH domains (residues 765-1138) was expressed in *E. coli* as described previously (20). Gao expression and purification in *E. coli* was described previously (21). BODIPY Texas Red (TR) guanosine 5'-O-(3-thiotriphosphate) (GTP γ S) was obtained from Molecular Probes—Invitrogen (Eugene, OR). [35 S] GTP γ S was obtained from PerkinElmer (Waltham, MA).

GTP γ S was obtained from EMD Biosciences (San Diego, CA). The non-ionic detergents IGEPAL and Lubrol were from Sigma (St. Louis, MO). The 10,000 structurally diverse chemical compounds were obtained from ChemBridge (San Diego, CA) as part of the collection of the University of Michigan Center for Chemical Genomics (CCG). The chemical similarity was low: at 80% similarity calculated with the ICM Pro (Molsoft LLC, La Jolla, CA) clustering algorithm, there were 4,390 clusters with a median size of 1 compound and mean size of 2.28 compounds.

Guanine nucleotide-binding FP assays

Exchange buffer (20 mM Tris HCl [pH 7.5], 150 mM NaCl, 10 mM MgCl₂, 10% glycerol, 0.01% IGEPAL, and freshly prepared 1 mM DTT) was added to each well of a black 96-well plate. Purified full-length human RhoA(C189S), purified DH/PH domain of human LARG, and BODIPY-FL-GTP γ S or BODIPY-TR-GTP γ S were added sequentially to each well to a final volume of 100 μ L per well. Fluorescein or Texas Red fluorescence polarization was read in a Victor² plate reader using excitation at 485 nm and emission at 535 nm for fluorescein or an excitation at 560 nm and emission at 630 nm for Texas Red. The measured values of polarization (mP) were calculated by using the following formula: $mP = (F_{||} - F_{\perp}) / (F_{||} + F_{\perp})$, where $F_{||}$ = fluorescence intensity parallel to the excitation plane, and F_{\perp} = fluorescence intensity perpendicular to the excitation plane. The statistical Z' factor used to assess assay suitability for high-throughput screening (HTS) was calculated by using the following formula: $Z' = 1 - [(3\sigma_{c+} + 3\sigma_{c-}) / (|\mu_{c+} - \mu_{c-}|)]$, where σ = standard deviation, μ = mean, c+ = with LARG, and c- = without LARG.

RhoA [³⁵S] GTPγS guanine nucleotide-binding assay

The indicated concentrations of the purified DH/PH domain of human LARG (0.5-2 nM, final) were added to a tube in buffer I (20 mM Tris [pH 7.5], 1 mM EDTA, 1 mM DTT, 50 mM NaCl, 0.1% Lubrol, 2 mM MgCl₂) in a final volume of 180 μL. To this mixture, 45 μL of purified human RhoA (C189S) in buffer I was added to yield a final concentration of 500 nM. The reaction was initiated by adding 225 μL of 2× binding buffer (100 mM Tris [pH 7.5], 1 mM EDTA, 2 mM DTT, 100 mM NaCl, 10 mM MgCl₂, 5 μM GTPγS, 0.1% Lubrol, 6.75 μCi [³⁵S] GTPγS) for a final reaction volume of 450 μL. Reaction mixtures were incubated at room temperature for 1, 5, 10, 30, 60, 120, and 180 min. Then, 50 μL of reaction mixture was removed and diluted in a tube containing 4 mL of ice-cold wash buffer (20 mM Tris [pH 8.0], 100 mM NaCl, 25 mM MgCl₂) to stop the reaction. An additional 4 mL of wash buffer was added to the tube and the sample filtered on a BA85 25-mm nitrocellulose filter using a Hoeffler filtration system. Filters were washed 2 times with 4 mL of wash buffer. Filters were dried under a heat lamp for 5 min. Filters were counted in 4 mL of scintillation fluid (Scintiverse, Fisher Scientific, Hampton, NH) for 1 min using a Beckman LS 5801 Scintillation Counter. The identical method was followed for RhoA [³⁵S] GTPγS binding studies without LARG, except reaction mixtures were incubated at room temperature for 1, 5, 10, 30, 60, 130, and 180 min.

Gao [³⁵S] GTPγS guanine nucleotide-binding assay

Purified Gα_o was diluted to a final concentration of 10 μM in 180 μL of Gα_o dilution buffer (10 mM HEPES [pH 7.7], 1 mM EDTA, 0.1% Lubrol, 1 mM DTT). [³⁵S]

GTP γ S binding was initiated by adding 180 μ L of Gao binding cocktail (50 mM HEPES [pH 7.7], 1 mM EDTA, 40 mM MgCl₂, 200 mM NaCl, 2 μ M GTP γ S, 6.75 μ Ci [³⁵S] GTP γ S, 1 mM DTT) and incubated at room temperature for 1, 5, 10, 30, 60, 90, and 120 min. Then, 40 μ L of the reaction mixture was diluted in a tube containing 4 mL of ice-cold wash buffer (20 mM Tris [pH 8.0], 100 mM NaCl, 25 mM MgCl₂). This reaction mixture was then filtered on a BA85 25-mm nitrocellulose filter using a Hoeffler filtration system. Filters were washed twice with 4 mL of wash buffer, then dried under a heat lamp for 5 min. Filters were counted in 4 mL of scintillation fluid for 1 min using a Beckman LS 5801 Scintillation Counter.

High-Throughput LARG-stimulated RhoA guanine nucleotide-binding FP screen

Using a Multidrop 384 (Thermo Scientific, Waltham, MA), exchange buffer was added to each well of a low-volume black 384-well plate (cat. 3676, Corning, NY); 20 μ L was added for the positive control wells (i.e., no LARG), and 15 μ L was added to all other wells. Using a 384-well pin tool on a Biomek FX liquid-handling workstation (Beckman Coulter, Fullerton, CA), approximately 250 nL of compound (stock concentration 0.75-4 mM; ChemBridge) or DMSO, for control wells, was added (producing final compound concentrations of ~6-30 μ M and 0.8% DMSO). Plates were then incubated at room temperature for 5 min. Using a Multidrop micro (Thermo Scientific), 5 μ L of purified DH/PH domain of human LARG in exchange buffer was added to the wells of the 384-well plate to produce a final concentration of 100 nM. Plates were then incubated for 5 min at room temperature. Using a Multidrop micro, 5 μ L of purified human RhoA (C189S) in exchange buffer was added to produce a final

concentration of 2 μM . Plates were then incubated for 2 min at room temperature. The reaction was initiated by using a Multidrop micro to add 5 μL of BODIPY-TR GTP γ S in exchange buffer to a final concentration of 500 nM and a final reaction volume of 30 μL . Plates were incubated for 20 min at room temperature, then read for fluorescence polarization with a PHERAstar (BMG LabTech, Offenburg, Germany) plate reader with a 575-nm band pass excitation filter, a 620-nm band pass emission filter, a dichroic mirror, and a dual-emission beam splitter to permit simultaneous recording of parallel and perpendicular fluorescence readings. Plates were individually incubated after each addition so that all plates would be read in the PHERAstar plate reader precisely at 20 min after GTP γ S addition (i.e., prior to saturation of the reaction time course). For follow-up dose-response studies of the primary hits, the same method was carried out as for the high-throughput screen, except reagents were added by hand with a multichannel pipet. In addition, compounds were added to the wells of the 384-well plate using serial 2-fold dilutions over a range of concentrations between 100 μM and 3.125 nM.

Compound Properties

Compound properties were calculated with ChemAxon JChem software. The LogP value method is described in Viswanadhan et al.(22).

Results

FP guanine nucleotide-binding assay

To study RhoA guanine nucleotide exchange in vitro, we used a novel FP guanine nucleotide-binding assay adapted from the standard fluorescence intensity guanine

nucleotide binding assay described previously by our laboratory (23, 24). This FP assay uses the non-hydrolyzable fluorescently labeled guanine nucleotide BODIPY-GTP γ S fluorophores. LARG-stimulated BODIPY-GTP γ S fluorophore binding to RhoA results in an increase in fluorescence polarization that can be read by a plate reader (Fig. 5-1A). The structures of the BODIPY-GTP γ S fluorophores used in this study are shown in Figure 5-1C.

Due to the importance of having a robust and reproducible assay for HTS, we compared the suitability of nucleotide binding to RhoA measured by fluorescence intensity (data not shown) versus fluorescence polarization (Fig. 5-2). Although both intensity and polarization assays gave signals for RhoA nucleotide binding, only the FP assay (Z' factor = 0.7) gave suitably reproducible data appropriate for doing HTS (Fig. 5-2). The FP assay takes into account fluorescence that is both parallel and perpendicular to the excitation plane, and the ratiometric nature of the measurement cancels many contributions to the noise (25). This most likely accounts for the difference between the Z' factors of the 2 assays. As a result, we conclude that fluorescence polarization should be a useful assay for HTS for small-molecule inhibitors of GEF-stimulated small GTPase guanine nucleotide binding. In addition, the assay has recently been used for general biological applications studying GEF activity upon small GTPases (26).

Comparison between the FP and [35 S] guanine nucleotide-binding assays

The standard [35 S] GTP γ S nucleotide-binding assay is generally not suitable for HTS due to time consumption, accumulation of environmental hazardous waste, and the complexity of adapting the assay to a 384-well plate format. Therefore, we chose the FP

assay to use for our high-throughput screen. We found that in both assays, LARG was able to stimulate RhoA (C189S) nucleotide binding in a concentration-dependent manner (Fig. 5-3A, B). However, the time courses for saturation in the 2 methods differed, with saturation occurring at 40 min for the FP assay and 180 min for the [³⁵S] radioactive assay. The basal rate constant for nucleotide exchange was slower with the [³⁵S] GTP γ S method. The faster kinetics of binding in the FP assay may be due, in part, to the higher concentration of RhoA, lower ratio of nucleotide to RhoA, the higher NaCl or MgCl₂ concentrations, or the non-native BODIPY nucleotide structure in the FP assay. However, plotting the rate constants on a graph both give a linear plot (Fig. 5-3C-D), suggesting that both the FP and radioactive nucleotide-binding assays are appropriate for measuring GEF-stimulated nucleotide binding to the Rho-family of proteins.

High-Throughput Screen for Inhibitors of LARG-stimulated RhoA nucleotide exchange

A 10,000 diverse chemical compound collection from ChemBridge was used to screen for small-molecule inhibitors of LARG-stimulated RhoA nucleotide exchange. The FP guanine nucleotide-binding assay using the purified DH/PH domain of LARG and RhoA (C189S) was used for the screen. Compounds were added to a black 384-well low-volume plate containing exchange buffer with a 384-well pin tool on the Biomek FX workstation. Then, the purified DH/PH domain of LARG, RhoA (C189S), and BODIPY-TR-GTP γ S were added to the plate in sequential order. After a 20-min incubation (non-saturating time point), polarization was read in a PHERastar plate reader, as shown in Figure 5-4A. The assay was tested for its suitability for HTS and reliability by using the *Z'* factor statistical measurement. Using purified RhoA (C189S) alone plus DMSO

(positive control for screen—100% inhibition) and the purified DH/PH domain of LARG and RhoA (C189S) plus DMSO (negative control for the screen—0% inhibition), the Z' factor in this HTS format was determined to be 0.52, indicating a suitable and reliable screen (Fig. 5-4B) (27). Although many FP-type screens give higher Z' factors than this, consideration should be taken of the fact that this is a kinetic assay done at a pre-saturation time point, so it would not be expected to have quite as good a Z' as a standard equilibrium FP binding assay.

Compounds that showed more than 30% inhibition or values of percent inhibition more than 3 standard deviations from the negative control were considered to be actives. Figure 5-4C shows 19 hits from the 30% inhibition criterion, and an additional 12 were found with the 3 standard deviation criterion, providing 31 initial actives (or a “hit” rate of 0.3%). There were several plates with clusters of compounds that just met the cutoff, and they were re-tested in duplicate using the primary screening assay methodology. Any that confirmed in either of the 2 measurements were retained in the actives list and were studied further in a concentration response study using the BODIPY-TR-GTP γ S FP assay. Of those 13 compounds, 7 (0.07% hit rate) did inhibit in this follow-up assay, and 6 compounds did not (<50% inhibition at 100 μ M; Fig. 5-4D). Of the 7 confirmed actives, 6 were available for resupply from ChemBridge for follow-up studies. The 3 most potent of these 6 compounds—CCG-14631 (4-{5-[(4,6-dioxo-2-sulfanylidene-1,3-diazinan-5-ylidene)methyl]furan-2-yl}-N-(1,3-thiazol-2-yl)benzene-1-sulfonamide) (ChemBridge, cat. 6192873), CCG-12529 (7-(3-nitrophenyl)-8-azatricyclo[7.4.0.0[^]{2,6}]trideca-1-(13),3,9,11-tetraene-10-carboxylic acid) (ChemBridge, cat. 5584249), and CCG-5849 (4-amino-2-(5-amino-1,3-benzothiazol-2-

yl)phenol) (ChemBridge, cat. 5312639) had IC₅₀ values between 3 and 10 μM (Fig. 4D and Table 1). The 3 remaining compounds-CCG-14113 ((N'Z)-2-[(3-methylphenyl)amino]-N'-[(2,4,6-tribromo-3-hydroxyphenyl)methylidene] acetohydrazide) (ChemBridge, cat. 6119878), CCG-13528 ((5Z)-3-(2H-1,3-benzodioxol-5-yl)-2-imino-5-[[5-(2-nitrophenyl)furan-2-yl]methylidene]-1,3-thiazolidin-4-one) (ChemBridge, cat. 5354792), and CCG-7167 (7-hydroxy-3-[2-(4-phenylphenyl)-1,3-thiazol-4-yl]-2H-chromen-2-one) (ChemBridge, cat. 5354792) were less potent, with IC₅₀ values between 32 and 65 μM (Fig. 5-4D and Table 5-1) in the FP assay.

Secondary screen in [³⁵S] GTPγS radioactive guanine nucleotide-binding assay

As mentioned previously, a potential mechanism for false positives in a fluorescence-based assay is quenching of the fluorescence signal. To address this

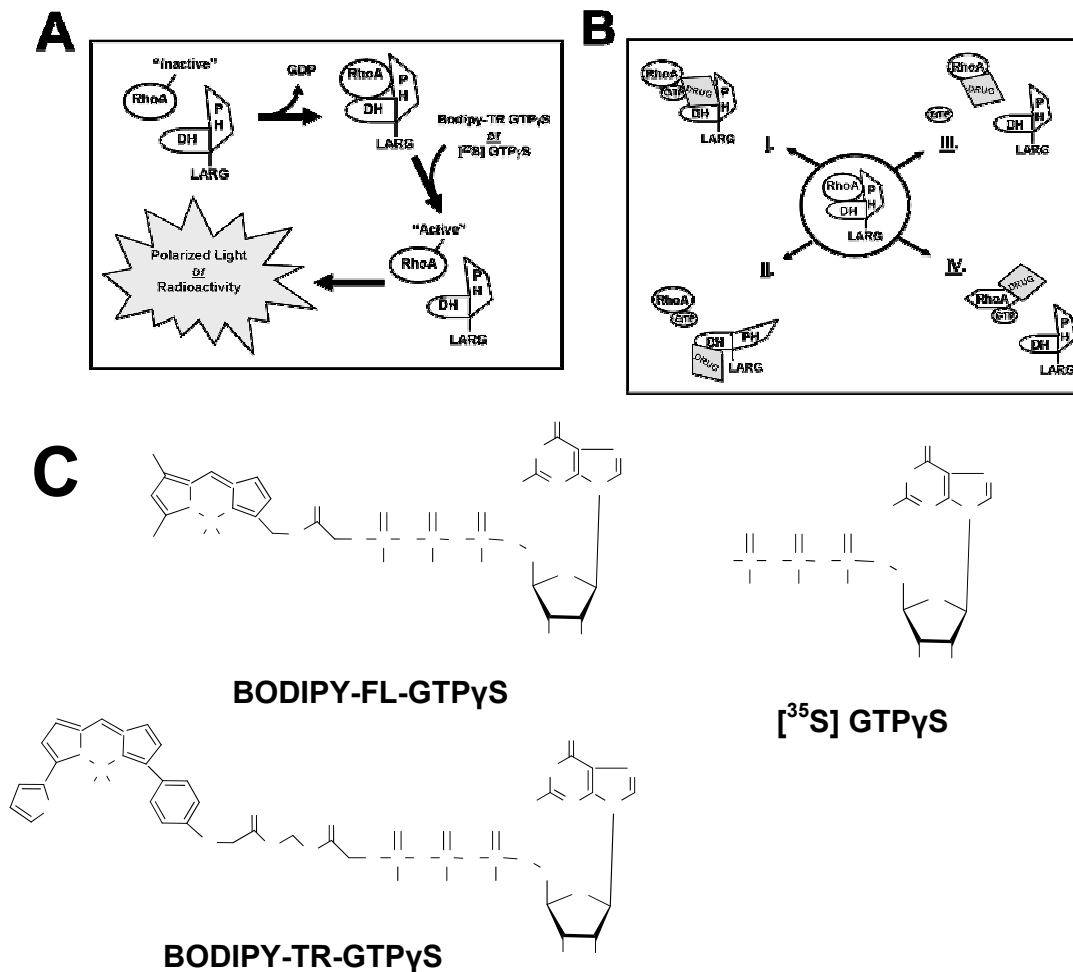


Figure 5-1. GTPase cycle, mechanisms of inhibition, and structure of guanosine triphosphate (GTP) analogs. (A) In its inactive form, the small GTPase RhoA is bound to both guanosine diphosphate (GDP) and Mg^{+2} . Upon the binding of the Dbl homology/pleckstrin homology (DH/PH) domain of the leukemia-associated RhoGEF (LARG, which is the catalyst of the guanine nucleotide exchange reaction), a conformational change occurs in the switch regions of the small GTPase RhoA, causing an intermediate to form that is free of nucleotide and Mg^{+2} . This enables the GTP and Mg^{+2} to bind to the small GTPase RhoA. In our in vitro assays described in this report, we use the BODIPY–Texas Red fluorescently labeled or [35 S] radioactive labeled nonhydrolysable form of the guanine nucleotide, GTP γ S. As a result, the GTP-bound RhoA can be released from the RhoGEF LARG in an active state. This results in a polarized light signal in our fluorescence polarization assay or a radioactive signal in our [35 S] radioactive assay that can be quantitatively measured. (B) There are several potential mechanisms of inhibition of LARG-stimulated RhoA nucleotide binding, which include (I) competitive inhibition at the site of interaction between LARG and RhoA, (II) allosteric inhibition by drug binding to LARG, (III) competitive inhibition at the site of nucleotide binding, or (IV) allosteric inhibition by drug binding to RhoA. (C) The chemical structures of the 3 non-hydrolysable forms of the guanine nucleotide, GTP γ S,

Figure 5-1. GTPase cycle, mechanisms of inhibition, and structure of guanosine triphosphate (GTP) analogs (continued) .used in both the fluorescence and radioactive in vitro assays described in this report are depicted.

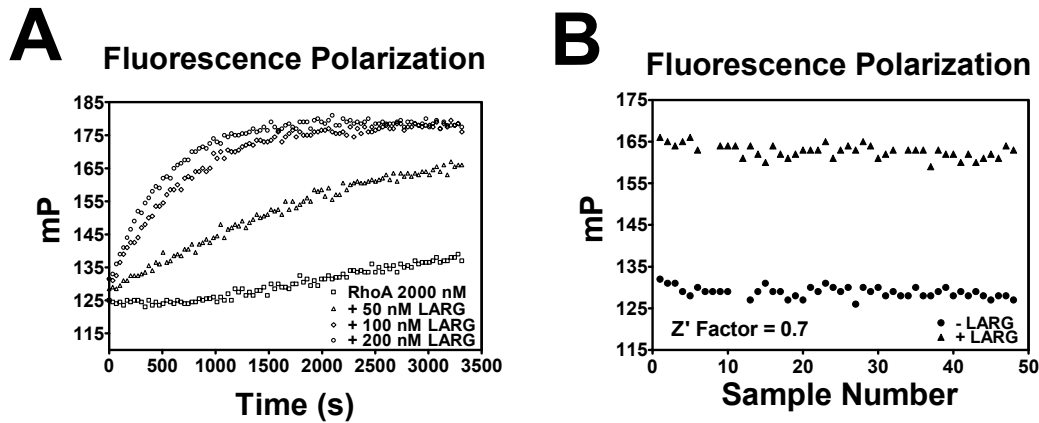


Figure 5-2. Fluorescence polarization RhoA nucleotide-binding assays. Purified Dbl homology/pleckstrin homology (DH/PH) domain of leukemia-associated RhoGEF (LARG; 200 nM) stimulated nucleotide binding of purified RhoA (C189S) (2 μ M) using BODIPY-FL-GTP γ S (1 μ M) and BODIPY-TR-GTP γ S (1 μ M). Values were measured in a Victor² plate reader as described in materials and methods. (A) LARG-dependent nucleotide binding to RhoA (C189S) (2 μ M, \square) stimulated by LARG (50 nM, Δ ; 100 nM, \diamond ; 200 nM, \circ) using BODIPY-TR-GTP γ S (1 μ M) was measured over a time course of 55 min for fluorescence polarization by using a Victor² plate reader, as described in materials and methods. (B) Fluorescence polarization measurements were taken from 48 wells not containing LARG (- LARG, \blacksquare) and 48 wells containing LARG (+ LARG, \blacktriangle) in a 96-well black plate after incubating for 20 min at room temperature. Data in panels A and B represent experiments performed in duplicate and are represented as mP polarization values. The Z' factor was calculated for the fluorescence polarization measurement. The Z' factor for the fluorescence polarization assay was 0.7, indicating an assay suitable for high-throughput screening.

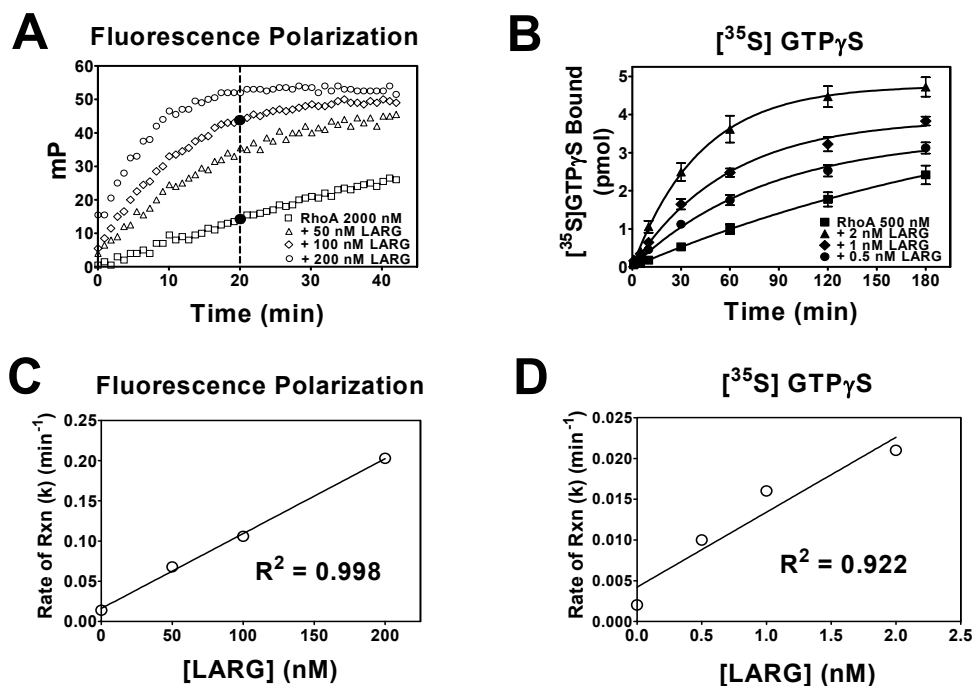


Figure 5-3. Dose-dependent leukemia-associated RhoGEF (LARG)-stimulated RhoA nucleotide binding. (A) Dose-dependent nucleotide binding to RhoA (C189S; 2 μM , \square) stimulated by LARG (50 nM, Δ ; 100 nM, \diamond ; 200 nM, \circ) using BODIPY-TR-GTP γ S (500 nM) was measured over a time course of 40 min in a Victor² plate reader, as described in materials and methods. (B) Dose-dependent nucleotide binding to RhoA (C189S; 500 nM, \blacksquare) stimulated by LARG (0.5 nM, \bullet ; 1 nM, \blacklozenge ; 2 nM, \blacktriangle) using [³⁵S] GTP γ S was measured over a time course of 180 min by a Beckman LS 5801 Scintillation Counter, as described in materials and methods. The black dotted vertical line and the solid black circles indicate the time point (incomplete saturation point) used for the high-throughput screen. (C, D) Rate constants for the reactions were plotted versus the concentration of LARG, yielding a linear plot for both the fluorescence polarization (FP) and radioactive binding assays. A linear regression plot was performed using Graphpad Prism 5, yielding R^2 values of 0.9. Rate constants were calculated using the 1-phase exponential association equation $Y = Y_{\text{max}} * (1 - \exp(-k * X))$ (k = rate constant for the reaction). Data in panel A were measured in duplicate and are representative data of $n = 3$. Data in panel A were background subtracted from BODIPY-TR-GTP γ S fluorescence alone. Data in panel B represent the Mean \pm SEM of 3 separate experiments ($n = 3$).

concern, we used the traditional radioactive [³⁵S] GTP γ S guanine nucleotide filter binding assay as a secondary follow-up assay for our 6 confirmed active compounds. For these experiments, we used a time point of 25 min, prior to saturation on the kinetic curve in Figure 5-5A. Five of the 6 candidate compounds showed dose-dependent inhibition in the [³⁵S] GTP γ S guanine nucleotide-binding assay. The 1 compound that was not active in the radioligand assay showed a marked effect on the total fluorescence, as calculated by F-parallel + 2*F-perpendicular (54% reduction). The 3 most potent compounds in this radioactive-based assay—CCG-13528, CCG-14631, and CCG-7167—had IC₅₀ values between 4 and 7 μ M (Fig. 5-5B and Table 5-1). The other 2 compounds, CCG-14113 and CCG-12529, were less potent, with IC₅₀ values around 30 μ M (Table 5-1). The IC₅₀ values for several of the compounds differ between the [³⁵S] GTP γ S and fluorescence polarization methods. These differences most likely can be attributed to experimental differences between the assays such as NaCl and MgCl₂ concentrations and the different nature of the detergent or nucleotide used. Despite these differences, the fact that 5 of the 6 tested compounds did show some activity in the [³⁵S] GTP γ S method is encouraging.

CCG-13528 and CCG-14631 satisfy all of Lipinski's rules for chemical compounds that have the most potential in becoming a drug with respect to their physical properties (28). CCG-7167 had only 1 violation of Lipinski's rule-of-5 due to a partition coefficient (log P) of 5.52 (Table 5-1). Interestingly, our 3 most potent compounds are all extended aromatic molecules. They have 4 (CCG-14631) or 5 (CCG-13528, CCG-7167) rings and are 16 (CCG-13528) or 18 (CCG-14631, CCG-7167) atoms in length (Fig. 5-5C). This suggests a potential pharmacophore for inhibiting LARG-stimulated RhoA

nucleotide exchange, which may be explained by the long shallow pocket of the LARG-RhoA interaction site (29).

Compound selectivity for LARG-stimulated RhoA nucleotide binding

Inhibition of LARG stimulation of RhoA nucleotide exchange can occur by 2 primary mechanisms. The compound could directly inhibit GTP binding to RhoA, or it could block LARG-mediated nucleotide exchange. Determining the exact mechanism of the inhibition of LARG-stimulated RhoA nucleotide exchange is beyond the scope of the present study, but we did determine whether the compounds inhibited GTP binding or LARG-mediated exchange in the [³⁵S] GTPγS guanine nucleotide-binding assay. [³⁵S] GTPγS binding to the small GTPase RhoA and the G-protein alpha subunit Gαo was determined at 60 min and 25 min, respectively (Fig. 5-6A, B). [³⁵S] GTPγS binding to RhoA and Gαo was tested in the absence of GEFs to determine whether the compounds inhibited GTP binding directly. As expected, all 5 compounds inhibited LARG-stimulated RhoA [³⁵S] GTPγS binding (≥50%), yet they had only modest or no effect on direct RhoA and Gαo [³⁵S] GTPγS binding at a maximal concentration of 100 μM (Fig. 5-6C). Therefore, the 5 compounds identified in the high-throughput screen described here do appear to inhibit the LARG-mediated nucleotide exchange in some manner.

Discussion

Radioactive and fluorescence assays are the primary approaches used to measure guanine nucleotide exchange of small GTPases. These approaches typically use

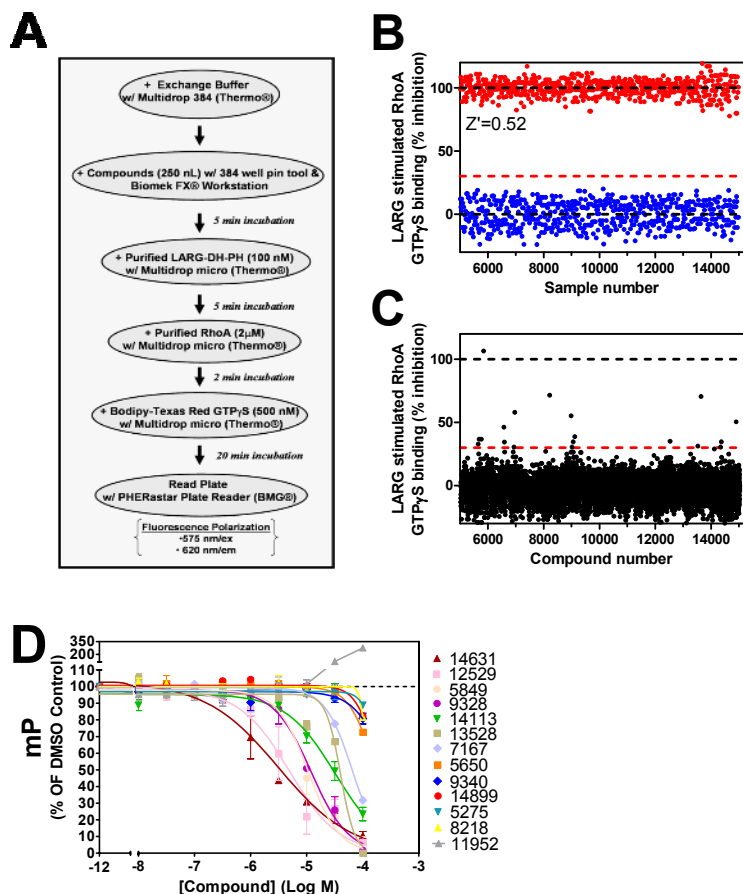


Figure 5-4. Fluorescence Polarization Screen for Inhibitors of LARG-stimulated RhoA nucleotide Binding. (A) Schematic of the protocol used for the 10,000 ChemBridge diverse chemical compound high-throughput screen (HTS) as described in the materials and methods. All samples, compounds and controls, contain 0.8% DMSO. (B) Control samples run on each plate include (100 nM) LARG as a negative (0% inhibition) control (•) and no LARG as a positive (100% inhibition) control (•). The statistical Z' – Factor measurement for the HTS was calculated to be 0.52 for this entire screen indicating suitable reproducibility. (C) Data from the 10,000 ChemBridge compound HTS (CCG compounds 5029-15028) are shown (•) with a 30 percent inhibition line indicated in red. (D) Dose-response follow-up of the hits from the HTS in the LARG-stimulated RhoA nucleotide BODIPY-TR-GTP γ S binding assay measured at a time point of 20 minutes. Data in panel D were measured in duplicate and are represented as percent change from the +LARG negative control (0%) compared to the no LARG positive control (100%).

Compound ID	Molecular Weight	Log P	IC₅₀ (μM) [TR-GTPγS]	Hill Slope [TR-GTPγS]	IC₅₀ (μM) [GTPγS35]	Hill Slope [GTPγS35]
CCG-13528	435.4	4.13	39.8	-3.4	4.6	-1.8
CCG-14631	460.5	1.89	3.1	-0.7	7.0	-1.1
CCG-7167	397.4	5.52	65.1	-1.8	4.2	-2.2
CCG-14113	520.0	5.40	32.2	-1.0	32.8	-7.1
CCG-12529	336.3	4.33	4.9	-1.0	27.5	-2.3
CCG-5849	257.3	1.97	10.7	-1.6	NA¹	NA¹

Table 5-1. **Chemical Compound Properties and IC₅₀ Values.** This table describes the chemical compound properties along with the IC₅₀s and Hill Slopes for the 6 compounds identified in the HTS. The IC₅₀ and Hill Slope values were taken from the dose-dependent data in both the BODIPY-TR-GTPγS and [³⁵S] GTPγS assays in Fig. 5-4D and Fig. 5-5B. The notation NA indicates the compound had no inhibitory activity.

radioactive [^3H] or [^{35}S] or fluorescent N-methyl-3'-O-anthranoyl (MANT) and boron dipyrromethene (BODIPY) analogs of guanine nucleotides. They either measure binding of the non-hydrolysable GTP analog, GTP γ S, to G-proteins or release of labeled GDP from G-proteins (23, 24, 30). Upon nucleotide exchange, the guanine nucleotide analogs yield either a measurable radioactive or fluorescence signal. Here, we describe a novel assay that uses fluorescence polarization rather than the standard fluorescence intensity approach to measure LARG-stimulated RhoA nucleotide binding. We chose the FP assay due to its better, initial baseline kinetics, signal-to-noise ratio, and Z' factor (data not shown). The Z' factor measures the reliability of a screen hit based on the dynamic range and intrinsic variability of the assay (27, 31). The Z' factor for the FP assay was 0.7 in pilot studies and showed a sustained level of 0.52 in our 10,000-compound screen. This should be sufficient for HTS and for general biological applications.

One major issue in fluorescence-based HTS assays is the type of fluorophore one chooses. The most commonly used fluorophores used to label guanine nucleotides, MANT and BODIPY-FL, have the drawback of being detected in the blue and green regions of the electromagnetic spectrum (32). This enhances the chance of false positives in high-throughput screens due to compounds absorbing light in this region of the electromagnetic spectrum. Therefore, in the work described here, we use a GTP γ S nucleotide labeled with the BODIPY-TR fluorophore (Fig. 5-1C), which is detected in the red region of the electromagnetic spectrum. This, along with the use of the ratiometric FP method, should decrease the chance of false positives due to non-specific compound absorbance. We compared the FP BODIPY-TR-GTP γ S binding assay as a measure of nucleotide exchange with the traditional radioactive [^{35}S] GTP γ S binding assay. We

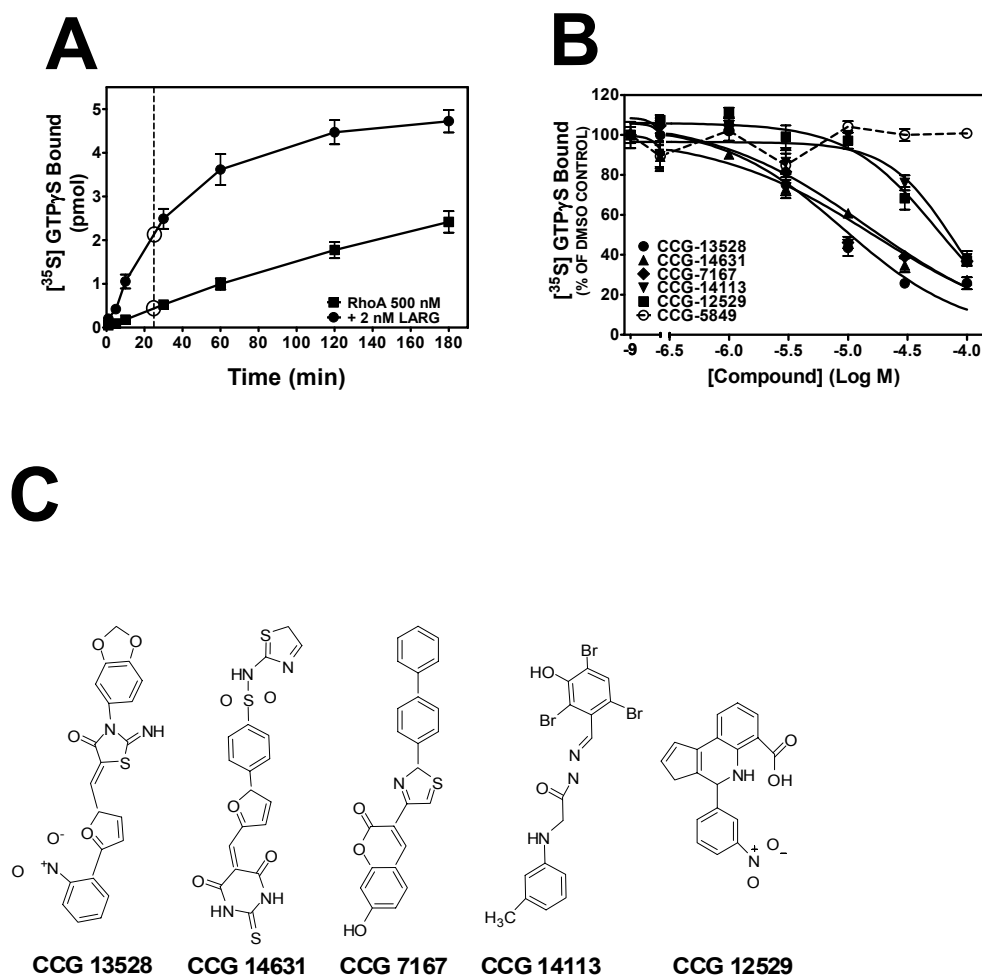


Figure 5-5. Dose-response inhibition of leukemia-associated RhoGEF (LARG)-stimulated RhoA [^{35}S] GTP γ S binding by high-throughput screening (HTS) hits. (A) Time course of guanosine nucleotide binding of RhoA (C189S; 500 nM, ■) stimulated by LARG (2 nM, ●) using [^{35}S] GTP γ S was measured over a time course of 180 min by a Beckman LS 5801 Scintillation Counter, as described in materials and methods. (B) Compound dose-dependent inhibition of LARG (2 nM) stimulated RhoA (C189S; 500 nM) guanosine nucleotide binding at a 25-min time point. (C) Chemical structures of the 5 compounds that show dose-dependent inhibition in panel B. Data in panels A and B were measured in duplicate and represent Mean \pm SEM of 3 separate experiments ($n = 3$). Data in panel B are represented as percentage of DMSO control for [^{35}S] GTP γ S binding.

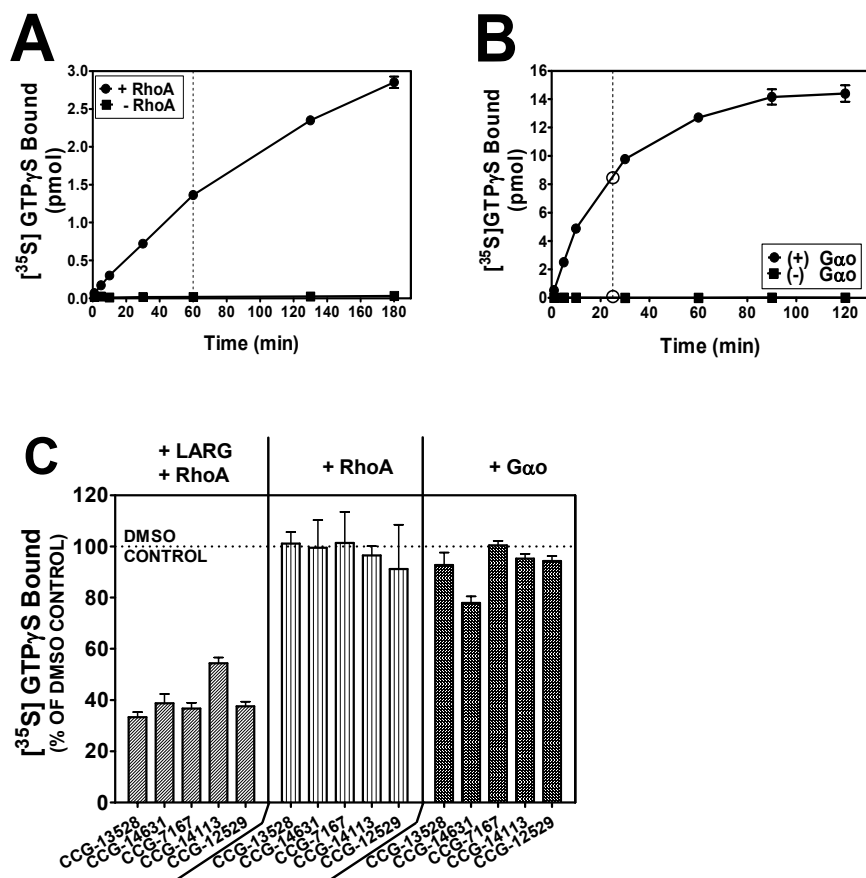


Figure 5-6. Compound selectivity for leukemia-associated RhoGEF (LARG)-stimulated RhoA [^{35}S] GTP γ S binding. (A) Time course of RhoA (C189S; 500 nM, ■) [^{35}S] GTP γ S binding over 180 min. (B) Time course of G α_o (250 nM, ●) [^{35}S] GTP γ S binding over 120 min. [^{35}S] GTP γ S alone is represented by ■ in both (A) and (B). (C) Bar graph representation of compound (100 μM) selectivity for LARG-stimulated [^{35}S] GTP γ S binding versus RhoA (C189S) and G α_o [^{35}S] GTP γ S binding. Binding was measured at a 60-min time point (indicated by the dotted vertical line) for RhoA (C189S) and 25-min time point (indicated by the dotted vertical line and open circles) for both G α_o and LARG-stimulated RhoA [^{35}S] GTP γ S binding. Data in panels A, B, and C measured in duplicate represent Mean \pm SEM for 3 separate experiments ($n = 3$). Data in panel C are represented as a percentage of DMSO control for [^{35}S] GTP γ S binding.

found both assays to be able to show concentration-dependent LARG-stimulated RhoA nucleotide binding with linear rate constants with respect to LARG concentration (Fig. 5-3). However, the 2 methods were different with respect to experimental conditions (i.e., buffers, protein concentrations, type of detergent and nucleotide) and reaction time. Despite the differences between assays, we chose the fluorescence polarization assay for a high-throughput screen for inhibitors of LARG-mediated nucleotide exchange based on its reliability, adaptability to a 384-well plate format, lack of production of environmental waste, and time efficiency.

There are several ways that one can molecularly target the function of RhoGEFs and Rho GTPases. One can inhibit the membrane localization of Rho GTPases through blockade of lipid modifications. Interestingly, using an HTS approach, Peterson et al. (33) describe the identification of a geranylgeranyl transferase type I small-molecule inhibitor (IC_{50} , 10 μ M) that inhibits Rho GTPase function. Another way to obstruct Rho function is through small-molecule stimulation of GAPs to stimulate intrinsic hydrolysis of Rho GTPases, promoting inhibition of function. Small-molecule stabilization of the association of GDP dissociation inhibitors (GDIs) with Rho GTPases can also be effective in disrupting the activation of Rho GTPases by preventing membrane localization (1). Also, small-molecule inhibition of GEFs would be effective in disrupting Rho function by preventing activation of Rho GTPases. Function can be abolished by directly targeting the Rho GTPase. Interestingly, Gao et al. (16) describe the identification of a direct small-molecule inhibitor of Rac1, NSC23766 (IC_{50} , 50 μ M), through a structure-based virtual screening approach. Another direct Rac1 inhibitor, EHT 1864 (K_d , 40 nM), selectively inhibits Rac1 through blocking the binding of the guanine

nucleotide to Rac1 (17, 18). Also, we recently identified an inhibitor downstream in the Rho-stimulated gene transcription pathway using a cell-based luciferase reporter screen (34). As a result, we describe here a FP high-throughput screen of a ChemBridge diverse chemical library for inhibitors of LARG-mediated RhoA nucleotide exchange. LARG was originally discovered as a chromosomal translocation fusion to MLL in a patient with acute myeloid leukemia (3). Therefore, from its initial identification, LARG has been linked to cancer. LARG gene expression was shown to be upregulated in patients with the preleukemic disorder Scwachman-Diamond syndrome (SDS) (35). LARG was first shown to have oncogenic activity in a NIH-3T3 transformation assay (8). Since then, LARG-mediated Rho activation has been shown to be important in prostate cancer (PC-3) and breast cancer (MDA-MB-435) cell morphology, motility, and invasion upon extracellular stimulation by the GPCR ligands bombesin, thrombin, and lysophosphatidic acid (6, 7, 36). In addition, LARG interaction with the adhesion receptor, CD44, or tyrosine kinase receptor, epidermal growth factor receptor (EGFR), and subsequent Rho activation has been shown to be necessary for cytoskeletal modification, motility, and invasion in head and neck squamous cell carcinoma (HSC-3) cells (9). Therefore, a small-molecule inhibitor of LARG-mediated RhoA nucleotide exchange would be a useful tool to elucidate cancer mechanisms and as a potential cancer therapeutic.

In addition to cancer, LARG also has the potential to play an important role in HIV or vascular diseases. LARG has been shown to be upregulated in rat vascular smooth muscle by angiotensin II and it is expressed in rat corpus cavernosum, thus potentially playing a vital role in contraction and calcium sensitization (11, 12, 37). Recently, LARG was determined to be the key RhoGEF involved in the development of

salt-induced hypertension (13). Interestingly, Hodges et al. (10) describe a role for LARG in HIV-1 pathogenesis via forming a complex with the C-type lectin receptor, DC-SIGN. Therefore, small-molecule inhibition of LARG-mediated RhoA nucleotide exchange may prove to be useful in the development of pharmacological tools and therapeutics for better understanding of disease pathogenesis and treatment of diseases and disorders, including HIV, hypertension, and erectile dysfunction (ED).

The 5 compounds identified in this study would be of interest for further development based on the multiple diseases and disorders that an inhibitor of LARG-mediated RhoA nucleotide exchange may have a positive impact on. All 5 compounds have potency in the micromolar range, which make them reasonable candidates for synthetic chemistry follow-up. In addition, the compounds do not inhibit GTP binding to RhoA or to G α . Therefore, they most likely inhibit LARG-mediated nucleotide binding by (i) binding to the LARG binding surface on RhoA; (ii) binding to the RhoA binding surface on LARG; (iii) allosterically binding to either LARG or RhoA, causing a conformational change; (iv) binding to both RhoA and LARG; or (v) covalently modifying RhoA or LARG. Further development, specificity studies, and mechanistic characterization are still needed, but the compounds identified in this study inhibit LARG-mediated RhoA nucleotide exchange with micromolar potency *in vitro*.

References

1. Rossman, K. L., Der, C. J., and Sondek, J. GEF means go: turning on RHO GTPases with guanine nucleotide-exchange factors. *Nat Rev Mol Cell Biol*, 6: 167-180, 2005.
2. Kjoller, L. and Hall, A. Signaling to Rho GTPases. *Exp Cell Res*, 253: 166-179, 1999.
3. Kourlas, P. J., Strout, M. P., Becknell, B., Veronese, M. L., Croce, C. M., Theil, K. S., Krahe, R., Ruutu, T., Knuutila, S., Bloomfield, C. D., and Caligiuri, M. A. Identification of a gene at 11q23 encoding a guanine nucleotide exchange factor: evidence for its fusion with MLL in acute myeloid leukemia. *Proc Natl Acad Sci U S A*, 97: 2145-2150, 2000.
4. Schmidt, A. and Hall, A. Guanine nucleotide exchange factors for Rho GTPases: turning on the switch. *Genes Dev*, 16: 1587-1609, 2002.
5. Booden, M. A., Siderovski, D. P., and Der, C. J. Leukemia-associated Rho guanine nucleotide exchange factor promotes G alpha q-coupled activation of RhoA. *Mol Cell Biol*, 22: 4053-4061, 2002.
6. Wang, Q., Liu, M., Kozasa, T., Rothstein, J. D., Sternweis, P. C., and Neubig, R. R. Thrombin and lysophosphatidic acid receptors utilize distinct rhoGEFs in prostate cancer cells. *J Biol Chem*, 279: 28831-28834, 2004.
7. Zheng, R., Iwase, A., Shen, R., Goodman, O. B., Jr., Sugimoto, N., Takuwa, Y., Lerner, D. J., and Nanus, D. M. Neuropeptide-stimulated cell migration in prostate cancer cells is mediated by RhoA kinase signaling and inhibited by neutral endopeptidase. *Oncogene*, 25: 5942-5952, 2006.
8. Reuther, G. W., Lambert, Q. T., Booden, M. A., Wennerberg, K., Becknell, B., Marcucci, G., Sondek, J., Caligiuri, M. A., and Der, C. J. Leukemia-associated Rho guanine nucleotide exchange factor, a Dbl family protein found mutated in leukemia, causes transformation by activation of RhoA. *J Biol Chem*, 276: 27145-27151, 2001.
9. Bourguignon, L. Y., Gilad, E., Brightman, A., Diedrich, F., and Singleton, P. Hyaluronan-CD44 interaction with leukemia-associated RhoGEF and epidermal growth factor receptor promotes Rho/Ras co-activation, phospholipase C epsilon-Ca²⁺ signaling, and cytoskeleton modification in head and neck squamous cell carcinoma cells. *J Biol Chem*, 281: 14026-14040, 2006.
10. Hodges, A., Sharrocks, K., Edelmann, M., Baban, D., Moris, A., Schwartz, O., Drakesmith, H., Davies, K., Kessler, B., McMichael, A., and Simmons, A.

- Activation of the lectin DC-SIGN induces an immature dendritic cell phenotype triggering Rho-GTPase activity required for HIV-1 replication. *Nat Immunol*, 8: 569-577, 2007.
11. Linder, A. E., Webb, R. C., Mills, T. M., Ying, Z., Lewis, R. W., and Teixeira, C. E. Rho-kinase and RGS-containing RhoGEFs as molecular targets for the treatment of erectile dysfunction. *Curr Pharm Des*, 11: 4029-4040, 2005.
 12. Teixeira, C. E., Ying, Z., and Webb, R. C. Proerectile effects of the Rho-kinase inhibitor (S)-(+)-2-methyl-1-[(4-methyl-5-isoquinolinyl)sulfonyl]homopiperazine (H-1152) in the rat penis. *J Pharmacol Exp Ther*, 315: 155-162, 2005.
 13. Wirth, A., Benyo, Z., Lukasova, M., Leutgeb, B., Wettschureck, N., Gorbey, S., Orsy, P., Horvath, B., Maser-Gluth, C., Greiner, E., Lemmer, B., Schutz, G., Gutkind, J. S., and Offermanns, S. G12-G13-LARG-mediated signaling in vascular smooth muscle is required for salt-induced hypertension. *Nat Med*, 14: 64-68, 2008.
 14. Collisson, E. A., Kleer, C., Wu, M., De, A., Gambhir, S. S., Merajver, S. D., and Kolodney, M. S. Atorvastatin prevents RhoC isoprenylation, invasion, and metastasis in human melanoma cells. *Mol Cancer Ther*, 2: 941-948, 2003.
 15. Sebti, S. M. and Hamilton, A. D. Farnesyltransferase and geranylgeranyltransferase I inhibitors and cancer therapy: lessons from mechanism and bench-to-bedside translational studies. *Oncogene*, 19: 6584-6593, 2000.
 16. Gao, Y., Dickerson, J. B., Guo, F., Zheng, J., and Zheng, Y. Rational design and characterization of a Rac GTPase-specific small molecule inhibitor. *Proc Natl Acad Sci U S A*, 101: 7618-7623, 2004.
 17. Desire, L., Bourdin, J., Loiseau, N., Peillon, H., Picard, V., De Oliveira, C., Bachelot, F., Leblond, B., Taverne, T., Beausoleil, E., Lacombe, S., Drouin, D., and Schweighoffer, F. RAC1 inhibition targets amyloid precursor protein processing by gamma-secretase and decreases Abeta production in vitro and in vivo. *J Biol Chem*, 280: 37516-37525, 2005.
 18. Shutes, A., Onesto, C., Picard, V., Leblond, B., Schweighoffer, F., and Der, C. J. Specificity and mechanism of action of EHT 1864, a novel small molecule inhibitor of Rac family small GTPases. *J Biol Chem*, 282: 35666-35678, 2007.
 19. Rossman, K. L., Cheng, L., Mahon, G. M., Rojas, R. J., Snyder, J. T., Whitehead, I. P., and Sondek, J. Multifunctional roles for the PH domain of Dbs in regulating Rho GTPase activation. *J Biol Chem*, 278: 18393-18400, 2003.

20. Kristelly, R., Earnest, B. T., Krishnamoorthy, L., and Tesmer, J. J. Preliminary structure analysis of the DH/PH domains of leukemia-associated RhoGEF. *Acta Crystallogr D Biol Crystallogr*, *59*: 1859-1862, 2003.
21. Roman, D. L., Talbot, J. N., Roof, R. A., Sunahara, R. K., Traynor, J. R., and Neubig, R. R. Identification of small-molecule inhibitors of RGS4 using a high-throughput flow cytometry protein interaction assay. *Mol Pharmacol*, *71*: 169-175, 2007.
22. Viswanadhan V.N., G. A. K., Revankar, G.R., Robins, R.K. Atomic Physicochemical Parameters for Three Dimensional Structure Directed Quantitative Structure-Activity Relationships. 4. Additional Parameters for Hydrophobic and Dispersive Interactions and Their Application for an Automated Superposition of Certain Naturally Occurring Nucleoside Antibiotics. *Journal of Chemical Information and Computer Sciences*, *29*: 163-172, 1989.
23. McEwen, D. P., Gee, K. R., Kang, H. C., and Neubig, R. R. Fluorescent BODIPY-GTP analogs: real-time measurement of nucleotide binding to G proteins. *Anal Biochem*, *291*: 109-117, 2001.
24. McEwen, D. P., Gee, K. R., Kang, H. C., and Neubig, R. R. Fluorescence approaches to study G protein mechanisms. *Methods Enzymol*, *344*: 403-420, 2002.
25. Owicki, J. C. Fluorescence polarization and anisotropy in high throughput screening: perspectives and primer. *J Biomol Screen*, *5*: 297-306, 2000.
26. Lutz, S., Shankaranarayanan, A., Coco, C., Ridilla, M., Nance, M. R., Vettel, C., Baltus, D., Evelyn, C. R., Neubig, R. R., Wieland, T., and Tesmer, J. J. Structure of Galphaq-p63RhoGEF-RhoA complex reveals a pathway for the activation of RhoA by GPCRs. *Science*, *318*: 1923-1927, 2007.
27. Zhang, J. H., Chung, T. D., and Oldenburg, K. R. A Simple Statistical Parameter for Use in Evaluation and Validation of High Throughput Screening Assays. *J Biomol Screen*, *4*: 67-73, 1999.
28. Lipinski, C. A., Lombardo, F., Dominy, B. W., and Feeney, P. J. Experimental and computational approaches to estimate solubility and permeability in drug discovery and development settings. *Adv Drug Deliv Rev*, *46*: 3-26, 2001.
29. Kristelly, R., Gao, G., and Tesmer, J. J. Structural determinants of RhoA binding and nucleotide exchange in leukemia-associated Rho guanine-nucleotide exchange factor. *J Biol Chem*, *279*: 47352-47362, 2004.
30. Remmers, A. E., Posner, R., and Neubig, R. R. Fluorescent guanine nucleotide analogs and G protein activation. *J Biol Chem*, *269*: 13771-13778, 1994.

31. Verkman, A. S. Drug discovery in academia. *Am J Physiol Cell Physiol*, 286: C465-474, 2004.
32. Rojas, R. J., Kimple, R. J., Rossman, K. L., Siderovski, D. P., and Sondek, J. Established and emerging fluorescence-based assays for G-protein function: Ras-superfamily GTPases. *Comb Chem High Throughput Screen*, 6: 409-418, 2003.
33. Peterson, Y. K., Kelly, P., Weinbaum, C. A., and Casey, P. J. A novel protein geranylgeranyltransferase-I inhibitor with high potency, selectivity, and cellular activity. *J Biol Chem*, 281: 12445-12450, 2006.
34. Evelyn, C. R., Wade, S. M., Wang, Q., Wu, M., Iniguez-Lluhi, J. A., Merajver, S. D., and Neubig, R. R. CCG-1423: a small-molecule inhibitor of RhoA transcriptional signaling. *Mol Cancer Ther*, 6: 2249-2260, 2007.
35. Rujkijyanont, P., Beyene, J., Wei, K., Khan, F., and Dror, Y. Leukaemia-related gene expression in bone marrow cells from patients with the preleukaemic disorder Shwachman-Diamond syndrome. *Br J Haematol*, 137: 537-544, 2007.
36. Kitzing, T. M., Sahadevan, A. S., Brandt, D. T., Knieling, H., Hannemann, S., Fackler, O. T., Grosshans, J., and Grosse, R. Positive feedback between Dial, LARG, and RhoA regulates cell morphology and invasion. *Genes Dev*, 21: 1478-1483, 2007.
37. Ying, Z., Jin, L., Palmer, T., and Webb, R. C. Angiotensin II up-regulates the leukemia-associated Rho guanine nucleotide exchange factor (RhoGEF), a regulator of G protein signaling domain-containing RhoGEF, in vascular smooth muscle cells. *Mol Pharmacol*, 69: 932-940, 2006.

Chapter VI

CONCLUSION

Cancer metastasis is a major health problem that results in thousands of deaths every year (1, 2). The complex process of metastasis requires tumor cells to escape their primary tumor site and to re-colonize at an alternate tissue site, such as the bone, lungs, liver, and brain (1-5). The RhoA transcriptional signaling pathway has been shown to play a role in the complex process of metastasis along with many of the cellular processes associated with it (6-26). However, there is still much to be elucidated with regard to the connection between signaling mechanisms of the RhoA transcriptional signaling pathway and to the progression and metastasis of multiple malignancies. Therefore, the major goal of my work here was to identify a small-molecule inhibitor of the RhoA transcriptional pathway that can be used as a pharmacological tool to further investigate the contribution of this pathway to the cell signaling mechanisms necessary for the progression and metastasis of these various malignancies. Also, another goal of my work was to identify a lead compound that can be potentially developed into a future cancer therapeutic.

In Chapter 2, using a two-thousand compound cell-based Rho-specific SRE.L-luciferase reporter assay high-throughput screen, I was able to identify two small-molecule inhibitors, CCG-977 and CCG-1423, of the RhoA transcriptional signaling pathway. In assessing the mechanism of action of the more potent compound, CCG-1423, the compound was found to work downstream of RhoA and RhoC and actin dynamics at the MKL1/SRF transcriptional signaling level. Given that CCG-1423 modulates

MKL1/SRF transcriptional activity, there are an abundance of potential cellular mechanisms, including: (i) inhibition of translocation of MKL1 into the nucleus, (ii) stimulation of MKL1 phosphorylation or sumoylation (27, 28), (iii) inhibition of the interaction between MKL1 and SRF, (iv) regulation of an element of transcriptional control, such as SPT16 (29), BRG1 (30), histone demethylases (31), histone acetyltransferases (HATs) (32), histone deacetyltransferases (HDACs) (32), and histone methyltransferases (HMTs) (32), or (v) inhibition of a novel regulatory protein. Interestingly, MKL1 and SRF have recently been shown to play a role in breast cancer and melanoma metastasis (17), thus solidifying the importance of the transcriptional portion of the RhoA signaling pathway in cancer biology. Therefore, development of more selective and less toxic analogs will be necessary to identify the molecular target of CCG-1423.

In Chapter 3, we utilized chemical synthesis to develop more potent, selective, and less toxic analogs of the RhoA transcriptional inhibitor, CCG-1423, that I identified in Chapter 2. The most promising analogs tested were less potent but more selective and less toxic than CCG-1423. The amide replacement class of analogs displayed the best activity with CCG-101425 showing the best activity and selectivity to date. This class of analogs should be most useful in identifying the molecular target of CCG-1423 and for development of a pharmacological tool that can be used *in vivo* to study the role of the RhoA transcriptional signaling pathway in prostate cancer metastasis. For assessing the effect of the compounds upon prostate cancer metastasis, a metastasis model described by Kalikin and colleagues will be used (33). Immunocompromised mice will be injected into the left ventricle with PC-3 prostate cancer cells stably expressing firefly luciferase, and

disease progression and metastasis will be monitored non-invasively by bioluminescent signals in real time without the need for sacrificing many mice (33).

Future mechanistic studies to identify the molecular target of CCG-1423 will utilize three compounds developed in Chapter 3. The approach that will be taken to identify the molecular target will be a compound affinity column. This approach has been successfully described previously to identify molecular targets of phenotypic screens (34-36). The small-molecule inhibitor, TWS119, a 4,6-disubstituted pyrrolopyrimidine, was identified in a high-throughput cell-based screen for inducers of neurogenesis in murine embryonic stem cells. Using an affinity-column approach, the molecular target of TWS119 was identified to be glycogen kinase-3 β (GSK-3 β) (34). Another study implemented an affinity-column approach to identify the molecular target of an inducer of glucose uptake in L6 myocytes via AMP-activated protein kinase (AMPK) activation, D942, a furancarboxylic acid derivative. The molecular protein target of D942 was identified to be NAD(P)H dehydrogenase [quinine 1] (complex 1) (35). For our column, the conformationally restrictive piperidine ring analog, CCG-100602, and the amide replacement analog, CCG-101425, will be used as active analogs for identifying the molecular target due their selective and efficacious functional activities (Fig. 6-1B-C). The amide analog, CCG-100686, will be used as an inactive analog for ruling out non-specific compound interactions with proteins due its lack of activity against both the Rho-specific SRE.L-luciferase and TK-*Renilla* luciferase responses (Fig. 6-1D). The compounds will be chemically linked to sepharose beads through a methoxy and polyethylene glycol (PEG) – amine linkage (Fig. 6-1A). PC-3 total cell lysate and nuclear extract will be used as the protein source for the column. Compound eluate will be run on

a SDS silver-stained gel. Protein bands specific for the active compounds (CCG-100602 and CCG-101425) versus the inactive compound (CCG-100686) will be submitted for matrix-assisted laser desorption/ionization (MALDI) - Mass Spectrometry analysis for determination of positive hits that may be the molecular target of CCG-1423. Upon identification of the molecular target, it can be used for more rational structure-activity relationship experimental studies for the development of a more specific pharmacological tool and cancer therapeutic.

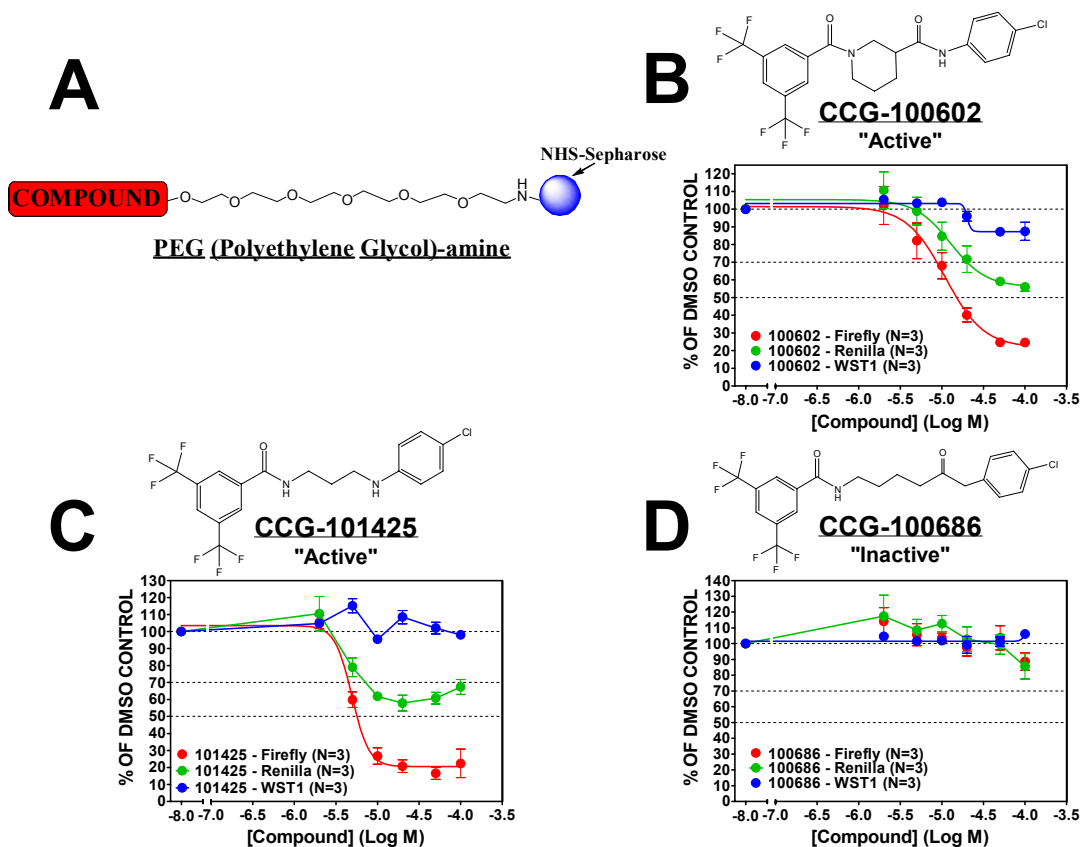


Figure 6-1. CCG-1423 Analogs and Affinity Column for Future Mechanistic Studies. (A) A schematic of the methoxy and PEG linkage that will be used to attach the compounds to the sepharose beads to make the affinity column. Dose-dependent inhibition of $G\alpha_{12}QL$ -stimulated SRE.L-luciferase expression, thymidine kinase (TK) driven *Renilla* luciferase expression, and PC-3 cell survival via the WST1 cell viability assay of the “active” compounds, CCG-100602 (B) and CCG-101425 (C), and the “inactive” compound, CCG-100686 (D) in PC-3 prostate cancer cells. The assays were carried out as described in the Materials and Methods in Chapter 3. Panels B-D represent the mean \pm SEM data performed in triplicate three separate times.

In Chapter 4, four candidate genes (*RGS4*, *RGS7*, *CTGF*, *SOX9*) were identified as potential CCG-1423 regulated genes that may play a role in the CCG-1423 inhibition of PC-3 cell Matrigel invasion described in Chapter 2. These genes were confirmed to be regulated by CCG-1423 by quantitative real time polymerase chain reaction (QRT-PCR) analysis. As described in Chapter 4, *RGS7* and *CTGF* were ruled out due to the differential effects that the two more selective and less toxic CCG-1423 analogs, CCG-100602 and CCG-101425, and the inactive analog, CCG-100686, had upon their gene expression in comparison to CCG-1423. Therefore, *RGS4* and *SOX9* were identified as my promising gene candidates that may regulate PC-3 prostate cancer cell Matrigel invasion and potentially metastasis. Future studies utilizing retroviral overexpression of *RGS4* and shRNA knockdown of *SOX9* expression in PC-3 cells will be necessary to assess the potential role of these gene candidates in functional studies. Initially, PC-3 cells stably expressing *RGS4* and shRNA *SOX9* will need to have *RGS4* protein overexpression and knockdown of *SOX9* protein expression confirmed by western blot. Then, these cells can be used in *in vitro* cancer cell functional assays, including cell growth, adhesion, migration, and invasion. In addition, these cells will be used in *in vivo* prostate cancer metastasis studies using the metastasis model described by Kalikin and colleagues (33).

In Chapter 5, we used a completely different biochemical molecular high-throughput screening approach to identify novel small-molecule inhibitors of the RhoA transcriptional signaling pathway. We performed a ten-thousand compound fluorescence polarization RhoA nucleotide binding screen for inhibitors of the interaction between the RhoGEF, LARG, and the Rho GTPase, RhoA, we identified five compounds that

selectively inhibit LARG-stimulated RhoA nucleotide binding. These compounds were also shown to selectively inhibit LARG-stimulated RhoA [³⁵S] GTPγS binding but not RhoA or Gα_o [³⁵S] GTPγS binding. Therefore, using another high-throughput screening approach, I was able to identify five promising lead compounds that inhibit the RhoA transcriptional signaling pathway that upon further development may lead to the development of pharmacological tools and therapeutics. Future biochemical studies utilizing this assay will assess the specificity of these compounds with respect to different RhoGEF and RhoGTPase interactions. In addition, future biochemical studies will assess the mechanism of action of these compounds, including the possibilities of (i) competitive inhibition at the site of interaction between LARG and RhoA, (ii) allosteric inhibition by compound binding to LARG, (iii) competitive inhibition at the site of nucleotide binding, or (iv) allosteric inhibition by compound binding to RhoA. Also, structure-activity relationship studies will be needed to develop analogs that can be used as pharmacological tools in cell-based and *in vivo* mouse experiments. As discussed in Chapter 5, cell-based inhibitors of LARG may lead to the development of therapeutics that may serve to be useful in multiple diseases and disorders, including leukemia (37, 38), human immunodeficiency virus (HIV) (39), hypertension (40), and erectile dysfunction (ED) (41-43).

Overall, in my thesis work described here, I have identified promising lead compounds that inhibit the RhoA transcriptional signaling pathway. These compounds should serve as a good start for the development of both pharmacological tools to assess the role of the RhoA transcriptional signaling pathway in the biology of cancer metastasis and future cancer therapeutics. Also, through the use of my RhoA transcriptional

signaling pathway inhibitor, CCG-1423, I have begun to elucidate a cancer gene signature that may be useful for identifying a population of future cancer patients that may be helped by drugs that target the RhoA transcriptional signaling pathway.

References

1. Nguyen, D. X., Bos, P. D., and Massague, J. Metastasis: from dissemination to organ-specific colonization. *Nat Rev Cancer*, *9*: 274-284, 2009.
2. Sawyer, T. K. Cancer metastasis therapeutic targets and drug discovery: emerging small-molecule protein kinase inhibitors. *Expert Opin Investig Drugs*, *13*: 1-19, 2004.
3. Christofori, G. New signals from the invasive front. *Nature*, *441*: 444-450, 2006.
4. Fidler, I. J. The pathogenesis of cancer metastasis: the 'seed and soil' hypothesis revisited. *Nat Rev Cancer*, *3*: 453-458, 2003.
5. Gupta, G. P. and Massague, J. Cancer metastasis: building a framework. *Cell*, *127*: 679-695, 2006.
6. Clark, E. A., Golub, T. R., Lander, E. S., and Hynes, R. O. Genomic analysis of metastasis reveals an essential role for RhoC. *Nature*, *406*: 532-535, 2000.
7. Collisson, E. A., Kleer, C., Wu, M., De, A., Gambhir, S. S., Merajver, S. D., and Kolodney, M. S. Atorvastatin prevents RhoC isoprenylation, invasion, and metastasis in human melanoma cells. *Mol Cancer Ther*, *2*: 941-948, 2003.
8. Faried, A., Nakajima, M., Sohda, M., Miyazaki, T., Kato, H., and Kuwano, H. Correlation between RhoA overexpression and tumour progression in esophageal squamous cell carcinoma. *Eur J Surg Oncol*, *31*: 410-414, 2005.
9. Hall, C. L., Dubyk, C. W., Riesenberger, T. A., Shein, D., Keller, E. T., and van Golen, K. L. Type I collagen receptor (alpha2beta1) signaling promotes prostate cancer invasion through RhoC GTPase. *Neoplasia*, *10*: 797-803, 2008.
10. Iizumi, M., Bandyopadhyay, S., Pai, S. K., Watabe, M., Hirota, S., Hosobe, S., Tsukada, T., Miura, K., Saito, K., Furuta, E., Liu, W., Xing, F., Okuda, H., Kobayashi, A., and Watabe, K. RhoC promotes metastasis via activation of the Pyk2 pathway in prostate cancer. *Cancer Res*, *68*: 7613-7620, 2008.
11. Ikoma, T., Takahashi, T., Nagano, S., Li, Y. M., Ohno, Y., Ando, K., Fujiwara, T., Fujiwara, H., and Kosai, K. A definitive role of RhoC in metastasis of orthotopic lung cancer in mice. *Clin Cancer Res*, *10*: 1192-1200, 2004.
12. Kelly, P., Moeller, B. J., Juneja, J., Booden, M. A., Der, C. J., Daaka, Y., Dewhirst, M. W., Fields, T. A., and Casey, P. J. The G12 family of heterotrimeric G proteins promotes breast cancer invasion and metastasis. *Proc Natl Acad Sci U S A*, *103*: 8173-8178, 2006.

13. Kelly, P., Stemmler, L. N., Madden, J. F., Fields, T. A., Daaka, Y., and Casey, P. J. A role for the G12 family of heterotrimeric G proteins in prostate cancer invasion. *J Biol Chem*, *281*: 26483-26490, 2006.
14. Li, X. R., Ji, F., Ouyang, J., Wu, W., Qian, L. Y., and Yang, K. Y. Overexpression of RhoA is associated with poor prognosis in hepatocellular carcinoma. *Eur J Surg Oncol*, *32*: 1130-1134, 2006.
15. Lin, M., DiVito, M. M., Merajver, S. D., Boyanapalli, M., and van Golen, K. L. Regulation of pancreatic cancer cell migration and invasion by RhoC GTPase and caveolin-1. *Mol Cancer*, *4*: 21, 2005.
16. Liu, N., Bi, F., Pan, Y., Sun, L., Xue, Y., Shi, Y., Yao, X., Zheng, Y., and Fan, D. Reversal of the malignant phenotype of gastric cancer cells by inhibition of RhoA expression and activity. *Clin Cancer Res*, *10*: 6239-6247, 2004.
17. Medjkane, S., Perez-Sanchez, C., Gaggioli, C., Sahai, E., and Treisman, R. Myocardin-related transcription factors and SRF are required for cytoskeletal dynamics and experimental metastasis. *Nat Cell Biol*, *11*: 257-268, 2009.
18. Pan, Q., Bao, L. W., Teknos, T. N., and Merajver, S. D. Targeted disruption of protein kinase C epsilon reduces cell invasion and motility through inactivation of RhoA and RhoC GTPases in head and neck squamous cell carcinoma. *Cancer Res*, *66*: 9379-9384, 2006.
19. Pille, J. Y., Denoyelle, C., Varet, J., Bertrand, J. R., Soria, J., Opolon, P., Lu, H., Pritchard, L. L., Vannier, J. P., Malvy, C., Soria, C., and Li, H. Anti-RhoA and anti-RhoC siRNAs inhibit the proliferation and invasiveness of MDA-MB-231 breast cancer cells in vitro and in vivo. *Mol Ther*, *11*: 267-274, 2005.
20. Sequeira, L., Dubyk, C. W., Riesenberger, T. A., Cooper, C. R., and van Golen, K. L. Rho GTPases in PC-3 prostate cancer cell morphology, invasion and tumor cell diapedesis. *Clin Exp Metastasis*, *25*: 569-579, 2008.
21. Sun, H. W., Tong, S. L., He, J., Wang, Q., Zou, L., Ma, S. J., Tan, H. Y., Luo, J. F., and Wu, H. X. RhoA and RhoC -siRNA inhibit the proliferation and invasiveness activity of human gastric carcinoma by Rho/PI3K/Akt pathway. *World J Gastroenterol*, *13*: 3517-3522, 2007.
22. van Golen, K. L., Bao, L., DiVito, M. M., Wu, Z., Prendergast, G. C., and Merajver, S. D. Reversion of RhoC GTPase-induced inflammatory breast cancer phenotype by treatment with a farnesyl transferase inhibitor. *Mol Cancer Ther*, *1*: 575-583, 2002.
23. van Golen, K. L., Davies, S., Wu, Z. F., Wang, Y., Bucana, C. D., Root, H., Chandrasekharappa, S., Strawderman, M., Ethier, S. P., and Merajver, S. D. A

- novel putative low-affinity insulin-like growth factor-binding protein, LIBC (lost in inflammatory breast cancer), and RhoC GTPase correlate with the inflammatory breast cancer phenotype. *Clin Cancer Res*, 5: 2511-2519, 1999.
24. van Golen, K. L., Wu, Z. F., Qiao, X. T., Bao, L. W., and Merajver, S. D. RhoC GTPase, a novel transforming oncogene for human mammary epithelial cells that partially recapitulates the inflammatory breast cancer phenotype. *Cancer Res*, 60: 5832-5838, 2000.
 25. Xiaorong, L., Wei, W., Liyuan, Q., and Kaiyan, Y. Underexpression of deleted in liver cancer 2 (DLC2) is associated with overexpression of RhoA and poor prognosis in hepatocellular carcinoma. *BMC Cancer*, 8: 205, 2008.
 26. Yao, H., Dashner, E. J., van Golen, C. M., and van Golen, K. L. RhoC GTPase is required for PC-3 prostate cancer cell invasion but not motility. *Oncogene*, 25: 2285-2296, 2006.
 27. Muehlich, S., Wang, R., Lee, S. M., Lewis, T. C., Dai, C., and Prywes, R. Serum-induced phosphorylation of the serum response factor coactivator MKL1 by the extracellular signal-regulated kinase 1/2 pathway inhibits its nuclear localization. *Mol Cell Biol*, 28: 6302-6313, 2008.
 28. Nakagawa, K. and Kuzumaki, N. Transcriptional activity of megakaryoblastic leukemia 1 (MKL1) is repressed by SUMO modification. *Genes Cells*, 10: 835-850, 2005.
 29. Kihara, T., Kano, F., and Murata, M. Modulation of SRF-dependent gene expression by association of SPT16 with MKL1. *Exp Cell Res*, 314: 629-637, 2008.
 30. Zhang, M., Fang, H., Zhou, J., and Herring, B. P. A novel role of Brg1 in the regulation of SRF/MRTFA-dependent smooth muscle-specific gene expression. *J Biol Chem*, 282: 25708-25716, 2007.
 31. Lockman, K., Taylor, J. M., and Mack, C. P. The histone demethylase, Jmjd1a, interacts with the myocardin factors to regulate SMC differentiation marker gene expression. *Circ Res*, 101: e115-123, 2007.
 32. Munshi, A., Shafi, G., Aliya, N., and Jyothy, A. Histone modifications dictate specific biological readouts. *J Genet Genomics*, 36: 75-88, 2009.
 33. Kalikin, L. M., Schneider, A., Thakur, M. A., Fridman, Y., Griffin, L. B., Dunn, R. L., Rosol, T. J., Shah, R. B., Rehemtulla, A., McCauley, L. K., and Pienta, K. J. In vivo visualization of metastatic prostate cancer and quantitation of disease progression in immunocompromised mice. *Cancer Biol Ther*, 2: 656-660, 2003.

34. Ding, S., Wu, T. Y., Brinker, A., Peters, E. C., Hur, W., Gray, N. S., and Schultz, P. G. Synthetic small molecules that control stem cell fate. *Proc Natl Acad Sci U S A*, *100*: 7632-7637, 2003.
35. Kosaka, T., Okuyama, R., Sun, W., Ogata, T., Harada, J., Araki, K., Izumi, M., Yoshida, T., Okuno, A., Fujiwara, T., Ohsumi, J., and Ichikawa, K. Identification of molecular target of AMP-activated protein kinase activator by affinity purification and mass spectrometry. *Anal Chem*, *77*: 2050-2055, 2005.
36. Leslie, B. J. and Hergenrother, P. J. Identification of the cellular targets of bioactive small organic molecules using affinity reagents. *Chem Soc Rev*, *37*: 1347-1360, 2008.
37. Kourlas, P. J., Strout, M. P., Becknell, B., Veronese, M. L., Croce, C. M., Theil, K. S., Krahe, R., Ruutu, T., Knuutila, S., Bloomfield, C. D., and Caligiuri, M. A. Identification of a gene at 11q23 encoding a guanine nucleotide exchange factor: evidence for its fusion with MLL in acute myeloid leukemia. *Proc Natl Acad Sci U S A*, *97*: 2145-2150, 2000.
38. Rujkijyanont, P., Beyene, J., Wei, K., Khan, F., and Dror, Y. Leukaemia-related gene expression in bone marrow cells from patients with the preleukaemic disorder Shwachman-Diamond syndrome. *Br J Haematol*, *137*: 537-544, 2007.
39. Hodges, A., Sharrocks, K., Edelmann, M., Baban, D., Moris, A., Schwartz, O., Drakesmith, H., Davies, K., Kessler, B., McMichael, A., and Simmons, A. Activation of the lectin DC-SIGN induces an immature dendritic cell phenotype triggering Rho-GTPase activity required for HIV-1 replication. *Nat Immunol*, *8*: 569-577, 2007.
40. Wirth, A., Benyo, Z., Lukasova, M., Leutgeb, B., Wettschureck, N., Gorbey, S., Orsy, P., Horvath, B., Maser-Gluth, C., Greiner, E., Lemmer, B., Schutz, G., Gutkind, J. S., and Offermanns, S. G12-G13-LARG-mediated signaling in vascular smooth muscle is required for salt-induced hypertension. *Nat Med*, *14*: 64-68, 2008.
41. Linder, A. E., Webb, R. C., Mills, T. M., Ying, Z., Lewis, R. W., and Teixeira, C. E. Rho-kinase and RGS-containing RhoGEFs as molecular targets for the treatment of erectile dysfunction. *Curr Pharm Des*, *11*: 4029-4040, 2005.
42. Teixeira, C. E., Ying, Z., and Webb, R. C. Proerectile effects of the Rho-kinase inhibitor (S)-(+)-2-methyl-1-[(4-methyl-5-isoquinoliny) sulfonyl] homopiperazine (H-1152) in the rat penis. *J Pharmacol Exp Ther*, *315*: 155-162, 2005.
43. Ying, Z., Jin, L., Palmer, T., and Webb, R. C. Angiotensin II up-regulates the leukemia-associated Rho guanine nucleotide exchange factor (RhoGEF), a regulator of G protein signaling domain-containing RhoGEF, in vascular smooth muscle cells. *Mol Pharmacol*, *69*: 932-940, 2006.

APPENDIX

<u>Symbol</u>	<u>Description</u>	<u>GenBank</u>	<u>Fold Change</u> (Log ₂ values)
S100P	S100 Calcium Binding Protein P	NM_005980	-5.40
RGS4	Regulator of G-Protein Signaling 4	BC000737	-4.28
RGS4	Regulator of G-Protein Signaling 4	AL514445	-4.44
RGS4	Regulator of G-Protein Signaling 4	NM_005613	-4.43
CXCL2	Chemokine (C-X-C motif) Ligand 2	M57731	-4.12
IL8	Interleukin 8	AF043337	-3.89
IL8	Interleukin 8	NM_000584	-3.81
PTGS2	Prostaglandin-Endoperoxide Synthase 2 (Prostaglandin G/H Synthase and Cyclooxygenase)	AY151286	-3.83
PTGS2	Prostaglandin-Endoperoxide Synthase 2 (Prostaglandin G/H Synthase and Cyclooxygenase)	NM_000963	-5.23
HMOX1	Heme Oxygenase (Decycling) 1	NM_002133	-3.59
ADAMTS5	ADAM Metallopeptidase with Thrombospondin Type 1 Motif, 5 (Aggrecanase-2)	NM_007038	-3.31
ADAMTS5	ADAM Metallopeptidase with Thrombospondin Type 1 Motif, 5 (Aggrecanase-2)	A1123555	-2.88
ADAMTS5	ADAM Metallopeptidase with Thrombospondin Type 1 Motif, 5 (Aggrecanase-2)	BF060767	-2.74
ADAMTS5	ADAM Metallopeptidase with Thrombospondin Type 1 Motif, 5 (Aggrecanase-2)	B1254089	-1.11
RGS7	Regulator of G-Protein Signaling 7	NM_002924	-3.27
HGF	Hepatocyte Growth Factor (Hepapoinetin A; Scatter Factor)	X16323	-3.26
HGF	Hepatocyte Growth Factor (Hepapoinetin A; Scatter Factor)	M77227	-2.91
HGF	Hepatocyte Growth Factor (Hepapoinetin A; Scatter Factor)	U46010	-1.72

APPENDIX

HGF	Hepatocyte Growth Factor (Hepapoin A; Scatter Factor)	M60718	-1.57
HGF	Hepatocyte Growth Factor (Hepapoin A; Scatter Factor)	M77227	-1.81
MFAP2	Microfibrillar-Associated Protein 2	NM_017459	-2.76
LIGAM	L1 Cell Adhesion Molecule	AI653981	-2.75
DST	Dystonin	NM_001723	-2.70
CXCL3	Chemokine (C-X-C Motif) Ligand 3	NM_002090	-2.69
MMP10	Matrix Metalloproteinase 10 (Stromelysin 2)	NM_002425	-2.68
CEBPB	CCAAT/Enhancer Binding Protein (C/EBP), Beta	AI564683	-2.66
ANXA1	Annexin A1	AUI55094	-2.60
ANXA1	Annexin A1	NM_000700	-1.87
VEGFA	Vascular Endothelial Growth Factor A	M27281	-2.60
VEGFA	Vascular Endothelial Growth Factor A	H95344	-2.49
VEGFA	Vascular Endothelial Growth Factor A	AF022375	-2.43
VEGFA	Vascular Endothelial Growth Factor A	AF091352	-2.76
RND3	Rho Family GTPase 3	BG054844	-2.58
LAMA3	Laminin, Alpha 3	BC033663	-2.35
LAMA3	Laminin, Alpha 3	AK024889	-1.11
ADRB1	Adrenergic, Beta-1-, Receptor	AI625747	-2.34
CDH7	Cadherin 7, Type 2	NM_004361	-2.20
ADAM17	ADAM Metalloproteinase Domain 17 (Tumor Necrosis Factor, Alpha, Converting Enzyme)	U86755	-2.11
ADAM17	ADAM Metalloproteinase Domain 17 (Tumor Necrosis Factor, Alpha, Converting Enzyme)	NM_003183	-1.98
FGF2	Fibroblast Growth Factor 2 (Basic)	M27968	-2.10
FGF2	Fibroblast Growth Factor 2 (Basic)	NM_002006	-1.83
IL6	Interleukin 6 (Interferon, Beta 2)	NM_000600	-2.02
ELF3	E74-Like Factor 3 (ETS Domain Transcription Factor, Epithelial-Specific)	U73844	-1.96
ELF3	E74-Like Factor 3	AA527180	-1.73

APPENDIX

	(ETS Domain Transcription Factor, Epithelial-Specific)		
ELF3	E74-Like Factor 3 (ETS Domain Transcription Factor, Epithelial-Specific)	AF017307	-1.86
HPSE	Heparanase	AF155510	-1.94
HPSE	Heparanase	NM_006665	-1.03
TNFAIP6	Tumor Necrosis Factor, Alpha-Induced Protein 6	NM_007115	-1.91
TNFAIP6	Tumor Necrosis Factor, Alpha-Induced Protein 6	AW188198	-2.05
CLDN12	Claudin 12	AL136770	-1.77
RTN4	Reticulon 4	N90377	-1.74
RTN4	Reticulon 4	CA428769	-1.42
RTN4	Reticulon 4	AW963634	-1.14
FLRT3	Fibronectin Leucine Rich Transmembrane Protein 3	N71923	-1.69
FLRT3	Fibronectin Leucine Rich Transmembrane Protein 3	NM_013281	-1.83
ITGAV	Integrin, Alpha V (Vitronectin Receptor, Alpha Polypeptide, Antigen CD51)	AA228366	-1.67
ITGAV	Integrin, Alpha V (Vitronectin Receptor, Alpha Polypeptide, Antigen CD51)	AW962458	-1.43
ITGAV	Integrin, Alpha V (Vitronectin Receptor, Alpha Polypeptide, Antigen CD51)	AU144005	-1.13
LY96	Lymphocyte Antigen 96	NM_015364	-1.63
CDH1	Cadherin 1, Type 1, E-Cadherin (Epithelial)	L08599	-1.61
CDH1	Cadherin 1, Type 1, E-Cadherin (Epithelial)	NM_004360	-1.61
IRAK2	Interleukin-1 Receptor-Associated Kinase 2	AI246590	-1.59
LUM	Lumican	NM_002345	-1.57
OPN3	Opn 3 (Encephalopsin, Panopsin)	AI074145	-1.56
C3	Complement Component 3	NM_000064	-1.52
NFE2L1	Nuclear Factor (Erythroid-Derived 2)-Like 1	H93013	-1.52
NFE2L1	Nuclear Factor (Erythroid-Derived 2)-Like 1	NM_003204	-1.44
NFE2L1	Nuclear Factor (Erythroid-Derived 2)-Like 1	AI361227	-1.13
ZFP36	Zinc Finger Protein 36, C3H Type, Homolog (Mouse)	NM_003407	-1.52

APPENDIX

CLDN14	Claudin 14	AF314090	-1.51
CCRL2	Chemokine (C-C Motif) Receptor-Like 2	AF015524	-1.50
AKAP12	A Kinase (PRKA) Anchor Protein (Gravin) 12	BF511276	-1.48
AKAP12	A Kinase (PRKA) Anchor Protein (Gravin) 12	AI672553	-1.46
AKAP12	A Kinase (PRKA) Anchor Protein (Gravin) 12	BF511276	-1.35
AKAP12	A Kinase (PRKA) Anchor Protein (Gravin) 12	AB003476	-1.13
KLF5	Kruppel-Like Factor 5 (Intestinal)	AB030824	-1.45
KLF5	Kruppel-Like Factor 5 (Intestinal)	AF132818	-1.64
BTG1	B-Cell Translocation Gene 1, Anti-Proliferative	AL535380	-1.44
BTG1	B-Cell Translocation Gene 1, Anti-Proliferative	NM_001731	-1.49
TPBG	Trophoblast Glycoprotein	NM_006670	-1.43
ACVR1	Activin A Receptor, Type I	NM_001105	-1.41
EDNRA	Endothelin Receptor Type A	NM_001957	-1.39
COL5A1	Collagen, Type V, Alpha 1	N30339	-1.36
COL5A1	Collagen, Type V, Alpha 1	AI983428	-1.06
WNT9A	Wingless-Type MMTV Integration Site Family, Member 9A"	BE220265	-1.34
ALCAM	Activated Leukocyte Cell Adhesion Molecule	BE502785	-1.31
ALCAM	Activated Leukocyte Cell Adhesion Molecule	BC041127	-1.33
NOS3	Nitric Oxide Synthase 3 (Endothelial Cell)	NM_000603	-1.31
CLDN7	Claudin 7	NM_001307	-1.29
BMP6	Bone Morphogenetic Protein 6	NM_001718	-1.26
GPC1	Glypican 1	NM_002081	-1.25
ERAP1	Endoplasmic Reticulum Aminopeptidase 1	BE551138	-1.24
PCDH7	Protocadherin 7	BE644809	-1.24
ADAMTS17	ADAM Metallopeptidase with Thrombospondin Type 1 Motif, 17	AA022668	-1.23
ADAMTS17	ADAM Metallopeptidase with Thrombospondin Type 1 Motif, 17	AA022668	-1.01
RRAS2	Related RAS Viral (R-Ras) Oncogene Homolog 2	NM_012250	-1.21
RRAS2	Related RAS Viral (R-Ras) Oncogene Homolog 2	AI753792	-1.18
RRAS2	Related RAS Viral (R-Ras) Oncogene Homolog 2	AI431643	-1.10

APPENDIX

CD24	CD24 Molecule	AA761181	-1.17
CD24	CD24 Molecule	L33930	-1.32
CD24	CD24 Molecule	AK000168	-1.18
CD24	CD24 Molecule	X69397	-1.09
CD24	CD24 Molecule	M58664	-1.18
CD24	CD24 Molecule	BG327863	-1.06
CELSRI	Cadherin, EGF LAG Seven-Pass G-Type Receptor 1 (Flamingo Homolog, Drosophila)	AL031588	-1.17
MPZL3	Myelin Protein Zero-Like 3	AA772172	-1.16
CEACAM1	Carcinoembryonic Antigen-Related Cell Adhesion Molecule 1 (BiliaryGlycoprotein)	M76742	-1.15
CEACAM1	Carcinoembryonic Antigen-Related Cell Adhesion Molecule 1 (BiliaryGlycoprotein)	X16354	-1.09
AGT	Angiotensinogen	NM_000029	-1.14
TYMP	(Serpine Peptidase Inhibitor, Clade A, Member 8)		
TYMP	Thymidine Phosphorylase	NM_001953	-1.14
TYMP	Thymidine Phosphorylase	AW613387	-1.25
AMIGO2	Adhesion Molecule with Ig-Like Domain 2	AC004010	-1.12
RHOB	RAS Homolog Gene Family, Member B	AI263909	-1.12
HDAC9	Histone Deacetylase 9	NM_014707	-1.10
GPR92	G-Protein Coupled Receptor 92	AW183080	-1.09
OR2A7	Olfactory Receptor, Family 2, Subfamily A, Member 7	AF327904	-1.09
BMP2	Bone Morphogenetic Protein 2	NM_001200	-1.04
CD58	CD58 Molecule	D28586	-1.04
ITGA2	Integrin, Alpha 2 (CD49B, Alpha 2 Subunit of VLA-2 Receptor)	N95414	-1.03
LAMA4	Laminin, Alpha 4	U77706	-1.03
SERPINE2	Serpine Peptidase Inhibitor, Clade E (Nexin, Plasminogen Activator Inhibitor Type 1), Member 2	AL541302	-1.03
SERPINE2	Serpine Peptidase Inhibitor, Clade E (Nexin, Plasminogen Activator Inhibitor Type 1), Member 2	AA703280	-1.49

APPENDIX

DSG2	Desmoglein 2	BF031829	-1.02
FERMT2	Fermiün Family Homolog 2 (Drosophila)	Z24725	-1.01
FERMT2	Fermiün Family Homolog 2 (Drosophila)	AW469573	-1.04
SCYL3	SCY1-Like 3 (S. Cerevisiae)	AI458463	-1.01
PDGFRA	Platelet-Derived Growth Factor Receptor, Alpha Polypeptide	NM_006206	1.00
EDG2	Endothelial Differentiation, Lysophosphatidic Acid G-Protein-Coupled Receptor, 2	AW269335	1.01
FN1	Fibronectin 1	AJ276395	1.01
SLIT2	Slit Homolog 2 (Drosophila)	AI692523	1.01
TGFB2	Transforming Growth Factor, Beta 2	M19154	1.01
TGFB3	Transforming Growth Factor, Beta 3	J03241	1.01
JUB	JUB, AJUBA Homolog (Xenopus Laevis)	NM_032876	1.02
TFPI2	Tissue Factor Pathway Inhibitor 2	L27624	1.02
CDK5	Cyclin-Dependent Kinase 5	NM_004935	1.03
MGLL	Monoglyceride Lipase	BC006230	1.03
ABI2	ABL Interactor 2	BF245400	1.04
NTNG1	Netrin G1	AV723308	1.04
SSX2IP	Synovial Sarcoma, X Breakpoint 2 Interacting Protein	R52678	1.04
TUBB3	Tubulin, Beta 3	NM_006086	1.04
TUBB3	Tubulin, Beta 3	AL565749	1.05
FZD4	Frizzled Homolog 4 (Drosophila)	NM_012193	1.05
FZD4	Frizzled Homolog 4 (Drosophila)	AB054881	1.15
GNAS	GNAS Complex Locus	AA401492	1.05
LOXL2	Lysyl Oxidase-Like 2	NM_002318	1.07
BAI2	Brain-Specific Angiogenesis Inhibitor 2	NM_001703	1.08
ITGB1	Integrin, Beta 1 (Fibronectin Receptor, Beta Polypeptide, Antigen CD29 includes MDF2, MSK12)	AF086249	1.08
NARG1	NMDA Receptor Regulated 1	NM_025085	1.08
LAMB1	Laminin, Beta 1	M20206	1.09
LAMB1	Laminin, Beta 1	NM_002291	1.12

APPENDIX

ATPIF1	ATPase Inhibitory Factor 1	NM_016311	1.11
ROBO1	Roundabout, Axon Guidance Receptor, Homolog 1 (Drosophila)	BF059159	1.11
CCDC88A	Coiled-Coil Domain Containing 88A	AB033038	1.12
ABHD2	Abhydrolase Domain Containing 2	BE671816	1.13
ABHD2	Abhydrolase Domain Containing 2	AI832249	1.12
CHST2	Carbohydrate (N-acetylglucosamine-6-O) Sulfotransferase 2	NM_004267	1.14
ITGB2	Integrin, Beta 2 (Complement Component 3 Receptor 3 and 4 Subunit)	NM_000211	1.15
ITGB2	Integrin, Beta 2 (Complement Component 3 Receptor 3 and 4 Subunit)	AW303397	1.38
PTGER4	Prostaglandin E Receptor 4 (Subtype EP4)	AA897516	1.15
ITGAE	Integrin, Alpha E (Antigen CD103, Human Mucosal Lymphocyte Antigen 1; Alpha Polypeptide)	NM_002208	1.17
VEGFC	Vascular Endothelial Growth Factor C	U58111	1.17
GAL	Galanin Prepropeptide	AL556409	1.19
GPSM2	G-Protein Signaling Modulator 2 (AGS3-like, C. Elegans)	NM_013296	1.19
GPSM2	G-Protein Signaling Modulator 2 (AGS3-like, C. Elegans)	AW195581	1.15
TRIP6	Thyroid Hormone Receptor Interactor 6	AF000974	1.19
ITGA10	Integrin, Alpha 10	AF112345	1.20
CD47	CD47 Molecule	AL118798	1.21
COL27A1	Collagen, Type XXVII, Alpha 1	AK021957	1.23
MAGI1	Membrane Associated Guanylate Kinase, WW and PDZ Domain Containing 1	AI141556	1.23
COCH	Coagulation Factor C Homolog, cochlin (Limulus Polyphemus)	AA669336	1.24
GNG2	Guanine Nucleotide Binding Protein (G protein), Gamma 2	AU118419	1.24
GNG2	Guanine Nucleotide Binding Protein (G protein), Gamma 2	AK026424	1.18

APPENDIX

GNG2	Guanine Nucleotide Binding Protein (G protein), Gamma 2	AF493870	1.05
ADAM9	ADAM Metallopeptidase Domain 9 (Meltrin Gamma)	AF495383	1.25
ADAM9	ADAM Metallopeptidase Domain 9 (Meltrin Gamma)	NM_003816	1.31
CDH3	Cadherin 3, Type 1, P-Cadherin (Placental)	NM_001793	1.29
CYFIP2	Cytoplasmic FMR1 Interacting Protein 2	AL161999	1.31
PXN	Paxillin	NM_002859	1.31
PXN	Paxillin	D86862	1.74
GPER	G-Protein-Coupled Estrogen Receptor 1	U58828	1.32
GPER	G-Protein-Coupled Estrogen Receptor 1	U63917	1.29
PDZD2	PDZ Domain Containing 2	AF338650	1.33
BMPR1B	Bone Morphogenetic Protein Receptor, Type IB	D89675	1.34
ITGA6	Integrin, Alpha 6	AV733308	1.35
MYH9	Myosin, Heavy Chain 9, Non-Muscle	AI827941	1.35
COL12A1	Collagen, Type XII, Alpha 1	AL096771	1.36
COL12A1	Collagen, Type XII, Alpha 1	AA788946	1.49
COL12A1	Collagen, Type XII, Alpha 1	U73778	1.08
EPHX2	Epoxyde Hydrolase 2, Cytoplasmic	AF233336	1.37
TGM2	Transglutaminase 2 (C Polypeptide, Protein-Glutamine-Gamma-Glutamyltransferase)	BC003551	1.38
TGM2	Transglutaminase 2 (C Polypeptide, Protein-Glutamine-Gamma-Glutamyltransferase)	AL031651	1.65
TGM2	Transglutaminase 2 (C Polypeptide, Protein-Glutamine-Gamma-Glutamyltransferase)	M98478	1.08
GRR5	G-Protein-Coupled Receptor Kinase 5	NM_005308	1.42
ARRGD1B	Rho GDP Dissociation Inhibitor (GDI) Beta	NM_001175	1.44
CDH11	Cadherin 11, Type 2, OB-Cadherin (Osteoblast)	NM_001797	1.45
CDH11	Cadherin 11, Type 2, OB-Cadherin (Osteoblast)	D21254	1.34
CDH11	Cadherin 11, Type 2, OB-Cadherin (Osteoblast)	AI040305	1.08
EDG3	Endothelial Differentiation, Sphingolipid G-Protein-Coupled Receptor, 3	AA534817	1.46
C21orf29	Chromosome 21 Open Reading Frame 29	BC021197	1.47

APPENDIX

GBX2	Gastrulation Brain Homeobox 2	AF118452	1.48
PI3	Peptidase Inhibitor 3, Skin-Derived (SKALP)	L10343	1.49
PI3	Peptidase Inhibitor 3, Skin-Derived (SKALP)	NM_002638	1.44
ITGAI1	Integrin, Alpha 1	X68742	1.51
SSPN	Sarcospan (Kras Oncogene-Associated Gene)	AW467136	1.52
SSPN	Sarcospan (Kras Oncogene-Associated Gene)	AL136756	1.30
SSPN	Sarcospan (Kras Oncogene-Associated Gene)	NM_005086	1.27
CALM3	Calmodulin 3 (Phosphorylase Kinase, Delta)	NM_005184	1.54
CALM3	Calmodulin 3 (Phosphorylase Kinase, Delta)	AV685208	1.16
GNG11	Guanine Nucleotide Binding Protein (G protein), gamma 11	NM_004126	1.55
ACHE	Acetylcholinesterase (Yt Blood Group)	NM_015831	1.56
FBN2	Fibrillin 2 (Congenital Contractural Arachnodactyly)	NM_001999	1.59
JAG1	Jagged 1 (Alagille Syndrome)	U73936	1.59
JAG1	Jagged 1 (Alagille Syndrome)	U77914	1.79
JAG1	Jagged 1 (Alagille Syndrome)	AI457817	1.37
JAG1	Jagged 1 (Alagille Syndrome)	U61276	2.01
JAG1	Jagged 1 (Alagille Syndrome)	AU151465	1.19
COL4A1	Collagen, Type IV, Alpha 1	AI922605	1.61
COL4A1	Collagen, Type IV, Alpha 1	NM_001845	1.28
SERPINE1	Serpin Peptidase Inhibitor, Clade E (Nexin, Plasminogen Activator Inhibitor Type 1), Member 1	NM_000602	1.61
SERPINE1	Serpin Peptidase Inhibitor, Clade E (Nexin, Plasminogen Activator Inhibitor Type 1), Member 1	AL574210	1.39
FBLN1	Fibulin 1	NM_006486	1.62
FBLN1	Fibulin 1	Z95331	1.18
DSC3	Desmocollin 3	NM_001941	1.67
DSC3	Desmocollin 3	AI797281	1.43
MMP13	Matrix Metalloproteinase 13 (Collagenase 3)	NM_002427	1.67
NEGR1	Neuronal Growth Regulator 1	AA115106	1.67
NEGR1	Neuronal Growth Regulator 1	AI123532	2.52
NEGR1	Neuronal Growth Regulator 1	NM_173808	1.40

APPENDIX

CNTNAP3	Contactin Associated Protein-Like 3	AF333769	1.68
CNTNAP3	Contactin Associated Protein-Like 3	AI433163	1.25
SPOCK1	Spare/Osteonectin, CWCV and Kazal-Like Domains Proteoglycan (Testican) 1	AF231124	1.70
NEXN	Nexilin (F Actin Binding Protein)	AF114264	1.71
NEXN	Nexilin (F Actin Binding Protein)	NM_144573	1.92
PGM5	Phosphoglucosmutase 5	AA706788	1.72
GPRC5B	G Protein-Coupled Receptor, Family C, Group 5, Member B	NM_016235	1.73
RGS2	Regulator of G-Protein Signaling 2, 24 kDa	NM_002923	1.77
GPR4	G Protein-Coupled Receptor 4	NM_005282	1.78
GPR4	G Protein-Coupled Receptor 4	U35399	1.15
COL6A3	Collagen, Type VI, Alpha 3	NM_004369	1.80
FABP4	Fatty Acid Binding Protein 4, Adipocyte	NM_001442	1.80
FAT	FAT Tumor Suppressor Homolog 1 (Drosophila)	NM_005245	1.86
LTPP1	Latent Transforming Growth Factor Beta Binding Protein 1	AI986120	1.86
LTPP1	Latent Transforming Growth Factor Beta Binding Protein 1	NM_000627	1.19
COL4A2	Collagen, Type IV, Alpha 2	X05610	1.90
COL4A2	Collagen, Type IV, Alpha 2	AA909035	2.12
TROAP	Trophinin Associated Protein (Tastin)	NM_005480	1.93
TROAP	Trophinin Associated Protein (Tastin)	AI199355	1.48
ITGB3BP	Integrin Beta 3 Binding Protein (Beta3-Endonexin)	NM_014288	1.95
CTNNA1	Catenin (Cadherin-Associated Protein), Alpha-Like 1	NM_003798	2.01
PCDH20	Protocadherin 20	AA040057	2.02
COL5A2	Collagen, Type V, Alpha 2	NM_000393	2.03
COL5A2	Collagen, Type V, Alpha 2	AL575735	2.01
KAL1	Kallmann Syndrome 1 Sequence	NM_000216	2.03
AOX1	Aldehyde Oxidase 1	AB046692	2.05
AOX1	Aldehyde Oxidase 1	NM_001159	1.97
HAPLN1	Hyaluronan and Proteoglycan Link Protein 1	U43328	2.08

APPENDIX

LOXL1	Lysyl Oxidase-Like 1	NM_005576	2.13
MCAM	Melanoma Cell Adhesion Molecule	BC006329	2.19
RELN	Reelin	BC041378	2.20
RELN	Reelin	BC041378	2.00
ELK3	ELK3, ETS-Domain Protein (SRF Accessory Protein 2)	AW575374	2.23
ELK3	ELK3, ETS-Domain Protein (SRF Accessory Protein 2)	NM_005230	1.53
CYR61	Cysteine-Rich, Angiogenic Inducer, 61	NM_001554	2.24
CYR61	Cysteine-Rich, Angiogenic Inducer, 61	AF003114	2.38
P2RY5	Purinergic Receptor P2Y, G-Protein Coupled, 5	NM_005767	2.24
HSPG2	Heparan Sulfate Proteoglycan 2	M85289	2.26
HSPG2	Heparan Sulfate Proteoglycan 2	AI991033	1.90
NTSR1	Neurotensin Receptor 1 (High Affinity)	NM_002531	2.27
PCDH18	Protocadherin 18	AW189885	2.27
LRP5	Low Density Lipoprotein Receptor-Related Protein 5	AB017498	2.33
IGFBP4	Insulin-Like Growth Factor Binding Protein 4	NM_001552	2.35
IL23A	Interleukin 23, Alpha Subunit p19	AF043179	2.37
IL23A	Interleukin 23, Alpha Subunit p19	M15564	1.60
IL23A	Interleukin 23, Alpha Subunit p19	AL559122	1.13
CSGALNACT1	Chondroitin Sulfate N-Acetylglucosaminyltransferase 1	NM_018371	2.38
F2RL1	Coagulation Factor II (Thrombin) Receptor-Like 1	BE965369	2.41
F2RL1	Coagulation Factor II (Thrombin) Receptor-Like 1	NM_005242	2.86
NF2	Neurofibromin 2 (Merlin)	NM_016418	2.49
NF2	Neurofibromin 2 (Merlin)	AF123570	2.18
NF2	Neurofibromin 2 (Merlin)	AF122828	2.33
NF2	Neurofibromin 2 (Merlin)	S73854	1.78
NF2	Neurofibromin 2 (Merlin)	BE313317	1.30
NF2	Neurofibromin 2 (Merlin)	AF122827	1.13
ANPEP	Alanyl (Membrane) Aminopeptidase (Aminopeptidase N, Aminopeptidase M, Microsomal	NM_001150	2.48

APPENDIX

	Aminopeptidase, CD13, p150)		
GPR87	G Protein-Coupled Receptor 87	NM_023915	2.54
F2R	Coagulation Factor II (Thrombin) Receptor	NM_001992	2.61
COL2A1	Collagen, Type II, Alpha 1	X06268	2.63
COL2A1	Collagen, Type II, Alpha 1	X16468	2.74
COL8A1	Collagen, Type VIII, Alpha 1	AL359062	2.63
CXCL6	Chemokine (C-X-C motif) Ligand 6 (Granulocyte Chemotactic Protein 2)	NM_002993	2.63
C5	Complement Component 5	NM_001735	2.69
RAMP1	Receptor (G protein-Coupled) Activity Modifying Protein 1	NM_005855	2.69
COL13A1	Collagen, Type XIII, Alpha 1	M33653	2.75
COL13A1	Collagen, Type XIII, Alpha 1	M59217	1.92
COL13A1	Collagen, Type XIII, Alpha 1	NM_005203	1.42
GRPR	Gastrin-Releasing Peptide Receptor	NM_005314	2.82
COL3A1	Collagen, Type III, Alpha 1 (Ehlers-Danlos Syndrome Type IV, Autosomal Dominant)	AU144167	2.89
COL3A1	Collagen, Type III, Alpha 1 (Ehlers-Danlos Syndrome Type IV, Autosomal Dominant)	AI813758	2.53
ITGBL1	Integrin, Beta-Like 1 (with EGF-Like Repeat Domains)	AI753143	2.99
ITGBL1	Integrin, Beta-Like 1 (with EGF-Like Repeat Domains)	AL359052	2.67
ITGBL1	Integrin, Beta-Like 1 (with EGF-Like Repeat Domains)	AK026784	2.70
ITGBL1	Integrin, Beta-Like 1 (with EGF-Like Repeat Domains)	NM_004791	1.82
NEDD9	Neural Precursor Cell Expressed, Developmentally Down-Regulated 9	AL136139	3.00
NEDD9	Neural Precursor Cell Expressed, Developmentally Down-Regulated 9	U64317	1.58
SOX9	SRY (Sex Determining Region Y)-Box 9 (Campomelic Dysplasia, Autosomal Sex-Reversal)	AI382146	3.00

SOX9	SRY (Sex Determining Region Y)-Box 9 (Campomelic Dysplasia, Autosomal Sex-Reversal)	NM_000346	2.97
GNAI4	Guanine Nucleotide Binding Protein (G protein), Alpha 14	NM_004297	3.15
PLA2G7	Phospholipase A2, Group VII (Platelet-Activating Factor Acetylhydrolase, Plasma)	NM_005084	3.20
LGR5	Leucine-Rich Repeat-Containing G Protein-Coupled Receptor 5	AL524520	3.23
LGR5	Leucine-Rich Repeat-Containing G Protein-Coupled Receptor 5	AF062006	1.75
PPAP2B	Phosphatidic Acid Phosphatase Type 2B	AV725664	3.29
PPAP2B	Phosphatidic Acid Phosphatase Type 2B	AB000889	3.16
PPAP2B	Phosphatidic Acid Phosphatase Type 2B	AA628586	2.89
CTGF	Connective Tissue Growth Factor	M92934	4.25
CLDN11	Claudin 11 (Oligodendrocyte Transmembrane Protein)	AW264204	4.49

APPENDIX

Table A-1. Summary of Metastasis-Related Gene Transcripts. The 2,142 genes changed by CCG-1423 were filtered using metastasis-related gene ontology (GO) categories, including: *angiogenesis, cell migration, cell adhesion, epithelial-mesenchymal-transition, extracellular matrix, G-protein coupled receptor protein signaling pathway, inflammatory response, and metalloendopeptidases*. This table lists the 203 unique metastasis-related genes identified using this criteria. For several genes, there are multiple probesets. Blue highlighted gene transcripts indicate genes stimulated by CCG-1423, and red highlighted gene transcripts indicate genes inhibited by CCG-1423. +